Development and optimisation of the lift beams topsides removal concept

Arso Karlicic

Technische Universiteit Delft

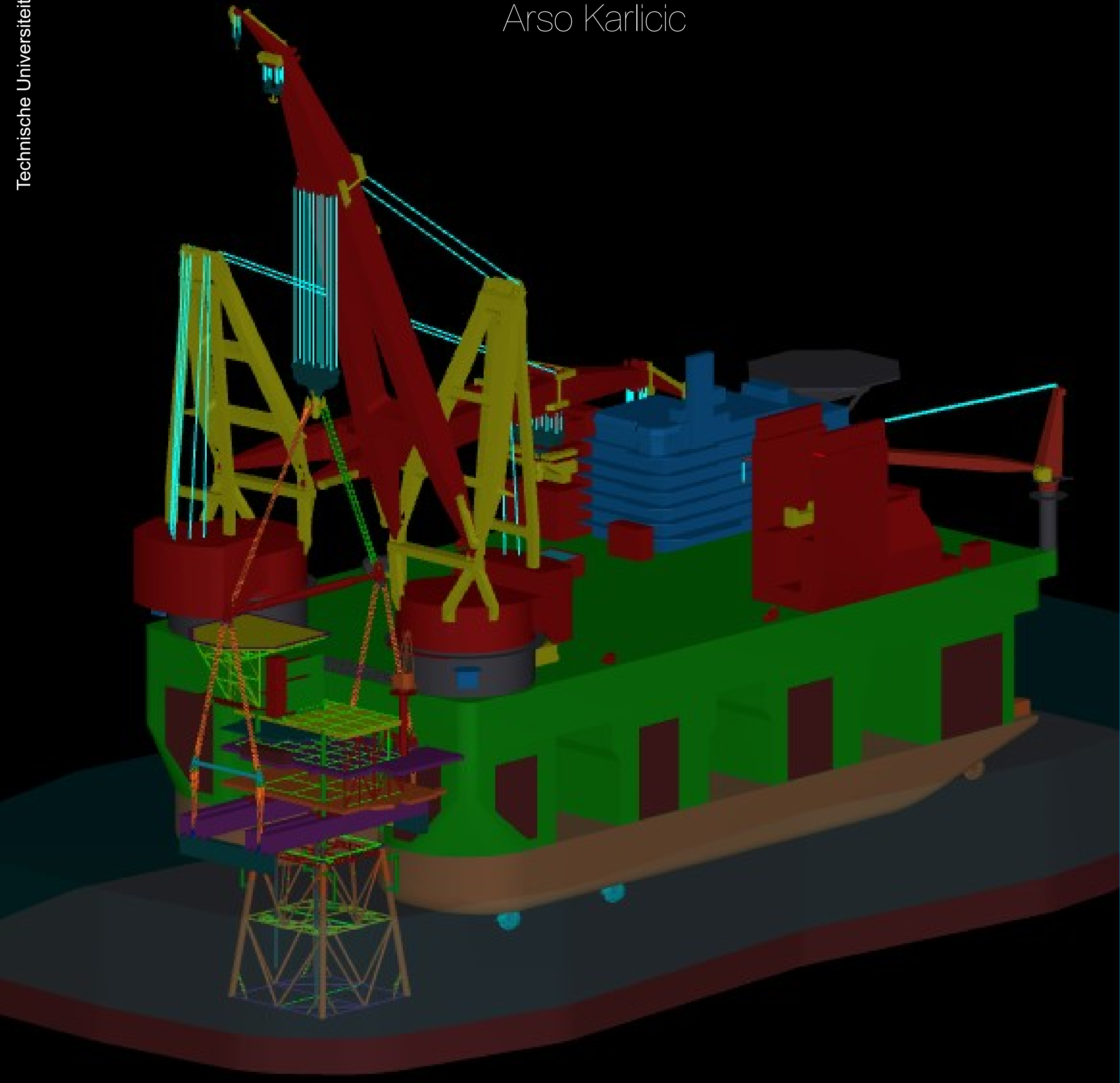

TU Delft

Development and optimisation of the lift beams topsides removal concept

by

Arso Karlicic

to obtain the degree of Master of Science
at the Delft University of Technology,
to be defended publicly on February 10, 2021 at 02:00 PM.

Student number:	4380584	
Project duration:	February 12, 2020 – February 10, 2021	
Thesis committee:	Ir. A.C.M. van der Stap,	TU Delft
	Ir. J.S. Hoving,	TU Delft
	Ir. P. Meeuws,	Heerema Marine Contractors
	Ir. J.P. Duvekot,	Heerema Marine Contractors

This thesis is confidential and cannot be made public until 10-02-2026.

Abstract

A large number of light, modular topsides in the southern North Sea is planned to be removed in the near future. Heerema Marine Contractors (HMC) is currently not the most competitive in this market as smaller contractors can often provide cheaper removal solutions with the use of smaller heavy lift vessels. HMC therefore aims to find a more economically attractive solution for the removal of these topsides.

Within HMC, a concept has been proposed to remove these modular topsides using so-called lift beams. The lift beams are large beams that are installed underneath the topsides, and are connected to the topsides' strong points. The ends of the lift beams provide lift points for the complete topsides, enabling removal in a single lift. Due to their high lifting capacity, and large available deck space, the modular topsides on the lift beams can easily be lifted by a single crane of one of the company's semi-submersible crane vessels (SSCV). Performing the lift by a single crane allows to put the topsides on deck of the SSCV for transportation. The concept is intended to be reused for a variety of modular topsides in the southern North Sea.

In this thesis, the lift beams are designed, and optimised, to withstand the governing load cases, while complying with the practical boundaries that each topsides imposes. Hereafter, it is investigated whether it is structurally feasible to lift the modular topsides using the lift beams. To determine this, structural integrity analyses are performed on a reference topsides using FEM software. Hereby the optimal lift beam setup to lift the topsides is determined. Furthermore, methods are designed for the connection between the lift beams and the topsides, and the installation of the lift beams.The efficiency of the final lift beams concept design is assessed by comparing its performance to conventional removal methods for modular topsides.

The lift beams are designed as stiffened box profile beams with a weight of more than 250 mT. The topsides is found to have sufficient capacity to withstand the loads during lifting. The optimal setup to lift the topsides consists of two lift beams per jacket leg row, and cross-beams at each end-on side of the lift beams. The cross-beams add stiffness to the lift beams and thereby redistribute the lift loads in a favourable manner over the connection points. Using a pin-hole connection between the lift beams and the topsides' legs is found to be most suitable. The lift beams are installed one-by-one using water as the counterweight component. Compared to conventional removal methods, the lift beams concept appears to be profitable after a relatively small number of topsides removals.

For future research, it is recommended to investigate the possibilities of performing the lift beams concept with a dual crane lift. It is expected that the practicality of the removal process can be improved in this manner. The increased lifting capacity also allows for removal of wider range of modular topsides. After lifting off its substructure, the topsides could be transported while suspended in the cranes.
Furthermore, it is recommended to extend the structural integrity analyses to the other topsides of interest. The structural limitations of the other topsides can be investigated, and the possibility to apply one-sided leg support can be considered. The weight and costs of the lift frame, as well as the installation procedure can be improved this way.

Preface

This master thesis report is the final deliverable to obtain the degree of Master of Science in Offshore and Dredging Engineering at Delft University of Technology. The project is done in cooperation with Heerema Marine Contractors.

The past year has been an incredible learning experience for me. Hereby I would like to show my gratitude to the people that have supported me throughout this journey. First I want thank my university supervisor Jeroen Hoving and committee chairman Andre van der Stap for their interest and support in completing this project. I have learned a lot from your feedback.

Furthermore I would like to thank Heerema Marine Contractors for providing me the opportunity to carry this project out. A special thanks goes out to my supervisors Pim Meeuws and Jan Pieter Duvekot. Your guidance and support throughout the project were essential in achieving this result. You have helped me a lot in linking theoretical knowledge with practical insights. I also appreciate all the other people within Heerema, that have shown interest in this project.

Finally I would like to thank my friends and family that have supported me through this time. Your motivation was of great importance to me.

Arso Karlicic
Rotterdam, February 2021

Nomenclature

Acronyms

CoG	Centre of Gravity
DAF	Dynamic Amplification Factor
DoF	Degree of Freedom
DNVGL	Det Norske Veritas Germanischer Lloyd
DP	Dynamic Positioning
FPSO	Floating Production Storage and Offloading
HLV	Heavy Lift Vessel
HMC	Heerema Marine Contractors
ILT	Internal Lifting Tool
IMO	International Maritime Organization
LAT	Lowest Astronomical Tide
LNG	Liquefied Natural Gas
LRFD	Load Resistance Factor Design
MCA	Multi-Criteria Analysis
MPM	Most Probable Maximum
MSF	Module Support Frame
mT	Metric Ton
NMA	Norwegian Maritime Authority
POI	Point Of Interest
RAO	Response Amplitude Operator
RP	Reference Point
SKL	Skew Load Factor
SNS	Southern North Sea
SPMT	Self Propelled Modular Transporter
SSCV	Semi-Submersible Crane Vessel
SWL	Safe Work Load
TLP	Tension Leg Platform
UC	Unity Check
UKCS	United Kingdom Continental Shelf

ULS Ultimate Limit State

WoW Waiting On Weather

Contents

1 Introduction to decommissioning of offshore oil and gas platforms

1.1. Decommissioning of platforms in the North Sea

In 1965 the first field producing commercial quantities of hydrocarbons was discovered in the southern North Sea [41]. A few years later the first offshore platform was installed in this basin. Hereafter more than 600 installations have followed in the North Sea. Approximately only 15% of the assets in the North Sea has been decommissioned so far [4]. Several reasons exist for the low number of decommissioned platforms:

- Decommissioning of offshore platforms is challenging and costly

  The scope of work in closing off operations and making the platform ready for removal is enormous. The state, size and complex layout of the platforms causes this to be a challenging and time consuming process. Removal of the platforms is in most cases only feasible with costly heavy lift vessels due to the size of the platforms and the rough surrounding environment. This all results in high decommissioning costs, which at times can be higher than the costs for installation.

- Platform lifetime extension

  Throughout its lifetime a platform undergoes various maintenance and refurbishment campaigns to secure its structural integrity and extend its initially intended structural lifetime. The production of a platform can be increased by expanding its sub-sea infrastructure to other nearby fields. This way a platform becomes economically viable for a longer period of time. Furthermore, the operational lifetime of a platform is often extended by transferring ownership to smaller operators. This is mostly done when the platform has surpassed its peak production.

- Long time path of decommissioning projects

  Once production has ceased permanently, it can still take several years of planning and preparation before actual platform removal is realized. The availability of the heavy lift vessels plays a role in this. There are also no regulations in the North Sea that set a time limit on platform removal after cessation of production. The relatively high costs for decommissioning are preferably postponed this way.

- Environmental impact

  An important aspect in the removal of platforms is that this process should have less environmental impact than leaving it in place to deteriorate. The removal process should therefore occur in an environmental friendly manner. Also, different types of species settle around a platform during its lifespan. Removal of the platform would affect the habitat of these species. In recent years the RELife project is initiated, where it is proposed to reuse old platforms for the production of renewable energy, such as hydrogen [43]. In most cases, the topsides requires extensive modifications to serve its new purpose.

However as decided in the OSPAR agreement in 1998, complete removal of platforms is required when they reach the end of their operating lifetime. An exception is made for gravity-based concrete substructures and 41 large steel substructures which were installed before the agreement [40].
Considering regulations and the increasing number of aging platforms in the North Sea, a rise in decommissioning activities is expected in the coming years.

1.2. Heerema Marine Contractors

HMC is a globally acknowledged pioneer in the installation, transportation and decommissioning of offshore structures. The company has an impressive fleet consisting of the two largest SSCV's in the world, the LNG-powered Sleipnir and the Thialf. In addition to this, the company owns HLV Aegir, SSCV Balder, and a large variety of barges, which are used for transportation and float-over of offshore facilities. The capacity and diversity of the fleet allows HMC to be active all over the world, in all kinds of waters. From the removal of aging platforms to the installation of newly built wind turbines. After all, the vision of HMC is to make the impossible possible offshore.

It is however of utmost importance that the company's activities are performed in a sustainable manner. HMC has therefore taken initiatives to further reduce its environmental footprint. The Sleipnir and the Thialf are for instance planned to be connected to a sustainable energy grid when moored on-shore to reduce the vessels' emissions and noise. This sustainable approach allows HMC to set the goal to become carbon-neutral by 2025. This mindset is also reflected in the mission of HMC which states to be the leading marine contractor creating sustainable values for clients and stakeholders.

1.3. Topsides decommissioning process

An offshore oil and gas platform can be divided in two parts: the topsides and the substructure. The topsides lies above the waterline and provides all the equipment for drilling, production and processing of hydrocarbons[28]. In case of a manned platform, the topsides also provides accommodation for the workmen. A distinction is made between modular topsides and integrated topsides. Modular topsides consist of multiple modules, which are supported by a module support frame (MSF). The MSF is the lower deck that carries the weight of the modules, and transfers it to the substructure. Integrated topsides on the other hand consist of a single primary structure.

The substructure keeps the topsides in place and is mostly submerged. Substructures can either be fixed or floating. Fixed substructures are founded on the seabed and can be further subdivided in concrete gravity based substructures (GBS) and steel substructures, which are either jackets or compliant towers. Floating substructures are applied in greater water depths and are present in the form of spars, TLP's, FPSO's and semi-submersibles. An impression of a typical steel structure based platform is provided in figure 1.1.

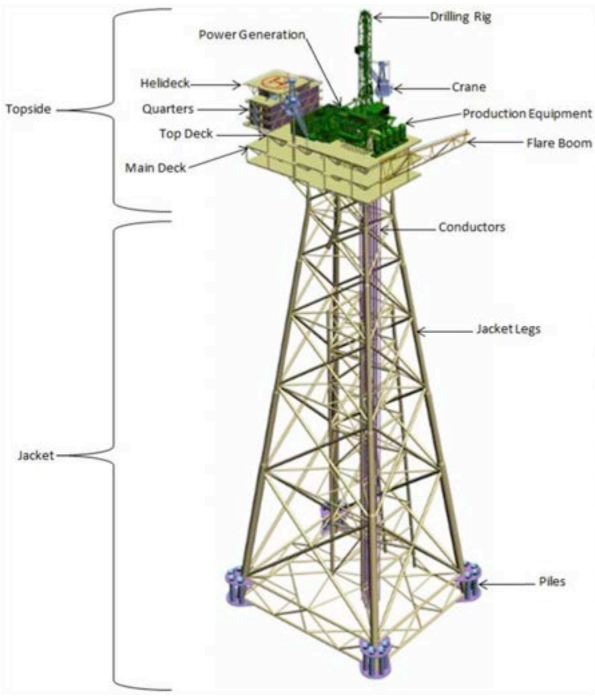

Figure 1.1: Modular topside with a jacket substructure [33]

The decommissioning of a platform consists of ending the platform operations and returning the ocean and seafloor to its pre-lease condition [2]. The platform decommissioning process can be divided in six stages, as presented in figure 1.2.

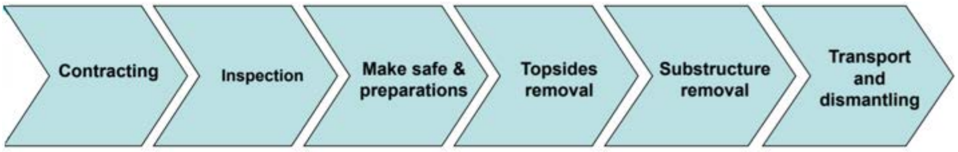

Figure 1.2: Phases of platform decommissioning[40]

Decommissioning of a platform is planned years in advance of its actual removal. Agreements are made with the assigned contractors about the planning, the scope of work and the method of removal. The platform is thoroughly inspected to get an accurate indication on its current state. Preparations follow to make the platform safe for removal. After removal, the topside and substructure are transported to shore, where the structures will be dismantled.
In this research the decommissioning of modular topsides with a fixed steel jacket substructure is of interest. This comprises the topsides make safe and preparations phase, the topsides removal phase and the transportation and disposal phase of the topsides.

1.3.1. Topsides make safe and preparations

The make safe and preparation phase regularly starts at the end of the platform's operational lifetime. The topsides has to be made ready for removal in this phase. Based on the method of removal, strengthening of the topsides might be required at specific locations. This is of significant importance as the topside has deteriorated over its years of service. During surveys defects such as excessive corrosion and fatigue cracks might have been detected. The original lift points that have been used during installation often have to be replaced. Connected modules have to be separated as they are likely to be removed one-by-one. Any interfering infrastructure such as piping and cables has to be cut free and removed. Also the risers and conductors that are travelling to the seabed must be separated from the topsides.

The topside has also undergone several modifications over its lifetime. Modules and equipment are possibly added, expanded or removed. It is important that these changes have been documented accordingly. Surveys are performed to get a best estimate on the current weight and layout of the topsides. The weight and CoG of the topsides and the separate modules are important input for the topsides removal phase.

1.3.2. Topsides removal

When the platform is deemed to be safe and all preparations have been completed, the topsides is ready to be removed. The topsides removal method depends on several factors:

- Topsides layout

  The composition of a topsides strongly determines the possible methods for removal. In case of modular topsides, removal is mostly achieved through multiple lifts, limited to a few modules a time. Each module has to be separately prepared for removal. Integrated topsides on the other hand can be removed in a single lift, since these structures have been designed for this operation. Removal of integrated topsides therefore requires significantly less preparation.

- Vessel characteristics

  Heavy lift vessels play an essential role in the removal of offshore platforms. The vessels can widely vary in their lifting capacity, operability and practicality. Based on the vessel characteristics different methods of removal can be considered. Since there is a select number of such vessels, their availability can not always be guaranteed.

- Topsides characteristics

  The size and weight of a topsides can limit the possible methods of removal. The state of the topsides can influence whether its safe and feasible to remove the topsides in a certain way. The topsides is allowed to plastically deform during this process, as it will no longer be in service. However the global structural integrity of the modules and the topsides must be ensured. Otherwise the safety of the removal process could be jeopardized . The vessel can get damaged in the process and parts of the platform can drop in the water and pollute the local environment.

Due to this, there is no generic solution for the removal of topsides. In this section the characteristics of the main removal methods are discussed.

Piece small removal
The topsides is dismantled and cut in smaller, more manageable pieces for removal. The dismantling is often done with an excavator, which is lifted onto the platform. An impression of this is provided in figure 1.3.

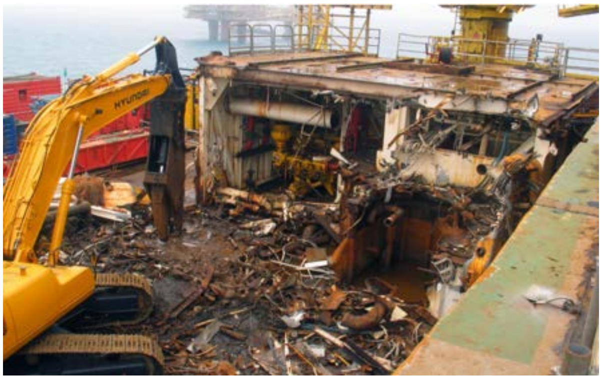

Figure 1.3: Piece small removal[19]

The pieces are loaded in containers, which are transported by a barge to a nearby yard. Piece small removal requires extensive offshore preparations and is used in absence of a heavy lift vessel. This method of removal is very time consuming and requires a lot of offshore manhours. Furthermore, piece small removal is considered to be less safe than the other removal methods due to its extensive scope consisting of hazardous operations.

Reversed installation
Reversed installation is the most commonly applied topsides removal method. Removal takes place in reversed order with respect to installation. No difficulties are expected as the modules are designed for the same load case during installation. If a module has undergone significant changes, it is advised to re-assess its structural integrity for the lift. If possible, the original installation lift points are used for removal. Additional strengthening of the modules might be required when signs of deterioration are visible. Prior to lifting, the modules have to be cut free and infrastructure between modules has to be removed.

Groups of modules
Multiple modules are removed together from the platform. This method is often selected for modules which are interconnected through infrastructure or by means of welding. The cutting and dismantling scope for these modules can be reduced this way. As the group of modules have not been lifted together before, extensive engineering is required to assess the structural integrity of the assembly. Besides, new lift points will have to be fabricated, which will serve for the whole group of modules. As this method is not applicable to all modules, it is often used in combination with reversed installation as a potential time and cost saver.

Single lift removal
The topsides can also be removed off its substructure in a single piece. This can either be done by lifting or reverse float-over. For the latter, float-over barges are used which can raise the topside by means of ballasting. For an integrated topsides, single lift removal can be considered as reversed installation. The topsides has been installed in a single lift and therefore has the structural capacity and the lift points to be lifted as a whole. In figure 1.4, the single lift removal of the Jotun B platform's integrated deck is depicted.

Figure 1.4: SSCV Thialf removing the Jotun B integrated deck in a single piece [26]

For modular topsides this method is rarely applied. Safe single piece removal of modular platforms requires extensive preparations and engineering. Besides, only a handful of vessels would be able to perform such an operation. Single lift removal saves a significant amount of preparation time and offshore HLV time compared to the aforementioned removal methods.

1.3.3. Transportation, offloading and dismantling of topsides
Depending on the removal method, the topsides is transported as a whole or in pieces. After lifting off its substructure, the topsides or module is placed on the HLV's deck or on a transportation barge. The removed object is placed on grillage and is sea-fastened to ensure its stability during the sail. In recent years an alternative method has been performed by HMC, where integrated topsides are transported while suspended in the cranes of the SSCV.

Eventually, the topsides is transported to a nearby yard, which has sufficient space and capacity to handle the size and weight of the topsides. At arrival the HLV or barge will offload the topsides on the yard's quay. The topsides is placed on load-in trailers, which will transport the topsides to its final destination. Here, the topsides is dismantled and mostly recycled.

1.4. The lift beams concept

A large number of lighter, modular topsides in the SNS is expected to be decommissioned in the coming years. HMC is not necessarily the most competitive in this market. The removal price per tonnage steel of these topsides is relatively high due to their light weight. Smaller contractors can often provide a cheaper removal solution with the use of smaller HLV's. HMC therefore aims to find a more economically attractive solution for the removal of these topsides. This way the company can re-establish its competitive position in this market.

Within HMC, a concept has been proposed to remove modular topsides in a single lift using so-called lift beams. The lift beams are large beams that are installed underneath the topsides, and are connected to the topsides' strong points. The ends of the lift beams provide lift points for the complete topsides, enabling removal in a single lift. The lift will be performed by one of the SSCV's because of their high lifting capacity and large available deck space. An impression of the lift beams concept is provided in figure 1.5.

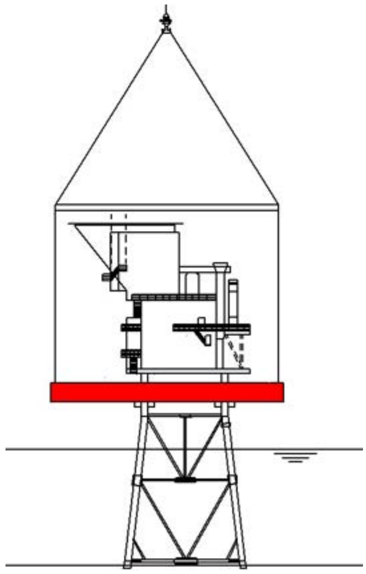

Figure 1.5: Impression of the lift beams concept

In this research the lift beams concept will be developed, and optimised to a certain degree. Compared to conventional reversed installation, it is expected that the amount of preparation time and offshore SSCV time can be reduced significantly with this removal concept. The capacity of the SSCV's will also be better utilized this way. The lift beams concept could therefore provide a more efficient and cost effective solution to remove modular topsides.
The two main criteria for this concept are listed below.

- Reusable

  The costs for the realization of this concept are expected to be relatively high. To make the concept economically viable, it is aimed to reuse the lift beams for a large variety of topsides. Project specific preparations and costs should be minimized in order for the concept to be cost-effective. The lift beams also have to be technically robust to withstand different load cases while complying with the practical boundaries that each topsides imposes. After removal, the lift beams should relatively easily be retrievable to be used for another removal project.

- Single crane single lift

  Another starting point for the lift beams concept is that the topsides will be removed in a single lift using a single crane. Lifting with a single crane allows to place the topsides on deck of the SSCV for transportation after removal. This will also provide the opportunity to subsequently remove the jacket substructure in the same campaign.

1.5. Problem definition

There are several challenges that have to be tackled to make this a feasible and efficient removal method. For each of the topside decommissioning phases discussed in section 1.3, important considerations and potential challenges are identified.

1.5.1. Preparation phase

Topsides preparations

The topsides has to be prepared for removal with the lift beams. Under-deck obstructions which could interfere with the installation or connection of the lift beams must be removed. It has to be assessed whether the connection points, and the remainder of the topsides, have sufficient capacity to withstand the loads during lifting. Additional strengthening might be required, as the topsides will be lifted in a manner it was not designed for.

During installation of the lift beams, it is possible that impact will occur between the lift beams and the topsides. A guide and bumper system could be equipped on the topsides to minimize the impact. Also, temporary supports have to be prepared for the lift beams to rest on, after their installation.
Preparations for the connection might also be required. The topsides' connection points have be outfitted with a connection interface, and work access platforms have to be installed to assist on the installation and connection phase.

Prior to topsides removal, the topsides has to be cut free from its substructure. It is hereby important that the topsides can maintain its lateral stability after cutting.

Lift beam preparations

On-shore the lift beams have to be prepared for the topsides lift. The lift beams are outfitted with connection elements and lift points are fabricated on the lift beams. Since the location of the connection points differs for each topside, the position of the connection elements must be adjustable in a relatively simple manner. Prior to each lift, the lift beams must be inspected on potential defects. If everything is set, the lift beams are loaded on deck of the SSCV. The rigging for installation of the lift beams and for removal of the topsides is also arranged in this stage.

1.5.2. Topsides removal phase

Installation and connection of the lift beams

Prior to topsides removal, the lift beams have to be installed and connected to the topsides. Installation of the lift beams might prove to be a challenging operation due to the limited under-deck space and the size of the lift beams. The lift beams are placed on their temporary supports, which are most likely provided by the MSF legs.

When the connection between the lift beams and the topsides is being established, the elements are preferably stress-free. This way initial stresses and displacements of the elements can be avoided. In practice this is however not feasible, and the initial stress state should be accounted for in the design of the connection. Any risks of disconnection or failure during removal must be eliminated. Furthermore, a quick connection time is desired in order to minimize the SSCV waiting time and the total topsides removal time.

Load transfer between the lift beams and the topsides

For the in-situ case, the weight of the topsides is carried by its jacket substructure. During lift-off the load is transferred from the jacket to the lift beams and is eventually borne by the SSCV. It is important that the load is transferred in a controlled and continuous manner.
Ideally, the topside is lifted under its MSF legs as this closely resembles the in-situ case, where mainly a vertical load is carried. This is likely not feasible and the type of connection will therefore strongly determine the types of loads that are introduced at the connection points. The design of the lift beams is also expected to be of influence here. The rigging arrangement and the position of the lift points are expected to play an important role in the load distribution over the connection points.

Structural integrity of the topsides
The structural integrity of the topsides is the main priority during the topsides removal phase. Local plastic deformations are allowed, however the global structural integrity of the topsides must be ensured. Due to the varying strength and stiffness of the topsides, failure might occur at several different locations. Strengthening might be required as the topsides will be loaded in a way it was not designed for. The structural integrity of the connection points and neighbouring elements is especially of importance here. Failure of these elements could directly lead to failure of the lift operation. The connection type and the design of the lift beams design are therefore crucial for the topsides' structural integrity.

Lift stability
During lifting it is important that the rotations and displacements of the topsides are limited. These motions are imposed by environmental loads and the lift loads, which load the topsides in an eccentric manner. The motions of the vessel directly influence the motions of the lift object, and therefore play an important role in this process. Lift analyses have to be carried out to determine suitable weather windows for the operation.

Tilt of the topsides should be limited to avoid collision between the topsides and the rigging. Similarly the off-lead angle should be limited to avoid collision between the topsides and the SSCV. Sufficient clearance and stability should therefore be maintained during this operation. The lift points are located below the topsides' CoG, which enhances the aforementioned instability phenomena. Accurate positioning of the hook with respect to the assembly's CoG and selecting appropriate rigging will reduce these effects.

1.5.3. Topsides transportation phase

On-deck transportation
After lifting off its substructure, the topsides is placed on the SSCV's deck for transportation. A single crane lift allows to rotate the assembly outwards onto deck. If both cranes would be used, the cranes would have to rotate the assembly inwards. This is not feasible due to the size of the topsides. For this operation it is important to maintain sufficient vessel stability. The SSCV deck should provide enough space for the cranes to lie on their boom rest.

Depending on the offloading phase, the SSCV will transport the assembly to the yard by itself or the assembly is transferred to a transportation barge. In case of the latter, the SSCV will have to sail to calm waters to perform the transfer. The topsides is placed on grillage, which will support the topsides during transportation. The lift beams could be used for this purpose. Additionally, the topsides has to be sea-fastened to ensure a stable voyage.

1.5.4. Topsides disposal phase

Offloading of the topsides
When the SSCV arrives at the destined yard, the topsides is offloaded at the yard's quay. As the water depth is relatively shallow, the SSCV will have to perform this operation at a low draught to maintain sufficient clearance with the seabed. The vessel should also maintain sufficient clearance with the quay during this operation. It is suggested that the hydrostatic stability of the SSCV is checked for this phase. If the clearance and stability criteria can't be satisfied, a barge will be used to transport the topsides to the yard. In this case, it is likely that offloading will happen by means of load-in trailers.

Detachment of the lift beams after disposal
Once the topsides has been offloaded at the yard, it is essential that the lift beams can easily be disconnected from the topsides and retrieved. This way the lift beams can relatively quickly be re-used for another removal project.

Yard capacity
Another aspect is the capacity of the yard where the topsides will be offloaded. As most yards are not used to receive such heavy and large structures in a single piece, it is very important to carefully plan disposal of the topsides. The yard should have sufficient space and capacity to handle the topsides and subsequently dismantle it.

1.6. Research objective and research questions

The objective of this research is to develop and optimise a method for single lift removal of modular built topsides using lift beams. The single lift must be performed by a single crane, and the concept must be reusable for a variety of topsides.

The lift beams will be designed and optimised, and it has to be investigated whether it's structurally feasible to remove modular topsides using lift beams. Hereby it is aimed to find the optimal lift beam setup for removal of the topsides. Furthermore, methods are designed for the connection between the lift beams and the topsides, and for the installation of the lift beams. Eventually, the efficiency of the lift beams concept will be assessed by comparing its performance to the conventional methods for modular topsides removal.

The focus of this research will lie on the topsides removal phase. However, the topsides preparation phase and the transportation and disposal phase are thoroughly considered throughout the process.

1.6.1. Research question

Through this research it is aimed to answer the following research question:

Is it feasible to efficiently remove modular topsides with a single crane lift using lift beams?

In order to adequately answer the research question, a set of sub-research questions is defined:

1. What are the lift beam requirements?
2. Can the topsides withstand it to be lifted by the lift beams?
3. How to connect the lift beams to the topsides?
4. How to install the lift beams underneath the topsides?

1.7. Research methodology

A structured approach is taken in developing the lift beams concept, and assessing its feasibility. The research is divided into six stages.

Literature study for the lift beams concept

At the start of this research, a literature study is conducted to get more insight on the requirements, boundaries and possibilities for the lift beams concept. First a market analysis is performed to get a better understanding on the current and future state of decommissioning projects in the North Sea. Data about the potential topsides for lift beams removal is obtained through a topsides analysis. This way the governing load case and the limiting global dimensions of the lift beams can be determined. The SSCV's lifting capabilities and hydrostatic stability are analysed to identify any operational limits for the lift beams concept. Finally, relevant literature regarding single lift modular topside removal and efficient lift beam design are discussed.

Design and optimisation of the lift beams

From the topside analysis, the required input data is obtained to design the lift beams. The global design of the lift beams is addressed in this phase. Phenomena such as bending, shear, torsion and buckling are taken into account. The local lift beam design is dependant of the connection type, and will therefore be addressed in the connection concept phase. The design of the lift beams is optimised to provide a light and cost-effective solution.

Topsides structural integrity analysis

Prior to designing the connection and installation concepts, the question has to be answered whether the topsides can withstand it to be lifted by the lift beams. A topsides structural integrity analysis is performed in SACS to answer this question. It is aimed to get more insight on the parameters that influence the load transfer between the lift beams and the topsides. Different lift beam configurations, connection possibilities and rigging arrangements are considered to find the most optimal solution regarding the topsides' structural integrity. This phase will also provide essential input for the connection concept design.

Connection concept design

Several types of connection concepts have been generated. Based on multiple assessment stages with HMC specialists and insights from the structural integrity analyses, three connection concepts are selected. These concepts are designed into more detail and a presentable manner is found to model the connections in SACS. This way the structural integrity of the topsides can be assessed for each connection type. Eventually the most suitable connection concept is selected based on a multi-criteria analysis.

Installation concept design

The final riddle to solve is how to install the lift beams underneath the topsides. The three most promising installation concepts are assessed in this stage. One concept is selected for further elaboration. The installation procedure of this concept is defined, and a lift analysis is performed to analyse the motions of the lift beam during installation. Based on the optimal installation setup, the workability of the installation concept can be determined.

Lift beams concept assessment

The final lift beams concept design is assessed through a case study. A detailed description of the complete topsides removal process is provided here. The performance of the lift beams concept is assessed for a specific topsides. Comparisons are drawn with the conventional method of removal. This way it can be determined whether the lift beams concept provides an improved solution for removal of modular built topsides.

An overview of the methodology structure is provided in figure 1.6. A strong correlation exists between the different phases of the lift beams concept. After completing all the phases, the final lift beams concept design is assessed through a case study.

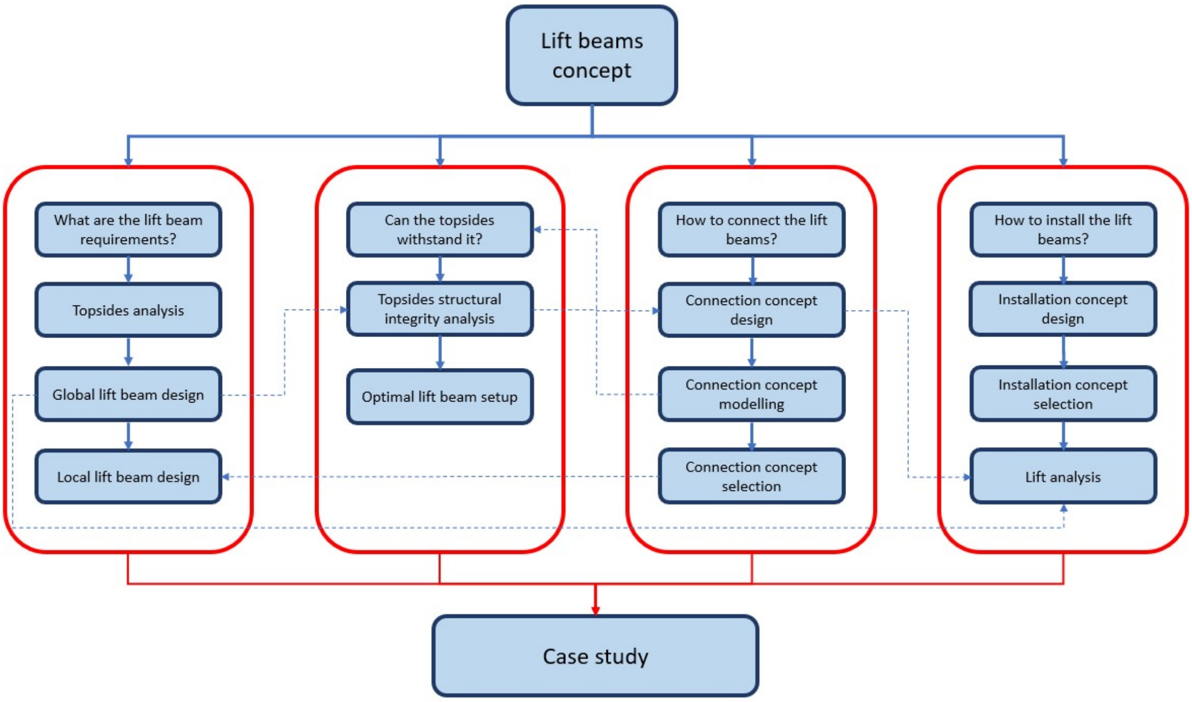

Figure 1.6: Overview of the methodology structure

1.8. Report structure

The structure of the report is illustrated in figure 1.7.

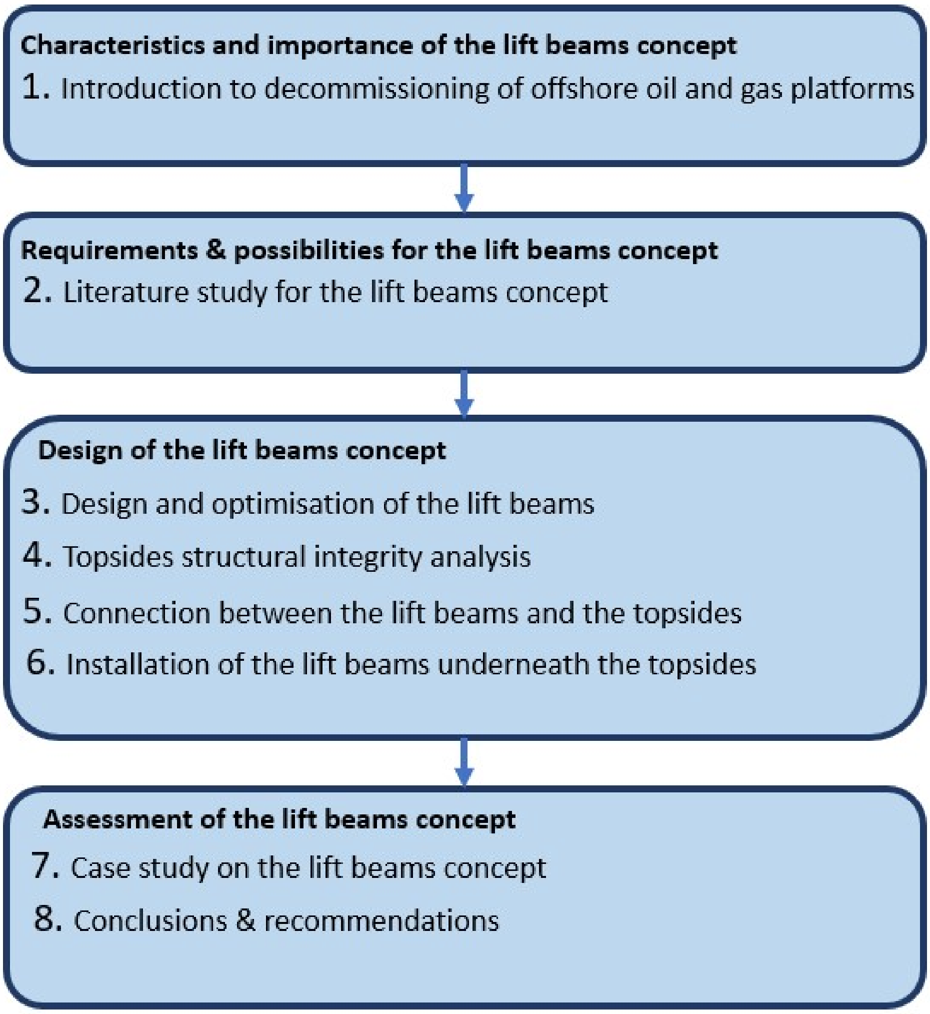

Figure 1.7: Overview of the report structure

2
Literature study for the lift beams concept

2.1. Market analysis

2.1.1. Current situation

The North Sea is densely populated by oil and gas facilities, with approximately 550 installations still in operation [21]. This number includes smaller installations functioning as wellhead, accommodation or satellite platforms. The map in figure 2.1 provides an overview of the platform population in the North Sea.

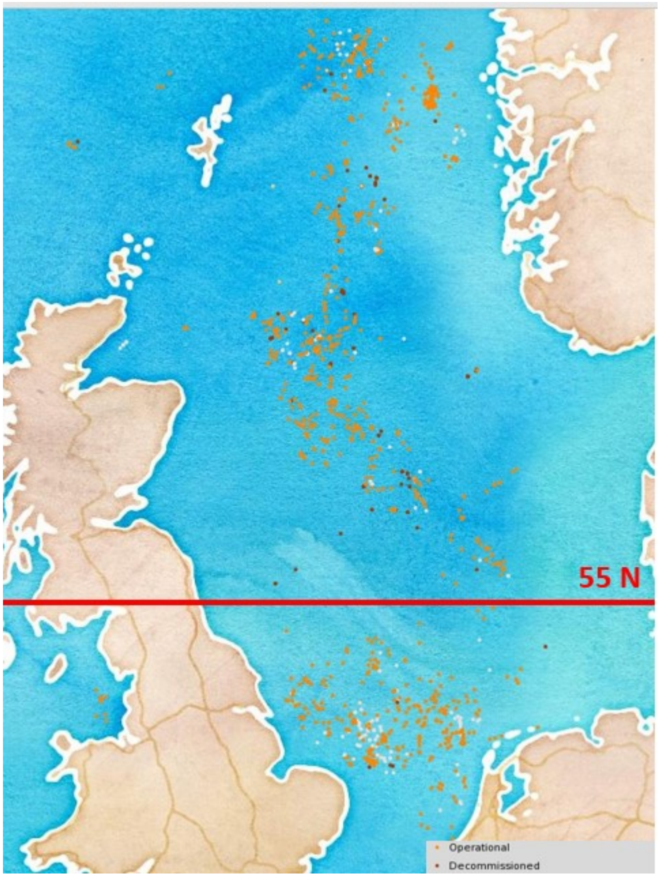

Figure 2.1: Overview of operational and decommissioned platforms in the North Sea [20]

The platforms in the southern North Sea mainly produce gas, and are in general lighter than oil producing facilities which are frequently found in the northern North Sea. In the central North Sea a mixture of both is found. Heavy modular topsides were mainly installed in the past, where decommissioning was not implemented in the topsides' life cycle. Current practices aim for more weight efficient, integrated, topsides.

The vast majority of the North Sea installations has a fixed steel substructure. No distinction is made between compliant towers and jackets. The latter is however the most commonly applied substructure type in this region. Figure 2.2 shows the substructure distribution for North Sea installations.

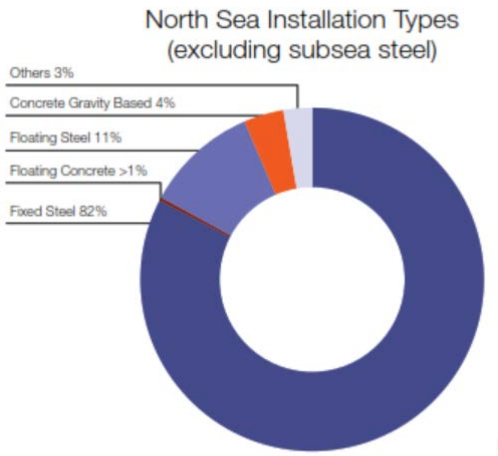

Figure 2.2: Substructure types of North Sea installations [17]

It can be seen that more than 80% of the platforms in the North Sea has a fixed steel substructure. The OSPAR installations inventory database is used to get an insight on the topsides weight of platforms with a fixed steel substructure. A distinction is made between the southern North Sea and the northern North Sea. The results are shown in figure 2.3.

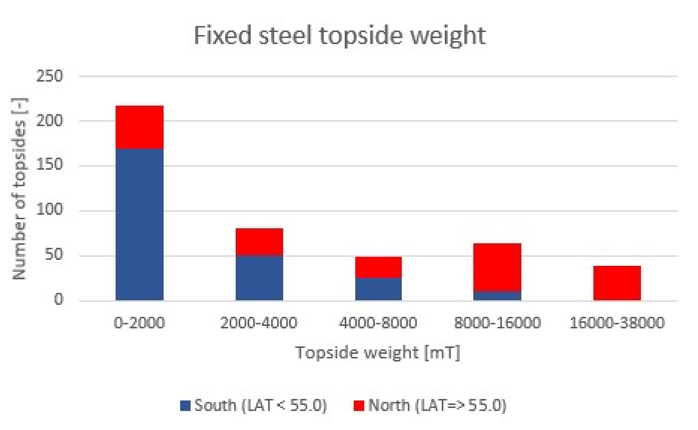

Figure 2.3: Weight of jacket supported topsides [21]

The topsides weight for jacket supported platforms in the North Sea ranges from 100 mT to 38.000 mT. It can be seen that the heavier topsides are located in the northern part of the North Sea, which is defined with a latitude greater than 55 degrees. .

The SNS is mostly populated by smaller topsides, which fall within the lifting capacity range of a Sleipnir single crane. The topsides in this region are mostly modular built. The SNS is therefore considered to be an ideal location for the lift beams concept.

A mere 15% of the platforms in the North Sea has been decommissioned so far, while the average asset age is found to be 25 years[4]. In some cases production of currently operating platforms dates back to 1967, presenting an operational lifetime of more than 50 years [21].

Decommissioning is preferably delayed as much as possible. The focus of operators lies on improving the economic viability of the assets rather than closing down operations. Production processes have become more efficient, and aging assets are sustained through exploitation of new fields and extending the asset's structural lifetime. Asset ownership is transferred to smaller operators, which are more

capable of investing in late-life fields[29]. The platform decommissioning liabilities are often included in the ownership transfer.
Decommissioning is nonetheless an inevitable part of an offshore asset's life cycle. In recent years an increasing amount of decommissioning projects has been undertaken. More experience is gained by the industry and it is aimed to further improve the decommissioning process.
In the UKCS, topsides removal on average takes up 8% of the total decommissioning costs. The highest costs are assigned to well decommissioning, presenting 49 % of the total platform decommissioning costs. Topsides preparations only take up 3 % of the total costs [29]. It has to be noted that higher topsides removal and preparation cost percentages are found in the SNS. The price per removed tonnage of topside is higher here due to the lower weight of the topsides. Nevertheless, operators have indicated to aim for further reduction of removal costs. Possible ways to achieve this are improved removal solutions and implementing decommissioning in the asset's long-term plans. Decommissioning can be planned in accordance with the removal vessels' availability this way. The removal costs can also be spread over a longer period of time.

2.1.2. Market forecast

The number of platforms in the North Sea reaching the end of their life cycle keeps on increasing. Decommissioning activities are therefore expected to continue rising in the coming years. More than 650,000 mT of topside weight is planned to be removed in the UKCS between 2020 and 2029 [29]. The distribution over this period is provided in figure 2.4.

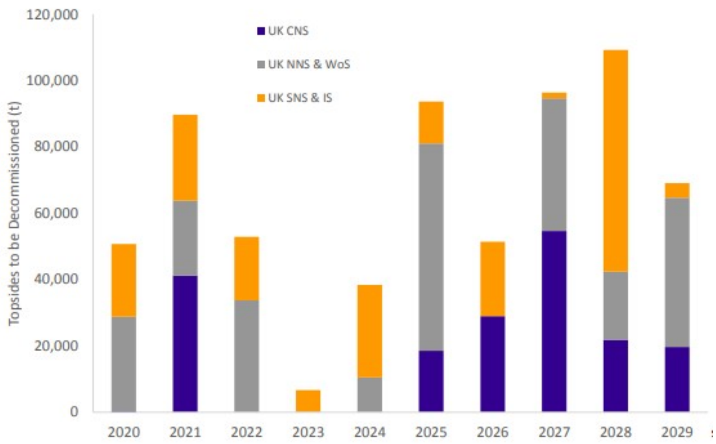

Figure 2.4: Topsides weight to be removed in the UKCS [29]

Approximately 32% of the to-be-removed topsides mass in the UKCS is assigned to the SNS. A total of 59 topsides are planned to be removed in this basin. This implies an average topsides weight of 3552 mT.

In the Netherlands, Denmark and Norway the to-be-removed topsides mass equals approximately 240,000 mT in this period [29]. The forecast over the years for the greater North Sea is provided in figure 2.5.

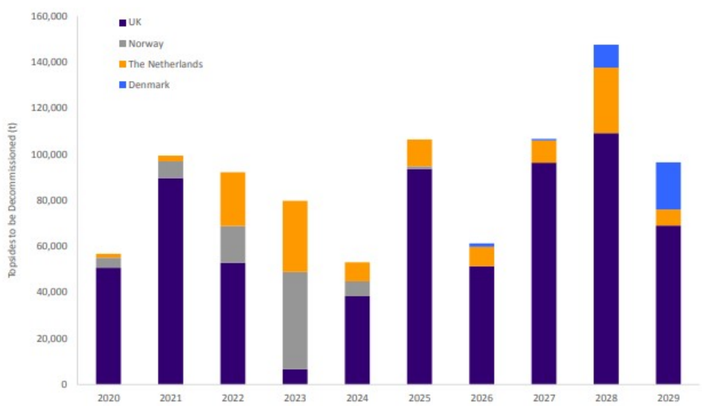

Figure 2.5: Topsides weight to be removed in the greater North Sea[29]

It can be seen that most of the topsides removal projects are scheduled from 2025. Fluctuations over the years are expected as each decommissioning project has a different time path. Unstable oil prices also strongly contribute to the fluctuating activity in the decommissioning market. After removal, the topsides are dismantled on-shore, where more than 90% of the total removed weight is expected to be recycled[24].

2.2. Topsides analysis

2.2.1. Topsides selection

A range of topsides has been selected for potential removal with the lift beams concept. The location of the topsides is indicated in figure 2.6.

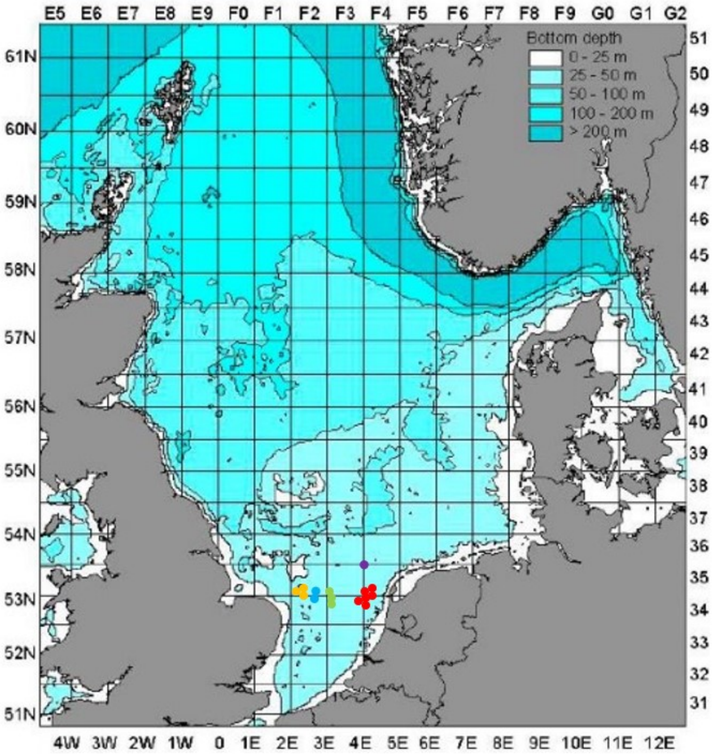

Figure 2.6: Water depth Greater North Sea [15]

The topsides are all located in the southern North Sea, where the water depth ranges between 25 and 50 meters. Each of these topsides is unique in their structural and geometrical properties. To make the concept reusable for each topsides, it is important that the boundaries and load cases, imposed by each topsides, are taken into account. This information is gathered by analysing structural drawings and installation manuals. Conservative assumptions are made in case data is missing or not up to date. Relevant topside characteristics for the lift beams concept are the topsides type, weight, size, location and substructure. The relevance of each characteristic is discussed below.

Topsides type

A distinction is made between modular topsides and integrated topsides. The majority of topsides that are planned for removal in the coming years are modular built. The lift beams concept could provide a cost-effective solution to remove modular topsides in a single lift. A significant reduction in preparation time and offshore SSCV time can be achieved this way. The offshore SSCV time is especially of importance as this is one of the driving factors for the total topsides removal costs.

Topsides weight

A platform undergoes various changes during it's lifetime. These changes are not always documented properly and some uncertainty exists about the exact weight of the topsides. Commonly weight reconciliations are performed, to assess the topsides' present inventory. The presence, weight and position of equipment and structural steel is analysed.

In this research conservative assumptions are made regarding the topside CoG in case of missing data. An offset of 10% in the CoG, with respect to the geometrical center, is taken in the most unfavorable directions. In practice, this offset in the CoG is considered to be a reasonable value for modular topsides. The CoG offset directly affects the assumed lift point loads acting on the lift object. Remaining uncertainty about the weight and CoG of the topside is expressed in a contingency factor. Based on in-house standard criteria for single crane lifts, a contingency factor of 1.1 is considered to be suitable [35]. The dry weight is additionally multiplied with a DAF to account for dynamic hook load fluctuations during lifting. The DAF is dependant on the lift object's mass, the environment and the lift vessel. For offshore single lift operations, performed by one of the SSCV's, a DAF of 1.1 can be taken for lift objects with a design weight greater than 100 mT [35]. The values for the contingency factor and DAF are provided in table 2.1.

DAF	1.1	[-]
μ_{cont}	1.1	[-]

Table 2.1: The contingency factor and DAF used for the topsides weight

The factored weight of the topsides, including the lift beams, must lie within the capacity of a Sleipnir single crane. The factored weight of the topsides under consideration is illustrated in figure 2.7. The dry weight of the topsides is obtained from the OSPAR installations inventory database.

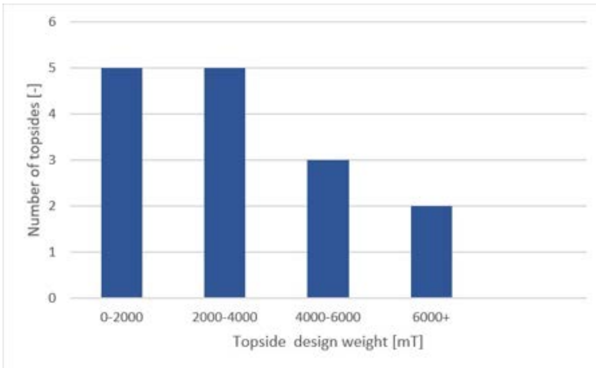

Figure 2.7: Topsides weight under consideration [20]

The maximum factored topsides weight is found to be 8100 mT. This implies that the design weight of the lift beams, including rigging is limited to approximately 1900 mT. It is therefore essential to minimise the weight of the lift beams. If this criterion can't be satisfied, it is advised to reduce the topsides weight by removing some modules prior to the single lift.

Topsides size

The topsides under consideration strongly vary in size. The minimum required length of the lift beams is determined by the maximum width of the topsides under consideration. Additional clearances are taken into account for this. Furthermore the size of the topsides affects the possible crane configurations during removal.

The maximum crane radius during removal is bounded by the topsides' weight and width. Sufficient clearances must be maintained between the crane boom and the topsides to prevent any risk of collision. Also the vessel should keep enough distance from the topsides during the lift operation. The advised clearances are dependant of the vessel and the operation that is performed. For the Sleipnir during a lift operation in DP mode, the following minimum clearances must be maintained [7]:

$$C_{boom-topside} = 3m$$

$$C_{vessel-topside} = 5m$$

Also, the required hook elevation during lifting is directly affected by the elevation of the topsides. The minimum required hook elevation is a function of the topsides elevation and the height of the upper rigging, taking additional clearances into account. The maximum hook elevation is a function of the crane radius. It can therefore be noted that the weight, the width and the height of the topsides determine the possible crane configurations during lifting.

Location
The selected topsides are all located in the SNS. The water depth in the SNS is known to be relatively shallow. The draught of the SSCV is therefore limited during installation of the lift beams and removal of the topsides. It is advised to assess the hydrostatic stability of the vessel during removal in such water depths. Based on the topside location, data can be extracted about the environmental conditions that are expected to be encountered. This data is used to determine the expected response of the vessel and the lift object during the lifting operations. The environmental conditions are assessed at a later stage in the report.

Substructure
The topsides of interest are supported by a fixed steel jacket substructure. The jackets strongly vary in size and layout. The limiting dimensions of the lift beams are determined by the under-deck layout, since it is expected that the lift beams will be installed within this space. The maximum width of the lift beams follows from the jacket leg spacing, whereas the maximum height is bounded by the distance between the MSF deck and the jacket top horizontal elevation. For both dimensions additional clearances have to be taken into account.

The lift beams are potentially connected to the MSF legs, as these are considered to be strong points of the topsides. The number of jacket leg rows indicates the potential number of lift beams to be used. The number of jacket legs per row indicates the number of possible connection points per lift beam. The number of jacket legs and their relative spacing therefore strongly influences the load case that is imposed to the lift beams. In the topside batch a wide variation of jackets is found, ranging from four-legged jackets to twelve-legged jackets.

2.2.2. Topsides data
The relevant topsides parameters are summarized in table 2.2.

Reference topside	Wdes [mT]	Width [m]	Elevation [m]	Water depth [m]	Jacket legs [-]
1	3831	40	49	36	2x2
2	1257	22	44	36	2x2
3	3025	28	44	36	2x2
4	8129	37	60	30	3x4
5	1332	25	50	30	2x2
6	4060	28	34	28	2x4
7	7754	46	47	31	2x4
8	2075	32	60	31	2x3
9	2048	32	31	31	2x3
10	4050	40	53	26	2x2
11	850	34	42	26	2x3
12	3910	46	53	26	2x2
13	850	32	26	26	2x3
14	4195	40	53	27	2x2
15	750	32	42	27	2x2

Table 2.2: Overview of the relevant parameters of the topsides under consideration

2.3. SSCV characteristics

The lift beams topside removal concept will be carried out by SSCV Sleipnir, which is the largest SSCV in the world.

2.3.1. Crane characteristics

The SSCV Sleipnir is equipped with two tub mounted cranes, each with a maximum lift capacity of 10,000 mT. The cranes have a main hoist, auxiliary hoists and a whip hoist. The maximum capacity is delivered by the main hoist, which has a maximum elevation of approximately 134 meters with respect to the waterline, at a regular operating draught of 27 meters. For the waterline, the governing value of the LAT is taken. This is also convenient, since the elevation of the topsides is indicated with respect to the LAT. The radius of the main hoist ranges from 27 meters to 103 meters with respect to the crane's ship-fixed vertical rotation axis, the so-called king pin. The distance from the king pin to the stern of the Sleipnir is equal to 15 meters. As the crane radius increases, the maximum lift height decreases, and the hook load capacity decreases for a crane radius in excess of 48 meters. The lift capacity of the main hoist as a function of the crane radius is plotted in figure 2.8.

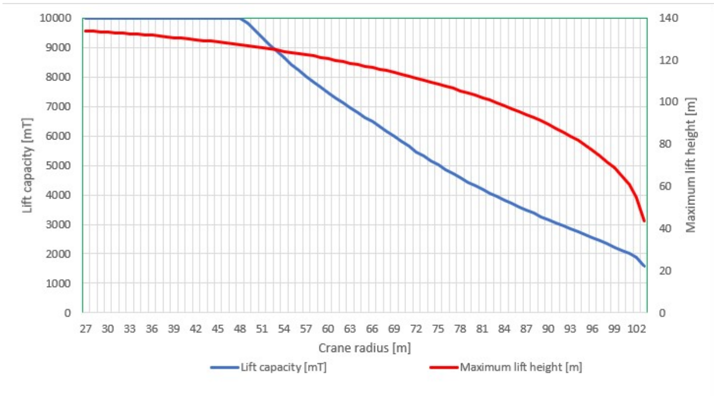

Figure 2.8: Sleipnir load curve main hoist

It is examined whether sufficient clearance can be maintained for the removal of the selected topsides. For the heaviest topsides in the range it is expected that the factored assembly weight will reach the maximum single crane capacity of 10,000 mT. To assess this, reference topsides 4 and 7 are used as the governing cases because of their size and weight. The maximum lift height is adjusted for a vessel draught of 20 meters, taking 10 meters clearance with the seabed into account. The maximum crane radius and lift height are indicated in figure 2.9.

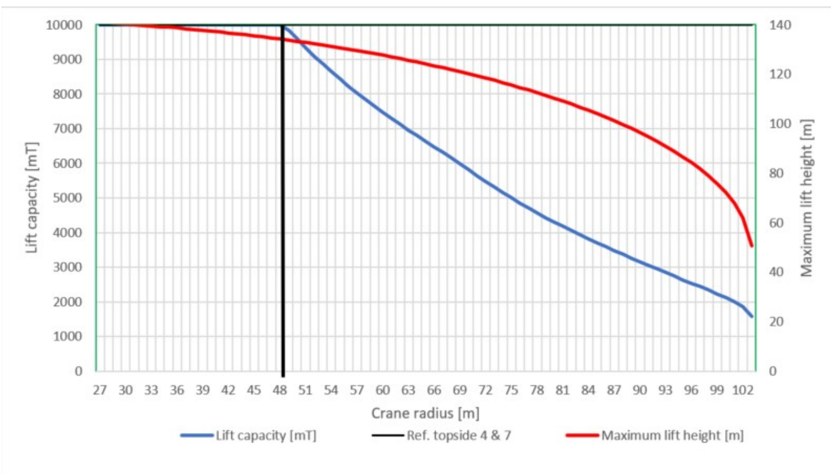

Figure 2.9: Sleipnir load curve main hoist for reference topside

Based on the maximum factored assembly weight of 10,000 mT, a maximum crane radius and a corresponding maximum lift height can be defined.

$$R_{max,topsides4/7} = 48m$$

$$H_{hook,max} = 141m$$

The minimum crane radius is determined by the clearance criteria discussed in section 2.2.1. Hereby, it is assumed that the main hook is positioned above the geometrical center of the topsides. The presence of the lift beams also has to be taken into account. The length of the lift beams is equal to 50 meters, and is determined by the maximum topside width, taking 2 meters of clearance on both sides into account. The reasoning for the clearances is further discussed in section 3.1.1. An impression of the governing lift cases is provided in figure 2.10.

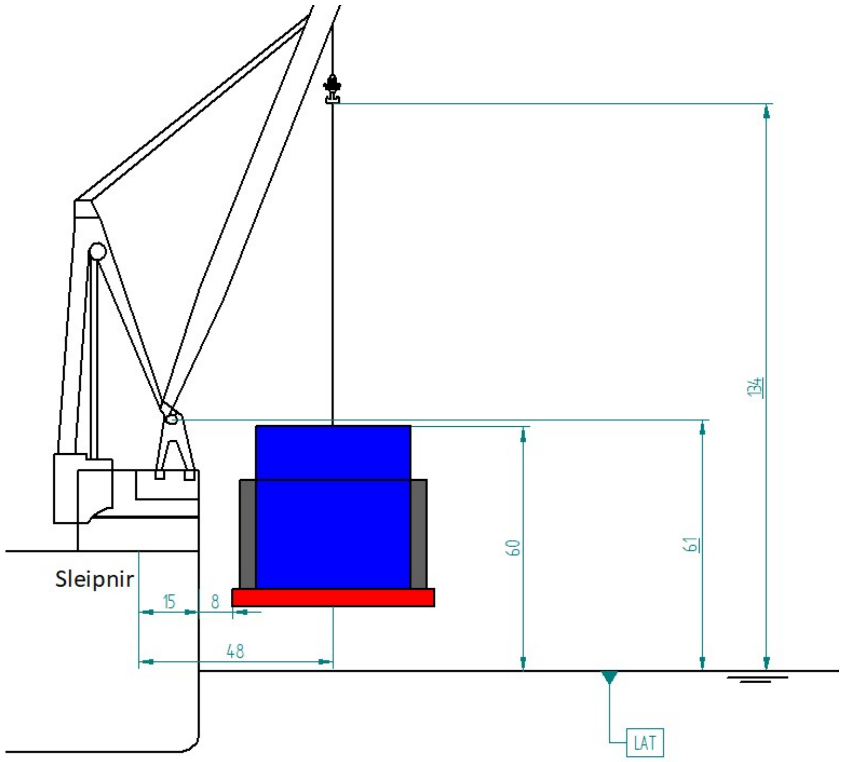

Figure 2.10: Governing lift cases with the Sleipnir, with reference topside 4 (blue) and reference topside 7 (grey)

The elevation of the boom's hinge point at a draught of 20 meters is equal to 61 meters with respect to the LAT. This is higher than the topsides' maximum elevation, and therefore sufficient clearance between the crane boom and topside is ensured. In this case the clearance between the vessel and the topside becomes governing. Looking at figure 2.10, the governing clearance criterion can be formulated as following:

$$\frac{W_{topside,max}}{2} + 2 + C_{vessel-topside} \leq R_{max} - 15 \text{ , where } C_{vessel-topside} \geq 5m$$

It can be seen that this criterion is satisfied, since 8 meters of clearance can be maintained between the Sleipnir and the lift object.

The required hook elevation follows from the elevation of the topsides and the height of the upper rigging. Hereby, additional clearances between the topside and the likely to-be-used spreader bar have to be taken into account. Based on offshore experiences, it has been advised to take a minimum clearance of 8 meters. An impression of this is shown in figure 2.11.

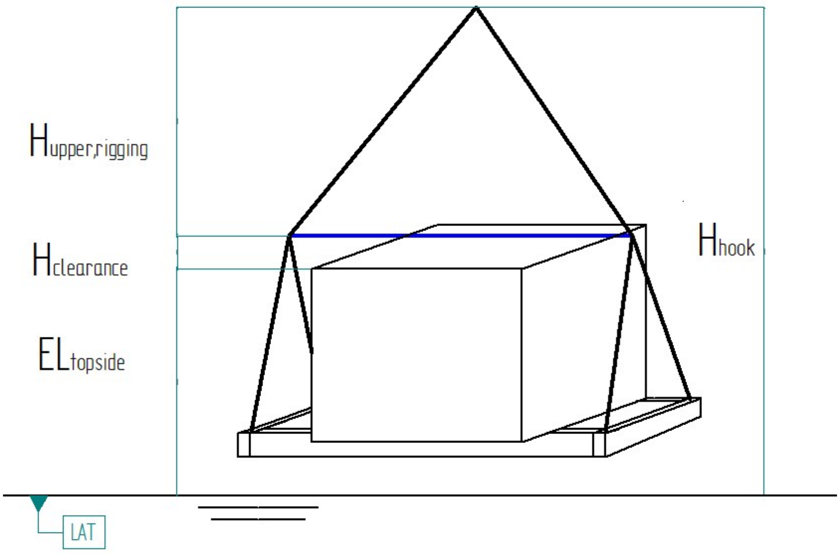

Figure 2.11: Required hook elevation

The height of the upper rigging is driven by the length of the spreader bar, which is approximately equal to the length of the lift beams. The angle of the slings should ideally lie between 60 and 75 degrees [35]. For angles below 60 degrees, it is considered that the horizontal component of the sling force becomes too large. Angles above 75 degrees are ideally prevented because of the resulting large hook height. Taking reference topside 4 as the governing case, this comes down to a minimum required hook elevation of:

$$H_{hook,min} \approx EL_{topside} + 8 + \tan(\alpha_{min}) * \frac{L_{beam}}{2} = 60 + 8 + tan(60) * 25 = 111m$$

It can be seen that the maximum lift height of 141 meters, with respect to the LAT, exceeds the minimum required hook height. Therefore no lift height restrictions are expected during topsides removal using the lift beams.

2.3.2. Hydrostatic stability

The water depth of the topsides' locations ranges from 26 meters to 36 meters, as shown in table 2.2. The clearance between the vessel's keel and the seabed must be at a minimum of 10 meters.
This means that the draught of the SSCV is limited to 16 meters in the shallowest case. The regular operating draught of the Sleipnir is between 27 and 32 meters. Lifting at a lower draught is possible, but is less stable than at the regular operating draught. The hydrostatic stability of the Sleipnir therefore needs to be assessed.

The Sleipnir has to satisfy the intact and damage stability criteria that are stated by the NMA, the IMO Modu code and HMC in the Sleipnir Stability Booklet. These stability criteria can be expressed in a maximum allowable VCG, which depends on the type of lift operation and the SSCV draught [23]. For the lift beams topsides removal concept, load cases 17, 18 and 19 in the Sleipnir stability booklet are of interest. These load cases represent a single lift over the bow of the SSCV.

Stability of the vessel can be ensured by adjusting the water content in the ballasting compartments of the SSCV. In-house sheet SSCV Ballast is used for this purpose. In this sheet, the aforementioned stability criteria are assessed as well. Excessive heeling of the SSCV is avoided by ensuring that the transverse component of the centre of gravity coincides with the transverse component of the centre of buoyancy. Similarly, trimming of the vessel is avoided by coinciding the longitudinal components. The Sleipnir's hydrostatic stability is assessed for removal of reference topsides 4, which is considered to be governing due to its weight and the water depth at this location. The maximum allowable crane radius and corresponding hook elevation for reference topside 4 are used as input. A slew angle of 180 degrees is taken.

It is found that the vessel can lift the governing topside at the required draught of 20 meters, while satisfying the stability and damage criteria. Under the setup, the VCG is found to be 37.7 meters, which is within limits for this operation. The heel angle and the trim angle are equal to 0.00 degrees under the given setup. An extract of the SSCV ballast sheet for the governing load case is provided in Appendix A.

2.4. Overview of single lift removal methods for modular topsides

In the past years, several types of single lift removal methods have been developed and executed for modular topsides. The characteristics and working principle of each method are briefly discussed in this section.

Pioneering Spirit

The best known example of single lift topsides removal is provided by SLV Pioneering Spirit, owned by competitor Allseas. The vessel has the capability to lift topsides with a weight of up to 48.000 mT. The size of the vessel and its active motion compensation system, allow the vessel to perform the lift operations in rough sea states [1]. Figure 2.12 shows the record-breaking removal of the Brent Delta topsides by the Pioneering Spirit.

Figure 2.12: Pioneering Spirit after lifting the Brent Delta topside [5]

The vessel is equipped with a Topsides Lifting System (TLS) consisting of sixteen large beams, which are paired into eight fork-lift units [25]. The TLS beams' ends contain lifting yokes, which are used to connect to the topsides' lift points. Lifting is provided by a combination of the yokes' hydraulically-actuated upward thrust and deballasting of the SLV [25].

Safe single lift removal of the modular topsides has shown to require extensive engineering and preparation. For removal of the GBS-supported Brent Delta and Brent Bravo topsides, under-deck lift points were created. For the Brent Delta platform, 140-tonnes-weighting steel lift points were used. The installation of these lift points and the required deck strengthening has shown to be very challenging and time consuming. For removal of the Brent Bravo topside, concrete lift points were used instead, which were created from the interior of the topside. This way it was aimed to reduce the under-deck preparatory work. In removing the jacket-supported Brent Alpha topside, the MSF legs were used as lift points. The legs required extensive strengthening to withstand the compression loads that the yokes exerted [25].

Versatruss
In 1996, the Versatruss concept was introduced by the company Versabar for the removal, installation and transportation of topsides [11]. Two standard barges are positioned along the length of the topside. The barges are equipped with three A-frame steel booms and hydraulic winches, providing a lift capacity of 7500 mT [16]. An impression of the Versatruss system is shown in figure 2.13.

Figure 2.13: The Versatruss lift system installing a topside [**?**]

The tip of the booms is connected to pre-installed pins, which are mounted on the platform's deck structure. The booms are allowed to rotate around their support point on the barge. Hydraulic winches are connected to the topsides' MSF legs, and pull the barges together. The angle of the booms increases this way, which results in an upward lift force. The working principle of the Versatruss system is illustrated in figure 2.14.

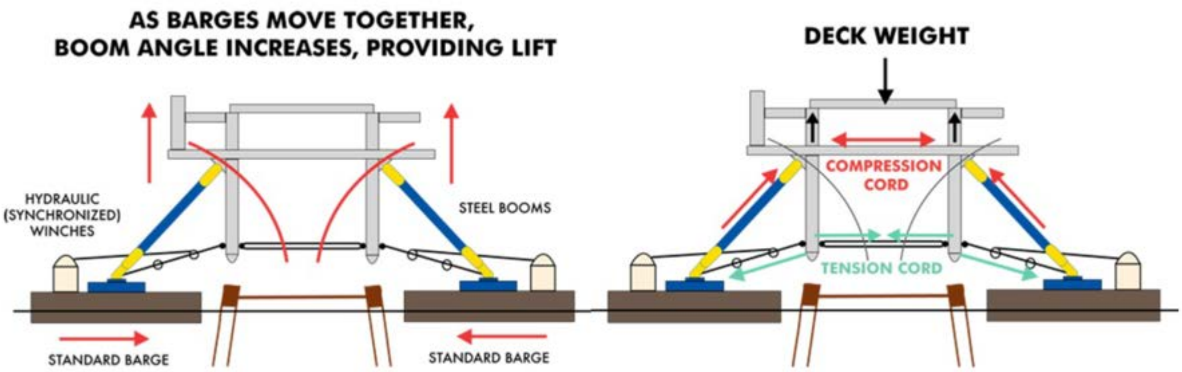

Figure 2.14: The Versatruss working principle [**?**]

The lifting capacity of the system could be improved by applying more booms, hence increasing the size of the barges. An advantage of this system is the relatively small preparation scope. Besides, lifting can be performed in very shallow water depths. One of the disadvantages of the Versatruss system is the poor wave response behaviour of the barges. It is therefore considered that this lift system is only applicable in relatively calm sea states.

VB10000
Another single lift topsides removal concept developed by Versabar is the VB10000. The VB10000 is a truss-type gantry crane which is mounted on two barges and has a lift capacity of 7500 mT [9]. The VB10000 is positioned above the topside, and the topside is removed in a single lift by means of hoisting. In case of an integrated topside, the topside is simply lifted by its lift points. For modular topsides, single lift removal is achieved by making use of a new lift device, named the Claw. An impression of this is provided in figure 2.15.

Figure 2.15: Modular topside removal using the Claw [8]

The claw consists of two 1100-tonnes-weighting steel jaws, which grab the topside below its MSF deck. The jaws are operated independently, but can be used in tandem for greater lift loads [**?**]. After lifting off its substructure, the topside is placed on a barge for transportation.

Petrodec skidding
In 2020, decommissioning specialist Petrodec has removed the Pickerill A and Pickerill B topsides with the Energy Endeavour jack-up rig. Topsides removal is achieved in a single operation by skidding the topsides onto the jack-up's deck. Figure 2.15 shows the Energy Endeavour being towed to shore after removing the Pickerill A topsides.

Figure 2.16: The Energy Endeavour towed to shore after topside removal [**?**]

First the jack-up hull is lowered, and skid beams are skidded onto temporary supports, which are installed on the topsides' MSF legs. These skid beams are then connected to skid beams which are positioned on deck of the jack-up. The topside is cut free from its substructure, and is subsequently elevated with the use hydraulic jacks, which are equipped on top of the skid shoes. Finally the topside is skidded on deck of the jack-up and is towed to shore. This removal concept is characterised by its weather robustness, as the jack-up is elevated above the waterline.

2.5. Efficient lift beam design

Different possibilities for the lift beams regarding the type of beam, the beam profile and the material type are discussed in this section. Considering the full range of possibilities will allow to come up with an efficient lift beam design.

2.5.1. Beam type

A distinction is made between a truss and a steel plated beam. Trusses are frequently used as a weight-efficient solution for large span support structures. A truss is a transparent structure, built up of multiple, often cylindrical, members. The members form triangular shapes, which provide the truss' global stiffness [32]. The members are connected to one another through joints. Different types of trusses can be identified based on the configuration of the inner members. An overview of the most commonly applied truss structures is provided in figure 2.17.

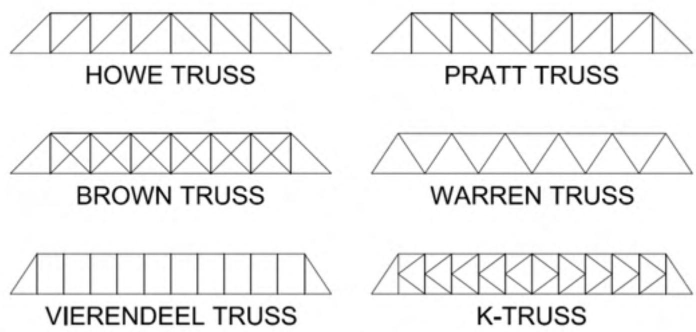

Figure 2.17: Most commonly applied truss variations [18]

The members are designed for axial loading only. The forces that are acting on the truss therefore have to be introduced at the joints. The force then travels through the vertical and diagonal members to the supports of the truss. Global moments that are acting on the truss are decoupled in axial loads acting on the members. A truss structure could be used for the lift beams to minimize the lift beam's weight. However the fabrication costs are expected to be significantly higher. The discrete load introduction for trusses could also introduce some practical challenges.

Steel plated beams, on the other hand, are continuous structures with a cross-sectional profile. The cross-sectional profile is created by welding different steel plate sections together. Since the structure is continuous, no restrictions are applied to the load introduction. Steel plated beams can therefore take up forces and moments in any direction at any location along its length. The resulting stresses are distributed over the cross-section, and travel along the length of the beam to the supports.

A variation on steel plated beams are tapered beams, which have a varying cross-section along their length. Tapered beams are mostly applied for large spans, where bending is the governing loading type. The cross-sectional properties gradually increase to the point where the largest bending moment is expected. An impression of a tapered beam is provided in figure 2.13.

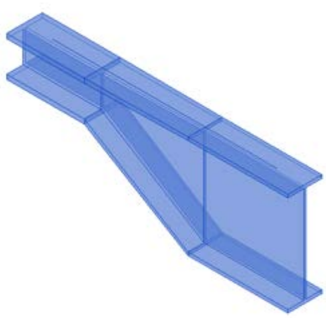

Figure 2.18: Tapered I-profile beam [22]

2.5.2. Beam profile

Truss structures are predominantly built up of tubular members. Tubular cross-sections are relatively easy to fabricate and have favorable axial and torsional properties. Since the cross-section is symmetric along all axes, no peak stresses are expected across the profile. The shear and bending properties of tubular members are however less favorable.

For steel plated beams subject to bending, I-profiles are most commonly applied. An I-profile can be proportioned for optimum bending properties around its major axis [30]. However, if the load is introduced eccentrically with respect to the cross-section's shear center, torsion is additionally introduced to the beam. The torsional shear stresses in open sections, such as an I-profile, work in opposite directions at opposite faces, resulting in significantly lower torsional resistance [30]. For closed cross-sections, the torsional shear stresses flow in the same direction, which results in much greater torsional resistance. The torsional shear stress flow for open and closed cross-sections is illustrated in figure 2.14.

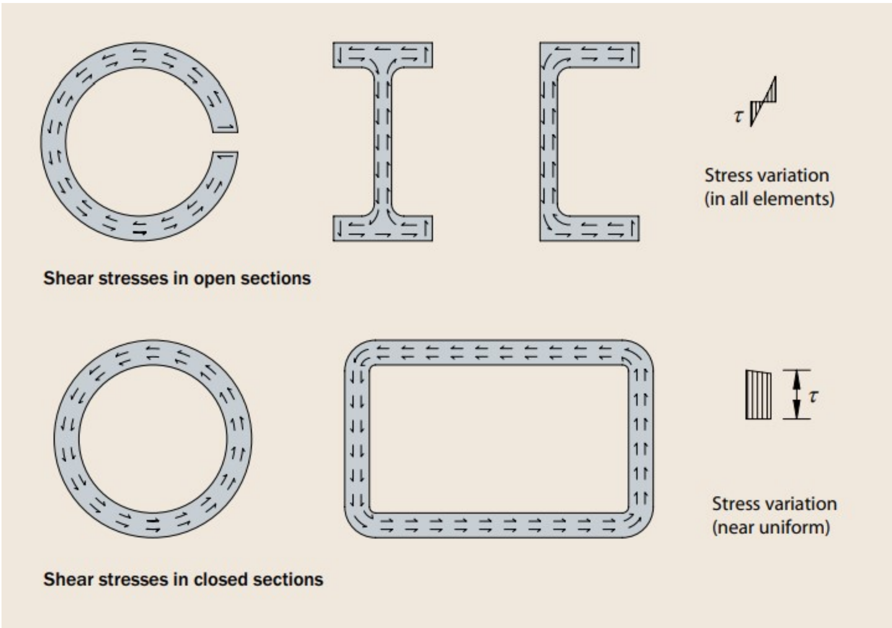

Figure 2.19: Torsional shear stress flow [30]

If the torsional shear stresses show to be significant, a closed cross-section might be preferred. A box-profile for instance is found to be torsionally very stiff [39], while also providing good bending properties around its major axis.

2.5.3. Steel grades

The materials that are considered for the lift beams are mild steel type S355 and high strength steel types S460 and S690. Important criteria for the steel grades are the yield strength, weldability, ductility, material toughness and fatigue behaviour.

The application of high strength steel allows for lighter, more slender structures. The price per kilogram of steel however increases as the yield strength of the material increases. It has to be noted that the specified yield strength decreases with an increasing material thickness. The yield strength reduction is applied to account for the effects of lower weldability for thicker materials [44].

The weldability of a steeltype strongly depends on its hardenability. Greater quantities of carbon and other alloying elements result in a higher hardenability and thus a lower weldability [44]. Higher strength steel types are therefore also less suitable for heat treatment.
The ductility of a material indicates the amount of plastic strain and plastic capacity before material failure. Ductility is therefore considered to be an important property, since it is necessary to prevent brittle failure. It can be noted that the ductility decreases as the yield strength of the material increases. In figure 2.15 the stress-strain curves of S355 and S690 steel are shown.

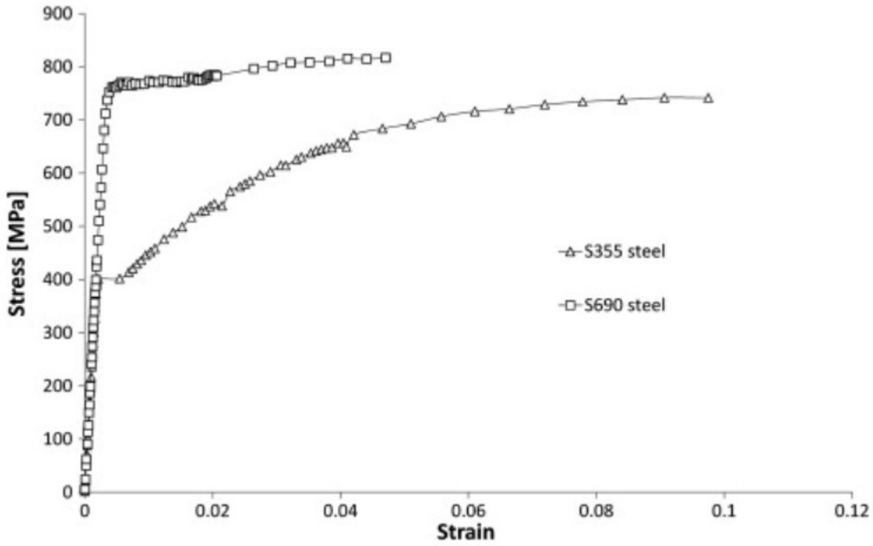

Figure 2.20: Stress-strain curve for S355 and S690 steel[31]

Looking at the stress-strain curve for S355, a clear yield plateau can be observed. The material also shows significant strain hardening after yielding. This type of behaviour can't be observed for S690 steel. It can be seen that there is minimal contingency after yielding, with brittle failure likely to occur. A minimum required ductility can be specified for which brittle failure won't occur. This value is mainly governed by the ratio between the ultimate tensile strength and the yield strength of the material. It has been found that steel grades up to S460 steel satisfy this criterion.

The modulus of resilience is used to indicate the material's resistance to deformations resulting from impact loading [36]. The modulus of resilience is a function of the material's yield strength and Young's modulus, as shown in equation 2.1.

$$u = \frac{\sigma_y^2}{2E} \tag{2.1}$$

It can be seen that the material's impact toughness increases as its steel grade increases.

Regarding the fatigue behaviour, it can be stated that lower steel grades show better fatigue behaviour for low-cycle fatigue regimes [31]. Lower steel grades show less resistance against crack initiation. However their resistance against crack propagation is found to be larger than that of higher steel grades.

2.5.4. Cross-sectional design

An efficient beam design should meet a set of general requirements, while minimizing its weight [36]. The requirements are listed below.

- The cross-section must have sufficient strength, which is quantified by its section modulus
- The cross-section must have sufficient stiffness, which is measured by its moment of inertia
- The web area must be great enough to carry the expected shear forces
- The cross-sectional design must withstand the occurrence of web buckling

The section modulus and moment of inertia provide resistance against bending of the beam, and are mostly driven by the height of the cross-section and the thickness of the flanges. These properties could be improved by applying longitudinal stiffeners along critical sections of the beam.

The web area is a product of the web height, d_w and the web thickness, t_w. The allowable shear stress in the web is governed by the occurrence of web buckling, which is related to the web slenderness, $K = \frac{d_w}{t_w}$ [36]. The allowable web slenderness is related to the yield strength of the material and the application of stiffeners. The stiffeners provide support to the web plates, hence increasing the critical web buckling stress. The use of stiffeners will therefore allow for more slender web design. Table 1 provides an overview of the limiting web slenderness ratio's. The values are based on plate girders, which are greatly used in the design of (long span) bridges.

TABLE 1—Limiting Ratios of Web Depth to Thickness

$$K = \frac{d_w}{t_w} = \frac{\text{web depth}}{\text{web thickness}}$$

AASHO (Bridges)

	Mild Steel A373, A36	Low Alloy Steel A441 or Weldable A242 46,000 psi yield	Low Alloy Steel A441 or Weldable A242 50,000 psi yield
No transverse stiffeners (1.6.80)	$K \leqq 60$	$K \leqq 52$	$K \leqq 50$
Transverse stiffeners (1.6.75)	$K \leqq 170$	$K \leqq 145$	$K \leqq 140$
Longitudinal stiffener with transverse stiffeners (1.6.75)	$K \leqq 340$	$K \leqq 290$	$K \leqq 280$

Figure 2.21: Web slenderness limits [36]

It can be seen that proper application of stiffeners will allow for more slender cross-sectional profiles. Approaching the slenderness limits is an essential step in minimizing the weight of the beam. It has to be noted that the limits provided in figure 2.16 are purely based on shear and bending.

3
Design and optimisation of the lift beams

In this chapter the design process of the lift beams is shown. The design of the lift beams meets the one-size-fits-all principle to comply with the complete range of topsides under consideration. Criteria for the size, strength and weight of the lift beams are obtained from the topsides analysis. Local design of the lift beams is dependant on the lift beam-to-topsides connection, and will therefore be discussed in Chapter 5. The structural requirements of the lift beams are based on the governing load case. For the lift beam design it is assumed that the lift beams are connected to the MSF legs. Here, a distinction is made between one-sided leg support and two-sided leg support. The required type of support is mainly driven by the topsides structural integrity, which is discussed in Chapter 4.

3.1. Design requirements

3.1.1. Dimensional requirements

In determining the maximum allowable dimensions of the lift beams, it is assumed that lift beams will have to be installed in the interface between the MSF deck and the jacket top horizontal elevation. The available space for the lift beams in this interface is limited, and it is therefore essential that clearances are taken into account for the dimensions of the lift beams. These clearances account for motions of the lift beams during installation, the presence of connection elements and installation offsets. For the height of the lift beams, a clearance of two meters is taken into account between the top of the lift beam, and the MSF deck. For the width and length of the lift beams, a clearance of two meters is considered on both sides of the lift beams. Further elaboration on the dimensional requirements, including corresponding drawings, is provided in Appendix B.1. The dimensional requirements for the lift beams are shown in table 3.1.

H_{max}	=	4.35	[m]
B_{max}	=	3.65	[m]
L_{min}	=	50.00	[m]

Table 3.1: Dimensional requirements for the lift beams

3.1.2. Structural requirements

The lift beams need to have sufficient structural capacity to withstand the maximum expected loads during lifting of the topsides under consideration. Based on the governing load case, which is further discussed in section 3.2, the structural capacity of the lift beams can be assessed. Assessment is based on the API WSD, which is commonly used for temporary offshore steel structures. The design codes are based on design within the elastic regime of the material. The stresses acting on the cross-section should be below the allowable stresses, which are is defined as a fraction of the yield strength of the material. The structural capacity of the lift beams is assessed in section 3.4.

3.1.3. Weight requirement

The factored weight of the lift beams-topsides assembly must lie within the maximum capacity of a Sleipnir single crane for a given crane radius. Based on the heaviest topsides in the batch, a maximum lift beam weight can be defined. The number of lift beams that are going to be used is unknown, and strongly depends on the connection between the lift beams and the topsides. Hereby, the topsides' structural integrity will play an important role. The use of more lift beams results in more support for the topsides. To obtain an estimate on the maximum lift beam weight, it is assumed that the lift beams are connected to the MSF legs. Here, a maximum lift beam weight can be defined for two cases: one-sided leg support and two-sided leg support.

$$W_{LB,max} = \frac{\frac{10000}{\mu_{DAF}*C_{rig}} - W_{topside} * \mu_{cont}}{n_{beams}} \tag{3.1}$$

Where:

μ_{DAF}	=	$\frac{DAF}{1.1}$ (= 1.0)	[-]
μ_{cont}	=	Contingency factor (= 1.1)	[-]
C_{rig}	=	Rigging weight factor (= 1.07)	[-]

the in-house standard code for single crane lift systems, it is suggested to take a contingency factor of 1.1 for the structural weight of the topside, and a rigging weight factor of 1.07 for rigging arrangements consisting of spreader bars [35]. The values for these factors are based on the early design phase and may be reduced at a later stage. In the topsides analysis it was found that the maximum topsides weight is provided by reference topsides 5, which has a dry weight of 6718 mT. The topsides is planned to be lifted over its width, parallel to four jacket leg rows. This implies that for one-sided leg support, four lift beams are planned to be used, and for two-sided leg support, eight lift beams. Substituting these values in equation (3.1), the maximum lift beam weights are found:

$$W_{LB,max} = 490[mT] \textit{ for one-sided leg support}$$

$$W_{LB,max} = 245[mT] \textit{ for two-sided leg support}$$

It has to be noted that for the maximum weight of the lift beams, the presence of potentially to-be-used cross-beams and connection elements is excluded. Especially the addition of cross-beams would significantly affect the maximum lift beam weight.

3.2. Governing load case

The strength requirements of the lift beams are based on the governing load case the lift beams are expected to be exposed to. The governing load case is a function of the topsides weight, the topsides CoG, the number of potential supports, or connection points, and the relative spacing of the supports. Hereby it is presumed that the MSF legs will be used as the connection points. It is found that the governing load case is caused by reference topsides 7 due to its weight and the number of supports and their relative spacing. Reference topsides 7 is depicted in figure 3.1.

Figure 3.1: Reference platform 7 [6]

The CoG of the topsides lies within the envelope of the MSF legs, since the topsides weight is transferred through these components. However due to a lack of data, the exact location of the topsides' CoG is unknown. For the design of the lift beams, it is assumed that the topsides' CoG has an offset of 10% with respect to the geometrical center of the MSF legs envelope. In practice, this value for the CoG offset is considered to be reasonable for modular topsides. The lift beams are presumably connected along the four jacket leg rows. Each lift beam is in this case supported at two points. With the lift beams being connected along four rows, the lift setup is statically undetermined and hence it is unknown how much of the topside weight is carried by the governing lift beam. If the load is equally distributed over the jacket rows, each row takes 25% of the topsides' weight. The inner jacket leg rows will most likely carry most of the topside load, due to the area that these rows cover. For the governing load case it is assumed that the inner jacket leg rows take twice as much of the topsides' weight compared to the outer rows. This implies that 33% of the topsides' weight is assumed to be carried by the governing lift beam.

3.2.1. Design lift loads

In determining the design lift loads, the total weight of the lift beams-topsides assembly is multiplied with a DAF and contingency factor. The DAF depends on the weight of the lift object, the surrounding environment, the lift vessel and the type of operation. The contingency factor accounts for uncertainty regarding the topsides weight and topsides CoG. For simplicity the maximum allowable lift beam weight for two-sided leg support is taken. The design lift loads can be updated, once the final weight of the lift beams has been determined. It is however expected that the differences will be relatively small.

DAF	=	1.1	[-]
μ_{cont}	=	1.1	[-]

Table 3.2: Factors used in determining the design lift loads

The load that is transferred per MSF leg to the lift beam is based on the position of the topsides' CoG in the direction of the lift beams. This load is modelled as a concentrated load acting on the edge of the lift beam, since it is most likely that the lift beams will be eccentrically loaded when connected to the MSF legs. The end-on sides of the lift beams are assumed to be pinned, because only forces can be transferred to the rigging. Figure 3.2 gives an impression of the load case that is considered for the design of the lift beams.

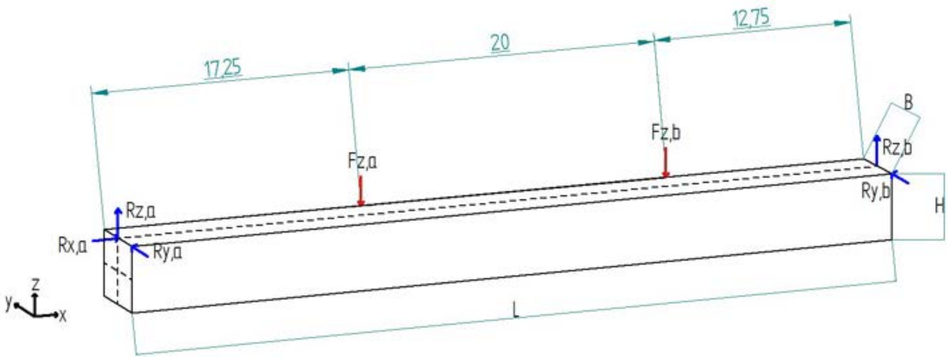

Figure 3.2: Loads acting on the lift beam

The vertical rigging loads $R_{z,a}$ and $R_{z,b}$ are first determined according to vertical force balance and momentum balance around the y-axis. Subsequently a SKL of 1.2 is applied such that the governing shear force-bending moment combination is obtained. The SKL takes the load distribution from the rigging arrangement into account, and is further discussed in chapter 4. The leg reaction forces $F_{z,a}$ and $F_{z,b}$ change accordingly due to this, which might have a significant effect on the structural integrity of the MSF legs. Additional side loads are assumed to act on the lift beam's ends, which take rigging misalignment and perpendicular dynamic loads into account [34].
A transverse side load is assumed to act on both lift beam ends.

$$R_{(y,a/b)\perp} = 0.05R_{z,a/b} \tag{3.2}$$

A longitudinal force is also taken into account, which is assumed to only act on one end.

$$R_{x,a\perp} = 0.05(R_{z,a} + R_{z,b}) \tag{3.3}$$

In case of two-sided leg support, an additional SKL of 1.1 is applied over adjacent lift beams. This implies that one of the lift beams takes 55% of the total leg loads. The SKL of 1.1 takes fabrication tolerances and friction over the spreader bar lift points into account. The governing rigging loads in case of one-sided and two-sided leg support are provided in table 3.3.

One lift beam per row			**Two lift beams per row**		
$R_{z,a}$	15669	[kN]	$R_{z,a}$	9782	[kN]
$R_{y,a}$	784	[kN]	$R_{y,a}$	489	[kN]
$R_{x,a}$	1319	[kN]	$R_{x,a}$	823	[kN]
$R_{z,b}$	10710	[kN]	$R_{z,b}$	6685	[kN]
$R_{y,b}$	536	[kN]	$R_{y,b}$	334	[kN]

Table 3.3: Overview of the design lift loads for one-sided leg support (left) and two-sided leg support (right)

The corresponding moments acting on the lift beam are determined with the following equations:

$$M_{x,max} = \frac{(R_{z,a} + R_{z,b})B}{2} + \frac{(R_{y,a} + R_{y,b})H}{2} \tag{3.4}$$

$$M_{y,max} = R_{z,a} * 17.25 + \frac{R_{x,a}H}{2} \tag{3.5}$$

$$M_{z,max} = R_{y,a} * 17.25 \tag{3.6}$$

3.3. Lift beam design selection

It is aimed to obtain a weight-efficient design for the lift beams, while satisfying the dimensional criteria and providing sufficient capacity to withstand the governing load case. In section 2.5 several options were proposed regarding the type of beam, the beam profile and the steel grade. The selection of these parameters is discussed in this section.

3.3.1. Beam type selection

It has been decided that for the lift beams it is most suitable to use a steel plated beam.
A tapered beam could provide a weight-efficient solution by narrowing the cross-section towards the lift beam's ends, where the moment decreases to zero. The location of the connection points and the maximum bending moment however varies for each topside. A tapered cross-section could therefore only be applied over a relatively short span. Taking the increased fabrication costs into account, this type of beam is considered to be unsuitable for the lift beams.
A truss was also considered as a potential weight-saving solution. Some practical challenges however would be introduced regarding the connection with the topsides. The load can only be introduced at discrete points, the joints, and the possibilities to house the connection elements are limited. Besides, the fabrication costs to weld the members together would be significant. An indicative design of the truss beam is determined to get an estimate on the potential weight saving. The design process of the truss is shown in Appendix B.2. It has to be noted that the vertical load is assumed to be equally spread over the truss planes, hence neglecting the effects of torsion. Also, no punching shear check has been performed. It is advised to account for these aspects in future consideration. Besides, the layout of the truss can be further improved.

Based on the indicative design, it was found that the lift beam weight reduces by roughly 12% compared to the steel plated beam. This doesn't weight up to the aforementioned disadvantages and hence it is decided to continue with a steel-plated beam.

3.3.2. Material selection

It has been decided to use S460 steel for the lift beams. This steel grade allows for slender structures, while providing ductile behaviour and impact toughness. The use of S355 steel would reduce the cost per kg of steel, however the size and weight of the lift beams would increase significantly. High steel grade S690 is considered to be unsuitable for the lift beams due to its brittle behaviour, once the material has started yielding, and its low weldability. The yield strength of steel grade S460NL, as a function of the material thickness, is provided in table 3.4.

Plate thickness [mm]	0-16	16-40	40-63	63-80	80-100	100-150
Yield stress [Mpa]	460	440	430	410	400	380

Table 3.4: Yield strength of S460NL steel as a function of material thickness

The Young's modulus of the material is independent of the steel grade or plate thickness, since the ductility is the same in the elastic region. The value for the Young's modulus is taken as; $E = 210GPa$.

3.3.3. Profile selection

The ideal lift beam profile strongly depends on the load transfer between the lift beams and topside. The exact load transfer is not known yet, but some preliminary assumptions can be made on the governing load types. Due to the large (free) span of the lift beams, it is likely that the global capacity of the lift beams is governed by bending stresses. The profile must therefore have great mass moment of inertia properties. Also, it is likely that the vertical load from the MSF legs is eccentrically introduced to the lift beams. The profile must therefore provide sufficient torsional resistance. Combining these criteria, it has been decided that a box-profile is most suitable for an efficient lift beam design. The profile is built up of plate thicknesses that are available for S460NL steel.

3.4. Global lift beam design

The lift beams are designed according to AISC 1989 WSD, which is commonly applied in the design of temporary steel offshore structures. The dimensional constraints and design loads, that have been discussed in the previous sections, are used as input for the design of the lift beams. Global phenomena such as bending, shear, torsion, buckling and lateral-torsional buckling are considered at this stage. The resulting stresses are classified as axial stresses, bending stresses and shear stresses. Each of these stresses must remain within the allowable limits. The combined effect of the stresses must be assessed as well. The maximum stresses in the cross-section are expected at either of the three critical points indicated in figure 3.3.

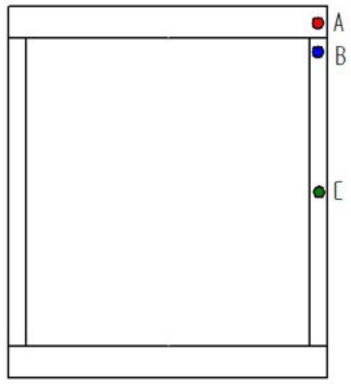

Figure 3.3: Critical cross-sectional points

Point A is located on the outer edge of of the compression flange. The maximum strong-axis and weak-axis bending stresses will occur at this point. The distance to the neutral axes of the cross-section is largest at this point. The combined effect of the compressive bending stresses and axial stresses is expected to be critical here.

Point B is located on the web, near the interface with the compression flange. Besides the aforementioned bending stresses, the vertical shear stress, which is carried by the webs of the cross-section, has to be taken into account. The combined effect of the axial stresses, bending stresses and shear stresses is expected to be critical at this point.

Point C lies on the horizontal neutral axis of the box-profile. The total shear stresses in the cross-section are expected to be largest at this point. The torsional shear stress is carried by the whole cross-section, but is expected to have a maximum in the webs because of the smaller expected thickness of these elements. The vertical shear stress, caused by the vertical rigging load, also has a maximum at the horizontal neutral axis of the box-profile.

Transverse intermediate stiffeners are applied over the length of the lift beam, which will increase the allowable shear stress in the cross-section. The spacing and design of the stiffeners is also elaborated in this chapter.

3.4.1. Cross-sectional properties

The magnitude of the stresses that will occur in the cross-section depends on the cross-sectional properties. The allowable stresses in each element of the cross-section depend on the element slenderness, its yield strength and whether the element is stiffened or not. Furthermore, it has to be noted that the height and width of the cross-section affect the moments that are acting on the cross-section, as described in section 3.2.1.

Element slenderness

The cross-sectional elements, i.e. the flanges and webs, are classified based on their slenderness. Three classes can be distinguished: $Compact(C)$, $Non-compact(NC)$ and $Slender(S)$. The allowable stress in the element depends on its slenderness class, and decreases as the slenderness of the element increases.

For compact sections subject to bending, the plastic moment capacity may be used, which is higher than the elastic moment capacity. The compact limit represents the slenderness limit at which the full plastic resistance can be attained. Slender members have a reduction in capacity because these members are prone to local buckling mechanisms.

The web slenderness is formulated as (h/t_w) , and the flange slenderness as (b/t_f). For stiffened elements h is the clear distance between the flanges and b is the clear distance between the webs. The web- and flange-slenderness limits are provided in Appendix B.3.

Stiffened elements

The allowable stresses are also dependant on whether the cross-sectional elements are stiffened. A distinction is made between closed cross-sections, which only contain stiffened elements, and open cross-sections, which can contain both stiffened and unstiffened elements. An element is considered to be stiffened when it is laterally supported on both edges. The elements of a box-profile can therefore all be considered as stiffened. The occurrence of local buckling mechanisms is more likely for unstiffened elements, because less support is provided for these elements.

3.4.2. Cross-sectional design

The cross-section of the lift beam is designed for the case of one-sided leg support and two-sided leg support. Both profiles satisfy the dimensional constraints that are set in section 3.1. It is aimed to minimize the cross-sectional area of the lift beams, in order to minimize the weight and costs of the lift beams. The cross-sectional properties must be sufficient to carry the stresses without yielding, hence satisfying the unity checks. The obtained thicknesses of the webs and flanges are rounded off to plate thicknesses that are available for S460NL steel. The optimized cross-section for one-sided leg support is provided in figure 3.4.

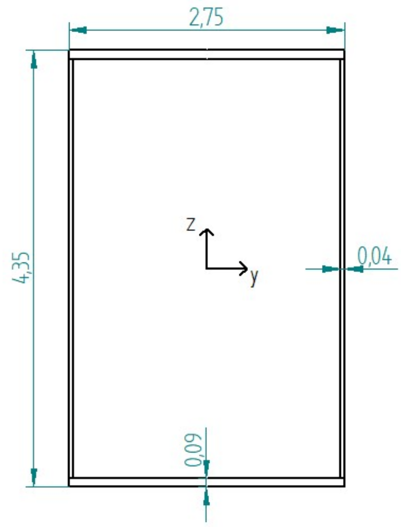

Figure 3.4: Lift beam box-profile dimensions for one-sided support

The cross-sectional properties for the one-sided support beam are given in table 3.5.

b/t_f	29.7	[-]
h/t_w	104.3	[-]
A	0.829	$[m^2]$
s	1.69	$[m]$
I_y	2.73	$[m^4]$
I_z	0.92	$[m^4]$
I_t	1.85	$[m^4]$
W_y	1.25	$[m^3]$
W_z	0.71	$[m^3]$
r_y	1.81	$[m]$
r_z	1.06	$[m]$
$F_{y,f}$	400	$[MPa]$
$F_{y,w}$	440	$[MPa]$
ρ_{st}	7.85	$[tn/m^3]$

Table 3.5: Cross-sectional properties of the box-profile for the one-sided support beam

The webs and flanges of the box-profile are identified as non-compact elements. The optimized cross-section for the two-sided leg support is provided in figure 3.5.

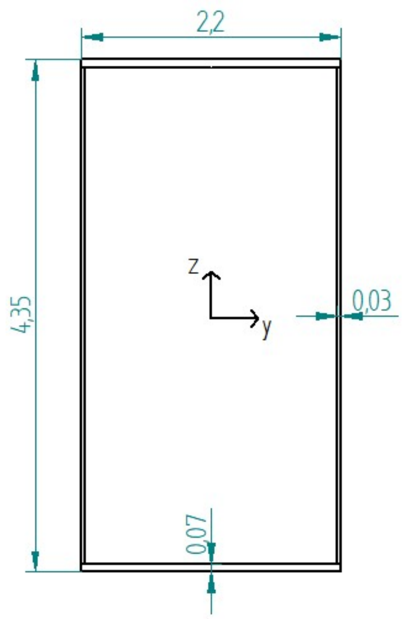

Figure 3.5: Lift beam box-profile dimensions for two-sided support

The cross-sectional properties for the two-sided support beam are provided in table 3.6.

b/t_f	30.9	[-]
h/t_w	140.3	[-]
A	0.563	$[m^2]$
s	1.65	$[m]$
I_y	1.80	$[m^4]$
I_z	0.43	$[m^4]$
I_t	1.01	$[m^4]$
W_y	0.83	$[m^3]$
W_z	0.39	$[m^3]$
r_y	1.79	$[m]$
r_z	0.87	$[m]$
$F_{y,f}$	410	$[MPa]$
$F_{y,w}$	440	$[MPa]$
ρ_{st}	7.85	$[tn/m^3]$

Table 3.6: Cross-sectional properties of the box-profile for the two-sided support beam

The cross-sectional elements for the two-sided support beam are classified as slender. Reduced cross-sectional properties are used in calculating the allowable stresses. This way the effects of potential local buckling are taken into account. For both cross-sections, the toe web radius, k, needed for welding the different plate sections together, is not included in the cross-sectional properties. In the allowable stress formula it is assumed that $k = t_w$.
Now that the dimensions of the lift beams are known, the moments acting on the cross-section can be determined. Table 3.7 provides an overview of the acting moments for one-sided leg support and two-sided leg support.

One lift beam per row			**Two lift beams per row**		
$M_{x,max}$	42437	[kNm]	$M_{x,max}$	19411	[kNm]
$M_{y,max}$	273159	[kNm]	$M_{y,max}$	170530	[kNm]
$M_{z,max}$	13515	[kNm]	$M_{z,max}$	8437	[kNm]

Table 3.7: Overview of the bending moments for one-sided support and two-sided support

3.4.3. Unity checks

The unity checks of the one-sided support beam and two-sided support beam are shown in this section. The cross-sections in figures 3.4 and 3.5, are designed to satisfy the unity checks and dimensional constraints for a minimum cross-sectional area. This is achieved by using a minimum solver for the function $A(H, B, t_w, t_f)$, and expressing the unity checks and dimensional constraints in terms of H, B, t_w and t_f. Derivation of the acting stresses and allowable stresses is provided in Appendix B.3.
The unity checks are assessed at the critical points in the cross-section, as indicated in figure 3.3. Calculation of the unity checks is also provided in Appendix B.3. The unity checks for the bending stresses, shear stresses, axial stresses and combined stresses is provided in table 3.8.

	One-sided support	**Two-sided support**
UC_b	1.00	0.95
UC_v	0.98	0.96
UC_a	0.01	0.01
UC_{b+a}	0.99	0.98
UC_{HUB}	0.99	0.93

Table 3.8: Overview of the unity checks for one-sided support beam and two-sided support beam

Except for the axial stresses, it can be seen that all unity checks are approaching the limit of 1.0. This implies that optimal use is made of the cross-sectional properties. For the two-sided support beam somewhat lower unity checks are found, which is mostly caused by rounding up the element thicknesses to available plate thicknesses.

3.4.4. Stiffeners

In this section the use of different types of stiffeners is discussed. It will be evaluated whether there is need for the type of stiffener. If so, its dimensions will be determined.

Intermediate transverse stiffeners

As discussed in Appendix B.3., the allowable web shear stress may be increased when intermediate transverse stiffeners are applied. It can be seen that the shorter the distance between stiffeners, a, the higher the allowable web shear stress. The web plate between two intermediate stiffeners can be imagined as an isolated plate. This plate is subject to horizontal shear stresses, caused by bending of the beam, and vertical shear stresses, caused by the vertical shear force and the torsional moment. The combination of these stresses results in a diagonal tension and compression force, as shown in figures 3.6 and 3.7.

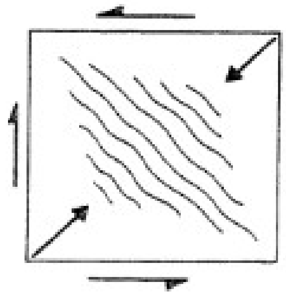

Figure 3.6: Compressive diagonal force due to horizontal and vertical shear

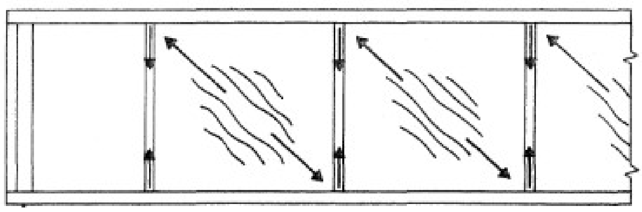

Figure 3.7: Tensile diagonal force due to horizontal and vertical shear

The compressive diagonal force could cause the plate to buckle. The plate won't fail in this case, since the bending stresses are carried by the flanges. The beam will instead act as a truss, where the web plate represents a tension diagonal which transfers the loads to compression struts, the transverse stiffeners [36].

The horizontal shear force is imposed to the web plate by the projecting flanges. The vertical shear force is imposed by the neighbouring web plates. Their resulting diagonal force is assumed to act under an angle of 45 degrees [36]. The stiffeners need to be designed to have sufficient capacity to withstand the vertical compression component of this force.

$$F_H = \frac{f_{b,y,max} * \frac{H}{2}}{2} * t_w \tag{3.7}$$

$$F_V = (f_{v,av} + f_{t,web}) * h * t_w \tag{3.8}$$

$$F_{Diag} = \sqrt{F_h^2 + F_V^2} \tag{3.9}$$

$$F_{c,st} = F_{Diag} * \cos 45 \tag{3.10}$$

$$A_{st} = \frac{F_{c,st}}{0.60 F_{y,st}} \tag{3.11}$$

The stiffener spacing, a, for one-sided support beam is taken at 3.75 meters and at 2.75 meters for the two-sided support beam. The spacing is taken such that the resulting shear unity check approaches 1.0.

$$a_{beam1} = 3.75[m]$$

$$a_{beam2} = 2.75[m]$$

The maximum allowable spacing criterion is also satisfied with these values.

$$a/h_w \leq \frac{260}{h_w/t_w} \leq 3.0$$

The governing case for the transverse stiffeners is taken at the location of the maximum bending moment of the beam, at $x = 17.25[m]$. The bending stress and hence the horizontal shear stress is largest here. The vertical shear force and torsional moment are constant over the panel width. An overview on the acting stresses and the governing plate panel are given in figures 3.8 and 3.9 respectively.

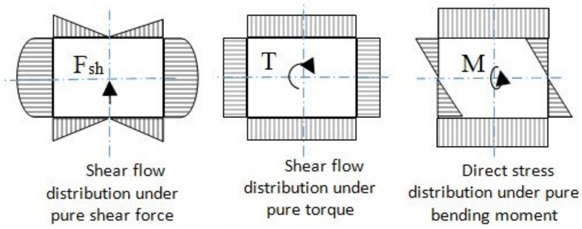

Figure 3.8: Stress distribution over the profile []

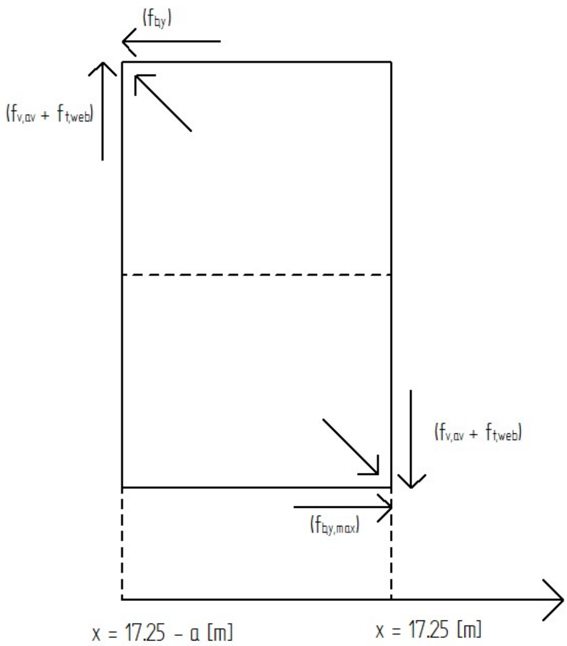

Figure 3.9: Governing panel []

For the one-sided support beam it is found that $F_{c,st,max1} = 13.9MN$, and for the two-sided support beam it is found that $F_{c,st,max2} = 9.1MN$. For the stiffeners the same yield strength is taken as for the web at 440 Mpa. It follows that $A_{st,1} = 0.052m^2$ and $A_{st,2} = 0.034m^2$. Here, A_{st} presents the required stiffener area per web plate.

Another way of determining the required stiffener area is by using the Bethlehem table, which can be found in Appendix B.3. In this table, the required stiffener area is expressed as a percentage of the total web area. Where necessary, the values from the table are interpolated. It is found that $A_{st,1} = 0.05 * A_{web,1} = 0.017m^2$ and $A_{st,2} = 0.06 * A_{cross,2} = 0.015m^2$. However, when a single plate is used as stiffener, the values have to be multiplied by a factor of 2.4 [36]. The final transverse stiffener area for the one-sided support beam and the two-sided support beam are equal to: $A_{st,1} = 2.4 * 0.017 = 0.04m^2$ and $A_{st,2} = 2.4 * 0.034 = 0.036m^2$.

The values are reasonably close to the values obtained from the first method. A possible reason for the relatively difference for the one-sided support beam is that the elements are not classified as slender. Also, the shear stresses due to torsion are not taken into account in the table. Eventually, the largest obtained area is used for the stiffeners.

The stiffeners are welded onto the compression flange and may be cut short from the tension flange over a distance of $4t_w$ [36]. This is allowed in case the stiffener is not used to directly bear a load. The stiffener area, A_{st}, is equal to $b_{st} * t_{st}$. The stiffener is applied over the whole interior width of the lift beam. It follows that:

$$t_{st,1} = \frac{0.052}{2.75 - 2 * 0.04} = 0.02m \tag{3.12}$$

And

$$t_{st,2} = \frac{0.036}{2.22 - 2 * 0.03} = 0.017m \tag{3.13}$$

The stiffener plate thickness for the two-sided support beam is rounded up to 0.02m.

For the one-sided support beam, a stiffener spacing of 3.75 meters allows for 12 intermediate transverse stiffeners. An end panel distance of 2.5 meters remains on either side. This end distance is within allowance.

$$a_{end,1} \leq \frac{11000 * t_{w,1}}{\sqrt{\tau_{max,1}}} = 3.6[m]$$

The total stiffener weight for the one-sided support beam equals:

$$W_{st,1} = 12 * (A_{st,1} * (H - 2 * t_{f,1} - 4 * t_{w,1})) * \rho_{st} = 20mT \tag{3.14}$$

The total weight for the one-sided support beam equals:

$$W_{beam,1} = A_{cross,1} * L * \rho_{st} + W_{st,1} + W_{extra,1} = 325.2 + 20 + 40 = 385.2mT \tag{3.15}$$

The extra weight is a preliminary assumption on the additional weight of the connection elements and other stiffener elements. For the two-sided support beam, a stiffener spacing of 2.75 meters allows for 17 intermediate transverse stiffeners. An end panel distance of 3 meters remains on either side. This end distance is also within allowance.

$$a_{end,2} \leq \frac{11000 * t_{w,2}}{\sqrt{\tau_{max,2}}} = 3.0[m]$$

The total stiffener weight for the two-sided support beam equals:

$$W_{st,2} = 17 * (A_{st,2} * \frac{0.02}{0.017}(H - 2 * t_{f,2} - 4 * t_{w,2})) * \rho_{st} = 23.1mT \tag{3.16}$$

The total weight for the two-sided support beam equals:

$$W_{beam,2} = A_{cross,2} * L * \rho_{st} + W_{st,2} + W_{extra,2} = 221.1 + 23.1 + 20 = 264.2mT \tag{3.17}$$

Plate buckling check
The transverse intermediate stiffeners are designed to have sufficient capacity to act as compression struts. This only applies when the critical buckling stress of the web plate is reached. It is therefore checked whether the web plate will buckle with the provided stiffener spacing. An in-house plating capacity sheet is used for this. The critical buckling stress is determined according to the Priest-Gilligan curve [36]. The extracts of the plating capacity sheets are provided in Appendix B.3.

For the one-sided support beam, it is found that the critical buckling stress,$\sigma_{cr,1}$ equals 65 MPa for a stiffener spacing of 3.75 meters. The acting shear stress is equal to 102.8 Mpa, implying that the web plate will buckle, and that the transverse stiffeners will be activated. For the two-sided support beam, a critical buckling stress of 68 MPa is found for a stiffener spacing of 2.75 meters, while the acting shear stress is equal to 86.4 Mpa.

Longitudinal stiffeners
Longitudinal stiffeners could be added to further reduce the dimensions of the isolated web plate and hence increase the critical buckling load. The presence of longitudinal stiffeners also improves the moment of inertia of the cross-section. For the lift beams, longitudinal stiffeners are considered to be unnecessary.

Local bearing stiffeners
Bearing stiffeners are implemented at select locations to provide extra bearing capacity for concentrated loads. Bearing stiffeners are used to prevent the occurrence of phenomena such as local web yielding, web crippling and sidesway web buckling. The need for local bearing stiffeners strongly depends on the interface between the lift beams and the topsides and will therefore be assessed in the connection concept phase. It is expected that single plate bearing stiffeners will be applied, which also have to be welded onto the tension flange. This way the load can be distributed over the entire cross-section.

3.5. Conclusions

- The lift beams are designed to withstand the governing load case, while complying with the dimensional criteria. The load case is modelled, presuming that the lift beams will be connected to the MSF legs. Two lift beam designs are provided; for one-sided leg support and for two-sided leg support.

- The lift beams are designed as steel-plated beams with a box profile, using high strength steel-grade S460NL.

- Design of the lift beams is based on global phenomena such as bending, shear, torsion and buckling. The cross-section of the lift beams is designed to satisfy the separate and combined unity checks of these phenomena.

- The design of the lift beams is optimised in order to minimise its weight and costs. The unity checks all approach a value of 1.0, implying that optimal use is made of the cross-sectional properties.

- Transverse intermediate stiffeners are applied over the length of the lift beams to allow for more slender webs and thereby reducing the total weight of the lift beams.

- The total lift beam weight for one-sided leg support is equal to 385 mT, which satisfies the weight criterion. For two-sided leg support, the total lift beam weight is equal to 264 mT, which exceeds the weight criterion. This implies that for the heaviest topsides in the batch, some weight has to be removed prior to the single lift.

4

Topsides structural integrity analysis

In the previous chapter, the lift beams have been designed to withstand the governing load case out of the topsides batch. Now the question arises whether the topsides can withstand it to be lifted by the lift beams. To assess this, a topsides structural integrity analysis is performed in SACS on reference topside 14. This is a widely applied software package to assess the structural response of offshore structures during installation, transportation and decommissioning. The results from this analysis will provide insight on whether the lift beams concept is structurally feasible and if so, under which conditions. A variety of models is analysed to understand how the load is transferred from the lift beams to the topsides and which parameters mostly influence this load transfer. This will provide important input on how to connect the lift beams to the topsides. The results of each model are analysed, and an assessment is made on the optimal lift beams setup for topsides removal.

4.1. SACS models

A variety of models is analysed, which differ in connection location, connection type, lift beams configuration and rigging load distribution. The results from these models are compared with one another to understand the influence of different parameters to the topsides' response during lifting.
A SACS model of reference topsides 14 was available to perform the analyses on.

Figure 4.1: Reference topsides 14 in-situ [3]

For this topsides definitive conclusions can be drawn on the ideal removal set-up, regarding its structural integrity during lifting. Also for the other topsides in the batch, this analysis will provide essential input on the topsides' response when lifted by the lift beams. However, as each topsides differs in size, strength and lay-out, it is advised to perform additional analyses to assess the structural integrity of the other topsides.

4.1.1. Connection location

Potential locations for the connection between the lift beams and the topsides are the topsides' strong points. The topsides strong points that have been identified are the MSF legs and the MSF deck. The members at these locations are considered to have sufficient capacity to take up the loads during lifting.

MSF legs

The MSF legs are evident strong points of the topside. In-situ, the topsides weight is transferred through the MSF legs to the jacket substructure. The number of MSF legs and their relative spacing differs for each topsides. These variables strongly determine the load case that is imposed to the lift beams and the topside. Also the possible lift beam configurations are influenced by this.
Reference topside 14 has four MSF legs, which are referred to as $PB10$, $PB50$, $PE10$ and $PE50$. The spacing between row 1 and 5 equals 18 meters and between row B and E 19.5 meters. An overview of the MSF legs is provided in figure 4.2.

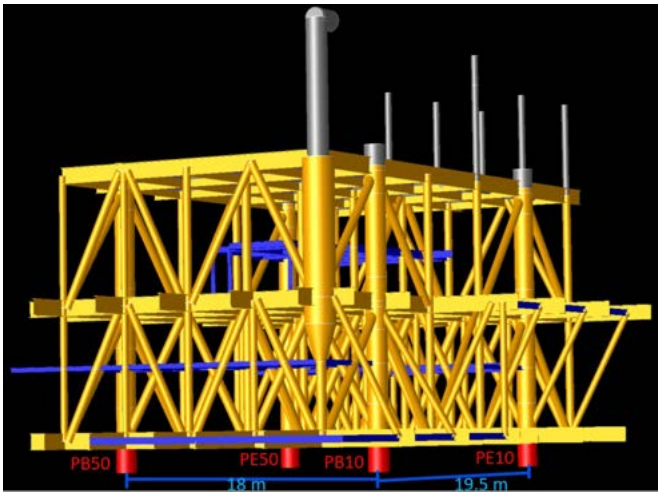

Figure 4.2: Overview MSF legs, reference topside 14

MSF deck

The lift beams could also lift the topsides by the MSF deck. The lift beams are connected to the rows containing the topsides' primary columns. In-situ the primary columns transfer the topsides load to the MSF legs and are therefore expected to have sufficient capacity to carry the lift loads. It is hereby important that sufficient columns participate in carrying the loads during lifting. The lift beams could potentially be connected to 24 columns. The large number of connection points will result in a good load spread, which is considered to be favorable for the structural integrity of both the topsides and the lift beams. The columns however differ in strength and consequently their structural properties should carefully be checked. The potential columns for connection are indicated in figure 4.3

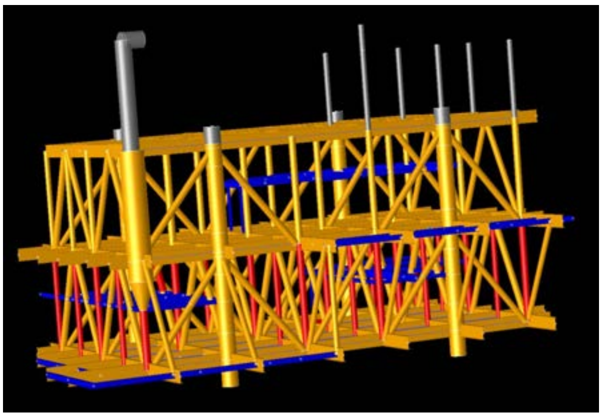

Figure 4.3: Potential columns for connection, reference topside 14

4.1.2. Connection type

The type of connection that is modelled in SACS depends on the connection location. For the MSF legs a fully pinned and fully clamped connection with the lift beams is initially considered. For the MSF deck an axial connection between the primary columns and the lift beams is modelled.

Pinned connection

For a pinned connection only forces are transferred between the lift beams and the topside. The lift beam is free to rotate with respect to the MSF leg, hence no resisting moments are introduced in the MSF legs. This is expected to be beneficial for the topsides' structural integrity, since the bending moments are completely taken by the lift beams. The lift beams will most likely be eccentrically loaded by the MSF legs, which results in twist of the lift beams. It is important that this rotation is restrained to ensure stability during lifting.

Clamped connection

The other MSF leg connection that is considered is a fully clamped connection. All relative displacements and rotations between the lift beams and the MSF legs are restrained in this case. This implies that both forces and moments are transferred to the MSF legs. It has to be examined how much of the leg capacity is taken by the resisting moments that are introduced with this connection type.

Axial connection

For the interaction between the lift beams and the primary columns, it is assumed that only axial compression forces are transferred between the elements. In reality also lateral loads due to friction are expected to be transferred. These loads are however considered to be negligibly small compared to the vertical load.

The interior columns will take up less of the vertical load in order to obtain momentum balance. Also after initial contact, the lift beam will deflect and contact with the interior primary columns can get lost. In order to properly activate the interior columns, shim plates are planned to be used at the interface with the exterior columns. The shim plates ensure that loads are only transferred after a specific displacement of the lift beam. This will result in more load transfer with the interior columns, and hence a better load spread. Lateral movements of the lift beams, due to wind loads or any type of side load should be limited, since this motion is unrestrained for this connection type.

4.1.3. Lift beam configuration

Several different lift beam configurations can be thought of, depending on the connection location and connection type. Each lift beam configuration imposes a different load case to the topsides. Varying the lift beam configuration will allow to analyse the influence of different design parameters on the load transfer between the lift beams and the topsides. The configurations are defined by the number of lift beams, the presence of cross-beams and the orientation of the lift beams. It should be noted that the total lift load increases when the number of components increases.

Number of lift beams

The MSF legs can be supported from one side or from both sides. It is likely that the MSF legs are loaded in a more favorable way when supported from both sides. The MSF legs will be loaded in a less eccentric manner this way, hence reducing the weak-axis bending moment of the MSF legs. For the MSF deck connection, the number of lift beams depends on the lift beam orientation. The use of more lift beams will result in a better load spread for both the lift beams and the topsides.

Cross-beam

A cross-beam could be added to the lift beams' ends for multiple reasons. When a pinned connection is used, a cross-beam will resist the aforementioned twisting of the lift beams. Also, any lateral loads during lifting are expected to be taken by the cross-beams. The addition of cross-beams will make the lift setup statically undetermined, which means that the load will be redistributed over the connection points. The stiffer load path will take up a larger portion of the load in this case. To ensure proper functioning of the cross-beams, it is essential that a rigid connection is realized between the lift beams and the cross-beams. There are also more options regarding the position of the lift points. It is expected that aligning the lift points with the connection points will have a positive influence on the topsides structural integrity. It has to be noted that the installation of the cross-beams might prove to be a challenging operation.

Lift beam orientation

Finally two possible orientations for the lift beams can be considered. The orientation of the lift beams determines the location of the rigging loads with respect to the connection points. The distance from the rigging loads to the connection points will influence the magnitude of the loads that are introduced to the topsides. Also, when the topsides is lifted off its equilibrium, a global moment is introduced to the assembly. The distance of the rigging loads to the topsides' CoG will therefore influence the global stability of the lift assembly.

4.1.4. Rigging load distribution

Different rigging arrangements can be thought of to lift the topsides with the lift beams. The rigging arrangement imposes a load case which lifts the topsides off its equilibrium. The deviation of the rigging load case with respect to the equilibrium load case is expressed in a SKL. Depending on the rigging arrangement a different SKL can be defined. The choice in rigging arrangement therefore influences the loads that are introduced to the lift object.

For a regular four-point lift, without spreader bars, a rigging load distribution of 75%-25% over any lift point diagonal can be assumed [35]. This rigging load distribution therefore represents a SKL of 1.5. For rigging arrangements consisting of floating spreader bars, a lower SKL may be assumed. Floating spreader bars are allowed to move to an equilibrium position without restraints, resulting in a load distribution which is closer to the equilibrium load case. Also, floating spreader bars are needed to prevent the slings from clashing with the topsides. Three possible rigging arrangements are identified for the lift beams concept, which are shown in figure 4.4.

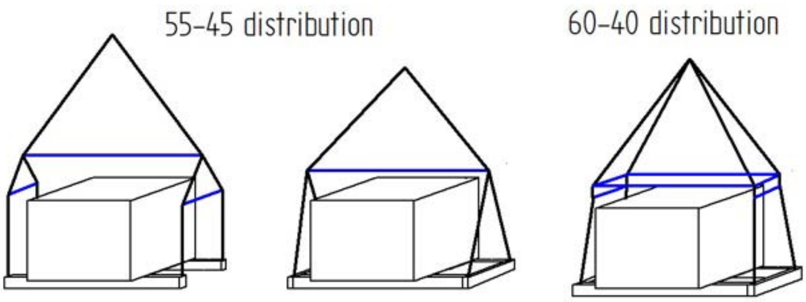

Figure 4.4: From left to right: Rigging arrangement A, Rigging arrangement B and Rigging arrangement C

According to the in-house standard code for single lifts, it is advised to take a SKL of 1.1 for rigging arrangements A and B, and a SKL of 1.2 for rigging arrangement C [35].

Rigging arrangement A consists of three floating spreader bars, one in longitudinal direction and two in transverse direction. The longitudinal spreader bar is allowed to move its CoG above the CoG of the lift object, resulting in a load case which is closer to the equilibrium case. Under this setup, only vertical rigging loads are imposed to the lift beams, as the slings are vertically attached to the lift points.

Rigging arrangement B provides an alternative solution for rigging arrangement A. As can be seen, this rigging arrangement only makes use of the longitudinal spreader bar. The costs and weight of the rigging setup can be reduced this way. The downside of this arrangement is that relatively large side loads are introduced to the lift beams, due to the angle of the slings. A cross-beam could be added to the lift beams to carry these loads.

Finally rigging arrangement C is considered, which follows a 60-40 load distribution. The rigging setup consists of two transverse floating spreader bars, which are attached to a spreader frame. The load distribution is further off the equilibrium case, resulting in a load case which is less favorable for the topsides. Also for this arrangement, a cross-beam will be required to take up the lateral components of the rigging loads.

Ideally, the rigging arrangements are re-used without need for project specific modifications. For the longitudinal spreader bar a fixed length can be taken, since it depends on the length of the lift beams. The size of the transverse spreader bars and the spreader frame is however strongly determined by the spacing of adjacent lift points. The spacing of these points differs for each topsides, and changing the dimensions of these elements is therefore considered to be inevitable.

4.2. Model set-up

In this section the set-up of the SACS models and implementation of the aforementioned characteristics are explained. The SACS model of reference topsides 14, which is used as the starting point, is initially made for another lift analysis. Due to this, the living quarter and helideck are not included in the model. Only for the position of the lift beams, the presence of these modules is taken into account.

4.2.1. Reference topsides 14

The topsides dry weight and CoG, excluding living quarter and helideck, are provided in table 4.1.

$W_{dry}[mT]$	CoG_x[m]	CoG_y[m]	CoG_z[m]
2176	0.95	15.22	8.24

Table 4.1: The dry weight and CoG of reference topsides 14

The CoG coordinates in x- and y-direction are with respect to the intersect of row A and row 3, as indicated in figure 4.5. The CoG z-coordinate is given with respect to the MSF deck.

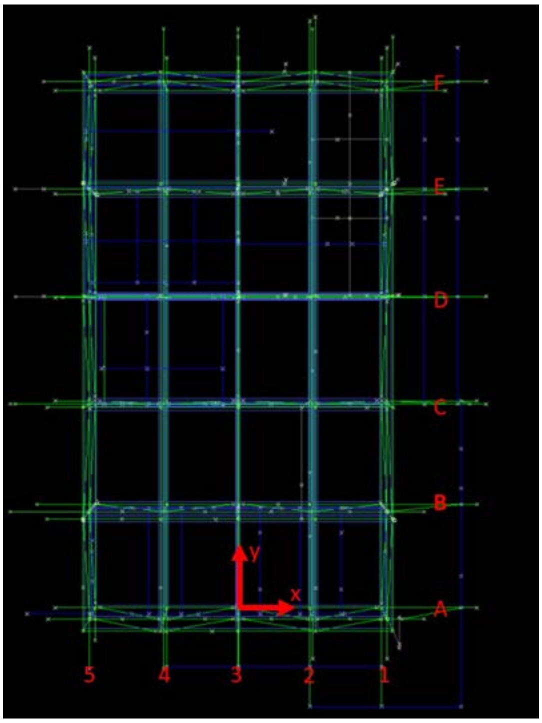

Figure 4.5: Top view of reference topsides 14 in SACS

The self-weight of primary and secondary steel is modelled as distributed loads, and equipment weight as concentrated loads. Different steel types are used for the members, with the yield strength ranging from 245 MPa to 360 MPa.
The MSF legs are cut-off 2 meters below the MSF deck in the SACS model. In reality, the MSF legs extend 7 meters till final cut-off. The structural properties of the MSF legs are provided in table 4.2.

OD [m]	WT [m]	Fy [MPa]	E [MPa]	G [Mpa]
1.22	0.05	335	210e3	81e3

Table 4.2: Structural properties of the MSF legs

For the primary columns, six different section groups are identified. Each section group has different structural properties, based on their design load. Given a good load spread, it is expected that the primary columns have sufficient capacity to withstand the loads during lifting.

4.2.2. Lift beams

Lift beam properties

For the lift beams the same properties are used as described in chapter 3. Hereby, the spacing of the transverse intermediate stiffeners is included. The lift beams that are used for connection with the MSF deck are assigned the same properties as the two-sided support beam. The exact load case for connection with the MSF deck can't be determined. However due to the greater load spread, it is presumed that the two-sided support beam will have sufficient capacity to withstand the loads when connected with the MSF deck.

For the buckling length factors K_y and K_z a value of 1.0 is assigned, which is recommended for beams that are pinned on both ends. The self-weight of the lift beams is modelled as a distributed load and equals $q_{beam1} = 76.2kN/m$ for the one-sided support beam and $q_{beam2} = 52.1kN/m$ for the two-sided support beam. For simplicity, the same properties are used for the cross-beams. The connection between the lift beams and the cross-beams is modelled to be fully rigid.

Lift beam position

The position of the lift beams depends on their orientation and the location of the connection. Figure 4.6 indicates the distances between the lift points and the MSF legs for orientation along rows 1-5 and for orientation along rows E-B.

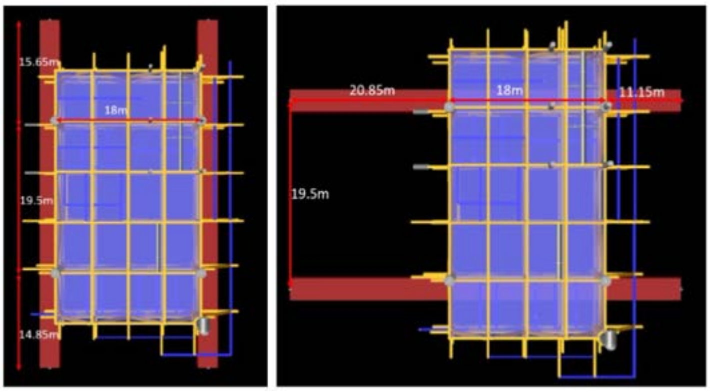

Figure 4.6: Relevant distances for the 1-5 orientation (left) and the E-B orientation (right)

For the MSF deck-connection models, the longitudinal position of the lift beams remains the same. The spacing of the lift beams however changes, since the lift beams are now connected to the rows containing the primary columns of the topsides. For the 1-5 orientation, the lift beams are positioned along rows 2, 3 and 4. For the E-B orientation, the rows A, C, D and F are used. The spacing of the primary column rows is presented in figure 4.7.

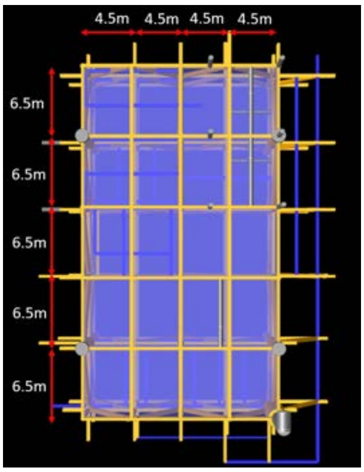

Figure 4.7: Column row spacing

4.2.3. Lift beams-to-topsides connection

Pinned

The pinned connection between the lift beams and the MSF legs is modelled with member end releases, which are set at (000111). This implies that the rotational DoF's 4, 5 and 6 are released and therefore unrestrained. The buckling length factors K_y and K_z of the MSF legs are set at 0.8, as recommended in Appendix C.1. Hereby, it is assumed that the fixed end of the MSF legs is stiff enough to be considered as fully fixed.

Clamped

For a clamped connection between the lift beams and the MSF legs, the leg end release is set at (000000). This implies that no DoF's are released, and therefore all relative displacements and rotations between the elements are restrained. The buckling length factors of the MSF legs are set at 0.65.

Axial

The axial connection between the lift beams and the primary columns is modelled with the use of dummy members. These members are able to transfer loads without affecting the structural behaviour of the connecting members. The dummy members are connected to the base of the columns, as can be seen in figure 4.8.

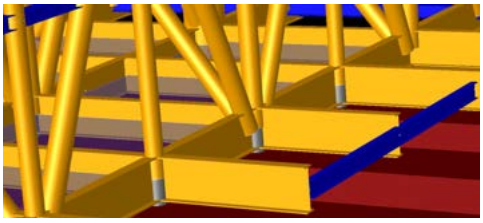

Figure 4.8: Dummy members shown in grey

The dummy members are assigned to be compression-only members. It is important to verify this by looking at the load out-put of these members.

4.2.4. Rigging loads

The rigging loads are modelled as vertical concentrated loads acting on the lift beams' end nodes. A horizontal, outwards directing, load component is added, which is equal to 5% of the vertical rigging load. The horizontal side load is used to take perpendicular dynamic loads and fabrication tolerances of the lift points into account [34]. Horizontal components of the rigging load due to the sling angle are neglected at this stage.

The first step in determining the rigging loads is to find the vertical equilibrium load distribution. The equilibrium load distribution provides the lift point loads at which the topsides is lifted in equilibrium. This load distribution is obtained by pinning the lift beams' ends to the world. Subsequently a SKL is applied, which corresponds to the rigging arrangement that is considered. The SKL takes additional loading caused by equipment and fabrication tolerances into account as well as uncertainties regarding asymmetry and force distribution in the rigging arrangement [38].

This implies that the topsides is lifted off its equilibrium. To ensure that the assembly remains stable, it is important that the load output per lift point row is equal to the equilibrium case. This will ensure that each row, containing the connection points between the lift beams and the topsides, will provide the same load output, while allowing for load redistribution within the row. An overview of the rigging loads for each model is provided in Appendix C.2.

Lift factors

The dry weight, and hence the rigging loads are multiplied by a DAF and contingency factor, both equal to 1.1. The DAF is used to account for dynamic load fluctuations, added to the static loads. The DAF is dependant on several factors as described in chapter 2. The contingency factor accounts for uncertainty about the weight and CoG of the lift object. An additional consequence factor is applied for members near the connection points. This way, extra safety is applied for these members, when assessing their structural integrity. This is needed to provide certainty that failure of these members won't occur. An overview of the lift factors is provided in table 4.3.

μ_{DAF} [-]	μ_{cont} [m]	$\mu_{cons} [MPa]$
1.1	1.1	1.15

Table 4.3: Overview of the lift factors

60-40 distribution

A 60-40 distribution implies that 60% of the hook load is taken by one diagonal and 40% by the other diagonal, which is equivalent to a SKL of 1.2. Since it's unknown which diagonal takes the larger portion of the load, both cases have to be considered simultaneously. This way an envelope is created, in which the governing UC's of each member are displayed. The 60-40 rigging load distribution is determined with the following equations:

$$F_{v,60} = F_{v,eq} + \frac{0.6 - \mu_{diag,eq}}{2} * F_{v,tot} \tag{4.1}$$

$$F_{v,40} = F_{v,eq} + \frac{0.4 - \mu_{diag,eq}}{2} * F_{v,tot} \tag{4.2}$$

In these equations, $\mu_{diag,eq}$ represents the portion of the hook load which is taken by the diagonal in the equilibrium load case.

55-45 distribution

The rigging loads with a SKL of 1.1 are determined with the following equations:

$$F_{v,55} = F_{v,eq} + \frac{0.55 - \mu_{diag,eq}}{2} * F_{v,tot} \tag{4.3}$$

$$F_{v,45} = F_{v,eq} + \frac{0.45 - \mu_{diag,eq}}{2} * F_{v,tot} \tag{4.4}$$

For the models consisting of four lift beams without a cross-beam, an additional SKL of 1.1 is applied over two adjacent lift points. Both of these lift points are connected to one spreader bar lift point. The SKL accounts for frictional effects over the spreader bar lift point, which result in additional load uptake by one of the slings. Two cases can be defined, where majority of the load is taken by either the inner or the outer lift point. An impression of this is provided in Appendix C.1.

4.2.5. Model stability

Stability of the model mainly refers to stability of the topsides. As the topsides is lifted off its equilibrium, a restoring moment has to be provided to prevent any rigid body motions and numerical instabilities. To achieve this, weak springs are applied at specific nodes of the topside. The spring reaction forces shouldn't have any significant impact on the structural integrity of the topsides. It is therefore important that the spring reaction forces are negligibly small compared to the rigging forces. The topsides springs are indicated in figure 4.19.

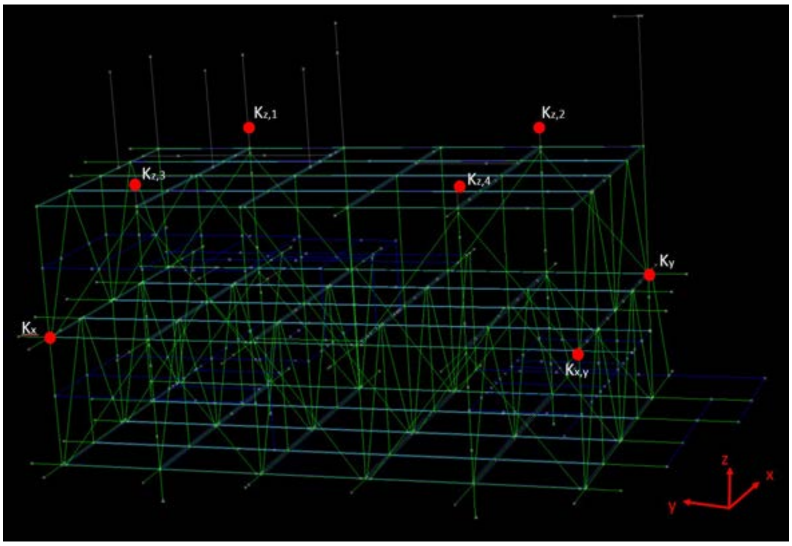

Figure 4.9: Topsides stability springs

Springs $K_{x,y}$, K_x and K_y are located between the two decks, on the edges of the topsides. The work line of the spring force couples must not intersect in order for them to be effective. Spring combinations $K_{x,y}$-K_x and $K_{x,y}$- K_y provide force couples which counteract excessive rotations of the topsides around the z-axis. The vertical distance between these springs and the topsides CoG must be relatively small to prevent additional overturning moments around the x- and y-axis.

The z-springs are located on the top elevation of the topsides. Spring combinations $K_{z,1}$- $K_{z,3}$ and $K_{z,2}$- $K_{z,4}$ provide a stabilizing moment around the y-axis. Excessive rotations around the x-axis are restrained by spring combinations $K_{z,1}$- $K_{z,2}$ and $K_{z,3}$- $K_{z,4}$. All springs are assigned a stiffness of 1MN/m. The spring forces should be relatively small compared to the rigging loads and should have a negligible influence on the structural integrity of the topsides.

For the lift beams, weak springs are only applied if necessary to assure numerical stability. Unnecessary restraint of the lift beams will stiffen the lift beams, and reduce their deflections. This results in a smaller load transfer to the MSF legs, and hence lower UC's. In case of a pinned connection without cross-beam, rotation around the longitudinal axis of the lift beam must be fully restrained on one of the lift beams' ends. The lift beams are eccentrically loaded when connected to the MSF legs. The torsional moment acting on the lift beams results in twisting of the lift beams. If this rotation is not restrained, the model becomes numerically unstable. In reality, this implies that a cross-beam or any type of local restraint is required to resist twisting of the lift beam.

4.3. Results

The topsides structural integrity for each model is assessed by the number of critical members, n_{crit}, and the number of failing members, n_{fail}. Critical members are defined as members with a UC ≥0.75, and failing members with a UC ≥1.0. These parameters give insight on the global capacity of the topsides for a given load case. It also allows for comparison between the models to understand which aspects are beneficial for the topsides structural integrity.

For the MSF leg connections, the UC's of the legs are observed. This way it can be investigated what types of loads are introduced to the leg and how much of the leg capacity is taken by each load type. Understanding the parameters that influence the load transfer will allow to reduce these loads or if possible eliminate them. For the MSF deck connections, the load output per dummy members is checked and the shim plate thicknesses are varied to improve the load spread to the topsides.

As the topsides will be out of service after removal, local failure of members in principle is allowed. However, failure of one member could lead to failure of other nearby members. Continuation of this process is known as progressive collapse and must be avoided at all times. Strengthening techniques could be applied to failing members in order to prevent progressive collapse. If possible, strengthening is avoided, since this is a costly and time consuming process. It is more effective to design a removal set-up, which loads the topside in a favorable manner. This way repetitive strengthening for each topsides can be prevented.

Failure of members that are part of the connection interface must be avoided, since it will likely result in collapse of the complete lift beams - topside assembly. When analysing the occurrence of progressive collapse, an additional consequence factor is applied to the loads to ensure that these members have sufficient capacity.

The current state of the topsides is assessed with offshore surveys. Remarkable signs of deterioration such as corrosion, plastic deformations or cracks are investigated and strengthening of these elements is advised prior to lifting. Other than that, it is assumed that the member capacity is the same as during installation. This gives rise to extra awareness when assessing the capacity of a specific member. It is therefore aimed to find a removal solution that doesn't take up the full capacity of the topsides' structural members.

4.3.1. In-situ

The in-situ case represents the topsides being supported by its jacket substructure. In SACS the MSF legs are pinned to the world to model the in-situ case. A DAF and contingency factor are applied, like in the other models, to make the results comparable. Figure 4.10 illustrates the in-situ topsides structural integrity.

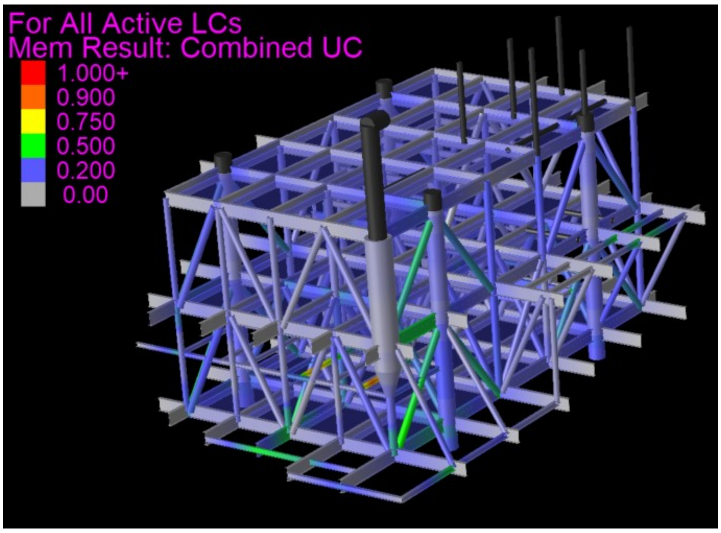

Figure 4.10: In-situ structural integrity of reference topsides 14

It can be seen that most of the members have a unity check below 0.5. Four critical members are identified, which are indicated in yellow. The combined UC's of the MSF legs are provided in table 4.4.

$UC_{PB10}[-]$	$UC_{PB50}[-]$	$UC_{PE10}[-]$	$UC_{PE50}[-]$
0.27	0.24	0.22	0.18

Table 4.4: In-situ combined UC of the MSF legs

4.3.2. MSF leg connection models

In this section the structural integrity results for the leg connection models are briefly discussed. The equilibrium load distribution and the rigging loads are provided in Appendix C.2. Evaluation of the results and further explanation is provided in Appendix C.3.

One-sided leg support

For one-sided support of the MSF legs, the lift beams are placed on the outer side of the legs. The top edge of the lift beams is connected to the bottom of the MSF legs. The total assembly weight, excluding factors, is equal to $2953mT$. The one-sided leg support models are shown in figure 4.11.

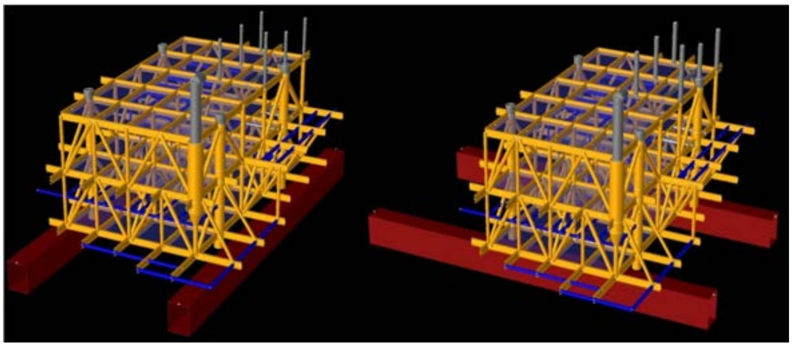

Figure 4.11: 1-5 direction (left) E-B direction (right) for one-sided leg support

It is unknown over which diagonal the majority of the hook load will be taken. Therefore both load cases are ran simultaneously, and the governing UC's from these cases are considered. For n_{crit} and n_{fail}, the number of unique members from both load cases is taken. The results are shown in tables below.

Direction 1-5	UC$_{PB10}$	UC$_{PB50}$	UC$_{PE10}$	UC$_{PE50}$	n$_{crit}$	n$_{fail}$
60-40 Pinned	0.59	0.52	0.54	0.47	35	10
55-45 Pinned	0.52	0.45	0.47	0.40	12	0
60-40 Clamped	1.83	1.53	1.73	1.46	>50	28
55-45 Clamped	1.72	1.42	1.62	1.36	>50	19

Table 4.5: Structural integrity results for one-sided leg support in 1-5 direction

Direction E-B	UC$_{PB10}$	UC$_{PB50}$	UC$_{PE10}$	UC$_{PE50}$	n$_{crit}$	n$_{fail}$
60-40 Pinned	0.60	0.62	0.54	0.51	29	13
55-45 Pinned	0.53	0.54	0.47	0.43	9	1
60-40 Clamped	1.78	1.81	1.52	1.51	>50	24
55-45 Clamped	1.68	1.68	1.42	1.37	44	11

Table 4.6: Structural integrity results for one-sided leg support in E-B direction

It can be seen that the MSF legs have sufficient capacity to withstand the loads in case of a pinned connection. Here, the maximum unity check of the legs is found at the interface with the MSF deck. Besides a vertical force, also lateral forces are transferred at the interface between the lift beams and the MSF legs. These forces cause a moment, which is largest at the fixed base of the MSF legs. The transverse force follows from the side loads that are applied to the lift beams' end nodes. Besides this force, a significantly larger longitudinal force is transferred to the MSF legs. This force is identified as a longitudinal shear force, which follows from the global bending moment acting over the supported span of the lift beams. It has to be noted that a fully pinned connection is not feasible, because there is no component restraining torsion of the lift beams. The lift beams' ends therefore are restrained in this direction. The torsional reaction moments, which are shown in Appendix C.2, also show to be relatively large.

The number of failing and critical members is still relatively high, especially for the 60-40 rigging load distribution. When a 55-45 distribution is applied, the number of critical members drops significantly, and almost no failing members are detected. The topside is lifted closer to its equilibrium, which shows to have a significant impact on the global structural integrity of the topsides. The main effect of the SKL is that the force uptake within the MSF leg row greatly changes compared to the equilibrium case. Here, the MSF leg closest to the increased lift point load, takes up the vast majority of the total leg row. The increased forces and resulting moments are then transferred to neighbouring elements. For certain members, this eventually results in a load case which exceeds the structural capacity of the member.

Looking at the clamped connections, it can be seen that the MSF legs have insufficient capacity to carry the loads. The vertical and transverse forces are approximately the same as for the pinned case. The longitudinal shear force however increases significantly. For a clamped connection, the lift beams experience more resistance against bending, which results in a much greater longitudinal shear force. Besides forces, also moments are transferred for this connection type. Based on the stiffness of the MSF legs, a portion of the lift beam's strong axis bending moment is taken by the MSF legs. Furthermore the torsional moment, due to eccentric vertical loading, is now completely taken by the MSF legs. This also implies that it is not necessary to restrain the lift beams against twisting. For a clamped connection, the UC's of the legs greatly exceed the limit of 1.0. The maximum value of the UC is found at the interface with the lift beams. It is found that the leg reaction moments take up most of the leg's capacity. Looking at n_{crit} and n_{fail}, it can be seen that the transfer of these moments to the remainder of the topsides is crucial for a large number of members.

Finally, it can observed that the orientation of the lift beams has a small influence on the structural integrity of the topsides. For the E-B direction somewhat better results are obtained. Several reasons are identified for this. Firstly, the position of the lift points with respect to the connection points is more favorable in this direction, resulting in smaller bending moments of the lift beams. Also the spacing of the MSF legs is smaller in this orientation. This results in less redistribution over the MSF leg row when a SKL is applied.

One-sided leg support with cross-beams

The cross-beams increase the dry weight of the assembly to $3228mT$, for the 1-5 direction, and $3351mT$ for the E-B direction. The cross-beams provide the lift points in this setup. Several locations have been investigated, and it is found that placing the lift points in-line with the MSF legs is most favorable regarding the topsides structural integrity. The position of the lift beams remains the same. Figure 4.12 gives an overview of the models for both directions.

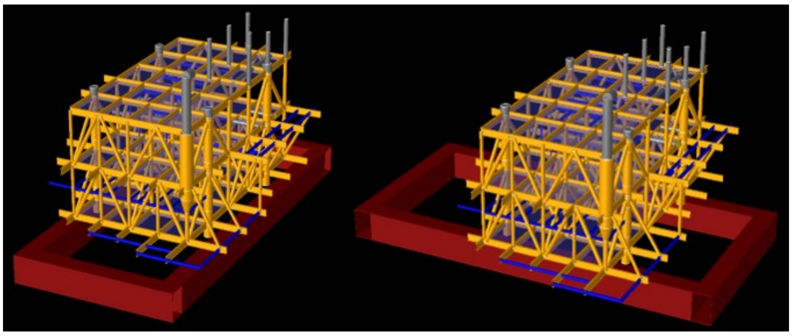

Figure 4.12: 1-5 direction (left) E-B direction (right) for one-sided leg support with cross-beams

Direction 1-5	UC$_{PB10}$	UC$_{PB50}$	UC$_{PE10}$	UC$_{PE50}$	n$_{crit}$	n$_{fail}$
60-40 Pinned	0.60	0.54	0.56	0.50	10	1
55-45 Pinned	0.56	0.50	0.52	0.45	9	0
60-40 Clamped	1.44	1.29	1.36	1.21	19	8
55-45 Clamped	1.35	1.20	1.27	1.13	17	6

Table 4.7: Structural integrity results for one-sided leg support in 1-5 direction

Direction E-B	UC$_{PB10}$	UC$_{PB50}$	UC$_{PE10}$	UC$_{PE50}$	n$_{crit}$	n$_{fail}$
60-40 Pinned	0.63	0.60	0.55	0.52	5	0
55-45 Pinned	0.59	0.55	0.51	0.47	5	0
60-40 Clamped	1.36	1.39	1.22	1.21	12	5
55-45 Clamped	1.29	1.30	1.15	1.12	10	4

Table 4.8: Structural integrity results for one-sided leg support in E-B direction

It is clearly visible that the addition of cross-beams is beneficial for the structural integrity of the topsides. Looking at the results for a pinned connection, a small increase in the UC of the MSF legs can be observed. This increase is mainly caused by the increased weight of the assembly, resulting in larger rigging loads.

Firstly it has to be noted that the load case has become statically undetermined. This implies that the load transfer is now dependent of the stiffness of the load path, with more load being transferred through the stiffer path. The SKL has less effect in this case, and the load transfer over the MSF leg row is now distributed in a better way. Furthermore, it is noticed that the transverse load acting on the MSF leg has reduced, implying that part of this load is taken by cross-beams. The longitudinal shear force on the other hand has increased, because the lift beams have become stiffer and thus provide more resistance against bending. Besides the favorable load redistribution, the cross-beams restrain twisting of the lift beams, hence allowing for a pinned connection between the lift beams and the MSF legs.

For the clamped connections, a significant reduction in the UC's can be observed. Especially the weak-axis bending moment of the MSF leg due to eccentric vertical loading has reduced. This follows from the fact that the lift beams are now able to take up a part of the torsional moments. The aligned position of the lift points with the MSF legs could also play a small role in this.

Especially the results for the E-B direction with a pinned connection are promising, with no failing members and just one additional critical member compared to the in-situ case. In general, when considering the number of critical and failing members, it can be concluded that the topsides is loaded in a more favorable manner under this setup.

Two-sided leg support
The MSF legs are supported from both sides when four lift beams are used. The properties of the lift beams are changed accordingly. The dry weight of the assembly increases to $3239mT$. In absence of a cross-beam, there is a total of eight lift points, one on each lift beam's end. Figure 4.13 shows the SACS models with four lift beams.

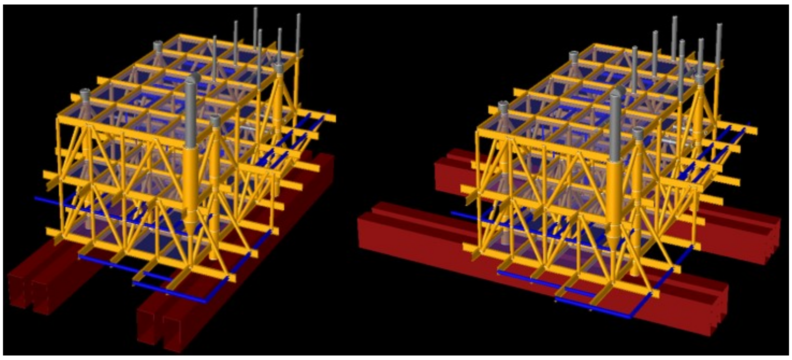

Figure 4.13: 1-5 direction (left) E-B direction (right) for two-sided leg support

The load out-put of neighbouring lift points in the equilibrium case is found to be roughly the same. It has to be noted that for a setup with eight lift points, rigging arrangement B can't be used due to the angle of the slings. The other two rigging arrangements can be applied, with each spreader bar lift point being connected to two lift beam lift points. In this case an additional SKL of 1.1 is applied over the lift points, as previously discussed. Two cases are considered. One case where 55% of the load goes to the outer lift points and the other case where 55% of the load goes to the inner lift points. This leads to a total of four load cases per rigging load distribution, which are shown in Appendix C.2. The topsides structural integrity results are shown in tables below.

Direction 1-5	UC_{PB10}	UC_{PB50}	UC_{PE10}	UC_{PE50}	n_{crit}	n_{fail}
60-40 Pinned	0.58	0.52	0.53	0.47	37	15
55-45 Pinned	0.51	0.45	0.47	0.40	12	0
60-40 Clamped	1.42	1.25	1.34	1.18	41	16
55-45 Clamped	1.25	1.09	1.17	1.02	18	6

Table 4.9: Structural integrity results for two-sided leg support in 1-5 direction

Direction E-B	UC_{PB10}	UC_{PB50}	UC_{PE10}	UC_{PE50}	n_{crit}	n_{fail}
60-40 Pinned	0.61	0.62	0.54	0.51	36	16
55-45 Pinned	0.54	0.54	0.48	0.43	10	1
60-40 Clamped	1.24	1.35	1.11	1.14	43	20
55-45 Clamped	1.15	1.21	1.02	1.0	15	5

Table 4.10: Structural integrity results for two-sided leg support in E-B direction

The results of the one-sided leg support and two-sided leg support models show small differences when a pinned connection is modelled. The vertical load acting on the MSF leg has slightly increased due to the increased weight of the assembly. The main difference that is observed is the reduced weak axis bending moment at the base of the leg. The transverse side load acting on the MSF leg has reduced, since the side loads acting on adjacent beams counteract each other. Moments due to eccentric loading are taken by the lift beams and therefore the effects of two-sided leg support aren't really visible for a pinned-connection.

Looking at the results for a clamped connection, a reduction in the unity checks and the number critical and failing members can be noticed. The MSF legs are supported from both sides and are therefore not subject to large weak axis bending moments. The legs are still slightly eccentrically loaded, because of a small difference in load carrying of adjacent lift beams. Most capacity of the MSF leg is taken by the strong axis bending moment, which follows from uptake of the lift beam's bending moment and the corresponding longitudinal shear force.

Comparing the results with the one-sided leg support with cross-beams, it can be concluded that the addition of a cross-beam is more beneficial for the topsides' structural integrity than supporting the MSF legs from both sides.

Two-sided leg support with cross-beams
The final lift beam setup to consider for the MSF leg connections consists of four lift beams with a cross-beam on each end. The dry weight is equal to $3488mT$ in 1-5 direction and $3504mT$ in E-B direction. In figure 4.15 an impression of the models in both directions is given.

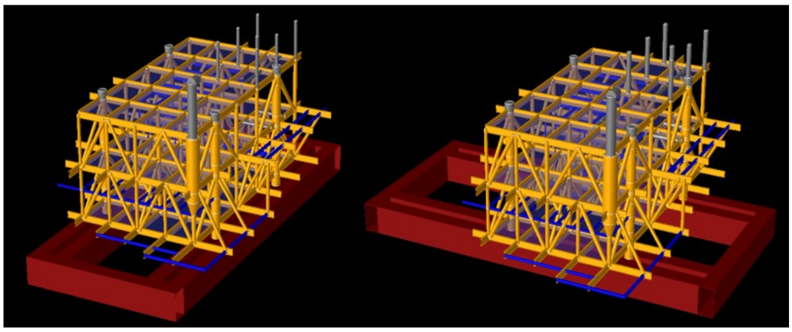

Figure 4.14: 1-5 direction (left) E-B direction (right) for two-sided leg support with cross-beams

This lift beam setup is the heaviest setup and supports the topsides the most. Rigging arrangement A can be used for this set-up as the number of lift points is reduced to four again. The UC's, n_{crit} and n_{fail} are provided below.

Direction 1-5	UC_{PB10}	UC_{PB50}	UC_{PE10}	UC_{PE50}	n_{crit}	n_{fail}
60-40 Pinned	0.56	0.49	0.51	0.45	11	1
55-45 Pinned	0.51	0.44	0.47	0.40	8	0
60-40 Clamped	1.30	1.16	1.22	1.09	14	5
55-45 Clamped	1.21	1.07	1.13	1.01	13	5

Table 4.11: Structural integrity results for two-sided leg support with cross-beams in 1-5 direction

Direction E-B	UC_{PB10}	UC_{PB50}	UC_{PE10}	UC_{PE50}	n_{crit}	n_{fail}
60-40 Pinned	0.57	0.57	0.51	0.46	6	0
55-45 Pinned	0.54	0.52	0.46	0.43	5	0
60-40 Clamped	1.22	1.25	1.09	1.07	13	5
55-45 Clamped	1.17	1.17	1.03	1.01	10	4

Table 4.12: Structural integrity results for two-sided leg support with cross-beams in E-B direction

Compared to the setup of one-sided leg support with cross-beams no significant improvements are observed for the pinned connection. For a clamped connection, the results have somewhat improved. The main difference is the reduced weak-axis bending moment since the MSF legs are loaded in a less eccentric manner. It has to be noted that the weight of the assembly is 260 mT heavier than the setup for one-sided leg support with cross-beams. It is however expected that for the heavier topsides, where the ratio of $W_{liftframe}$ / $W_{topside}$ is lower, the benefits of two-sided leg support with cross-beams will become better visible. For the smaller topsides on the other hand it is suggested that one-sided leg support with cross-beams will be more suitable.

4.3.3. MSF deck connection models

For connection of the lift beams with the MSF deck, a cross-beam is considered to be required in order to provide lateral stability to the lift beams. This is necessary since the connection only transfers an axial compressive force, and therefore doesn't restrain lateral motions. In this section only the number of critical members and failing members are considered. The connection elements are checked on their load out-put, which can be found in Appendix C.2. The same holds for the rigging loads. An additional non-linear gap analysis is run, where the dummy members are assigned to be gap elements. Gap elements only allow load transfer after reaching a certain displacement, the gap size. If these gap elements wouldn't be used, the load would mostly be taken by the exterior columns. The use of gap elements on the exterior column rows will therefore allow to activate the interior columns as well. It is aimed to obtain a better distributed load spread this way. In practice, the gap elements represent shim plates which essentially provide the same functioning.

1-5 direction

In the 1-5 direction, three column rows are available for connection with the lift beams. The spacing of the primary column rows is provided in figure 4.7. Over the three lift beams, 16 connection members are positioned. This removal set-up is found to be very unstable. This is due to the position of the topsides CoG, and the short distance between the lift beams and therefore the lift points. The result is that the topsides tends to tilt to the right handed beam, as this beam has to take most of the load. An aggressive shift in CoG or excessive tilting could result in the CoG falling out of the lift point envelope and the topsides could potentially topple over. In addition to the topsides springs, weak springs are applied to the lift beams' ends to maintain stability. The total dry weight of the assembly is equal to $3091 mT$. Figure 4.15 shows the SACS model and the location of the dummy members.

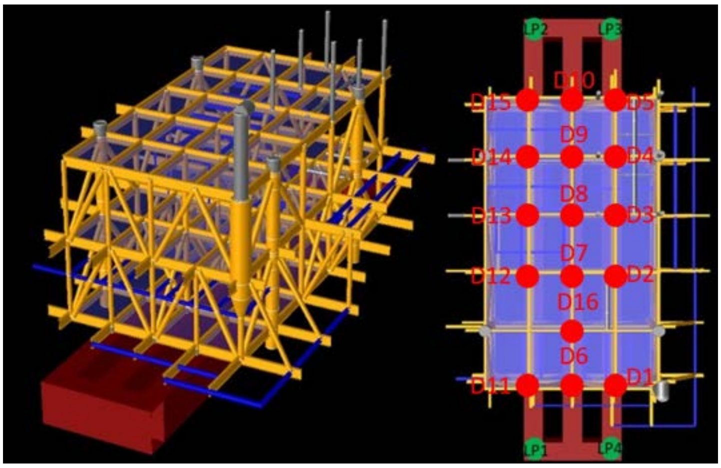

Figure 4.15: MSF deck connection model in 1-5 direction (left) and the position of the connection elements (right)

An overview of the maximum combined UC of each topsides member for the 60-40 and 55-45 rigging load distribution is shown in figure 4.16.

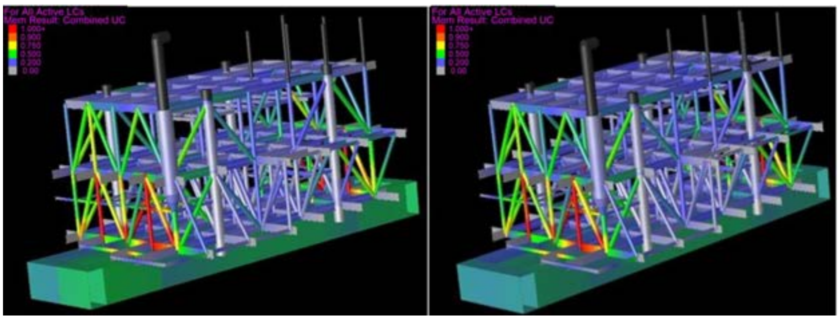

Figure 4.16: The maximum combined UC's for a 60-40 distribution (left) and a 55-45 distribution (right) without gap elements in 1-5 direction

It can be seen that primarily the exterior column rows A and F are loaded. As the lift beams are loaded by the topsides, the lift beams bend and only contact with the exterior column rows is maintained. These second order effects are only considered in the non-linear gap analysis. For the basic static analysis, which is performed here, the dummy members can be modelled as supports. The outer supports, located along rows A and F, deliver most of the reaction force in order to obtain momentum balance over the lift beam. The reaction forces on the outer supports are found to be too large for the columns to withstand. The number of critical and failing members is given in table below.

60-40 distribution		55-45 distribution	
n_{crit}	n_{fail}	n_{crit}	n_{fail}
48	24	43	19

Table 4.13: Structural integrity results for the 1-5 direction without gap elements

It is clear that the topsides doesn't have sufficient capacity to withstand the lift loads under this setup. It is expected that activation of the interior column rows will significantly improve the topsides structural integrity results. As previously discussed, this is achieved by using shim plates, which are modelled as gap elements in SACS. The optimal gap size per connection point is determined through iteration. An overview of the gap sizes is found in Appendix C.2. The maximum combined UC overview with the optimal shim plate thicknesses is provided in figure 4.17.

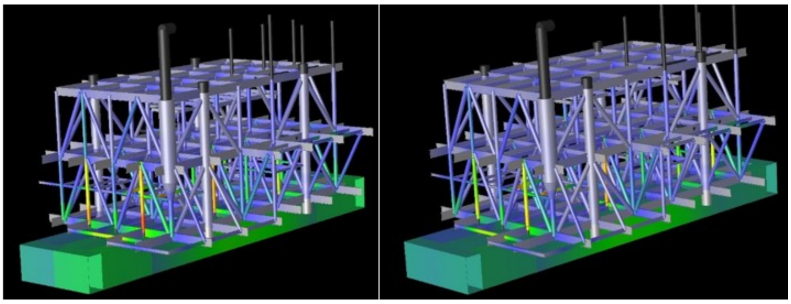

Figure 4.17: The maximum combined UC's for a 60-40 distribution (left) and a 55-45 distribution (right) with gap elements in 1-5 direction

A significant improvement in load distribution over the connection elements and primary columns can be observed. It is clear that it is essential to activate the interior columns for this load transfer concept to be structurally feasible. The values for n_{crit} and n_{fail} are given in table 4.14.

60-40 distribution		55-45 distribution	
n_{crit}	n_{fail}	n_{crit}	n_{fail}
10	0	7	0

Table 4.14: Structural integrity results for the 1-5 direction with gap elements

It can be seen that no failing members are detected and that the number of critical members is reduced to an acceptable amount. Extra attention should be paid to the exterior columns along rows 2 and 4. These columns are designed for a lower design load, and the diagonals that are connected to these columns are considered to be the main load carrying components. If necessary, the gap size could be further increased for these columns to reduce the load uptake.

E-B direction
Four lift beams are used in the E-B direction, resulting in a total dry weight of $3607mT$. The beams are positioned along rows A, C, D and F, as indicated in figure 4.7. On each lift beam five connection elements are applied. The assembly is much more stable under this set-up. The topsides CoG has a more central position, and the lift points are spread over a greater distance. Also, the distance between the topsides CoG and the CoF of the rigging is smaller. The shorter this distance, the smaller the overturning moment and hence the tilting of the topside. Under this setup, the load is also more equally spread over the lift beams.

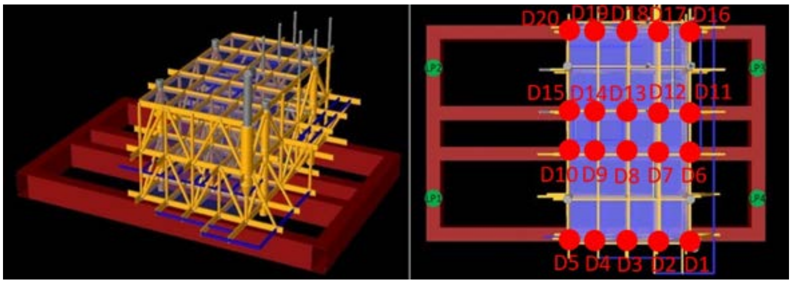

Figure 4.18: MSF deck connection model in E-B direction (left) and the position of the connection elements (right)

The maximum combined UC's of the topsides members for both load distributions is shown figure 4.19.

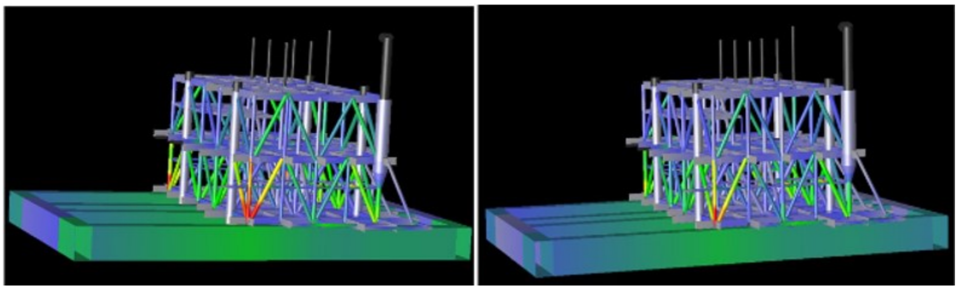

Figure 4.19: The maximum combined UC's for a 60-40 distribution (left) and a 55-45 distribution (right) without gap elements

60-40 distribution		55-45 distribution	
n_{crit}	n_{fail}	n_{crit}	n_{fail}
23	2	16	1

Table 4.15: Structural integrity results for the E-B direction without gap elements

The number of critical and failing members is significantly lower compared to the setup for the 1-5 direction. More column rows are activated and the topsides is loaded with less eccentricity. The deflection of the lift beams is also smaller, because on average each lift beam takes up a smaller portion of the topsides weight. This is due to the increased number of lift beams, and the more central position of the topsides CoG. However, tt can be seen that the exterior column rows are still heavily loaded. The results with the use of gap elements are provided in figure 4.20 and table 4.16. An overview of the gap element sizes is found in Appendix C.2.

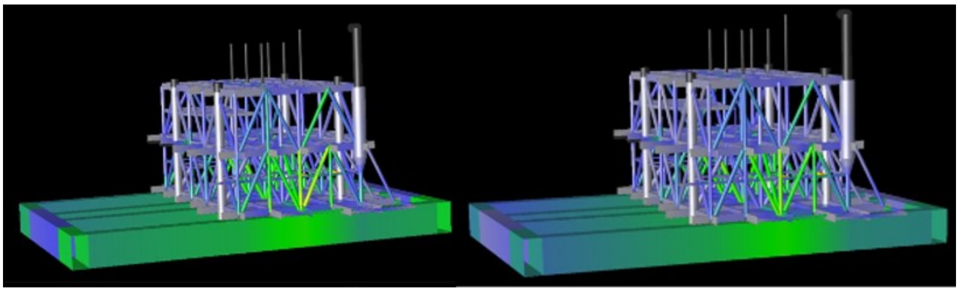

Figure 4.20: The maximum combined UC's for a 60-40 distribution (left) and a 55-45 distribution (right) with gap elements in E-B direction

60-40 distribution		55-45 distribution	
n_{crit}	n_{fail}	n_{crit}	n_{fail}
8	0	7	0

Table 4.16: Structural integrity results for the E-B direction with gap elements

Promising results are obtained as there are no failing members and a small number of critical members compared to the in-situ case. It can be seen that the highest UC's are located on row A, where most of the topsides weight is carried. The columns in this row are all braced and therefore the load can easily be transferred to other neighbouring members.

4.4. Verification

It is important that the obtained results are verified prior to drawing conclusions on the models. Different aspects of the models can be verified, such as the rigging loads, the boundary conditions, the UC's and stability of the model. The rigging loads are verified by checking whether the load per row remains the same under different rigging load distribution. The boundary conditions are verified by following the load path and ensuring that the loads are transferred as expected. The UC's are verified by determining whether the loads, introduced to the MSF legs, result in the appropriate acting stresses. Finally stability of the model is checked by looking at the topsides' displacements and the magnitude of the topsides' restoring spring forces compared to the rigging loads. Verification of the rigging loads is provided in Appendix C.2. The boundary conditions and the UC's are assessed in Appendix C.3.

4.5. Neutral axis

Verification of the model results, shown in Appendix C.3, has shown that a large portion of the MSF leg capacity is taken by a longitudinal shear force and the corresponding moment at the fixed base of the leg. It is found that transfer of the longitudinal shear force to the MSF leg can be prevented by connecting the lift beams at their neutral axis to the MSF legs. The resulting MSF leg UC's, and the number of critical and failing members are shown in tables below.

1-5 direction, one-sided support	UC_{PB10}	UC_{PB50}	UC_{PE10}	UC_{PE50}	n_{crit}	n_{fail}
60-40 pinned	0.56	0.5	0.51	0.45	29	9
55-45 pinned	0.46	0.41	0.41	0.35	9	0
60-40 clamped	1.52	1.25	1.44	1.20	o50	28
55-45 clamped	1.45	1.18	1.37	1.13	50	18

Table 4.17: Structural integrity results for one-sided leg support in 1-5 direction with neutral axis connection

E-B direction, one-sided support	UC_{PB10}	UC_{PB50}	UC_{PE10}	UC_{PE50}	n_{crit}	n_{fail}
60-40 pinned	0.54	0.55	0.52	0.46	31	11
55-45 pinned	0.44	0.45	0.41	0.36	9	1
60-40 clamped	1.57	1.54	1.34	1.27	o50	24
55-45 clamped	1.46	1.43	1.23	1.16	38	9

Table 4.18: Structural integrity results for one-sided leg support in E-B direction with neutral axis connection

1-5 direction, one-sided support + cross	UC_{PB10}	UC_{PB50}	UC_{PE10}	UC_{PE50}	n_{crit}	n_{fail}
60-40 pinned	0.31	0.27	0.28	0.23	6	0
55-45 pinned	0.26	0.23	0.22	0.18	4	0
60-40 clamped	1.06	0.95	0.98	0.87	10	1
55-45 clamped	0.97	0.86	0.90	0.79	9	0

Table 4.19: Structural integrity results for one-sided leg support with cross-beams in 1-5 direction with neutral axis connection

E-B direction, one-sided support + cross	UC_{PB10}	UC_{PB50}	UC_{PE10}	UC_{PE50}	n_{crit}	n_{fail}
60-40 pinned	0.36	0.33	0.32	0.27	6	0
55-45 pinned	0.31	0.28	0.26	0.22	5	0
60-40 clamped	1.00	1.01	0.89	0.87	10	1
55-45 clamped	0.93	0.93	0.82	0.79	9	0

Table 4.20: Structural integrity results for one-sided leg support with cross-beams in E-B direction with neutral axis connection

1-5 direction, two-sided support	UC_{PB10}	UC_{PB50}	UC_{PE10}	UC_{PE50}	n_{crit}	n_{fail}
60-40 pinned	0.37	0.33	0.34	0.3	34	13
55-45 pinned	0.30	0.26	0.27	0.23	9	0
60-40 clamped	1.02	0.90	0.94	0.83	34	14
55-45 clamped	0.88	0.77	0.81	0.71	12	1

Table 4.21: Structural integrity results for two-sided leg support in 1-5 direction with neutral axis connection

E-B direction, two-sided support	UC_{PB10}	UC_{PB50}	UC_{PE10}	UC_{PE50}	n_{crit}	n_{fail}
60-40 pinned	0.39	0.39	0.37	0.32	35	16
55-45 pinned	0.32	0.31	0.29	0.24	10	1
60-40 clamped	0.90	0.96	0.81	0.80	41	16
55-45 clamped	0.81	0.84	0.73	0.69	13	1

Table 4.22: Structural integrity results for two-sided leg support in E-B direction with neutral axis connection

1-5 direction, two-sided support + cross	UC_{PB10}	UC_{PB50}	UC_{PE10}	UC_{PE50}	n_{crit}	n_{fail}
60-40 pinned	0.31	0.28	0.28	0.23	5	0
55-45 pinned	0.26	0.23	0.22	0.19	4	0
60-40 clamped	0.73	0.65	0.66	0.58	5	0
55-45 clamped	0.65	0.58	0.59	0.51	4	0

Table 4.23: Structural integrity results for two-sided leg support with cross-beams in 1-5 direction with neutral axis connection

E-B direction, two-sided support + cross	UC_{PB10}	UC_{PB50}	UC_{PE10}	UC_{PE50}	n_{crit}	n_{fail}
60-40 pinned	0.34	0.33	0.32	0.24	6	0
55-45 pinned	0.31	0.28	0.26	0.22	5	0
60-40 clamped	0.69	0.70	0.63	0.56	5	0
55-45 clamped	0.64	0.63	0.57	0.52	5	0

Table 4.24: Structural integrity results for two-sided leg support with cross-beams in E-B direction with neutral axis connection

4.6. Consequence factor

To ensure the structural integrity of crucial members an additional consequence factor is applied to the loads. The UC's of members around the connection points are revised under this load case. If the maximum combined UC of any of these members exceeds 1.0, preventive strengthening is strongly advised. Also their failure will be included in the progressive collapse analysis, which is described in the next section.
The members that are considered as crucial depends on the connection location. For the MSF leg connections, the crucial members are indicated in red in figure 4.21.

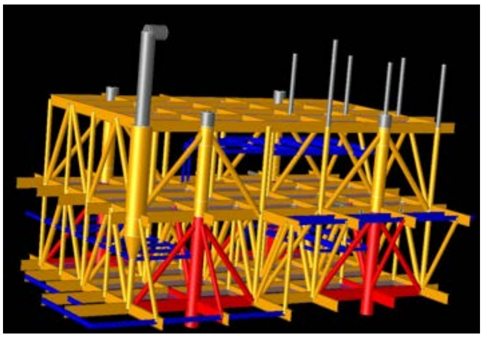

Figure 4.21: Crucial members for the MSF leg connection models

For the MSF deck connection models, the UC of each member in the loaded rows is revised under the consequence load case. This is done because of the large number of connection points and members that are connected to these connection points. The consequence factor is applied in combination with the shim plates.
The consequence load case is only applied to models which have no more than five failing members and don't have any failing MSF legs under the design load case. For the other models progressive failure is considered to be inevitable unless strengthening is applied. The number of newly found failing members, $n_{cons,fail}$, for the eligible models is provided in table 4.17.

	1-5 direction	E-B direction
Model	$\mathbf{n_{cons,fail}}$	
2 beams (55-45,pinned)	0	0
2 beams + cross (60-40,pinned)	0	0
2 beams + cross (55-45,pinned)	0	0
2 beams + cross (55-45,clamped)	2	2
4 beams (55-45,pinned)	0	0
4 beams (55-45,clamped)	1	1
4 beams + cross (60-40,pinned)	0	0
4 beams + cross (55-45,pinned)	0	0
4 beams + cross (60-40,clamped)	0	0
4 beams + cross (55-45,clamped)	0	0
Deck (60-40)	4	0
Deck (55-45)	2	0

Table 4.25: Overview of the number of newly found failing members under the consequence load case

4.7. Progressive collapse

Failure of one member could lead to failure of other members. When this process repetitively continuous, it is called progressive collapse. The load that was carried by the failed member has to be taken over by other, neighbouring members. This is especially of importance for crucial members,braced members, or members carrying a large load.

Failure of a member in SACS is modelled with the use of member releases. This way any loads acting on the failing member can be transferred to the other members. The member release on one end is set at (000011) and for the other end at (100111). This implies that the axial load is transferred on one end, while the transverse loads are transferred on both ends. The member remains statically determined under this setup. Furthermore, all moments are released, except for torsion on one end. This is done to ensure stability of the failed member.

Progressive collapse is assessed for models with a maximum of five failing members, including $n_{cons,fail}$. However if one of the failing members is a MSF leg, progressive collapse will definitely occur. The lift beam loses one of its two connection points and the load case becomes unstable, since no momentum balance can be obtained. For the cases with more than five failing members, it is also presumed that progressive collapse certainly will occur. The progressive collapse results for the removal setups under consideration are shown in table 4.18.

Model	$n_{fail,tot}$	Progressive collapse
2 beams E-B (55-45,pinned)	1	No
2 beams+cross 1-5 (55-45, clamped)	2	Yes
2 beams+cross E-B (55-45, clamped)	2	Yes
4 beams E-B (55-45,pinned)	1	No
4 beams 1-5 (55-45,clamped)	2	Yes
4 beams E-B (55-45,clamped)	2	Yes
MSF deck 1-5 (60-40)	4	Yes
MSF deck 1-5 (55-45)	2	Yes

Table 4.26: Progressive collapse overview

The total number of failing members consists of the initially found failing members, and the newly found failing members when a consequence factor is applied. To assess the occurrence of progressive collapse, the design load case is used.

4.8. Structural feasibility

Three cases are defined in assessing the structural feasibility of the different models to lift reference topsides 14 using the lift beams. A distinction is made between three cases:

- Yes. The topsides has sufficient structural capacity to withstand the lift loads without need for strengthening.
- Conditional. The topsides can be lifted under the given setup, however strengthening of a select number of members will be required.
- No. The lift is physically unstable, which is the case for the models where torsion of the lift beams is unrestrained. Or, too many failing members are identified and strengthening of all these members is considered to be inefficient.

MSF leg connection	Rigging load distribution	Connection type	Structurally feasible?
One-sided leg support 1-5 direction	60-40 distribution	Pinned	No, torsion needs to be restrained
		Clamped	No, too many failing member
	55-45 distribution	Pinned	No, torsion needs to be restrained
		Clamped	No, too many failing member
One-sided leg support E B direction	60-40 distribution	Pinned	No, torsion needs to be restrained
		Clamped	No, too many failing member
	55-45 distribution	Pinned	No, torsion needs to be restrained
		Clamped	No, too many failing member
One-sided leg support with cross-beams 1-5 direction	60-40 distribution	Pinned	Yes
		Clamped	Leg strenghtening
	55-45 distribution	Pinned	Yes
		Clamped	Leg strenghtening
One-sided leg support with cross-beams E-B direction	60-40 distribution	Pinned	Yes
		Clamped	Leg strenghtening
	55-45 distribution	Pinned	Yes
		Clamped	Leg strenghtening
Two-sided leg support 1-5 direction	60-40 distribution	Pinned	No, torsion needs to be restrained
		Clamped	No, too many failing member
	55-45 distribution	Pinned	No, torsion needs to be restrained
		Clamped	Leg strenghtening
Two-sided leg support E B direction	60-40 distribution	Pinned	No, torsion needs to be restrained
		Clamped	No, too many failing member
	55-45 distribution	Pinned	No, torsion needs to be restrained
		Clamped	Selective strenghtening
Two-sided leg support with cross-beams 1-5 direction	60-40 distribution	Pinned	Yes
		Clamped	Yes
	55-45 distribution	Pinned	Yes
		Clamped	Yes
Two-sided leg support with cross-beams E-B direction	60-40 distribution	Pinned	Yes
		Clamped	Yes
	55-45 distribution	Pinned	Yes
		Clamped	Yes
MSF deck 1-5 direction	60-40 distribution	Axial	Column strengthening rows A & F
	55-45 distribution	Axial	Column strengthening rows A & F
MSF deck E-B direction	60-40 distribution	Axial	Yes
	55-45 distribution	Axial	Yes

Figure 4.22: The number of critical members in the 1-5 direction for a 60-40 distribution (left) and a 55-45 distribution (right)

4.9. Conclusions

- A topsides structural integrity analysis is performed in SACS on reference topsides 14. A variety of options has been investigated. The models differ in connection location, connection type, lift beam configuration and rigging load distribution.
- The MSF legs and the MSF deck are both found to be suitable connection locations for the lift beams.
- The rigging load distribution has shown to have a great impact on the topsides' structural integrity. An increase in eccentric loading results in significantly larger reaction loads at some of the connection points. These effects become clearly visible when looking at the number of critical and failing members. The corresponding global moment, acting on the topsides, has shown to be of less significance.
- For the MSF leg connection models, a pinned connection is found to be most suitable. This type of connection is only feasible if outward twisting of the lift beams is restrained. In case of a clamped connection, the leg reaction moments have shown to take up majority of the MSF leg capacity, resulting in failure of the MSF legs.
- The addition of cross-beams is essential for the structural integrity of the topsides. For the MSF leg connections, the addition of cross-beams enables a pinned connection, since it restrains twisting of the lift beam. For the MSF deck connections, the cross-beam provides lateral stability to the lift beams. An important characteristic of the cross-beams is that the load case becomes statically undetermined, which results in redistribution of the load over the connection points in a favorable manner.
- Connecting the lift beams at their neutral axis with the MSF legs provides a significantly improved load transfer. The longitudinal shear force, which was found to take up a large portion of the MSF leg capacity, is not transferred in this manner. Also a clamped connection between the lift beams and the MSF legs can be applied this way, without occurrence of failure.
- Two-sided leg support with cross-beams is found to be the optimal lift beam setup for the MSF leg connection models. The difference in results with one-sided leg support with cross-beams is negligibly small for a pinned connection. This is partially due to the increased weight of the frame and hence the rigging loads. When a clamped connection is applied an improvement in the results can be observed. This is mainly due to a smaller weak-axis bending moment of the MSF leg.
- For the MSF leg connections, the orientation of the lift beams has shown to have little influence on the structural integrity of the reference topsides. The main factor here is the distance between the lift points and the connection points. It is hereby preferred to have a short distance between the heaviest loaded lift points and the connection points.
- For the MSF deck connections, it is essential that the interior primary columns are activated. This is achieved with the use of shim plates, which are applied on the exterior column rows. The position of the topsides CoG with respect to the connection points and especially the lift points, plays an important role in the structural integrity and stability of the topsides.

5
Connection between the lift beams and the topsides

In the previous chapter it was shown under which conditions the topsides can withstand it to be lifted by the lift beams. The lift beam set-up and the type of connection between the lift beams and the topsides are found to be decisive. The connection type determines where the load is transferred and in which form. The concept generation process has continuously been updated through this research. Where possible, important findings from the structural integrity analysis are implemented in the concept design. The three most promising connection concepts are discussed in this chapter; Two MSF leg connection concepts, the pin-hole connection and the geometric lock, and one MSF deck connection concept, the hydraulic jacks. The full range of connection concepts is provided in Appendix D.1. Important criteria for the connection concepts are the preparation – and connection time, the load transfer mechanism, the robustness and the costs. The connection concepts are designed for the two-sided support beams.

5.1. Connection concept criteria

The load transfer mechanism has shown to be of great influence for the topside structural integrity. However, there are also other aspects that are included in the assessment of the connection concepts. To evaluate each concept appropriately, four criteria have been defined: Preparation- and connection time, load transfer mechanism, robustness and costs. Evaluation of the concepts has been done through one-on-one sessions and panel sessions with company experts. The feedback from these sessions and an improving understanding of each concept's working principle have led to continuous development of the concepts. Below, the relevance of each criterion is briefly discussed.

Preparation -and connection time

The time required for the connection can be split up in preparation time and connection time. Preparations for the connection are mostly performed in the preparation phase, well before actual topside removal. The connection time is the time that is required to establish the connection between the lift beams and the topside and lies on the critical path of the topsides removal phase. A short preparation time will reduce the offshore man hours and total costs of the removal project.

Due to management of change, it is likely that a support vessel will have to be stationed while the preparations are ongoing. Management of change occurs when cessation of production is reached, which causes a shift of activities on the topsides. It is therefore uncertain whether the topsides can provide accommodation for the workmen. The support vessel will be needed for the transportation and housing of equipment, materials and workmen. It has to be noted that the preparation campaign would have to be repeated for each topsides in the batch.

Connection of the lift beams to the topsides falls between the installation of the lift beams and the removal of the topsides. Minimizing the connection time will therefore have a significant impact on the topsides removal time and the critical weather windows in which the operations can be performed.

Load transfer mechanism
The load transfer mechanism depends on the connection type and the location of the connection. Both the MSF legs and the MSF deck have proven to be potential connection locations for the lift beams concept. The type of connection determines the kind of loads are introduced at these locations. This has shown to be critical for the structural integrity of the topsides. Implementing the important findings from the structural integrity analysis are an important step in designing an appropriate connection.

It is aimed to design a connection for which strengthening of the topside is not required. Ideally, only vertical loads are transferred that are necessary to lift the topside off its substructure. In practice this is likely not feasible and therefore it is important to know which types of loads can be withstood by the topsides. The loads that are introduced to the lift beams are of less importance as the design of the lift beams can be adjusted to the load transfer. It is considered to be more efficient to strengthen the lift beams on-shore rather than repetitively strengthening the topsides off-shore.

Robustness
The robustness expresses the practicality, re-usability and durability of a connection type. It is important that the connection can relatively easily be applied in practice. Factors that influence the practicality are the size and weight of the connection element, it's working principle and the need or dependency of auxiliary tools.

The connection concept should be re-usable for a variety of topsides, without needing significant project specific modifications. Hereby, it is also important that the connection can easily be disconnected from the topsides once offloading has taken place. This way the lift beams can quickly be reused for another topsides removal project. The connection concepts must satisfy different topside layouts and geometries, and should therefore be movable, or integrated along the length of the lift beam. The durability of the connection elements also influences the concept's re-usability and is characterised by the fragility of the elements and the risk of malfunction.

Costs
Finally, the costs of the connection concept have to be taken into account. The lift beams topsides removal concept will only be applied when it shows to be cost-effective. The purpose of the lift beams concept is eventually to reduce the costs for topsides removal, and will only be economically viable when it can be used for multiple topsides. The costs for the connection concept are composed of the connection element costs and preparation costs. The latter includes the costs for a support vessel, materials required for the preparation scope and offshore man-hours.

5.2. Connection concept design

In this section the design of the connection concepts is discussed. The governing topsides load case and geometrical properties are used as input. Design of local lift beam modifications such as bearing stiffeners are also included in this section. The connection concept design is primarily based on hand calculations in accordance with API and DNV-GL guidelines. For the geometric lock an additional FEM analysis is performed in Abaqus to get a better understanding of the contact forces for this connection type.

5.2.1. Pin-hole connection

The pin-hole connection is a connection that previously has been used for the lifting and upending of large diameter piles. The pin is hydraulically driven into a hole that is prepared on the MSF leg. Lifting is based on bearing between the pin and the shell of the MSF leg. It is therefore expected that this method provides a quick, but safe and secure connection with the MSF legs. On each end, the pin is supported by a support frame, which is attached to to one of the adjacent beams. The frame can be skidded over the lift beam to the connection location, and can this way be applied to different topside layouts. The concept design is split up in a pin design and a support frame design.

Pin design

Design of the hydraulic pin is based on a combination of the highest MSF leg reaction force and the smallest MSF leg wall thickness. The MSF leg's shell thickness and the diameter of the pin determine the bearing area. The larger this area, the smaller the bearing stresses will be. The bearing capacity of the MSF leg could therefore be the governing factor for the pin design.

It has been decided to use a single pin rather than two separate pins. When two separate pins are used, the possibility exists that during lifting the pin is pushed out of the hole. As the pin makes contact with the shell of the leg, the pin will deflect and the orientation of the contact force changes, which could cause this effect. With a single pin this phenomenon can not occur. The downside of a single pin is however that the holes should align in order to properly install the pin and prevent eccentric loading of the MSF leg.

The pin capacity is examined with the LRFD method, which is in accordance with Eurocode 3, section 3 [13]. It has to be noted that the design of the hydraulic system is not considered. The relevant material properties of the pin are provided in table 5.1.

Element	Material	Diameter [mm]	Yield strength [MPa]	Tensile strength [MPa]
Hydraulic Pin	30NiCrMo8	625	590	780

Table 5.1: Properties of the hydraulic pin

Figures 5.1 and 5.2 provide a side view and a top view of the load case that is used for the design of the hydraulic pin and the support frame.

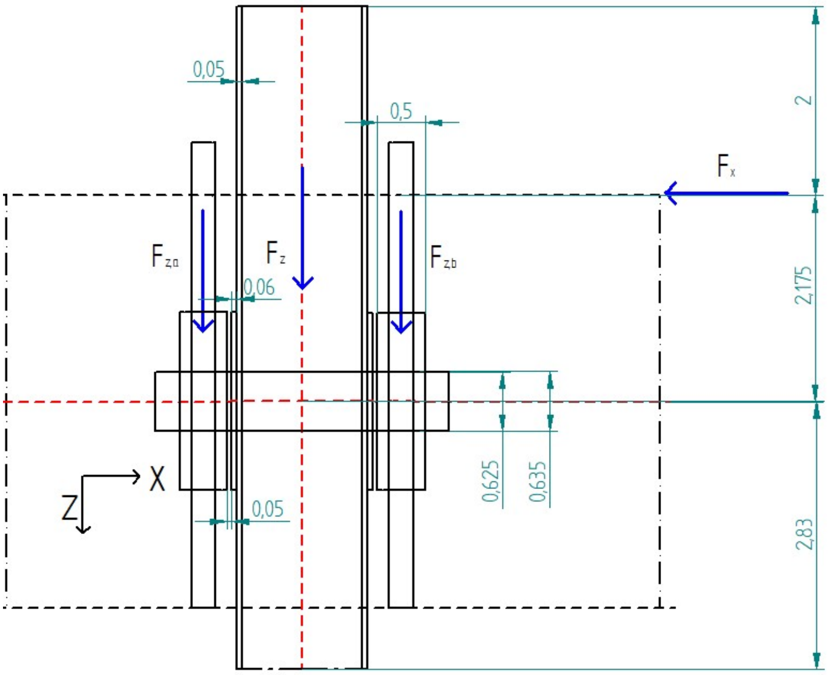

Figure 5.1: Side view pin-hole connection

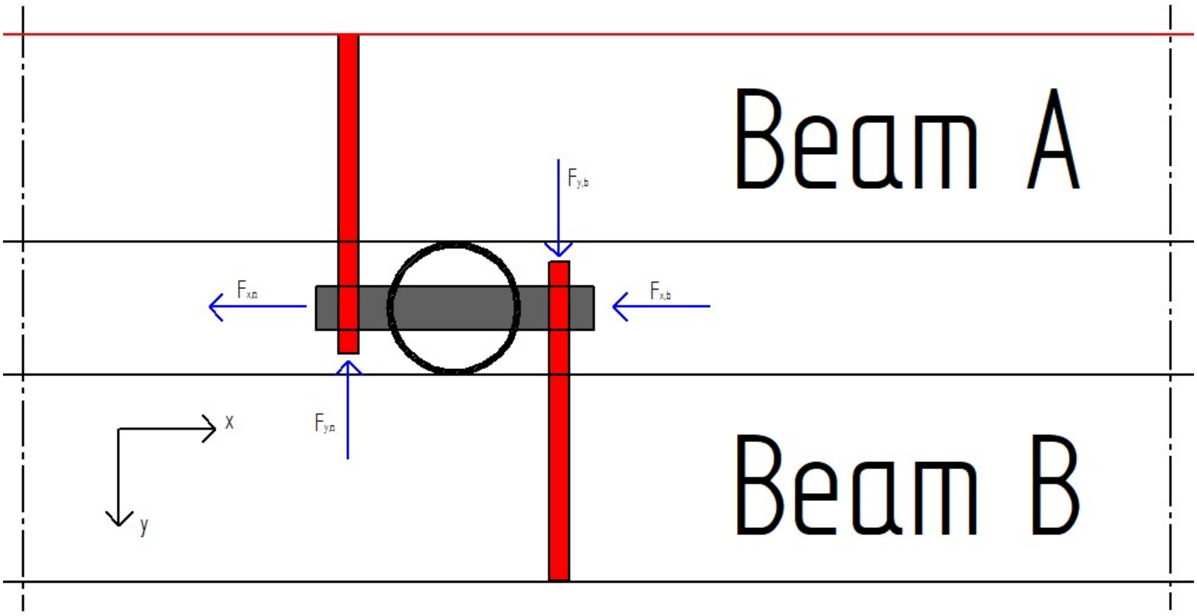

Figure 5.2: Top view pin-hole connection

The dimensions shown in figure 5.1 are summarized in table below.

D_{leg}	1372	[mm]
t_{leg}	50	[mm]
L_{leg}	7000	[mm]
e_1	4175	[mm]
e_2	2825	[mm]
D_{pin}	625	[mm]
D_{hole}	635	[mm]
$t_{spacerplate}$	60	[mm]
x_{offset}	50	[mm]
$t_{mainplate}$	250	[mm]
$t_{cheekplate}$	125	[mm]

Table 5.2: Properties of the hydraulic pin

The governing lift load, F_z, is the largest found leg reaction force, and is equal to 22.4 MN. For the design load, the governing lift load is multiplied with a consequence factor, μ_{CF}, of 1.3. The load distribution factor, μ_{dist}, over the two support frames is taken as 0.55. It is assumed that 55% of the lift load is taken by lift beam A. Additional side loads, F_x and F_y, which are equal to 5% of the vertical force, are considered to act simultaneously on the pin. Table 5.3 provides an overview of the design loads and load factors.

$F_{d,z}$	29.12	[MN]
$F_{d,z,A}$	16.02	[MN]
$F_{d,z,B}$	13.10	[MN]
$F_{d,y,A}$	801	[kN]
$F_{d,y,B}$	655	[kN]
$F_{d,x,A}$	801	[kN]
$F_{d,x,B}$	655	[kN]
μ_{CF}	1.3	[-]
μ_{dist}	0.55	[-]

Table 5.3: The design loads and corresponding load factors used for the pin design

The UC's for the leg's bearing capacity and the pin's structural capacity are shown in table below. Derivation of the UC's is provided in Appendix D.2.

$UC_{br,leg}$	0.98	[-]
$UC_{v,pin}$	0.20	[-]
$UC_{b,pin}$	0.46	[-]
$UC_{comb,pin}$	0.25	[-]
$UC_{br,pin}$	0.93	[-]

Table 5.4: The UC's of the pin and the MSF leg

It can be seen that the leg's bearing capacity is governing in the design of the hydraulic pin. As the diameter of the pin increases, the bearing surface between the pin and the leg increases, resulting in more bearing capacity. An alternative to increase the bearing capacity, and hence reduce the dimensions of the hydraulic pin, is to create the pin-hole connection below the MSF leg's stabbing cone. This way the bearing capacity is provided by the shells of the MSF leg and the jacket leg. Creating the holes for the connection would be more complicated under this set-up, since holes would have to be burned through two separate shells.

Support Frame design

The pin support frame is designed in compliance with API WSD and HMC's standard code for lift point design [34]. Figure 5.3 provides a front view of the support frame.

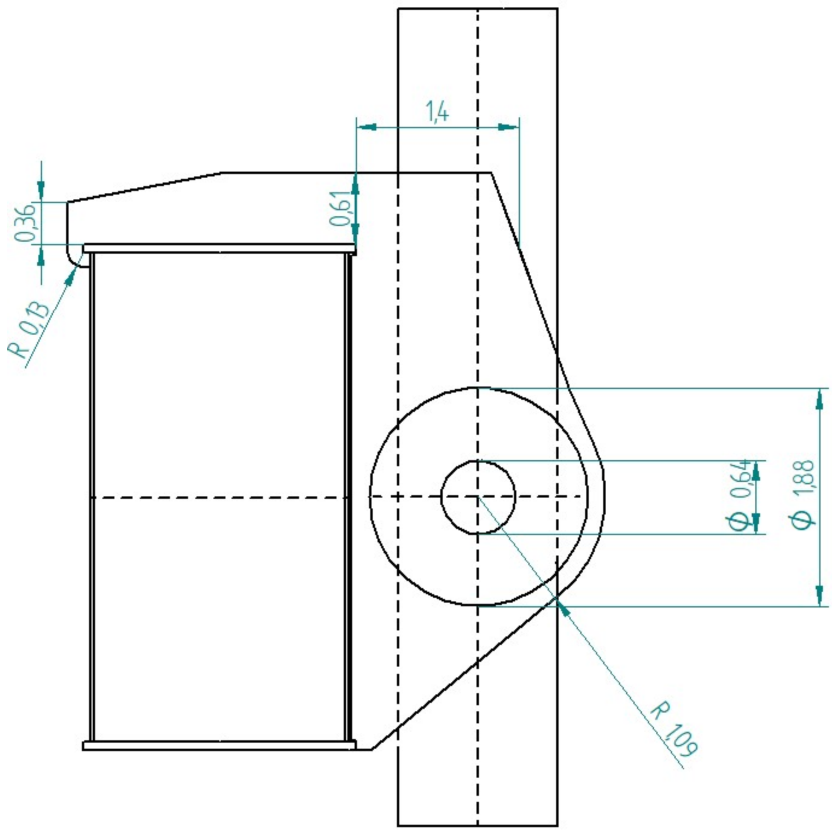

Figure 5.3: Front view of the pin support frame

The hole is positioned at the center line of the lift beam to avoid transfer of longitudinal shear forces, as discussed in section 4.5. The center of the hole also aligns with the center line of the MSF leg. On the top left corner, the frame is hooked onto the compression flange to restrain relative rotation of the frame with respect to the lift beam. At the right bottom, the frame is cut short from the tension flange to ensure the flange is only axially loaded.

After determining the shape of the support frame, the first step is to obtain the main plate and cheek plate properties. The cheek plate is welded to the main plate to provide sufficient capacity for peak stresses that occur around the hole. A range for the radius and thickness of the plates can be determined with rules of thumb, which are expressed in terms of the pin diameter [34]. Derivation of these parameters is provided in Appendix D.2. Steel grade S355J2+N is used for the support frame. The yield strength of the plates is reduced according to the plate thickness. The design properties of the support frame are provided in table 5.5.

t_{main}	250	[mm]
r_{main}	1094	[mm]
$F_{y,main}$	255	[MPa]
t_{cheek}	125	[mm]
r_{cheek}	938	[mm]
$F_{y,cheek}$	295	[MPa]

Table 5.5: Design properties of the support frame

For the design of the support frame it is assumed that only a vertical load is transferred between the pin and the support frame. In reality it is likely that also a transverse and longitudinal load component are transferred. Their magnitude is expected to be negligibly small compared to the vertical load, and hence these loads are not considered. The assumed load case for the support frame is illustrated in figure 5.4.

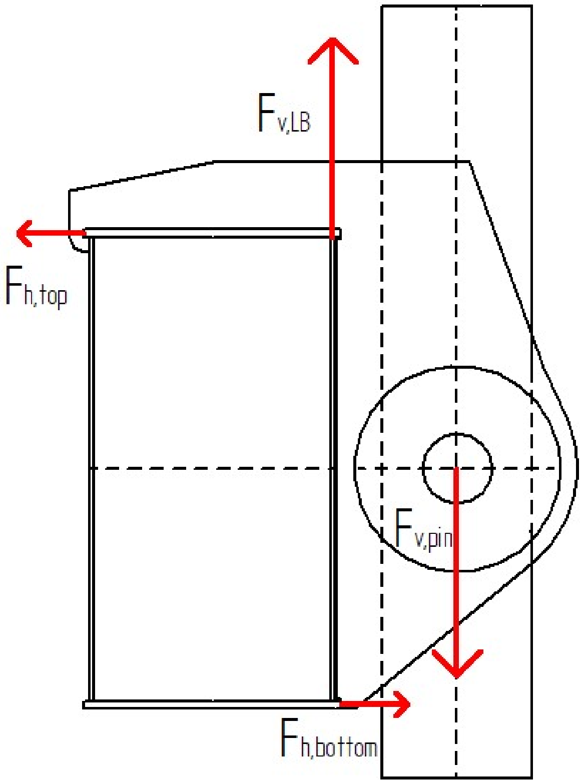

Figure 5.4: Pin support frame load case

During lifting, the lift beam will rotate towards the MSF leg due to eccentric loading. In this case the frame will lean against the web closest to the MSF leg. To make the load case statically determined, it is assumed that this web will completely provide the upward reaction force. The downward force from the pin and the upward force from the lift beam's web form a couple. This couple has to be counteracted by a horizontal force couple in order to obtain momentum balance. These horizontal reaction forces are assumed to be provided by the flanges of the lift beam.
The downward force transferred by the pin is assumed to be 55 % of the leg load, as discussed in the previous section. The upward force is equal in magnitude to provide vertical equilibrium. The horizontal forces are obtained by considering in-plane momentum equilibrium.

$$F_{v,pin} = F_{v,LB} = 0.55 * 22.4MN = 12.3MN \tag{5.1}$$

$$F_{h,top} = F_{h,bottom} = \frac{F_v * x_v}{z_h} = 3.2MN \tag{5.2}$$

Where:

$$x_v = r_{main} + \Delta + \frac{t_w}{2} = 1094 + 20 + 15 = 1129mm \tag{5.3}$$

$$z_h = H_{LB} - t_f = 4350 - 70 = 4280mm \tag{5.4}$$

Here, Δ represents the offset between the lift frame and lift beam web. The lift frame is checked on axial stresses, bending stresses and shear stresses. The resulting combined plate stresses are checked as well. This is done at critical sections of the support frame, which are indicated in figure 5.5.

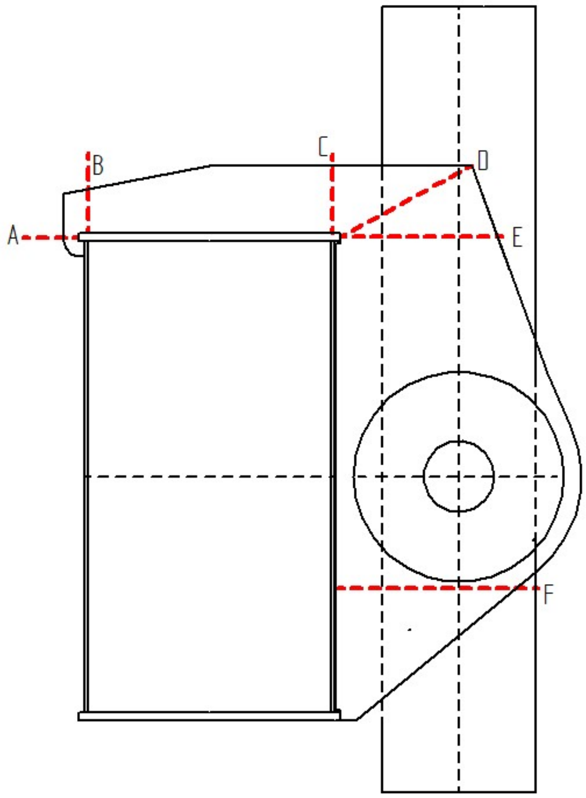

Figure 5.5: Critical sections support frame

The critical sections are defined where the reaction forces are introduced to the frame and where the largest bending moments are expected. The governing UC for each section is provided in table 5.6.

$UC_{A,v}$	0.98	[-]
$UC_{B,a+b}$	1.00	[-]
$UC_{C,VM}$	1.00	[-]
$UC_{D,VM}$	0.93	[-]
$UC_{E,a+b}$	0.92	[-]
$UC_{F,VM}$	0.20	[-]

Table 5.6: Governing UC of the critical sections

At sections C, D and F the Von Mises stress was found to be governing. For cuts B and E the combination of tensile stresses and bending stresses results in the largest stress combination. Finally , the shear stress was the governing stress in section A. The bottom of the frame, connected to the tension flange, experiences the same load case as section A and therefore is assigned the same dimensions. Derivation of the stresses and the UC's is provided in appendix D.2.

Lift point check

To verify whether the stresses around the hole are within limits, a padeye capacity check is performed using an in-house sheet. The extract of this sheet can be found in Appendix D.2.

Local lift beam stiffeners

Bearing stiffeners are applied at locations of concentrated loads to avoid phenomena such as local web yielding, local web crippling and sidesway web buckling. If the UC for one of these phenomena is exceeded, bearing stiffeners will have to be applied. The UC's are provided in Appendix D.2.
It is found that the occurrence of sidesway web buckling can be neglected. Local web yielding and web crippling are however expected to occur and therefore bearing stiffeners will be required. The case of local web yielding is governing in this, with a unity check of 3.53. The required area to prevent web yielding equals:

$$A_{tot} = \frac{R}{\sigma_a} = \frac{12.3}{0.6 * F_{y,w}} = 0.047m^2 \tag{5.5}$$

For a single plate interior stiffener it may be assumed that a portion of the web, equal to $25t_w$, participates in the load carrying [36]. The remaining area has to be taken by the stiffener.

$$A_{st} = A_{tot} - A_{web} = 0.047 - (25 * 0.03) * 0.03 = 0.025m^2 \tag{5.6}$$

A single plate bearing stiffener is aimed to be used. The required stiffener area has to be multiplied with a factor of 2.4, as discussed in section 3.4.4. The thickness of the stiffener plate becomes:

$$t_{st} = \frac{2.4 * A_{st}}{b, red} = 0.03m \tag{5.7}$$

It has to be noted that the location of the concentrated loads differs for each topside, and therefore bearing stiffeners would be needed at different locations for different topsides. Two possible solutions are considered for this problem. Firstly, the bearing length could be increased such that the UC's for local web yielding and local web crippling are satisfied. The plate thickness of the support frame, which represents the bearing length, would have to be increased significantly. This can be avoided by using a transition piece at the interface between the pin lift frame and the lift beam flange. The transition piece distributes the concentrated load over a greater surface.

Another option is to use the transverse intermediate stiffeners as bearing stiffeners. This is allowed since the bearing stiffeners don't have to be at the exact location of the concentrated load. The thickness of the stiffeners would have to be increased from 0.02 to 0.03 m. The bearing stiffeners are applied over the full interior height in order to transfer the load to the complete cross-section.

For the first option the bearing length has to be increased to 1.3 meters. The transition piece can be a footing plate at the interface between the support frame and the compression flange. The plate would have to be designed such that it can withstand the loads and equally distribute them over its length. If the second option is chosen, the stiffeners have to be checked on their compression column buckling capacity. To assess this the slenderness of the stiffener is determined.

$$I = \frac{t_s * b_f^3}{12} + \frac{(25t_w - t_s) * t_w^3}{12} = 0.025m^4 \tag{5.8}$$

$$A = t_s * b_f + (25t_w - t_s) * t_w = 0.086m^2 \tag{5.9}$$

$$r = \sqrt{\frac{I}{A}} = 0.54m \tag{5.10}$$

$$\frac{KL_e}{r} = \frac{1 * 0.75 * (4.35 - 2 * 0.07)}{0.54} = 5.85[-] \tag{5.11}$$

$$F_a = 260MPa \approx 0.6 * 440 \tag{5.12}$$

The buckling criterion is satisfied and a stiffener plate thickness of 0.03 m will therefore suffice.

5.2.2. Geometric lock

The geometric lock is a connection that creates an enclosed shape between the lift beams and the MSF leg when the lift beams are lifted. The upward lift force is initially driven by a combination of friction and normal forces. When the two bodies have fully settled, lifting is assumed to be completely provided by the normal forces. This scenario is considered to be governing, since the horizontal contact forces would be largest in this case. Different variations can be thought of for the geometric lock. The chosen design is provided in figure 5.6.

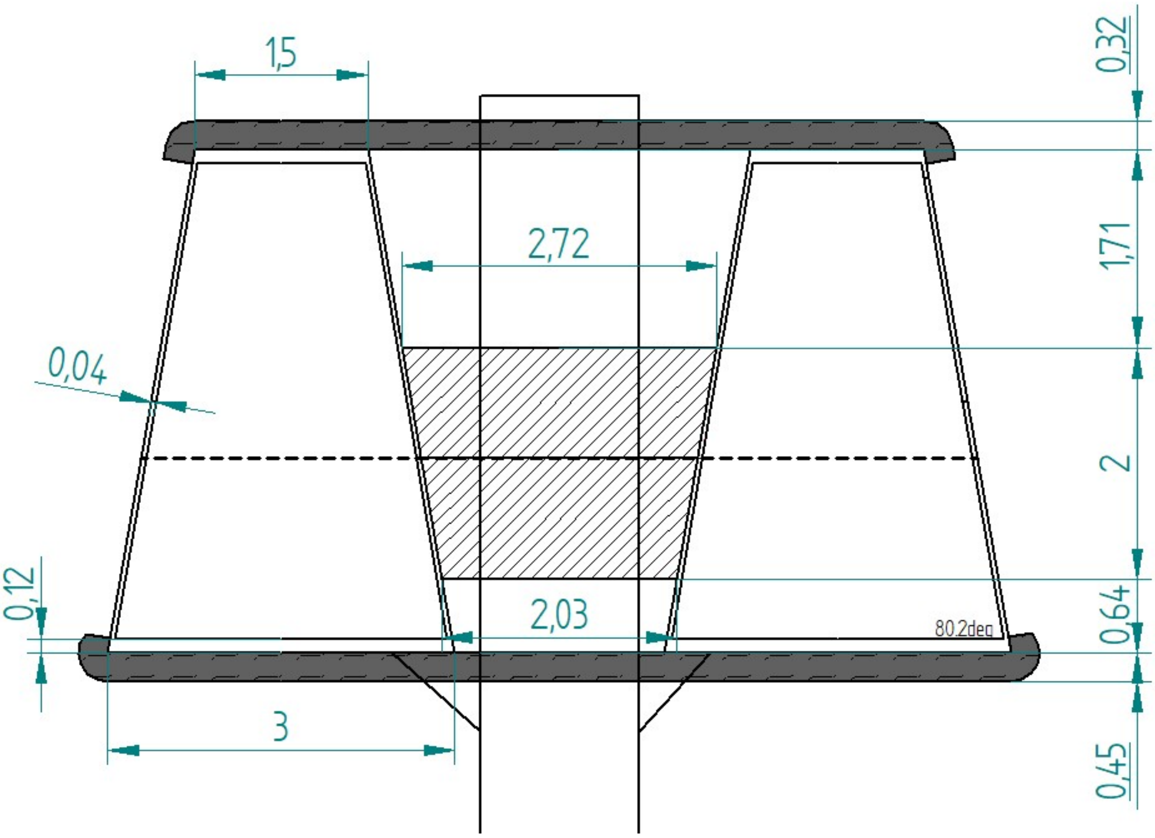

Figure 5.6: Geometric lock cross-sectional design

The enclosed shape is formed by the trapezoidal shaped lift beam profile and a steel wedge that is welded on the MSF leg. The centre line of the lift beam is aligned with the centre line of the wedge. This way the contact forces will act through the center line of the lift beam and additional moments are avoided. During lifting the lift beams are pushed outwards by the contact forces. This motion is resisted by the tension rods, which take up most of the horizontal component of the contact load. To provide momentum balance, it is necessary that tension rods are applied at the top and bottom of the lift beams. The angle that is taken for the contact surface is a trade-off between the size of the lift beams and the magnitude of the contact load. For larger angles the width of the lift beams can be reduced, and the lift beams can be positioned closer to the MSF leg. However, the normal component of the contact loads will increase when the angle of the contact surface increases. The height of the lift beams must provide sufficient sliding length, while maintaining enough spacing between the tension flange and the MSF leg.

Lift beam design

The horizontal component of the contact loads, that act on the lift beams, are taken by the tension rods. Bearing stiffeners will be needed to initially absorb the contact forces, and subsequently transfer them to the rest of cross-section and eventually to the tension rods. This way, the tension rods will resist torsion and weak-axis bending of the lift beams. The trapezoidal lift beam profile can therefore be designed for the same global load case as described in section 3.2. As for the box-profile lift beams, S460NL steel has been used. The cross-sectional properties are provided in table 5.7.

$(b/t_f)_{top}$	12.2	[-]
$(b/t_f)_{bottom}$	24.0	[-]
h/t_w	104.3	[-]
A	0.869	$[m^2]$
s	1.34	$[m]$
I_y	2.75	$[m^4]$
I_z	0.71	$[m^4]$
I_t	1.41	$[m^4]$
W_y	0.84	$[m^3]$
W_z	0.33	$[m^3]$
r_y	1.78	$[m]$
r_z	0.91	$[m]$
$F_{y,f}$	380	$[MPa]$
$F_{y,w}$	440	$[MPa]$
ρ_{st}	7.85	$[tn/m^3]$

Table 5.7: Overview of the cross-sectional properties of the trapezoid beam

The flanges are classified as compact and the webs as non-compact. The same sectional allowable stresses are used as described in Appendix D.2. The UC's of the cross-section are provided below.

$$UC_{(b,A)} = \frac{f_{b,y,max} + f_{b,z,max}}{0.60 F_{y,f}} = 0.92$$

$$UC_{(v,C)} = \frac{f_{v,z,max} + f_{v,t,w}}{0.18 F_{y,w}} = 0.98$$

$$UC_{(a)} = \frac{f_a}{min(F_{a,bckl}, F_{a,ltb})} = 0.01$$

$$UC_{(n,A)} = max(\frac{f_a}{F_a} + \frac{C_{my} f_{by}}{(1 - \frac{f_a}{F'_{ey}}) F_{by}} + \frac{C_{mz} f_{bz}}{(1 - \frac{f_a}{F'_{ez}}) F_{bz}}, \frac{f_a}{0.60 F_y} + \frac{f_{by}}{F_{by}} + \frac{f_{bz}}{F_{bz}}) = 0.92$$

$$UC_{(HUB)} = max(\frac{\sqrt{(f_{b,y,B} + f_{b,z,B} + f_a)^2 + 3 * (f_{v,z,av} + f_{v,t,B})^2}}{0.66 F_{y_w}}, \frac{\sqrt{(f_{b,y,A} + f_{b,z,A} + f_a)^2 + 3 * (f_{v,y,av} + f_{v,t,A})^2}}{0.66 F_{y_f}}) = 0.93$$

Over the length of the lift beam, nine intermediate transverse stiffener plates are used with a spacing of 5 meters. The thickness of the stiffener plates is equal to 0.02m. The use of transverse intermediate stiffeners will allow for larger allowable shear stresses in the webs. The spacing of the stiffeners is chosen such that a shear stress UC of 1.0 is approached. The thickness of the stiffener plates is the same as for the box-profile beams. This is allowed since the same global load case is applied.

As previously mentioned, bearing stiffeners are also required to absorb the contact loads at the lift beam-wedge interface. Figure 5.7 provides an overview of the contact loads.

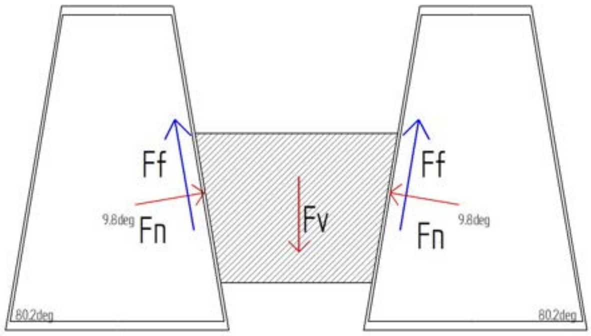

Figure 5.7: Contact loads for the geometric lock

The contact loads can be decomposed in a friction force ,F_f, and a normal force, F_n. The kinematic friction force is active while the lift beams are sliding with respect to the wedge. Once sliding of the two objects has stopped, a static friction force acts on the contact surfaces which has a maximum value of $F_{f,s,max} = \mu_s * F_n$. The actual magnitude of the static friction force however is unknown. Therefore the worst case must be assumed, which is the case without friction. The vertical leg load, F_v, is counteracted by the normal forces in this case. The maximum static friction force and the normal force are determined with equations 5.13 and 5.14.

$$F_n = \frac{0.5 * F_v}{sin(9.8)} = \frac{0.5 * 22.4}{sin(9.8)} = 65.8MN \tag{5.13}$$

$$F_{f,s,max} = \mu_s * F_n = tan(9.8) * 72.4 = 11.4MN \tag{5.14}$$

The webs of the lift beam are designed to take up the maximum static friction force. The bearing stiffeners are single plates that are designed as compression columns to take up the total normal force. In reality the flanges will also contribute in the load uptake, but the load first has to be borne by the bearing stiffeners before it can be transferred to the other elements. The bearing stiffeners also need to provide sufficient stiffness to the web's contact surface in order to maintain continuous contact with the wedge.

The bearing stiffeners should ideally be placed at the center of the contact area. This will allow for a continuous and relatively equally spread load transfer. The location of the contact area on the lift beam however differs for each topsides. An envelope can be created in which all of the potential contact areas lie. This is shown in figure 5.8.

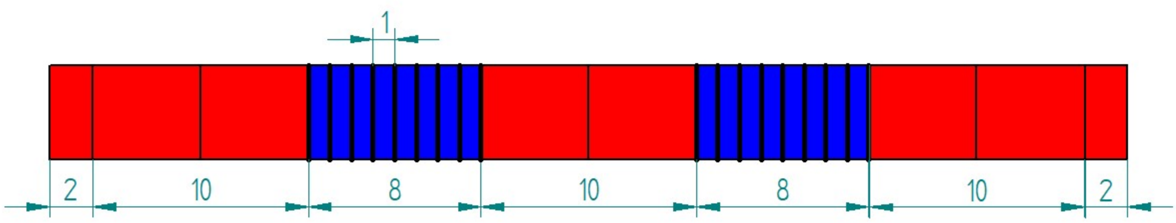

Figure 5.8: Overview of the bearing stiffener location on the lift beam

The potential contact areas lie in the blue area, which has a total length of 16 meters. The connection points of some topsides lie reasonably close to each other. To approach the center of each contact area, it is decided to apply a bearing stiffener spacing of 1.0 meter. This implies that each wedge will activate at least two bearing stiffeners. It has to be noted that the inactive bearing stiffeners will act as transverse intermediate stiffener, and hence no intermediate stiffeners need to applied in the blue region. The thickness of the bearing stiffener plates is determined with equations 5.15 to 5.20.

$$A_{st} = \frac{65.8 * 0.5}{0.6 * F_{y,w}} = 0.125m^2 \tag{5.15}$$

$$t_{st} = \frac{2.4 * A_{st}}{(H - 2 * t_f)/sin(80.2)} = 0.075m \tag{5.16}$$

$$I_{st} = \frac{0.075 * ((4.35 - 2 * 0.12)/sin(80.2))^3}{12} = 0.45m^4 \tag{5.17}$$

$$A_{st} = 0.075 * (4.35 - 2 * 0.12)/sin(80.2) = 0.31m^4 \tag{5.18}$$

$$r = \sqrt{\frac{0.45}{0.31}} = 1.2m \tag{5.19}$$

$$F_a = 263MPa \approx 0.6 * 440 \tag{5.20}$$

It can be seen that a thickness of 0.075m suffices for the bearing stiffener plates. In the red regions intermediate transverse stiffeners are applied as single plates with a plate thickness of 0.02m. Their spacing is equal to 5 meters, which results in two intermediate stiffeners on the outer red regions, and one intermediate stiffener in the central red region. The end panel distance is equal to 2 meters, and satisfies the end panel distance limit.
The dry weight of the trapezoid lift beam is equal to:

$$W_{dry,beam} = 0.869 * 50 * 7.85 = 341mT$$

The total dry weight of the stiffeners is equal to:

$$W_{stiffeners} = (18*(H_{red}*(B_{top,red}+B_{bottom,red})/2*t_{st,br})+5*(H_{red}*(B_{top,red}+B_{bottom,red})/2*t_{st,int}))*7.85 = 101mT$$

The total weight of the trapezoidal lift beam is therefore equal to $442mT$. Based on the weight it can be seen that the load case is unfavorable for the lift beam. This is due to the shape of the lift beam and the contact loads which are much higher than the required vertical load to lift the topsides off its substructure.

FEA model setup

To get a better understanding on the contact loads and the system's response to these loads, it has been decided to model the geometric lock with FEA software. Abaqus is chosen for this purpose, since this software is useful to grasp complex local phenomena such as contact interaction. The beams and MSF legs are modelled as shell elements, because of their slender profile. The wedge is modelled as a solid element. The weld between the leg and the wedge is modelled as a tie constraint acting over a surface that is equal to the fillet weld size. An impression of the model is provided in figure 5.9.

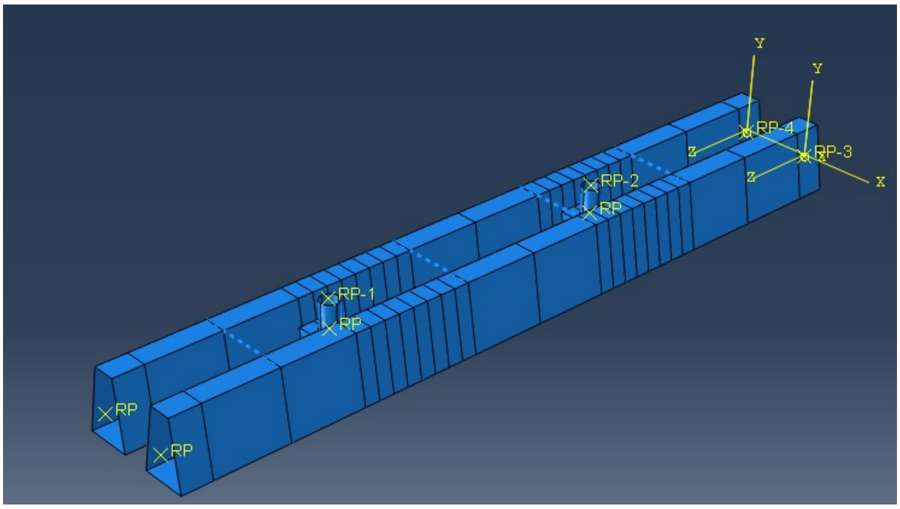

Figure 5.9: Geometric lock modelled in Abaqus

The stiffeners are modelled as shell elements, and are applied at the partitions as discussed in the previous section. The top of the MSF legs is modelled to be fully fixed. In reality the fixed base of the MSF leg has a finite stiffness. However due to the stiff support of the MSF leg's base it is considered that assuming a fully fixed base is reasonable.

The lift beams' ends are unrestrained, and the governing load case is applied as described in section 3.2. Weak springs in z-direction are applied to one of the lift beam's ends to ensure model stability. The interaction between the lift beams and the wedge is modelled as hard contact, which implies that only normal forces are generated at the contact area. No friction is considered as it will provide a more beneficial load case for both the lift beams and the MSF leg. The load case that is modelled can therefore be considered as governing.

In the contact interaction the lift beams' webs are assigned to be the master surface and the wedge as the slave surface. Several rules exist in determining the master surface and slave surface. The master surface should be the stiffer surface as it will impose the loads, and its response to the loads, to the slave surface. It is therefore important that the master surface doesn't experience local buckling phenomena. This way it can be ensured that contact between the surfaces is maintained. It is also preferred that the master surface is the longer surface to avoid that the surfaces will slip off. Regarding the mesh, it is advised to take a coarser mesh for the master surface to prevent penetration of the master nodes into the slave surface. The interaction surfaces are indicated in figure 5.10.

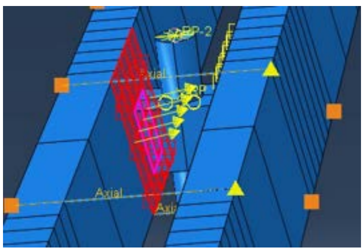

Figure 5.10: Master surface (in red) and slave surface (in pink)

The arrows indicate the direction of the normal force, which is imposed by the master surface onto the slave surface. The tension rods are modelled as elastic axial connectors, and can take up both a compression and a tension force. It is therefore important to verify whether the axial load acts in tension. The rods are attached to the outer nodes of the lift beams' flanges. Tension rods are applied on the top and bottom of the lift beams to provide rotational stability. A stiffness is assigned to the tension rods according to equation 5.21.

$$k_{rod} = \frac{EA_{rod}}{L_{rod}} \tag{5.21}$$

$$A_{rod} = \frac{F_t}{0.6 * F_{y,r}} \tag{5.22}$$

The tension rods prevent relative motions between the lift beams, and the wedge, in x-direction. The rods can only absorb tension, and the cross-section is therefore designed to withstand the maximum tensile force. A yield strength of 355 MPa is taken for the tension rods. The length of the tension rods is fixed and equals 6.2 meters at the top and 7.7 meters at the bottom. Their position is indicated in figure 5.11.

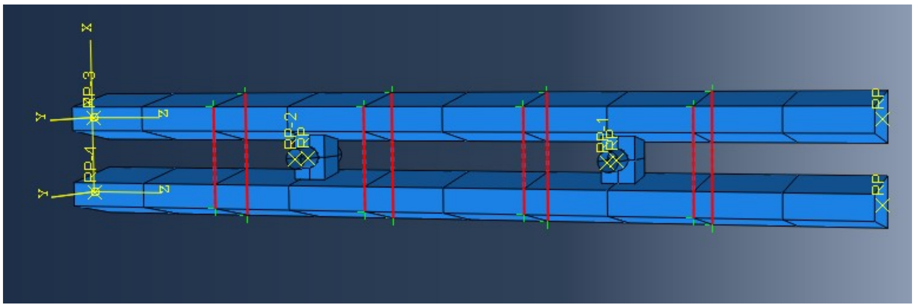

Figure 5.11: Position of the tension rods

An initial stiffness is assigned to the tension rods, which is iteratively updated based on the resulting maximum tension force. Longitudinal motions of the tension rods are restrained thereby ensuring that contact is maintained. Finally, for the analysis a static load step is used, where the load is built up linearly over a period of 1 second. An energy dissipation term of 2e-4 is used to provide stability for the interaction. This is often necessary when a force-driven model is considered.

FEA results

With the FEA it is aimed to get an insight on the contact forces and the resulting stresses in the lift beam, the wedge and the MSF leg. The system's response is analysed once all parameters are set. Therefore, first the maximum axial load in the tension rods is determined and the stiffness is correspondingly updated until the difference with the previous iteration step is negligibly small. Hereafter it is determined whether the lift beams and the MSF leg can withstand the governing load case. The results are validated by checking the reaction forces and moments and the system's energy output. If the reaction forces and moments are as expected, it is assumed that the system is modelled correctly. The dissipated energy term, used to obtain model stability, shouldn't affect the system's response. Therefore a limit is put on the dissipated energy, which is equal to 1% of the system's internal energy.

A different axial stiffness is defined for the upper and the lower tension rods. This follows from a difference in length and a difference in force uptake. Since the tension rods at the bottom are closer to the lift beams' neutral axis, these rods will absorb a larger portion of the contact force. The maximum axial connector forces for the top and the bottom tension rods is plotted in appendix D.2. It can be seen that the tension rods only provide a tension force. The maximum tension force for the top tension rods is equal to 16.6 MN and for the bottom tension rods 33.6 MN. The cross-sectional area and stiffness of the rods is then equal to:

$$A_{rod,top} = \frac{16.6}{0.6 * 355} = 0.078 m^2 \tag{5.23}$$

$$k_{rod,top} = \frac{210e9 * 0.0855}{6.2} = 2640MN/m \tag{5.24}$$

$$A_{rod,top} = \frac{33.6}{0.6 * 355} = 0.158m^2 \tag{5.25}$$

$$k_{rod,top} = \frac{210e9 * 0.169}{7.7} = 4302MN/m \tag{5.26}$$

$$D_{rod,top} = 0.32m \tag{5.27}$$

$$D_{rod,bottom} = 0.45m \tag{5.28}$$

The maximum Von Mises stresses in the lift beam are shown in Appendix D.2. It can be seen that globally the stresses are within limits. However, peak stresses are observed, as high as 464 MPa, at the contact surface with the wedge. The peak stresses mainly occur at the interface between the lift beam's web and the bearing stiffeners. These stresses are most likely caused by a sudden stiffness change in the contact surface. Due to this, the stiffer cells will take up a larger portion of the load. This is mainly a result of discretization in the numerical analysis and the mesh size. It is assumed that in reality the stresses are distributed across the continuum.
Furthermore it can be noticed that the flanges of the lift beams and neighbouring stiffeners are also activated in the load uptake. This implies distribution of the stresses from the contact surface to the rest of the cross-section. Excluding the peak stresses, it is found that the Von Mises stresses in the contact surface are limited to approximately 272 MPa. It is therefore assumed that the lift beam has sufficient capacity to withstand the governing load case.

$$UC_{VM,web} = \frac{272}{0.66 * 440} = 0.94[-] \tag{5.29}$$

The maximum Von Mises stresses in the governing leg are also provided in Appendix D.2. Peak stresses are observed at the interface with the wedge, which represents the weld between the two elements. All stresses acting on the wedge near the tied surface are transferred to the leg's tied surface. This results in a condensed load transfer over a relatively small surface, which is 0.1m in height. The peak stresses are as high as 250 MPa. It can be seen that the loads are subsequently distributed over the height of the leg. Excluding the peak stresses, the maximum Von Mises stress in the governing leg is found to be 190 MPa. This means that the leg has sufficient capacity to withstand the governing load case. The yield strength of the leg is equal to 335 MPa.

$$UC_{VM,leg} = \frac{190}{0.66 * 335} = 0.86[-] \tag{5.30}$$

Finally the maximum stresses in the wedge are shown in Appendix D.2. Yet again peak stresses are observed at specific nodes, which lie on the interface with the stiffeners. In general it can be said that the wedge has sufficient capacity to withstand the load case.
The results are verified by looking at the system's energy output and the reaction forces and moments at the boundaries. Verification of the results can be found in Appendix D.2.

5.2.3. Hydraulic jacks

From the topsides structural integrity analysis it was found that a small change in gap size results in large deviation of the transferred load. This implies that lifting the topsides using shim plates is sensitive to potential fabrication offsets. The result is an uncontrolled load transfer. The use of hydraulic jacks on the other hand will provide a predictable and remotely controlled load output.

The hydraulic jacks are designed to have sufficient capacity to withstand the maximum expected axial load. The jacks also need to have sufficient height and stroke capacity to overbridge surrounding obstacles and establish contact with the connection point. This way sufficient clearance is maintained between the lift beams and the MSF deck.

The jacks are positioned under the primary columns of the topsides ,as discussed in chapter 4, and are divided in three groups. In each group the jacks are hydraulically linked to provide an equal load output. This load output is independent of the stiffness of the lift beams or the rigging load distribution. It is not known yet how much load is transferred at each connection location. However, the topsides should be lifted in a stable manner, which means that moment equilibrium should be achieved around the topsides' CoG. The load out-put for each jack group is therefore dependant on their location with respect to the topsides' CoG. For each hydraulically linked group a resultant force can be defined. The load case becomes statically determined when three separate groups are defined. The topside can only be lifted stably when the topsides CoG lies within the resultant force triangle. Figures 5.12 5.13 give an overview of this.

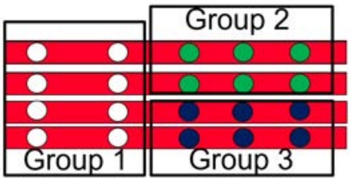

Figure 5.12: Top view of the hydraulic jack groups

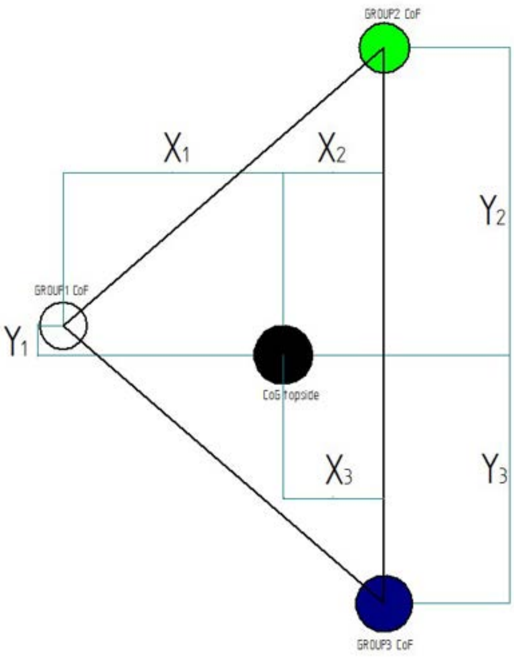

Figure 5.13: Statically determined load case with the resultant forces of each jack group

When the distances between the CoF of each group and the topsides CoG are known, the resultant forces can be determined based on vertical force equilibrium and moment equilibrium around the x- and y-axis. This is presented by equations 5.29, 5.30 and 5.31.

$$F_{Res1} + F_{Res2} + F_{Res3} = F_{topside} \tag{5.31}$$

$$F_{Res1} * x_1 - F_{Res2} * x_2 - F_{Res3} * x_3 = 0 \tag{5.32}$$

$$F_{Res1} * y_1 - F_{Res2} * y_2 + F_{Res3} * y_3 = 0 \tag{5.33}$$

The force per jack is then determined by dividing the resultant force by the number of jacks in the group.

$$F_{jack} = \frac{F_{Res}}{n_{jacks}} \tag{5.34}$$

The topsides CoG and the location of the hydraulic jacks can be determined from drawings and additional offshore surveys. The jacks are designed to withstand the maximum expected load. Due to a lack of data, it is assumed that for the governing load case, the topsides load can be distributed over 20 jacks. Each group has a different load output, depending on its location. To be conservative it is assumed that the governing jack group takes 50% of the total load.

$$F_{jack,max} \approx \frac{10000 * 0.5}{6} = 833.3mT \tag{5.35}$$

Assuming S245 steel, this results in a minimum piston diameter of 0.27 m. The height and stroke capacity of the jacks should also be large enough to maintain sufficient spacing with the MSF deck. Different types of hydraulic jacks are found on the market which satisfy the lifting capacity. The relevant properties of the reference jack are shown in table below. The jacks are equipped with swivel eye bolts, which enable lifting under an angle.

Capacity	1000	[mT]
D_{piston}	0.38	[m]
D_{body}	0.53	[m]
$H_{extended}$	0.66	[m]
H_{stroke}	0.15	[m]

Table 5.8: Properties of the reference jack

The load output from the jacks is also considered to be favorable for the structural integrity of the lift beams, since the load is distributed over multiple points. The exact location and magnitude of the loads is unknown. It is however expected that the load case is more favorable than when the lift beams are connected to the MSF legs. Therefore the lift beam design for two-sided leg support is used. It is assessed whether bearing stiffeners are required in this case. The UC's for web yielding and web crippling are provided below. Their derivation can be found in Appendix D.2.

$$UC_{webyielding} = 0.99$$

$$UC_{webyielding} = 1.04$$

It can be seen that under the current configuration web crippling is expected to occur. This could be prevented by adding bearing stiffeners. The location of the hydraulic jacks however changes for each topsides. Increasing the bearing length, the base diameter of the jacks, is therefore considered to be more cost-effective. To satisfy both UC's, the base diameter of the jacks would have to be increased to 0.75m. For this sake, a transition piece can be used between the jacks and compression flange.
It is suggested to house the hydraulic system within the lift beams. Holes have to be created for the hydraulic instrumentation that travels between the lift beams. The fluid capacity and pressure at capacity should be sufficient to provide the required jack loads. Design of the hydraulic system is out of the scope of this project and will not be discussed any further.

5.3. SACS Implementation

In this section it is shown how the connection concepts are modelled in SACS. This allows to investigate the influence of each connection concept to the topsides' structural integrity. The connection concept is also generalized in this way, which means that it can easily be implemented for different load cases or lift beam setups.

5.3.1. Pin-hole connection

The pin-hole connection is modelled with the MSF leg's member end releases, which are set at (001101) for direction 1-5 and (010110) for direction E-B. It is assumed that only forces in vertical and transverse direction are transferred, since only forces in these directions are applied. Also looking at the pin-hole interface, it can be seen that the pin is only restrained in these directions. In reality a longitudinal friction force between the pin and leg could be acting. This force component is considered to be negligibly small compared to the other forces. Weak springs are applied in this direction at one of the lift beam's ends to ensure model stability.

Rotations around the lift beam's strong axis are fully restrained, which means that there are no relative rotations between the pin and the lift beam in this direction. This restraint is considered to be valid, assuming that the pin is stiff enough, and therefore won't undergo additional rotations. This results in a portion of the lift beam's bending moment being transferred to the MSF leg. Rotations around the other axes are unrestrained and therefore no moments around these axes are transferred. In reality a non-zero stiffness could be defined in these directions. Their stiffness is however expected to be negligibly small compared to the strong axis rotational stiffness. These fixity's are considered to valid assumptions.
The length of the MSF legs is extended to 4 meters below deck. The lift beams are connected at their neutral axis with the MSF legs. An impression of this is shown in figure 5.14.

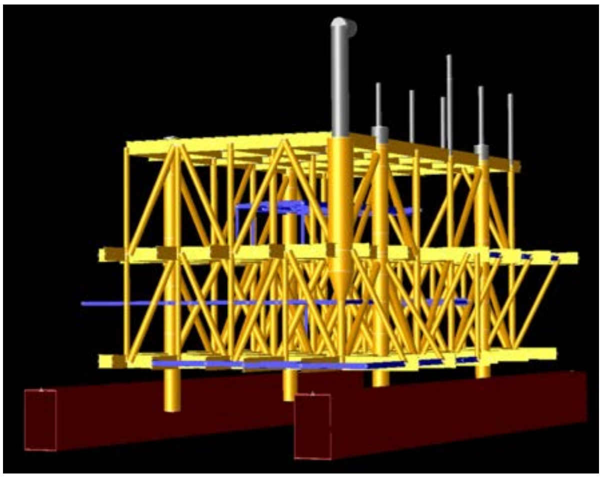

Figure 5.14: Lift beams connected at their neutral axis with the MSF leg's free end

The UC's of the MSF legs and the number of critical and failing members for direction 1-5 and direction E-B are shown in tables below. It has to be noted that torsion of the lift beams is unrestrained for this connection type, and therefore the lift beam setups consisting of cross-beams are only considered.

Direction 1-5	UC_{PB10}	UC_{PB50}	UC_{PE10}	UC_{PE50}	n_{crit}	n_{fail}
One-sided leg support + cross, 60-40	0.55	0.48	0.49	0.42	5	0
One-sided leg support + cross, 55-45	0.49	0.42	0.42	0.36	4	0
Two-sided leg support + cross, 60-40	0.51	0.44	0.45	0.38	5	0
Two-sided leg support + cross, 55-45	0.45	0.39	0.39	0.33	5	0

Table 5.9: Topsides structural integrity results for the pin-hole connection in 1-5 direction

Direction E-B	UC_{PB10}	UC_{PB50}	UC_{PE10}	UC_{PE50}	n_{crit}	n_{fail}
One-sided leg support + cross, 60-40	0.48	0.46	0.42	0.39	6	0
One-sided leg support + cross, 55-45	0.42	0.40	0.37	0.33	5	0
Two-sided leg support + cross, 60-40	0.44	0.42	0.40	0.35	8	0
Two-sided leg support + cross, 55-45	0.39	0.36	0.34	0.30	5	0

Table 5.10: Topsides structural integrity results for the pin-hole connection in E-B direction

The topsides structural integrity results show that the topsides can withstand it to be lifted with the pin-hole connection. Furthermore it has to be noted that no progressive collapse occurs in any of the models.

5.3.2. Geometric lock

The geometric lock is also implemented in SACS with the use of leg end releases. In Abaqus it was confirmed that for this connection concept negligibly small forces are transferred to the MSF legs in longitudinal direction of the lift beams. The transverse and vertical direction are considered to be fully fixed, as no relative motions are expected in these directions between the lift beams and the MSF leg. Furthermore, it is assumed that all three rotational DoF's are fully fixed. This assumption is not completely valid, since relative rotations are likely to occur. It is therefore advised to further investigate the rotational stiffness of the connection.

For the 1-5 direction this comes down to a member end release of (001000) and (010000) for direction E-B. To verify whether these assumptions are reasonable, the leg reaction forces and moments from SACS and Abaqus are compared with each other for the same load case. To make the comparison valid, the lift beam's properties are adjusted to represent the structural properties of the trapezoidal shaped cross-section, shown in figure 5.6. The resulting reaction forces and moments for direction 1-5 and direction E-B for leg PB10 are shown below.

1-5 direction	**Abaqus**	**SACS**
Fx [kN]	60	154
Fy [kN]	3	0
Fz [kN]	12800	12550
Mx [kNm]	3286	2656
My [kNm]	2068	2360
Mz [kNm]	18	47

Table 5.11: Comparison of the MSF leg reaction forces and moments in SACS and Abaqus for the 1-5 direction

E-B direction	**Abaqus**	**SACS**
Fx [kN]	4	4
Fy [kN]	2.5	0
Fz [kN]	7400	7800
Mx [kNm]	903	760
My [kNm]	820	660
Mz [kNm]	9	28

Table 5.12: Comparison of the MSF leg reaction forces and moments in SACS and Abaqus for the E-B direction

Looking at the results it can be noticed that the obtained reaction forces are relatively close to each other. Regarding the reaction moments, clear differences can be observed, especially for the 1-5 direction. Several reasons exist for the differences in results:

- In Abaqus a fully fixed boundary is taken for the legs, while in SACS a finite stiffness is assigned to the base of the leg. In general this results in larger reaction moments in Abaqus. Also the influence of the remainder of the topside is not included in Abaqus. The leg reaction moments in SACS therefore may include terms that originate from other members or from global moments acting on the topsides.
- A part of the loads in Abaqus is absorbed by the wedge. The dimension of the wedge and hence the arm of the contact forces are also not included in SACS.
- Non-linear second-order effects are not included in SACS.
- The lift beam is stiffer at the contact surface due to the presence of bearing stiffeners. This is not included in SACS. This could be done by splitting up the lift beam in multiple sections, and locally assigning the corresponding properties.

Since no better modelling solution is obtained, it has been decided to use the aforementioned leg end releases to assess the influence of the geometric lock to the topsides structural integrity. The structural integrity results are provided in tables 5.13 and 5.14.

Direction 1-5	UC_{PB10}	UC_{PB50}	UC_{PE10}	UC_{PE50}	n_{crit}	n_{fail}
Two-sided leg support, 60-40	0.66	0.60	0.60	0.55	31	13
Two-sided leg support, 55-45	0.53	0.47	0.47	0.42	8	0
Two-sided leg support + cross, 60-40	0.69	0.61	0.62	0.55	5	0
Two-sided leg support + cross, 55-45	0.63	0.56	0.57	0.50	5	0

Table 5.13: Topsides structural integrity results for the geometric lock in 1-5 direction

Direction E-B	UC_{PB10}	UC_{PB50}	UC_{PE10}	UC_{PE50}	n_{crit}	n_{fail}
Two-sided leg support, 60-40	0.54	0.53	0.52	0.47	39	16
Two-sided leg support, 55-45	0.44	0.44	0.43	0.37	10	1
Two-sided leg support + cross, 60-40	0.41	0.36	0.33	0.29	6	0
Two-sided leg support + cross, 55-45	0.34	0.31	0.30	0.25	5	0

Table 5.14: Topsides structural integrity results for the geometric lock in E-B direction

It can be seen that the topsides can withstand it to be lifted with the geometric lock connection. Only when a 60-40 distribution is applied, without a cross-beam, a large number of critical and failing members is observed, with progressive collapse as a consequence. For the other models it was found that no progressive collapse will occur. Some uncertainty exists about the way the connection is modelled. It is therefore strongly advised to investigate the rotational spring stiffness for strong-axis bending and weak-axis bending of the connection. To ensure that the MSF legs have sufficient capacity to take up the contact loads, the stresses in the governing leg for load case L641 in 1-5 direction are provided in Appendix D.2.

5.3.3. Hydraulic jacks

The hydraulic jacks are modelled in SACS as concentrated loads acting on the MSF deck's connection points, the primary columns. The magnitude of the loads depends on the lift beam set-up, the location of the connection points, and how the hydraulic jack groups are defined. For the 1-5 direction, three lift beams are used with a total of 16 connection points. The definition of the groups is provided in figure 5.15.

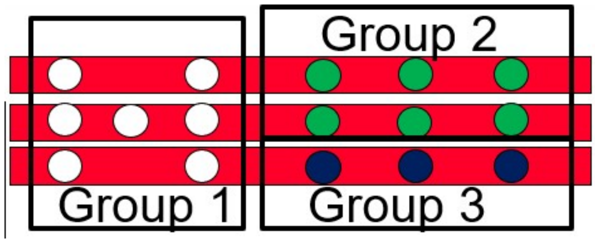

Figure 5.15: Hydraulic jack groups in 1-5 direction

For each group a resultant force can be defined, acting at the geometrical center of the group, the CoF. The topsides CoG lies within the triangle that is formed by the CoF's of the three groups, therefore stable lifting is possible. It is aimed to define the groups such that the difference in their distance to the topsides' CoG is as small as possible. This will allow for a more equal load distribution over the hydraulic jacks. The distances are provided in figure 5.16.

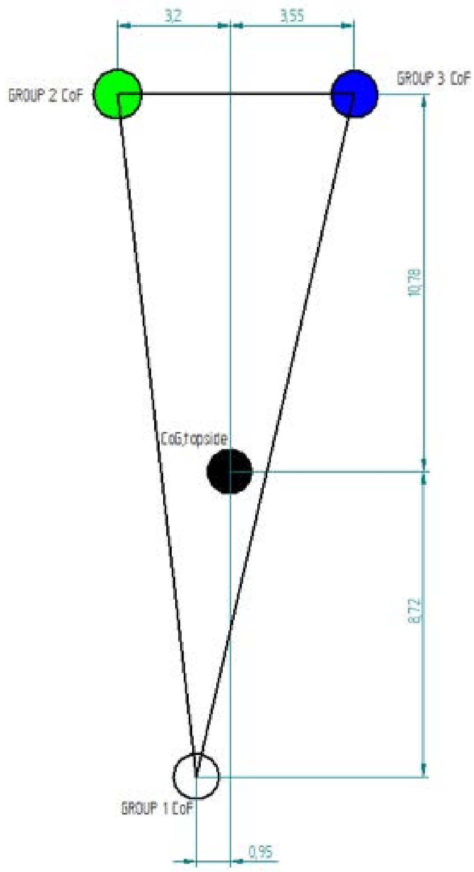

Figure 5.16: Hydraulic jacks force balance overview in 1-5 direction

The CoG of the topsides clearly tends to one side. This is due to the relatively short spacing between the lift beams , the small number of lift beams that is used, and the eccentricity of the topsides' CoG in this direction. The effects are clearly visible in the load distribution over the jack groups. The jack forces are provided in table below. Derivation of the forces is provided in Appendix D.2.

$F_{jack,1}$	2040	kN
$F_{jack,2}$	676	kN
$F_{jack,3}$	2501	kN

Table 5.15: Overview of the jack force per jack group in 1-5 direction

A large deviation is found in the load output of the hydraulic jacks. This is considered to be unfavorable for the design of the jacks, but especially for the structural integrity of the primary columns.
For the E-B direction, four lift beams are used over which 20 connection points are spread. The increased number of lift beams and connection points and the greater relative spacing allow for a better load distribution over the jack groups.

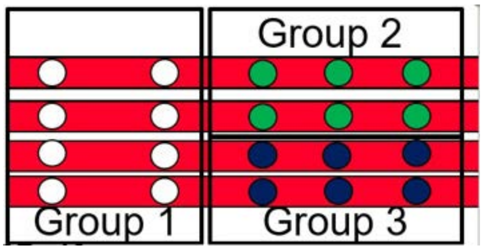

Figure 5.17: Hydraulic jack groups in E-B direction

Also the number of jacks per group is better distributed for this set-up. The relevant distances are shown in figure 5.18.

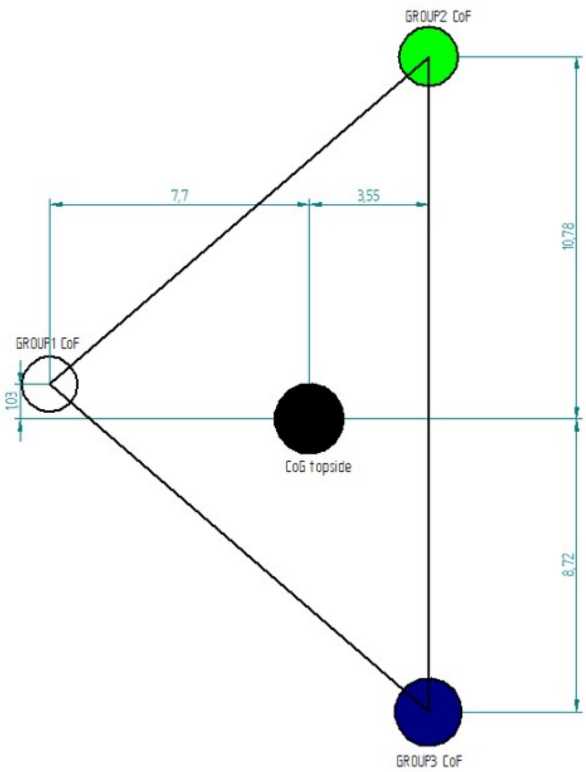

Figure 5.18: Hydraulic jacks force balance overview in E-B direction

The corresponding jack forces are provided in table below. Their derivation can be found in Appendix D.2.

$F_{jack,1}$	1018	kN
$F_{jack,2}$	1248	kN
$F_{jack,3}$	1701	kN

Table 5.16: Overview of the jack force per jack group in E-B direction

The jack forces are implemented in SACS as concentrated loads, as shown for direction E-B in figure 5.19.

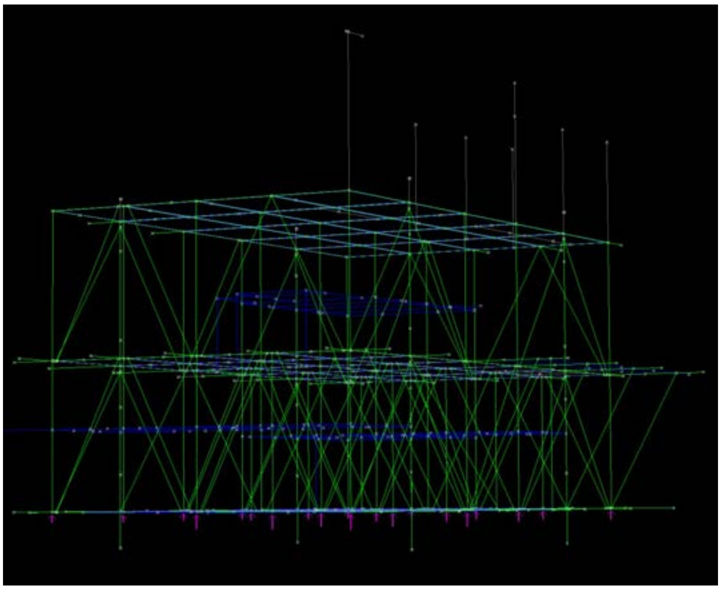

Figure 5.19: Hydraulic jack forces (in pink) in SACS for E-B direction

Additionally a 5% horizontal acceleration is considered to be acting on the topsides CoG. This implies that for each vertical load component, a horizontal component is added, acting at the same location. The horizontal component is perpendicular to the direction of the lift beams. This is a standard procedure in the analysis of hydraulic multi-axle load-outs. It was found that the effects of the horizontal acceleration are negligible for the structural integrity of the topsides. However, if the side load is eccentrically applied, an overturning moment would be acting on the topsides. This overturning moment could be counteracted by monitoring the pressure variation per jack group and accordingly adjust the load output. The number of critical and failing members for both directions is shown in table below.

	n_{crit}	n_{fail}
1-5 direction	5	0
E-B direction	4	0

Table 5.17: The topsides structural integrity results for the hydraulic jacks in both directions

It can be concluded that the topsides can be lifted in a favorable manner with the use of hydraulic jacks. The number of critical members and failing members is approximately equal to the in-situ case, and no progressive collapse will occur.

5.4. MCA evaluation

The connection concepts are evaluated on the previously discussed criteria: preparation- and connection time, load transfer, robustness and costs.

5.4.1. Pin-hole connection

Preparation -and connection time

The amount of required preparation -and connection time for the pin-hole connection is considered to be relatively short. The main activity is creating the holes in the MSF legs. The leg would have to be cleaned and tested prior to this. It is also important that prior to creating the holes, it is investigated whether some obstructions such as ring stiffeners are present within the MSF leg.

The holes can be created by means of burning or drilling. For the latter, the hydraulic pin could be used. The design of the pin would require extensive modifications for this, which would result in an inefficient pin design. It has therefore been decided to burn the holes in the MSF legs. The main concern in this method is alignment of the holes. To ensure alignment, a pin support sleeve could be used, which is attached to the pin support frame. Proper alignment can therefore only be achieved once the lift beams, including hydraulic pin and support frame, are in position.

The position of these elements is prepared on-shore, prior to lift beam installation. Burning of the holes therefore falls within the connection time. The burning process can be done simultaneously for all legs. Penetration of the pin into the hole is hydraulically driven and will therefore require a short period of time. After installation of the pin, the pin's ends are secured with bolts.

Load transfer mechanism

Regarding the load transfer, only forces in vertical and transverse direction are transferred to the MSF legs. These force components are required to lift the topside off its substructure, and transfer the transverse rigging loads to the topside. The hole is positioned on the center line of the MSF leg and therefore results in centric loading of the MSF leg. However, the strong-axis bending moment of the lift beams is also partially transferred to the MSF legs. It was found that these moments can take up a significant portion of the MSF leg's capacity. Looking at the topsides structural integrity results for the pin-hole connection, it can be seen that the topsides has sufficient capacity to be lifted with this connection type.

An alternative to the current pin-hole design is to rotate the pin's orientation by 90 degrees. This way transfer of the lift beam's strong-axis bending moment is prevented. Instead, a smaller weak-axis bending moment due to eccentric loading will be introduced. This setup is expected to be more favorable for the MSF leg, but provides difficulties in the installation procedure. Also the connection between the pin and lift beam is challenging for this setup.

Finally, the lift beam has shown to need some additional strengthening to provide sufficient capacity to withstand local failure mechanisms. The requirements for the bearing stiffeners are found to be relatively low.

Robustness

The pin-hole connection has previously been used for the lifting and upending of large diameter piles. The technology can therefore be considered as proven.
Extension of the pin is hydraulically driven and can be operated remotely in a controlled manner. The connection can only be established properly if the holes are aligned. This shouldn't be a problem with the aforementioned method. In preparation, the presence of ring stiffeners in the MSF leg should be checked, as the pin can't penetrate these elements. This connection type is considered to be safe and durable, with little risk of failure or malfunctioning. The pin itself is also quite robust considering its size and material properties.

Disconnection of this concept happens in reversed order and can relatively quickly be achieved. This way the connection can easily be reused for the removal of other topsides. The size of the lift frame does impose some limits to the lift beam's heave and sway motions during installation. This is however considered to be manageable. In general it can be concluded that this connection concept is quite robust.

Costs
The total costs for this connection concept are mainly composed of costs for the pin and the corresponding hydraulic system. These components are quite costly. However, it has to be noted that these costs are one-time investments for the removal of multiple topsides. The repetitively ongoing preparation costs and offshore man hours on the other hand are relatively low. The pin-hole connection is therefore considered to be cost-effective.

5.4.2. Geometric lock

Preparation- and connection time
The geometric lock requires significant preparation time. The wedge is fabricated on shore, transported to location, hoisted to the required elevation, and finally welded onto the MSF leg. Welding of the wedge onto the MSF leg is considered to be very time consuming and requires a lot of offshore man hours. Work access platforms have to be installed for the welders. To hoist the wedge, entrances have to be created in the MSF deck for the winch to pass through.

Prior to topsides removal, the lift beams are accurately positioned against the wedge. Once the position is set, tension rods have to be installed prior to lifting. This is expected to be a complex operation due to the location of the tension rods and their size. This activity falls within the critical path of the topsides removal process and could therefore result in serious delays.

Load transfer mechanism
The normal component of the contact forces has shown to be much higher than the required vertical lift load. Large bearing stiffeners are implemented in the lift beams to absorb the contact loads and subsequently transfer them to the tension rods. In this process, local yielding of the web's contact surface might occur due to peak stresses in the interaction surface.

The connection between the lift beams and the topsides is modelled as fully fixed, except for displacements in longitudinal direction. It was shown that the resulting stresses in the MSF legs are within limits, given that the wedge has sufficient capacity to absorb a portion of the contact loads. Also the remainder of the topsides has shown to be able to take up the loads for this connection concept. Considering the strengthening requirements, it can be concluded that the load transfer for the geometric lock is inefficient.

Robustness
To maintain contact during lifting, it is essential that the tension rods act properly. Failure of the tension rods directly leads to disconnection and failure of the removal process. It is therefore of great importance to select the right length and structural properties for the tension rods. Also their connection to the lift beams has to be performed precisely under limited conditions. To deal with varying connection points, a large number of bearing stiffeners will be implemented in the lift beams. Hereby, most of the stiffeners are not activated during the removal of a specific topsides.

An advantage of the geometric lock is that no connection elements are needed, other than the tension rods. The connection concept is therefore considered to be quite durable. Also, installation of the lift beams is expected to be relatively easy due to the limited size of the connection elements. After offloading, disconnection is simply achieved by lowering the lift beams.

Finally it is important to mention that a cross-beam is not necessarily needed for this connection concept, since the tension rods restrain the twisting motion of the lift beams. This could significantly improve the installation time of the lift frame.

Costs
The costs for this connection concept are considered to relatively high. The lift beams require extensive strengthening which has a significant impact on the total weight of the lift beam. Installation of the wedges for each topsides is not cost-effective and requires a lot of materials and offshore man hours in the preparation phase. It is likely that a support vessel will be needed during the preparation phase to accommodate and mobilize the workforce and equipment for the extensive welding scope. However, the ease of installation and disconnection could compensate for the total costs of this connection concept.

5.4.3. Hydraulic jacks

Preparation- and connection time

In the preparation phase, the MSF deck has to be prepared for connection with the hydraulic jacks. An even and clean contact surface has to be created. Any significant obstructions near the connection points have to be removed. Additionally guides are installed to ensure that the jacks are properly aligned with the topsides' primary columns. These guides also intend to ensure contact is maintained between the jacks and the primary columns. Prior to establishing the connection, the lift beams will rest on temporary supports, just like for the other connection concepts. However, due to the location of the primary columns, an extensive support structure will be required for this.

Prior to topside removal, the jacks have to be hydraulically linked, which could proof to be challenging. The hydraulic instrumentation travels between lift beams and therefore linking of the jacks can only be done after installation of the lift beams. Work access platforms have to be installed to make this possible. The connection of the hydraulic jacks can therefore be very time consuming. This process lies in the topsides removal phase and therefore serious delays have to be taken into account. After all the required preparations have been performed, the topsides can relatively quickly be lifted off its substructure.
Onshore, the jacks are positioned on the lift beams based on the structural layout of the topside. The hydraulic system is housed in the lift beams and must be prepared and tested.

Load transfer mechanism

The load transfer for this connection concept is favorable for both the lift beams and the topsides. From the topsides analysis, the position of the jacks can be determined and the optimal jack grouping can be defined. By hydraulically linking the jacks, it is ensured that there will be a constant load output per jack. This way the load transfer to the topsides can occur in a controlled and predictable manner. Also, no other forces than the vertical lift load are introduced for this connection concept. In practice, friction between the jacks and the connection points can occur. This force is however considered to be negligibly small.

The topsides structural integrity analysis has shown that removal with the hydraulic jacks is favorable, since a large number of columns can be activated. Looking at the lift beams, this connection type is also very favorable. The load is distributed over multiple points in the shear center line of the lift beam. Furthermore, there is no need for additional strengthening of the lift beams. Local failure is prevented by placing the jacks on a footing plate, which increases the bearing length.

Robustness

The hydraulic jacks are considered to be robust in their lifting capabilities, as the load transfer occurs in a predictable and remotely controlled manner. Their position on the lift beam however has to be altered for each topsides, and the hydraulic instrumentation has to be adjusted accordingly. The durability of the hydraulic jacks system depends on several components and it is therefore advised that the system is thoroughly checked prior to each topsides removal project. After topsides removal, a quick disconnection can be realized by lowering the lift beams.

Costs

The costs for the jacks and the corresponding hydraulic system are expected to be relatively high. Due to their favorable load transfer, no strengthening will be required for both the lift beams and the topsides. However, a large temporary support frame will be required to accurately position the lift beams underneath their connection row. This can result in relatively high costs.

5.4.4. MCA results

A score between 1 and 5 is assigned to each connection concept, based on the previously discussed evaluation criteria. Each criterion has a different weight, taking its importance for the total lift beams concept into account. The weighting of the criteria is shown in table below.

Preparation and connection time	30%
Load transfer	20%
Robustness	30%
Costs	20%

Table 5.18: Weighting of the connection concept criteria

Preparation and connection time, and robustness are given a greater weight since these criteria resemble the lift beam concept's long term performance. The preparation and connection time are important parameters that directly determine the topsides removal time for each topsides. The robustness indicates the ease of repetitive application of the lift beams concept. A robust concept will therefore require little project specific modifications and will limit the challenges of the lift beams concept.

The costs are the main driving factor for the realization of the lift beams concept. It is however considered to be more cost-effective to have higher initial investment costs than continuous project specific costs. This way more costs can be saved in the long term. The load transfer between the lift beams and the topsides is also important, as this will result in lower costs for the lift beams. Also strengthening of the topsides can be prevented this way. As long as progressive collapse of the topsides won't occur it is not paramount how much of the topsides' capacity is required. Table 5.19 gives an overview of the scoring for each connection concept.

Connection concept	Preparation and connection time	Load transfer	Costs	Robustness	Total
Pin-hole connection	4	3.7	3.3	4	**3.8**
Geometric lock	2.3	3.2	3	3.5	**3.0**
Hydraulic jacks	3.2	4.5	2.5	3	**3.3**

Table 5.19: MCA results of the connection concepts

It can be seen that the overall highest score is achieved by the pin-hole connection. This connection concept is therefore selected as the most suitable for the lift beams concept, and will be considered as the designated connection in the remainder of this report. It has to be mentioned that a change in weighting of the criteria results in a change in the total score. However, looking at the scores per criterion, it can be seen that the pin-hole connection has the highest score on each category except for the load transfer criterion.

5.5. Conclusions

- Three connection concepts have been analysed: the pin-hole connection, the geometric lock and the hydraulic jacks.
- The connection concepts are designed to withstand the governing load case. For the pin-hole connection and the geometric lock bearing stiffeners are locally applied on the lift beam to take up the concentrated connection loads. For the hydraulic jacks an alternative solution is considered, where the bearing width of the connection is increased.
- The effect of each connection concept to the topsides' structural integrity has been investigated. It was found that the reference topsides has sufficient capacity to be lifted with each of the connection types.
- The connection concepts are evaluated on four criteria: preparation and connection time, load transfer, robustness and costs.
- Through a MCA it has been decided that the pin-hole connection is most suitable for the lift beams concept.

6 Installation of the lift beams underneath the topsides

In the previous chapter the connection between the lift beams and the topsides has been discussed. After analysing the concepts, it was found that the pin-hole connection is most suitable for the lift beams concept. What rests to determine is how to install the lift beams beneath the topsides. Several installation concepts have been generated to find the optimal method for installation of the lift beams. In this chapter, the three most promising installation concepts are discussed. The full range of concepts can be found in Appendix E. After evaluation, one installation concept will be selected for further analysis. For this concept, the installation procedure will be defined and its installation performance will be assessed. The concepts are evaluated on installation time, practicality, costs and robustness. A distinction is made between frame installation and beam-per-beam installation.

6.1. Installation concept criteria

Assessment of the installation concepts is based on four criteria: installation time, practicality, costs and robustness. Evaluation of the concepts has been done through one-on-one sessions and panel sessions with HMC experts. Important input from these sessions are especially the limitations of each concept and the requirements to make the concept practically feasible. Below, the relevance of each criterion is briefly discussed.

Installation time

The installation time of the lift beams directly influences the total topsides removal time. The critical weather windows in which the operations can be performed also plays an important role here. The critical weather windows are a function of the duration of the operation and the limiting motions that are imposed to the lift beams during installation.

The installation time indicates the total time that is required to complete the installation of the complete lift beam setup. The installation starts with attaching the rigging and ends with laying the lift beams down onto temporary supports. For the frame installation concepts, installation is expected to be completed in one or two operations, and the installation time of these concepts is therefore expected to be shorter. For the beam-per-beam installation concepts, each component of the lift setup is installed one-by-one and will therefore require a longer time to complete.

Practicality

Another important aspect to consider is the practicality of the installation concepts. The practicality indicates the practical feasibility of the installation concept and is mainly characterized by the limitations that each concept imposes. For the frame installation concepts the practicality is in general considered to be lower due to the size and weight of the frame and the layout of the frame. As the size and weight of the frame increases, there are more limitations to the lift operation. It is therefore likely that the workability of the concept also reduces. Due to the size and weight, the operation can only be performed by one of the SSCV's. Due to the lay-out of the frame the motions during installation become more limited, because clearance has to be maintained for multiple locations simultaneously.

Costs
The costs of the installation concept are also of importance as this will directly add up to the total costs for the lift beams concept. The costs for the installation concepts are composed of costs for required installation equipment, any necessary mechanics for the installation concept's working principle and the costs for the installation vessel. It is most likely that installation of the lift beams will be performed by one of the SSCV's during the topsides removal phase.

However, the opportunity also exists to perform the installation in the preparation phase with a smaller HLV. This is mostly useful for the beam-per-beam installation concepts, because of the lower lift requirements. This means that installation of the lift beams falls out of the critical path of the topsides removal phase. The offshore SSCV time can be reduced significantly this way, since the SSCV would only be used to lift the topsides off its substructure. In this case, the lift beams would need to rest on their temporary supports for an undisclosed period of time. The design of the connection and the temporary supports needs to take into account the occurrence of a potential storm.

Robustness
Finally the robustness of the installation concepts must be considered. The robustness of the installation concept mainly indicates its reusability and the limitations that it imposes to the complete lift beams concept. This includes project specific modifications for the installation, the lift beams-to-topsides connection, and the transportation and offloading phase. Another important aspect is the installation concept's dependency of auxiliary tools for its installation and working mechanism. The likelihood of failure or malfunctioning of such components is considered to be higher than that of 'raw' steel.

6.2. Installation concepts

6.2.1. Frame installation concepts

Rectangular frame
The rectangular frame consists of two lift beams attached to a cross-beam on each end. The idea of this concept is to lift the frame over the topsides and subsequently lower it below deck elevation. Once the frame is hanging on the right elevation, the lift beams are allowed to skid over the cross-beams to the connection points. Skidding can be performed either hydraulically, with the use of pushing strokes, or mechanically. For this installation concept, the only possible connection points are the MSF legs. An impression of the rectangular frame is given in figure 6.1.

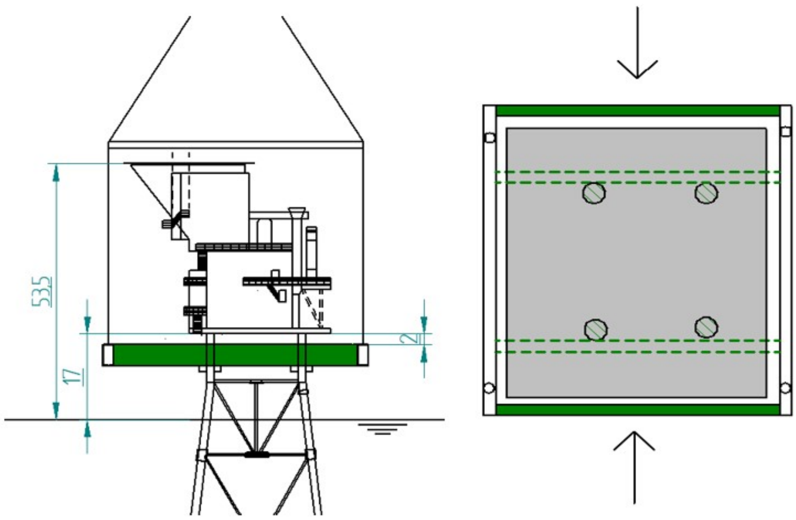

Figure 6.1: Impression of the rectangular frame

The length of the cross-beams must be approximately 60 meters in order for the frame to fit over all the topsides under consideration. An advantage of this is that the frame doesn't need to be modified for different topsides. Also there would be no need to separately install any of the cross-beams.

The lift points, located on the cross-beams, are used for both the installation and removal phase. The opportunity exists to remove the topsides right after connection, without need to attach the removal rigging. The rigging must have sufficient capacity for both load cases, without the occurrence of slack. Also a shift in CoG of the lift object occurs. Due to this, direct removal could only be feasible for the smaller topsides in the batch.

Forklift frame
For the forklift frame, the lift beams are attached to a cross-beam on one end. To provide momentum balance, a counterweight is attached to the other side of the cross-beam. The lift points for installation of the frame are provided by the counterweight. An impression of this is given in figure 6.2.

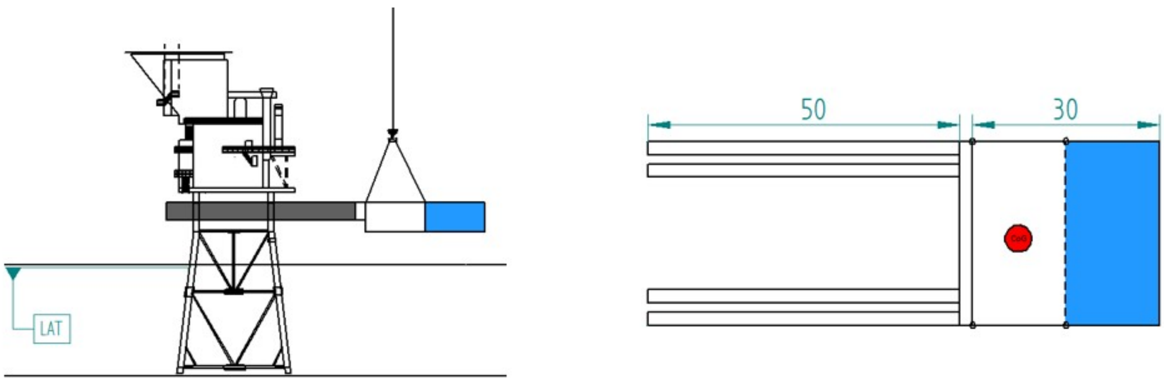

Figure 6.2: Impression of the forklift frame

Prior to installation, the lift beams are accurately positioned on the cross-beam, based on the location of the topsides' connection points. Due to the length and weight of the lift beams, a large counterweight will be required. A cheap solution for this is to use a steel box, in which seawater is used as the counterweight component. The steel box consists of two compartments, where the outer compartment is filled with water, providing a lever arm with respect to the assembly's CoG. The counterweight will significantly increase the size and weight of the frame during installation. An alternative solution is to split up the forklift frame per two lift beams to improve its ease of installation.

After installation of the lift frame, the outer compartment is drained, and the CoG shifts towards the cross-beam-counterweight interface. Hereby it is important that the counterweight CoG remains within the lift points envelope and the occurrence of slack in the rigging should be prevented. Another option is to drain the water from the outer compartment to the inner compartment after installation of the lift beams. This can be driven by gravity, using a tilted bottom for the counterweight. Hereby it is important that a quick disconnection between the cross-beam and the counterweight can be achieved in order to reduce the waiting time.

6.2.2. Beam-per-beam installation concepts

The lift beams can also be installed one-by-one. Two solutions are defined for this. The first option is to use a counterweight as described in the previous section. The size and weight of the counterweight are much lower in this case. For this procedure, one counterweight could be used for the installation of all lift beams, or for each lift beam a separate counterweight could be used. The latter option will improve the installation time, since there is no need to refill the steel box. The available deck space however would decrease with the presence of multiple counterweights.
Another option is to install the lift beams sideways with the use of a spreader bar, which is oriented parallel to the lift beams, as indicated in figure 6.3. It has to be noted that this method of installation is only possible for lift beams on the outer side of the MSF legs.

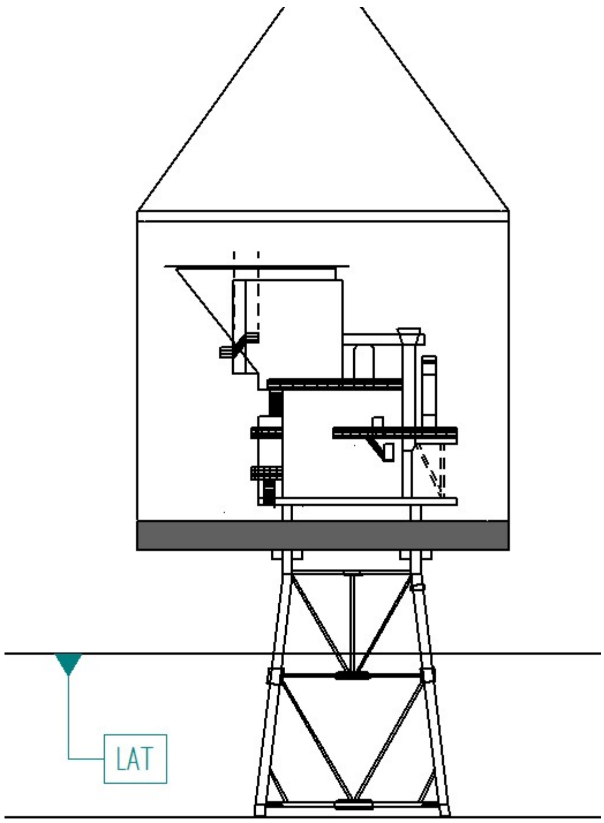

Figure 6.3: Side way lift beam installation using a spreader bar

6.3. Installation concept evaluation

The connection concepts are evaluated on four criteria: installation time, practicality, costs and robustness. At the end of this section a score between 1 and 5 is assigned for each criterion. The installation concept with the highest total score will be selected as the optimal installation concept for the lift beams.

6.3.1. Rectangular frame

Installation time

Installation of the rectangular frame is expected to be a sensitive operation due to the size and weight, and the manner of installation of the frame. After lifting off the SSCV's deck, the frame is accurately positioned above the topsides. The position of the frame must be such, that when lowered clearances are maintained along all sides. It is expected that the positioning and lowering of the frame, under calm conditions, will take a reasonable amount of time. Once lowered, the lift beams skid towards the connection points, which should to be a relatively short operation. In general it can be said that the lift operation is sensitive for motions during installation and can likely only be performed under limited conditions. The installation time is however considered to be short, as installation is completed after a single lift.

Practicality

Some practical challenges arise for installation of the rectangular frame. To install the frame a rigging setup consisting of at least two floating spreader bars will be required. The slings that are attached to the lift points will need a length that is sufficiently greater than the height of the topsides. This way the frame can be lowered without the risk of rigging clashing with the topsides. The rigging arrangement and the installation method, e.g. lifting over the topside, require a large hook elevation. Prior to topsides removal, the drilling derrick and flare boom would likely have to be removed due to this. During lowering of the frame, it has to be checked whether the crane boom maintains sufficient clearance with the topsides. From the topsides analysis it was found that this installation method is not feasible for the larger topsides, as the crane boom envelope intersects with some of the topsides during lowering. The motions of the frame should also be limited during skidding of the lift beams. The frame itself moves relative to the platform due to the SSCV's motions. When moving components are included, these relative motions will only increase. A heave compensator could be used to dampen the motions of the frame during the critical operations.

The rectangular frame can most likely only be applied to topsides that have a maximum of two MSF leg rows. For topsides with more MSF leg rows, the rectangular frame can't be connected to the interior rows, and therefore can't provide sufficient support to lift the topsides. As discussed before, the opportunity exists to directly remove the smaller topsides. In this case, there is no need to install temporary supports for the frame to rest on. However, in order to establish the connection, the frame would have to hang still. This could be achieved by hanging the frame off the topsides once lowered. Additional strengthening of the topsides could be needed in this case. For most topsides, direct removal is not possible and the frame would need to be laid down onto pre-installed temporary supports.

Transportation and installation of the frame can only be performed by one of the SSCV's. Taking the sensitivity of the lift operation and the practical limitations of this concept into account, this concept can only be applied for a limited period of the year, for a limited number of topsides.

Costs

The costs for the installation concept are mainly driven by the installation vessel, costs for the frame and costs for any additional installation equipment and mechanics. As previously mentioned, the rectangular frame can only be installed with one of the SSCV's, which is costly. The costs for the skidding mechanism, including the maintenance costs, are expected to be relatively high. Additional costs for auxiliary tools during installation, to limit the frame's motions, also need to be taken into account. Overall it can be said that the costs for the rectangular frame are relatively high.

Robustness
The rectangular frame is finally evaluated on its robustness. The rectangular frame can't be applied to each topsides. Also the sensitivity of the operation, would make the application of this installation concept limited. Frame-wise, this concept is also not considered to be very robust. Any defects during the skidding phase lead to direct delays or potential failure of installation. If the malfunction happens when the lift beams are beneath the topside, there is no point of return. The frame itself is also not braced, which implies that the frame could deform due to skidding of the lift beams.

Furthermore, the rectangular frame only provides lift beams on the outer side of the MSF legs. The topsides' support during lifting is therefore limited. As shown for reference topsides 14, removal under such a setup is possible. However for larger topsides, consisting of multiple rows of MSF legs, lifting with just two lift beams is considered to be insufficient. Also looking at the connection concepts, the rectangular frame can only be combined with the pin-hole connection.

6.3.2. Forklift frame

Installation time

The forklift frame provides a relatively quick solution for simultaneous installation of multiple lift beams, also between the MSF leg rows. The frame has a large size and weight due to the presence of the counterweight. Positioning of the frame is challenging as this has to be done for multiple lift beams simultaneously, without colliding with the topside. Installation of the frame is therefore considered to be a sensitive operation. Due to the lift beams' free ends, significant sway and heave tip motions are expected. The lift operation is considered to be precise and time consuming, but after completion multiple lift beams are installed. Hereafter, only the installation of one cross-beam is left. To improve the sensitivity of the operation, the size of the forklift frame can be reduced per two lift beams. This could result in a quicker operation, which can be performed over a large period of the year.

Practicality

The lift beams are positioned on the cross-beam onshore. This has to be done very accurately. The spacing between the lift beams has to be large enough to prevent collision with the topsides, but also small enough to approach the connection points as close as possible. Guides and bumpers are therefore most likely necessary to limit potential impact with the topsides' vital components.

The counterweight is filled and attached to the forklift frame onshore. It is essential that the counterweight is filled properly to ensure momentum balance during lifting. Sloshing effects within the counterweight are considered to be negligible. After installation of the lift beams, the counterweight must be quickly detachable from the cross-beam to avoid serious delays. After detachment, the counterweight is lifted back on deck. It is important that during this phase the CoG remains within the lift points envelope.

Another practical challenge is to install the second cross-beam and connect it rigidly to the lift beams while suspended. This is expected to be a challenging operation. Another option is to use a lift frame consisting of one cross-beam. The effects of this modification on the structural integrity of the topsides would have to be assessed in this case. To reduce the weight and size of the frame, and hence improve its workability, it can be decided to reduce the forklift frame to two lift beams.

Costs

Installation of the forklift frame has to performed by one of the SSCV's. However if the forklift frame is reduced to two lift beams, installation could be performed by a smaller HLV. Because of lower vessel stability this operation could likely only be performed in the summer seasons. The duration of installation increases as well, and it is therefore advised to install the lift frame in the preparation phase in this case. A relatively cheap solution is used for the counterweight. To dampen the lift frame's motions tugger lines can be used. Additionally, winches could be deployed on the topsides, which are connected to the lift beams' free ends. This way the lateral motions can be reduced and the lift beams can be guided in the right direction. Due to the short, fixed spacing between the lift beams it is likely that a guide a bumper system will be needed to limit the impact loads. Taking all of this into account, it can be said that the costs for this installation concept are reasonable.

Robustness

The forklift frame is considered to be relatively robust. To improve its installation time and expand its potential installation period, the number of lift beams on the forklift frame can be reduced. The counterweight is provided by water, and its weight can therefore relatively easily be adjusted. It is important that a good working drainage system is applied to the counterweight. The water mass should also be checked prior to lifting.

Furthermore, the position of the lift beams on the cross-beam would have to be adjustable to comply with different topsides layouts. A temporary, rigid connection should therefore be used, which is integrated over the entire length of the cross-beam. If the forklift frame is combined with a MSF leg connection concept, impact with the MSF legs will likely occur due to the short fixed distance between adjacent lift beams.

6.3.3. Beam-per-beam installation concepts

The most straightforward way to install the lift beams is one-by-one. The lift beams can be installed with the use of a counterweight, similarly to the forklift frame but now consisting of one lift beam. On the outer side of the MSF legs, the lift beams could also be installed with a spreader bar. As discussed in chapter 4, it is desired to also have lift beams on the interior of the MSF legs. Therefore the counterweight method is assessed in this section.

Installation time

Installation of a single lift beam is a less sensitive operation as there is more space for motions of the lift beam during installation. The operation can therefore be carried out over a larger period of the year. The waiting on weather time is reduced and the lift operation can be completed relatively quickly. The total installation time of the frame is longer since it consists of multiple sequenced operations. Especially the installation of the cross-beams is expected to be a challenging and time-consuming operation.

The lift preparation is similar to the forklift frame and mainly consists of filling the counterweight box. Filling can be performed quickly with the available pumping capacity of the SSCV. Alternatively the water can be drained from one compartment to the other. It is also possible to eliminate this step by having a separate counterweight for each lift beam. Considering the costs and the required deck space, this option is not further considered.

Practicality

As the size and weight of the lift object decreases, it is easier to maintain stability and clearance during installation of the lift beams. Besides, the lift beams can be installed under a wider range of conditions. Furthermore, installation of the lift beam could be done in the preparation phase by a smaller HLV.

After installation, it is important that a quick disconnection with the counterweight can be achieved. A downside of this concept is that both cross-beams would have to be installed after installation of the lift beams, which is considered to be a challenging operation. Other than that, no practical challenges are identified.

Costs

The costs related to this installation concept are considered to be minimal as there is no need for additional tools or components to install the lift beams. Also, installation of the lift beams could be done with a smaller HLV in the preparation phase. This would significantly reduce the risks of delay, since installation is now out of the critical path of topsides removal. The offshore SSCV time and hence the removal costs would reduce due to this. However, additional costs would have to be taken into account during the preparation phase, since a vessel would be required with a certain lift capacity.

Robustness

The beam-per-beam installation method is considered to be very robust, as there are minimal limitations and no project specific modifications. Installation can also be performed throughout a large period over the year, and is not necessarily dependant on the availability of the SSCV's. Tugger lines could be used to dampen the lift beam's motions during installation. This is most likely only beneficial in the winter seasons. During the summer seasons in general benign sea states are expected for which the limiting motions are not governing. The installation time could potentially be improved if multiple lift beams are simultaneously installed one-by-one. In all of this, it will be essential to find an efficient method to install the cross-beams.

6.3.4. MCA evaluation

In this section the grading of the concepts for each criterion is shown. The criteria are each assigned a different weight, based on their relative importance to the lift beams concept. The concept with the highest combined score is selected, and a lift analysis is performed for this concept. An overview of the criteria weight is provided in table below.

Criterion	Weight [%]
Installation time	20
Practicality	30
Costs	20
Robustness	30

Table 6.1: Weighting of the installation concept criteria

The practicality and robustness criteria have the highest assigned weight, set at 30%. The practicality of the concept is important, because the installation should relatively easily be performed. This means that the concept can be applied with minimal limitations, over a wide range of conditions. This way the lift beams topsides removal concept can be applied over a large period over the year. The SSCV's generally have busy summer seasons, where installation projects often bring in more revenue than the removal projects. If the installation of the lift beams can be performed out of the peak period, it would be commercially very attractive. It will also provide more flexibility to the method, and potentially a greater usage of the concept. The possibility to install the lift beams with another HLV enhances this. It can therefore be said that a more practically feasible solution eventually has a large impact on the performance of the concept.

The robustness of the concept is also important because the concept is intended to be reused for various different topsides. If the concept requires minimal project specific modifications, the concept can be reused with minimal costs and preparation time. It is desired that the lift beams can relatively easily be installed, and retrieved to be used for another topsides removal project.

A short installation time is obviously desired. The lift beams concept however already provides a quick solution for the removal of modular topsides. It might therefore be more beneficial to choose a practical and robust concept rather than the quickest one. It has to be noted that the installation time is less of importance when installation of the lift beams is performed in the preparation phase.

The costs of the installation concept are also important, since costs are the driving factor for the generation of the lift beams concept. Lower removal costs make HMC more competitive in the market. It is however considered to be more cost-effective to have a flexible and easily applicable concept rather than a cheapest one. A concept with great reusability and practicality will allow for the removal of more topsides, which eventually will improve the return on investment.

The results from the MCA are provided in table 6.2.

Installation concept	Installation time	Practicability	Costs	Robustness	Total
Rectangular frame	4	3	2	2	**2.6**
Forklift frame	4.3	3.3	3	4	**3.6**
Beam-per-beam	3	4	4	4.7	**4.0**

Table 6.2: Results of the MCA of the installation concepts

The beam-per-beam installation concept has been selected as the optimal concept. Its flexibility and ease of application make it the most promising installation method. It has to be mentioned that the results are dependent of the weight that is assigned to the criteria. A sensitivity analysis could be performed, where the weight of each criterion is varied. However looking at the table it can be seen that the beam-per-beam installation concept scores the highest in each category, except for installation time. Unless the installation time is assigned a weight of 50% or higher, the beam-per-beam concept will end up with the highest overall score.

6.4. Analysis of motions during lift beam installation

A lift analysis is performed on the beam-per-beam installation concept using a counterweight. The installation process can be divided in a sequence of stages. In this section the critical stage is assessed where the lift beam is moved under the topsides. In chapter 7 a complete overview of the installation procedure can be found.

Different lift configurations are analysed to investigate the system's response. Eventually it is aimed to find the lift setup with the highest yearly workability. To obtain the system's dynamic response to a range of different wave frequencies and wave directions, the installation setup is modelled in the in-house software LiftDyn. Limits are set on the allowable motions of the lift beam to avoid collision with the MSF legs or MSF deck. Using the system's RAO's and limiting criteria, the operability of the system can be determined. The operability shows the maximum allowable wave height as a function of the wave peak period and wave direction under which the operation can be performed, while satisfying the limiting criteria.

To determine the workability of the lift setup a wave time-series data set of 20 years is used for a location near the southern North Sea. This will allow to predict the percentage of time over the year, in which installation of the concept can be executed. It is aimed to reach a high workability also out of the summer season. In general the SSCV's have a busy summer season with lots of installation and removal projects scheduled. If installation of the lift beams could be performed out of this season, more projects can be undertaken by the SSCV's. The workability in the winter months could be improved by analysing whether a dominant wave direction is present and adjust the orientation of the SSCV accordingly. The lift analysis is performed for reference topsides 14.

6.4.1. LiftDyn model setup

SSCV Sleipnir

Installation of the lift beams by SSCV Sleipnir is modelled for reference topsides 14, which lies in a water depth of 26 meters. A minimum clearance of 10 meters with the seabed has to be taken into account, which results in a vessel draught of 16 meters. This is out of the range of the Sleipnir's regular operating draught. The hydrostatic properties of the vessel under the given lift setup are determined with the in-house SSCV ballast sheet. The SSCV's radii of gyration, mass including ballast, and it's CoG are used as input. These parameters are dependant of the lift object's mass and location and will therefore change for different crane radii and slew angles. The hydrodynamic properties of the Sleipnir are obtained from WAMIT, and is mainly dependant on the vessel's draught. Therefore the hydrodynamic properties remain the same under different lift setups. Figure 6.4 gives an impression of the LiftDyn model.

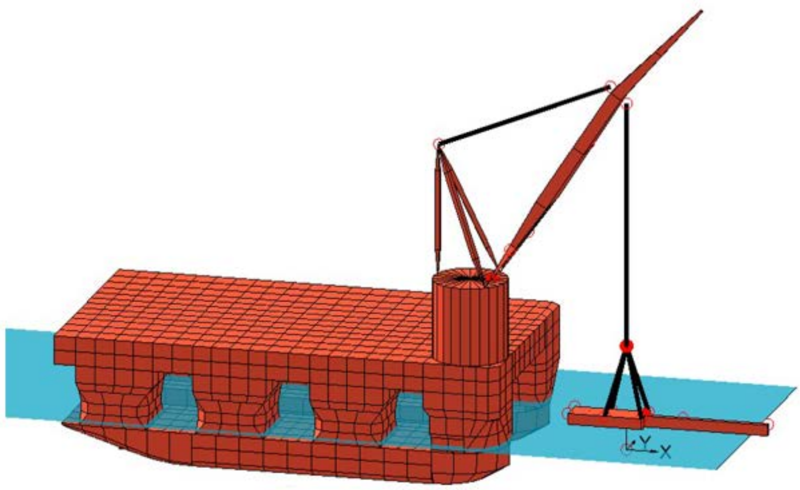

Figure 6.4: Unrestrained LiftDyn model for beam-per-beam installation

SSCV crane
Different crane radii are considered for installation of the lift beams. The crane radius influences the hydrostatic properties of the vessel and the eigenmodes of the system. The location of the mass with respect to the SSCV changes, and also the stiffness of the system. This means that the response of the SSCV and the lift beam changes for different crane radii. A larger crane radius is expected to result in larger heave motions of the lift beams. The arm with respect to the SSCV increases, and hence pitching of the SSCV will result in larger heave motions of the lift beam. The crane is also more sensitive for pitch for a larger radius.

It must therefore first be investigated what the ideal crane radius is for a given heading and seastate. Four crane radii are considered for this purpose, ranging from the minimum installation radius to the maximum installation radius. The minimum crane radius follows from the minimum distance between the crane boom's hinge to the main block, taking a clearance between the lift object and the SSCV of 8 meters into account. The maximum crane radius during installation is taken such that there is sufficient clearance with the topsides during the operation. The crane radii under consideration are shown in table 6.3.

R_1	45.5	[m]
R_2	63.5	[m]
R_3	82	[m]
R_4	100	[m]

Table 6.3: Considered crane radii for installation of the lift beams

Lift beam and counterweight
For the lift beam and counterweight, the dry weights are multiplied with a lift factor of 1.21, composed of a DAF and a contingency factor. The radii of gyration are determined with equations 6.1 to 6.3.

$$r_{roll} = \sqrt{1/12 * \theta_{roll} * (B^2 + H^2)} \tag{6.1}$$

$$r_{pitch} = \sqrt{1/12 * \theta_{pitch} * (L^2 + H^2)} \tag{6.2}$$

$$r_{yaw} = \sqrt{1/12 * \theta_{yaw} * (B^2 + L^2)} \tag{6.3}$$

Here θ represents the mass distribution factor for the given rotation, and is taken as 1.5 for the lift beam and 2.25 for the counterweight. The higher value for the counterweight follows from its eccentric CoG location. The lift points are located on the counterweight's edges. The design weight of the lift beam is equal to 325.7 mT. The counterweight needs to be heavy enough and large enough to provide rotational equilibrium. Figure 6.10 gives an impression of the counterweight.

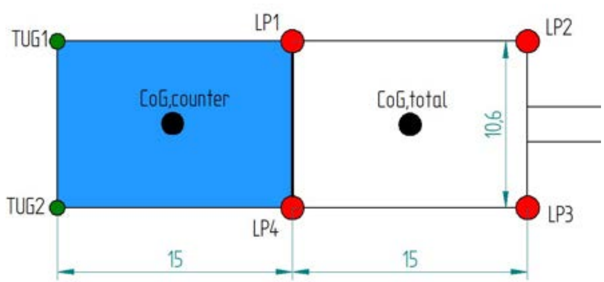

Figure 6.5: Overview of the counterweight

The mass of the counterweight, excluding the mass of the steel box is determined with equation 6.4.

$$W_{CW,des} = \frac{W_{LB,des} * (25 + 7.5)}{15} = \frac{325.7 * 32.5}{15} = 705.7mT \tag{6.4}$$

The dimensions of the compartment are such that the required counterweight is reached when the compartment is completely filled with water. The counterweight is assigned the same height as the lift beam to ease the assembly's handling.

$$W_{water} = 1.025 * 10.6 * 4.35 * 15 = 705.7mT \tag{6.5}$$

Rigging
The slings are modelled as inline-connectors with a defined spring stiffness and pre-tension. The spring stiffness is a property of the sling. The pre-tension is equal to the rigging load under the given setup, and is determined from a static lift analysis in AGES. Existing slings are selected for installation of the lift beam-counterweight assembly. More information about this can be found in Appendix E.2.

Limiting criteria
A limit is set on the sway and heave motion of two points on the lift beam, the lift beam's tip and the point of the lift beam that touches the last MSF leg. This way it is aimed to ensure that the limiting criteria are satisfied throughout the entire operation. The limiting motions are defined to avoid collision with the MSF legs or MSF deck. The governing case for the sway motions follow from the MSF leg spacing, with one of the interior lift beams already installed. The limiting heave motion is defined by the distance between the MSF deck and the jacket top horizontal elevation. The lift analysis is performed on reference topsides 14, which offers more under-deck space than the smaller topsides in the batch. As concluded in chapter 4, it is sufficient for such topsides to be lifted with one-sided leg support. This implies that only lift beams on the exterior of the MSF legs have to be installed. This results in a significant increase in the available space during installation, and hence the defined limiting criteria. The workability for lift beam installation for these topsides eventually improves this way. Derivation of the limiting criteria for reference topsides 14 is provided in Appendix E. It has to be noted that the dimensions of the pin support frame are taken into account for this. An overview of the limiting criteria, and the points for which the criteria are defined, are shown in figure 6.6.

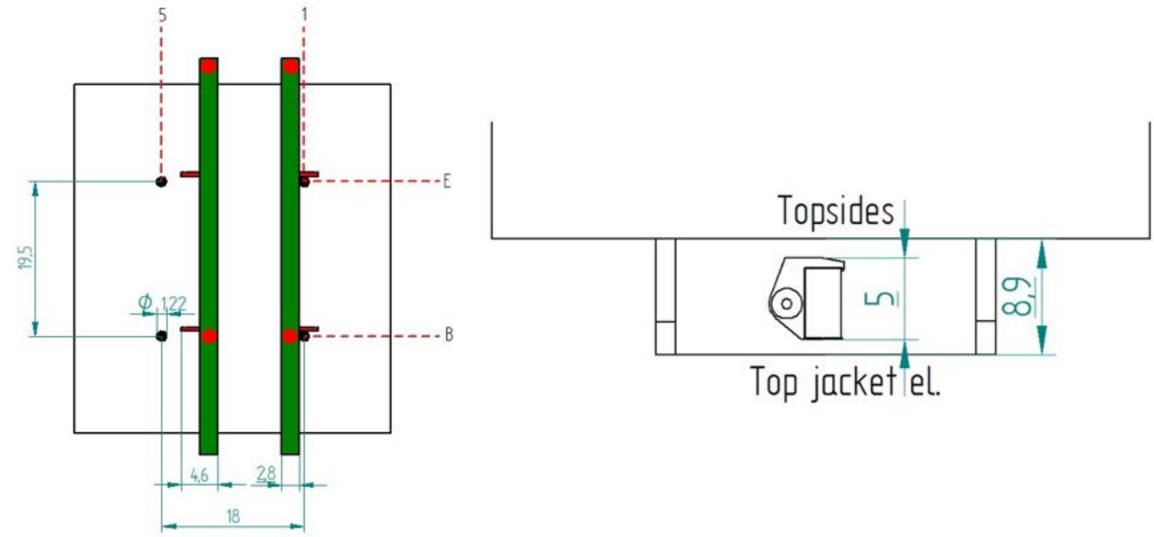

Figure 6.6: Limiting criteria for the lift beam motions during installation

The maximum allowable sway single amplitude with the pin-hole connection is equal to 4.7 meters in 1-5 direction and 5.4 meters in E-B direction. The limiting heave single amplitude is found to be equal to 1.95 meters. For now a conservative estimate of 3 hours is made on the duration for installation a single lift beam. The limiting criteria are therefore set for the 3 hour MPM response. An overview of the limiting criteria is provided in table below. It has to be noted that the criteria do not account for the SSCV's DP footprint.

Limiting single amplitude	1-5 direction	E-B direction
Sway [m]	4.70	5.40
Heave [m]	1.95	1.95

Table 6.4: Limiting motions of the lift beam during installation

Spectrum

A JONSWAP spectrum is used to obtain the system's RAO's. The JONSWAP spectrum represents a sea state that is not fully developed and consists of irregular seawaves, which is the case in the North Sea. The spreading factor is set at 2.0 and the peak enhancement factor at 3.3. The magnitude of second order non-linear interaction effects of the waves is represented by the enhancement factor. Peak wave periods between 0 and 16 seconds are of interest as most of the wave energy is contained in this range. Extra attention should be paid to eigenmodes, whose eigenperiods fall within this range.

6.4.2. Lift analysis results

Two possible headings are defined for installation of the lift beams for reference platform 14. The headings of the SSCV are indicated in figure 6.7.

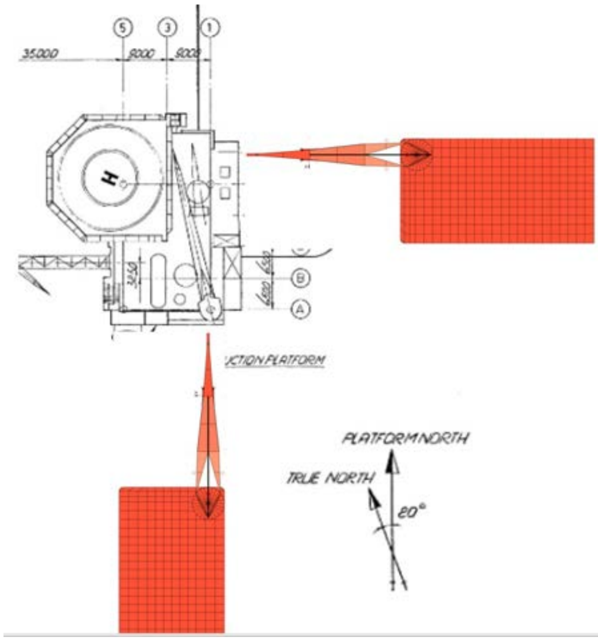

Figure 6.7: Possible SSCV headings

The headings are equal to 250 degrees for the E-B direction, and 340 degrees for the 1-5 direction, with respect to the true north. For the sea state, an available wave time-series of the Doggerbank is used, which is located North of the southern North Sea, and is considered to have a presentable sea state. The location of the measurements is shown in figure 6.13.

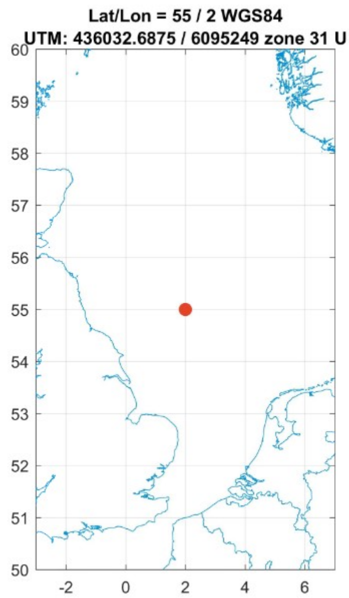

Figure 6.8: Location of the Doggerbank measurements

Unrestrained case

The unrestrained case is first analysed, where no auxiliary tools are used during the lift operation. Through the unrestrained case it is aimed to find the ideal heading and crane radius for the lift setup. As the crane radius changes, new eigenmodes are found and the natural period of reoccurring eigenmodes changes. The eigenmodes, with an eigenperiod between 0 and 16 seconds, for each considered crane radius can be found in Appendix E.

First the operability for each lift setup is plotted, which can be found in Appendix E. The operability plots provide a maximum wave height, as a function of the wave period and wave direction, for which the limiting criteria are satisfied. These plots give insight on the wave directions and wave periods that are governing for the limiting motions of the lift beam. The plots therefore give an indication on the system's sensitivity for the operation to certain types of waves. In the operability plots, all wave directions with a step size of 15 degrees are considered and all wave periods between 0 and 16 seconds. The results however don't show the wave frequencies and wave directions that are expected to be encountered at the location of the platform. It also doesn't provide information about the wave energy content for each direction and frequency. The system's response during installation therefore strongly depends on the sea state it is exposed to and the SSCV's heading in this environment.

To get an indication on each lift setup's performance, for a specific location, the average waiting on weather time is determined for the different headings and crane radii. The average waiting on weather time shows the time that is required to reach a 3 hour sea state in which the limiting criteria are satisfied. The lower the average weighting time, the higher the workability of the lift configuration. The in-house Sequencetool is used for this, which takes the RAO's of the two lift beam points, the limiting criteria for these points, the SSCV's heading and the sea state as input. An additional operational limit is set for the wind speed at 25 knots. The results are plotted in figure 6.9. The numerical values are provided in Appendix E.

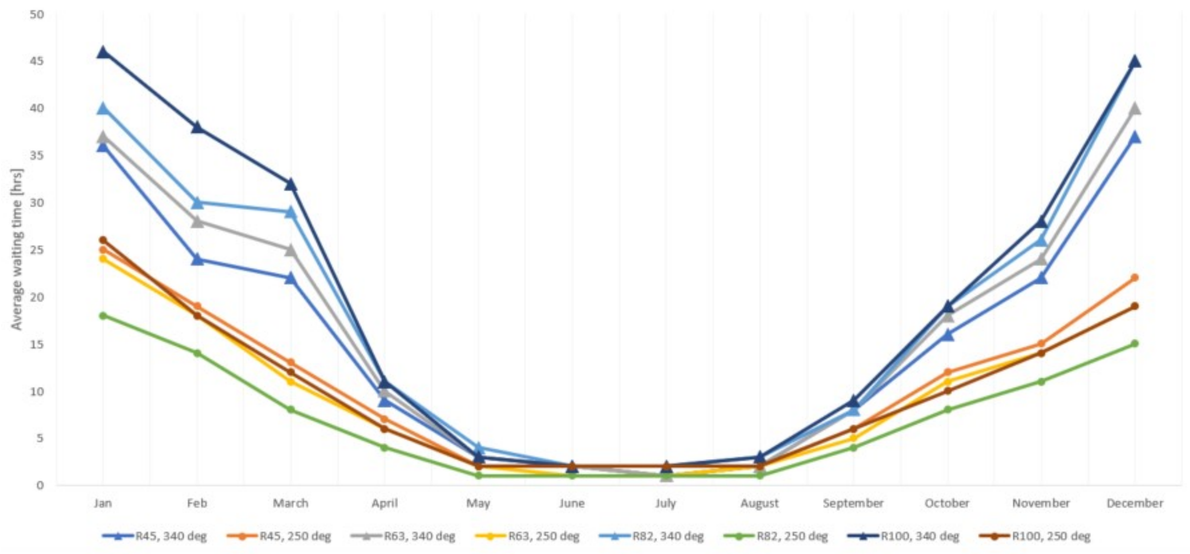

Figure 6.9: Average waiting on weather time

Between April and September the average waiting on weather time for each setup is similar as the sea state is calm in this period. However looking at the other months, strong differences in waiting time are observed. The lift setup with a radius of 82 meters and a heading of 250 degrees results in the lowest average waiting time. In general it can be noticed that significantly better results are obtained for the 250 degrees heading. Looking at the wave directions at the Doggerbank, it is found that most waves and wave energy comes from the North. When the vessel lies at a heading of 340 degrees, the pitch motion of the vessel and hence of the lift beam's heave motion is excited most. The heave motion of the lift beam is thereby governing. When lying on 250 degrees, the same waves mainly result in a roll motion of the SSCV and a sway motion of the lift beam, which is less governing than the heave motion. This is mainly due to the limiting criteria that are set for the sway and heave motion. The wave height distribution over the year as a function of the wave direction is provided in Appendix E.

The monthly workability of the optimal lift setup, at 250 degrees heading and a crane radius of 82 meters, is shown in figure 6.10.

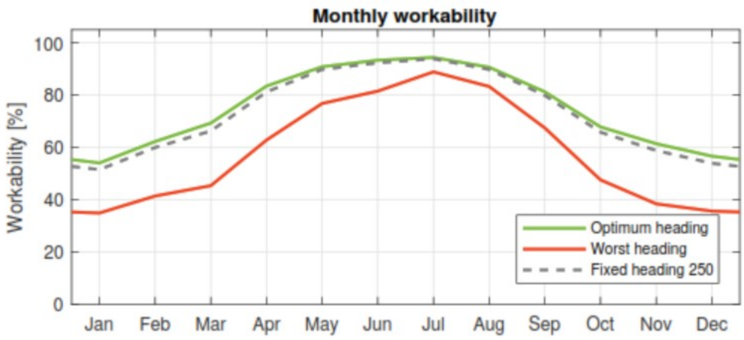

Figure 6.10: Monthly workability

The workability for a heading of 250 degrees is plotted with the optimal and worst headings. It can be seen that the workability for a 250 degrees heading lies very close to the optimal heading for installation of the lift beams under the current lift setup. In the summer season the workability ranges between 80 and 94%. The workability drops as low as 50 % in the winter months. This comes down to a yearly workability of 74%. In figure 6.11, the workability per limiting criterion is plotted.

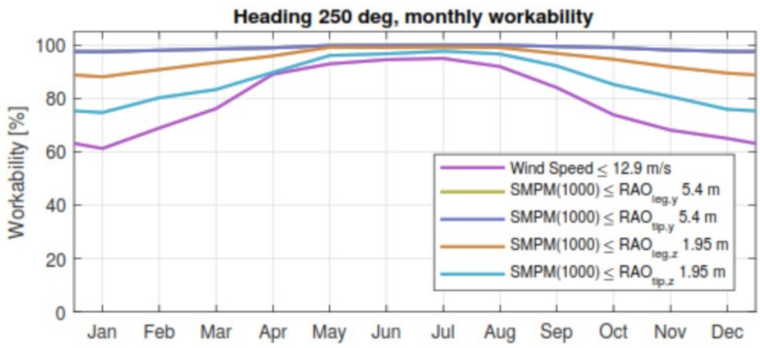

Figure 6.11: Monthly workability per limiting criterion

Looking at the workability per limiting criterion, it can be seen that the wind speed criterion is governing. However, when the limiting criteria for the lift beam's response are combined, a lower workability is obtained. The difference with the wind speed criterion is relatively small, implying that little improvements can be made under the current setup. The wind speed limits the yearly workability to approximately 80%, as shown in Appendix E. This means that a potential increase in workability of 6% can be reached. Regarding the lift beam's response, it can be noticed that the tip's heave motion is the most critical criterion, as expected.

Figure 6.12 provides an overview of the optimum and worst headings for the combined limiting criteria.

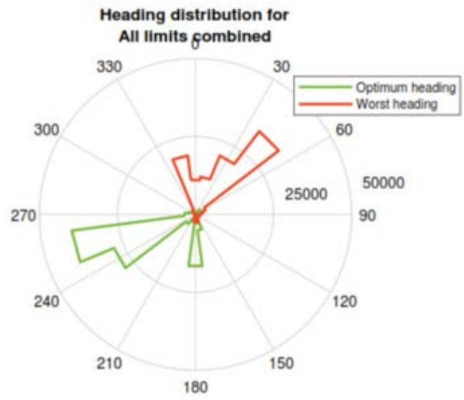

Figure 6.12: Optimum and worst heading

It can be seen that a heading of 340 degree degrees is considered to be one of the worst headings, while a heading of 250 degrees is found to be one of the optimal headings. This follows from the dominant wave direction, which comes from the North. These waves result in pitch of the SSCV for a heading of 340 degrees, and roll of the SSCV for a heading of 250 degrees.
Regarding the SSCV's heading no improvements can be made under the current setup. However, the workability in the winter months can still be improved by improving the lift setup. Also, it can be investigated whether the dominant wave direction in the winter months differs from the yearly dominant wave direction. The heading of the SSCV could be adjusted accordingly for these months. This way the potential usage of the lift beams concept can be improved. In the next section the addition of tugger lines is discussed.

Tugger lines
Tugger lines are connected to the counterweight to dampen its motions in heave and pitch. If the tugger lines are crossed, the working line of the tugger lines changes, and more damping in sway and roll direction is achieved. Figure 6.13 indicates the tugger lines in the LiftDyn model.

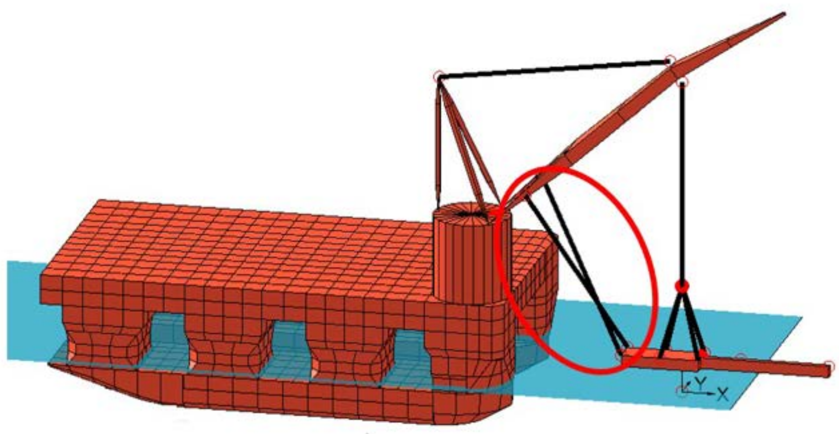

Figure 6.13: LiftDyn model of the lift beam-counterweight assembly with tugger lines

The tugger lines are connected to the crane boom at a distance of 18.5 meters from the crane boom's pivot. The tugger lines are modelled as connectors with spring damping. The spring damping can be determined with equation 6.6. The properties of the tugger wires that are equipped on the Sleipnir are used.

$$Damping = \frac{T_{max} - T_{min}}{V_{max}} = 392.4kN/s \tag{6.6}$$

Where:
T_{max} = Maximum tension in the tugger wire (= 40 mT)
T_{min} = Minimum tension in the tugger wire (= 0 mT)
V_{max} = Maximum velocity in the tugger wire (= 1 m/s)
Looking at the RAO's of the lift beam tip and lift beam leg point, a significant reduction in the heave RAO peaks can be noticed. Due to the angle of the lines, damping for the sway motion is found to be negligibly small. The tip's sway and heave RAO's for the case with tugger lines is provided in Appendix E. The monthly workability is shown in figure 6.14.

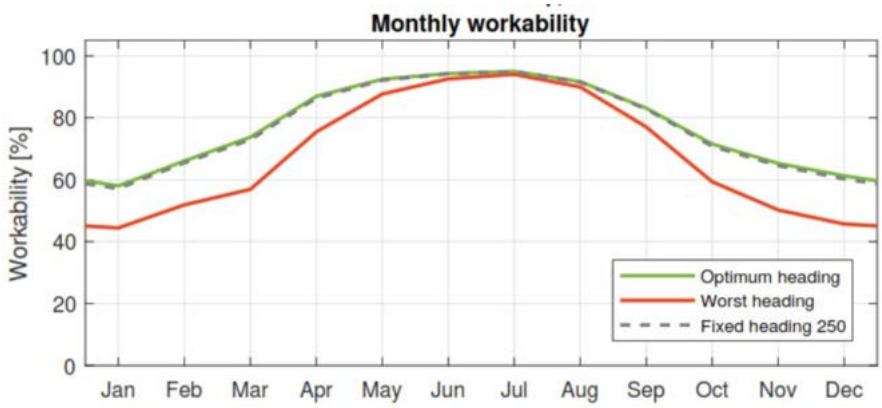

Figure 6.14: Monthly workability with tugger lines, 250 degrees heading

It can be seen that the workability has especially improved in the winter months, ranging from 57 to 71 %. The monthly workability is compared for the case without tugger lines in table below.

Month	Unrestrained	Tugger lines
Jan	51.5	57.2
Feb	59.9	65.5
Mar	66.3	73.0
Apr	81.2	86.3
May	89.8	92.2
Jun	92.3	94.2
Jul	93.9	94.9
Aug	89.8	91.5
Sep	79.9	82.9
Oct	65.8	70.8
Nov	58.8	64.6
Dec	53.9	60.3
Yearly	**73.6**	**77.8**

Table 6.5: Monthly workability of the optimal lift setup for the unrestrained case and the case with tugger lines

It can be seen that on average, the workability has improved by roughly 4 %. Especially in the winter months a significant improvement is achieved of up to almost 7%.

The workability per limiting criterion is shown in figure 6.15.

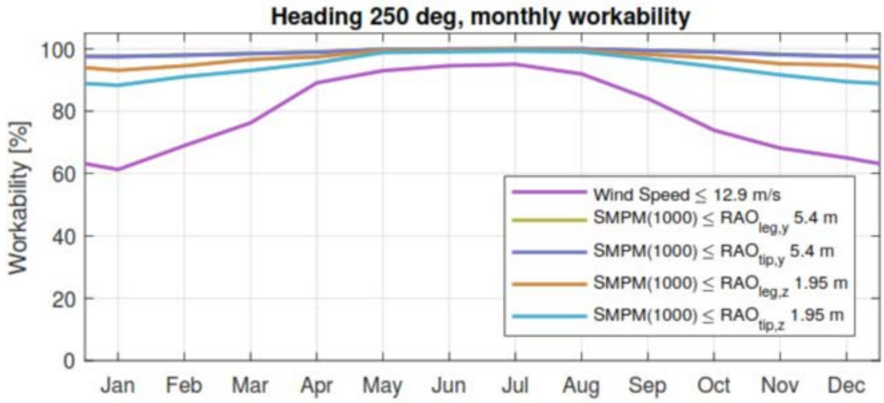

Figure 6.15: Monthly workability per limiting criterion with tugger lines

It can be seen that the workability for the tip's heave motion has improved significantly, representing the damping effect of the tugger lines. The wind speed is a characteristic of the location and the heading of the vessel, and can't be influenced by the design. In the next section it is investigated whether the addition of a winch could further improve the workability.

Winch

Finally the influence of a winch to the lift beam's response is analysed. A distinction between two types of winches can be made, a constant tension winch and an active winch. A constant tension winch pulls the lift beam's tip with a constant force, whereas an active winch behaves like a spring, where the force is dependent of the lift beam's motions. It has been decided that a constant tension winch is more suitable for installation of the lift beams. The winch is installed on the other side of the topside's main deck. The dimensions of the winch should therefore be limited. The capacity of the winch should be sufficient to dampen the lift beam's motions. A constant tension winch with a pull force of 30 mT has been chosen for this purpose.
The winch is modelled in LiftDyn as a pre-tension only connector. The pretension is equal to 294.3 kN. The pull point of the winch is modelled 1 meter above the outer edge of the main deck, and therefore has a vertical upward component. It is of interest whether this component will positively affect the tip's heave motion. The monthly workability is compared to the case with only tugger lines in table below.

Month	Tugger lines	Tugger lines + CT30 winch
Jan	57.2	56.5
Feb	65.5	64.8
Mar	73.0	72.1
Apr	86.3	85.8
May	92.2	91.9
Jun	94.2	94.0
Jul	94.9	94.8
Aug	91.5	91.4
Sep	82.9	82.5
Oct	70.8	70.2
Nov	64.6	63.9
Dec	60.3	59.5
Yearly	**77.8**	**77.3**

Table 6.6: Monthly workability of the optimal lift setup for the tugger lines case and the case with tugger lines and a CT winch

It can be seen that the workability decreases with the addition of a CT winch. It shows that the upward component of the winch has a negative effect on the heave motion of the lift beam. Also, a new eigenmode in roll of the lift object is noticed, with a natural period of 15.90 seconds. It can be concluded that a winch is not favored for installation of the lift beams, as it increases the heave motion of the lift beam, and introduces a new eigenmode that excites wagging of the lift beam's tip. Also, the effort to install the winch on the topsides and connect it to the lift beam's tip will result in a more complicated installation procedure.

Slew angle
The slew angle can also be rotated to 90 degrees. It is expected that clear differences in the system's response will be observed. An impression of the LiftDyn setup with a slew angle of 90 degrees is shown in figure 6.16.

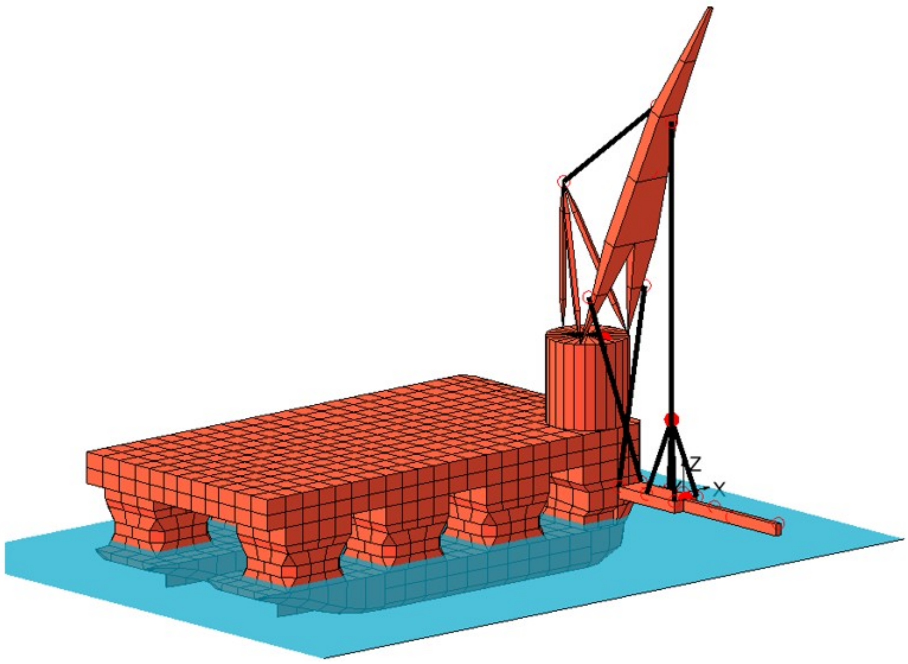

Figure 6.16: LiftDyn model with a 90 degrees slew angle

The position of the lift object with respect to the vessel changes, and hence the response of the system changes. Pitching motions of the vessel will result in roll motions of the lift beam and vise versa. This also implies that the crane radius of 82 meters might not be optimal anymore. It is assumed that the case with crossed tugger lines is still the best option regarding the rigging setup. The SSCV headings change as well, as the orientation of the SSCV with respect to the platform changes. The headings for a slew angle of 90 degrees are equal to 160 degrees, for installation in E-B direction, and 250 degrees, for installation in 1-5 direction. The average waiting on weather time has been plotted in figure 6.17.

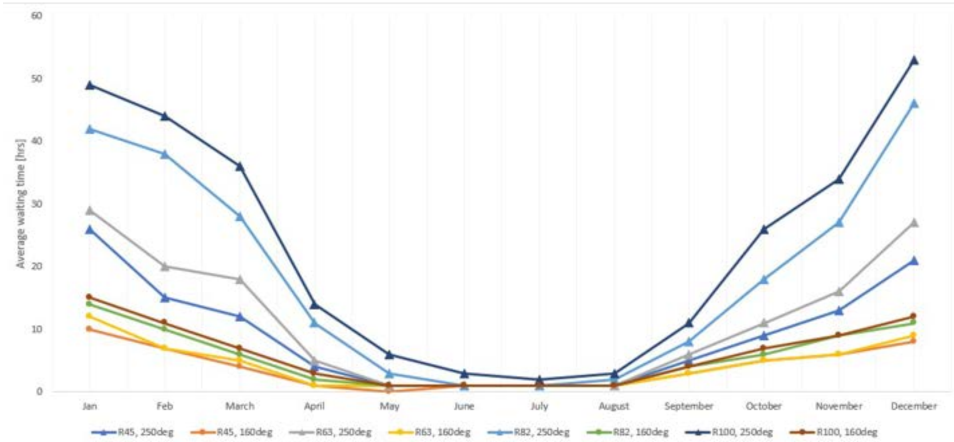

Figure 6.17: Average waiting on weather time for a slew angle of 90 degrees

As expected, a heading of 160 degrees gives the best results. For this heading, pitching of the vessel results in less governing roll and sway motions of the lift object. For the 250 degrees heading the opposite holds. The optimal lift setup is found to be at a radius of 45.5 meters. The distance of the lift object to the stern of the vessel is smallest for this radius. This implies that the arm for the roll motion is minimal, therefore resulting in smaller motions in this direction. The workability for a heading of 160 degrees is provided in figure 6.18.

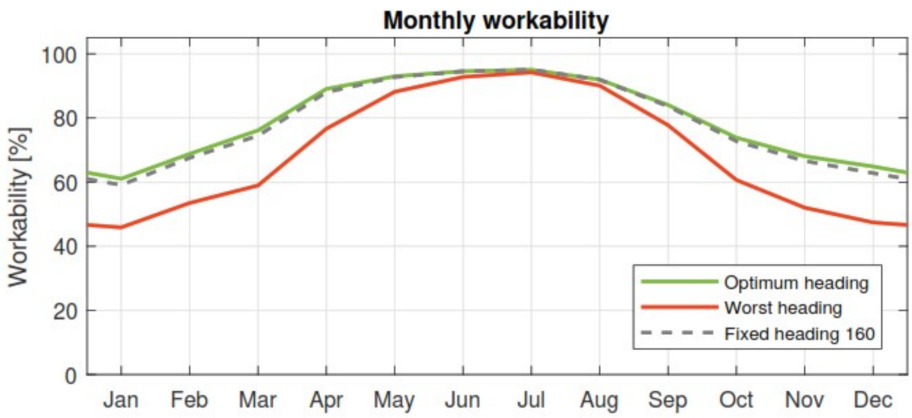

Figure 6.18: Monthly workability for the optimal lift setup

The workability per limiting criterion is shown in figure 6.19.

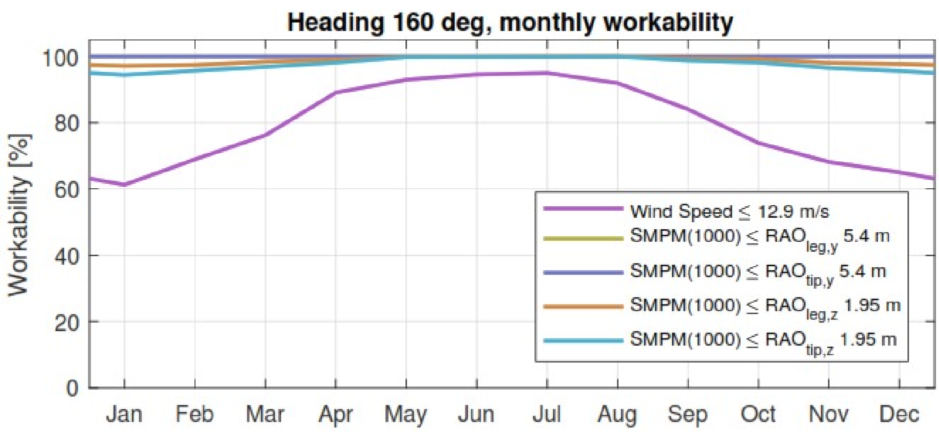

Figure 6.19: Monthly workability per limiting criterion for the optimal lift setup

It can be seen that the workabilities per limiting criterion of the lift beam's response lie much closer to each other. The smaller the difference in these workabilities, the less sensitive the system is to specific motions, and hence the better the lift setup. In table below, the workability is compared with the optimal workability for a slew angle of 180 degrees.

Month	SL90,R45,H160	SL180,R82,H250
Jan	59.1	57.2
Feb	67.6	65.5
Mar	74.5	73.0
Apr	88.0	86.3
May	92.7	92.2
Jun	94.5	94.2
Jul	95.0	94.9
Aug	91.9	91.5
Sep	83.6	82.9
Oct	72.7	70.8
Nov	66.6	64.6
Dec	62.8	60.3
Yearly	**79.1**	**77.8**

Table 6.7: Monthly workability of the optimal lift setup for a slew angle of 90 degrees and a slew angle of 180 degrees

Throughout the year, better results are obtained for the 90 degrees slew angle setup, with an increase of 1.3 % in the yearly workability. Furthermore, it can be noted that this lift setup has almost reached the maximum possible yearly workability of 80 %, implying that there is minimal room for improvement. It can be concluded that for installation of the lift beams for reference topsides 14, a heading of 160 degrees, with a slew angle of 90 degrees, and a crane radius of 45.5 meters is the ideal lift setup. The addition of tugger lines has proven to have a positive influence on the installation since it especially dampens the governing heave motions of the lift beam.

6.5. Conclusions

- Three lift beam installation concepts have been analysed: the rectangular frame, the forklift frame and beam-per-beam installation.
- Through a MCA it has been decided that the beam-per-beam installation concept, using a counterweight, is most suitable for the lift beams concept. The evaluation criteria are: installation time, practicality, costs and robustness.
- The general properties of the beam-per-beam installation concept have been determined and a lift analysis has been performed. For the lift analysis a 20 year-dataset of the Doggerbank is used.
- The optimal lift setup is found to be for a SSCV heading of 160 degrees, a slew angle of 90 degrees, and a crane radius of 45.5 meters. Under this setup the SSCV's pitching motions result in less governing sway and roll motions of the lift beam.
- The addition of tugger lines shows to effectively dampen the heave motions of the lift beam during installation, resulting in a yearly workability of 79 %. This is 1% below the maximum possible yearly workability, which is limited by the maximum wind speed during operation. Installation of the lift beams can therefore be performed over a wide range over the year.

7

Case study on the lift beams concept

In this section the lift beams topsides removal concept is assessed by comparing its performance with the conventional method of removal, reversed installation. For this purpose reference topsides 14 is used, because for this topsides an estimate is available on the duration for removal with reversed installation.

In chapters 3 and 4 it was shown that the lift beams and the reference topsides have sufficient capacity for topsides removal with the lift beams. It was found that the ideal lift beam setup consists of two-sided leg support, with a cross-beam on each end of the lift beams. The pin-hole connection was chosen as the optimal connection between the lift beams and the topsides. Hereby the lift beams are installed one by one using a counterweight.

In this section the complete removal procedure of reference topsides 14 will be discussed. The costs and removal time will be estimated and used as the main indicators for the performance of the lift beams concept. The topsides removal time will be compared with the topsides removal time for reversed installation. Including the costs for the realization of the lift beams concept, will allow to draw an economic comparison. Eventually it is aimed to get an estimate on how much topsides are required to be removed in order for the lift beams concept to become profitable.

7.1. Lift beams topsides removal procedure

The lift beams topsides removal procedure can be divided in six stages. The main activities and characteristics of each stage will be shortly described.

7.1.1. Preparation phase

First the platform has to be prepared for removal with the lift beams. The preparation scope takes place well before actual removal of the topsides. In this phase a platform support vessel will be required to mobilize and demobilize equipment, materials and workmen to the platform. Due to management of change, the activities on the topsides will change and it is thereby uncertain whether there will be accommodation on the platform for the workmen. Accommodation should therefore be provided by the support vessel. This implies that the support vessel will have to be stationed at the platform while the preparation phase is going on.

On-deck preparations are performed, where the topsides might be strengthened at select locations. Also equipment and materials that will be required during the preparation phase will be installed on deck. It is likely that entrances for winches will have be created that will be used to transfer equipment and materials on deck or below deck. The main activities for the under-deck preparations are welding of temporary supports onto the MSF legs and cutting the MSF legs free from the jacket. Prior to this work access has to be created and the leg has to be prepared for these operations. Also any potential obstructions have to be cut off to create space for the preparation activities and for installation of the lift beams. After the leg has been prepared and an adequate working habitat is created, the temporary supports are hoisted from the support vessel's deck to the required elevation of the MSF leg. The temporary supports are hoisted with vertical winches that are installed on the topsides' cellar deck. Therefore entrances have to be created for the winches to pass through. For each MSF leg, two temporary supports have to be welded. The welders need 1 meter of free space on each side to perform the welding. The temporary supports for each MSF leg can be welded simultaneously.

In figure 7.1 the temporary supports are shown in yellow.

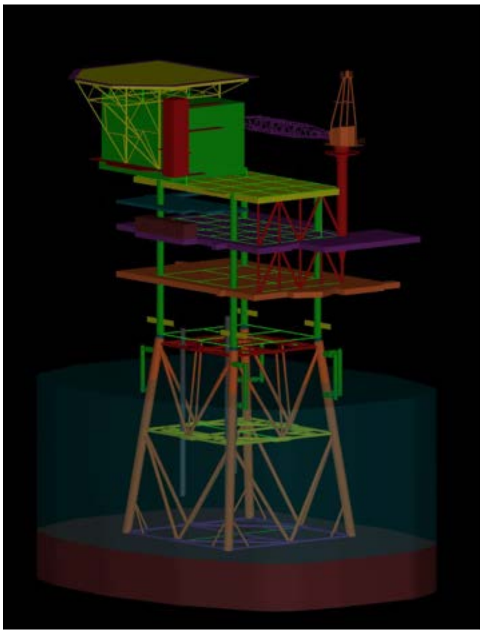

Figure 7.1: The topside in the preparation phase, with the temporary supports indicated in yellow

The temporary supports are welded 6.5 meters below the MSF deck, and are designed as H-profile beams with a height of 1 meter. The dimensions of the temporary supports are given in Appendix F.1.

After completing the welding activities, the MSF legs are cut free from the jacket substructure. It is aimed to use a castellated cut, since this way the topside can maintain its lateral stability after cutting. An example of a castellated cut is provided in figure 7.2.

Figure 7.2: Castellated cut [42]

In case it turns out that a castellated cut is not feasible, alternative cutting solutions could be used that also provide lateral stability after cutting. This could for example be achieved using shear restraints.

The cut is ideally performed above the MSF leg's stabbing cone. This will ensure that the cut is made above the transition to the jacket legs, which will ease the cutting process. Prior to cutting it must be checked if any obstructions in the interior of the leg are present. During the cutting process it is preferred that the leg is stress free to avoid initial stresses and strains, which could lead to inaccuracies in the cutting process. In practice this is likely not feasible, and the initial stress state of the leg should be accounted for.

Onshore the lift beams and the counterweight are prepared. The lift beams are outfitted with their connection elements and final checks are performed to identify any possible flaws. The counterweights are filled with water and it is checked whether the desired water content is reached. Lift points are prepared on the counterweight which are used during installation of the lift beams. Additionally connection points are created on the back end of the counterweight to attach the tugger lines to. The elements are then lifted on deck and are accurately positioned to enhance an efficient installation procedure. The required installation and removal rigging and any auxiliary tools are loaded on deck as well.

7.1.2. Lift beam installation phase

The vessel sails to location, takes its installation position and the DP functioning is tested. A landing area is prepared on the topsides and a gangway is installed. Final checks are performed around the platform to ensure that everything is as expected. Some final preparations are performed prior to start of the lift beam installation procedure. Required equipment for these activities is transferred onto the topsides. During these preparations, the installation setup is prepared. The installation rigging and the tugger lines are attached to their respective points on the counterweight . Once the final preparations are completed, the crane will lift the lift beam-counterweight assembly off deck and rotate to the predefined slew angle. The main hook is lowered to the required installation elevation at a radius of 45.5 meters. The lift beams are then carefully moved underneath the topsides. The SSCV will perform this operation in DP mode. When the lift beams are accurately positioned, the lift beams are laid onto their temporary supports. Installation of the lift beam is illustrated in figure 7.3.

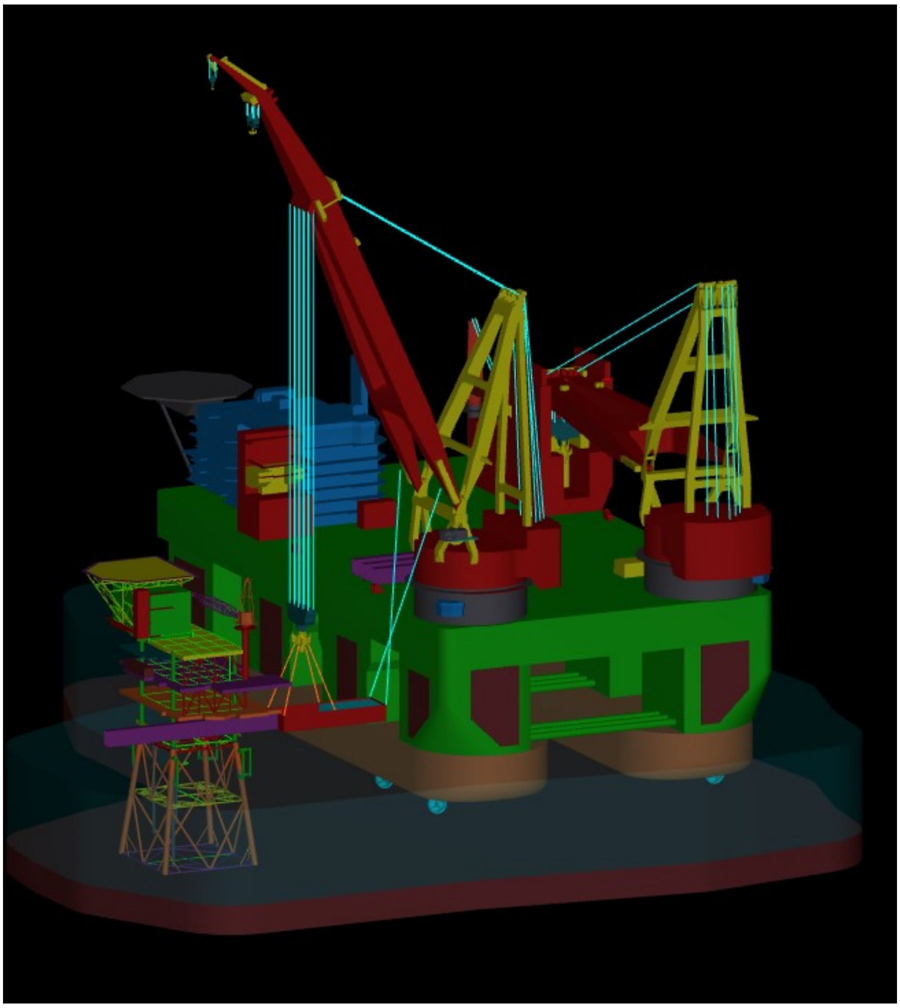

Figure 7.3: Installation of the lift beam

7.1.3. Counterweight detachment phase

After installation of the lift beam, the counterweight has to be detached and lifted back on deck. It is important that the disconnection can happen in a relatively quick manner in order to continue with the installation of the other lift beams. First the counterweight is drained, which will result in a CoG shift to the interface between the lift beams and the topside. The connection consist of two hooks, a larger hook at the top, and a smaller hook at the bottom. When the rigging is lowered, the smaller hook decouples first and the counterweight tilts until decoupling of the upper hook is reached. Figure 7.4 gives an impression of the connection. In figure 7.5 the sequence of counterweight detachment is illustrated.

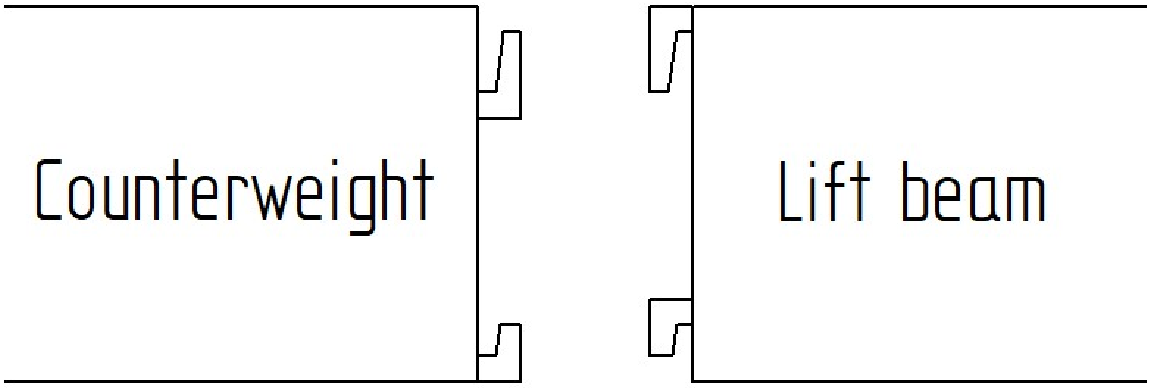

Figure 7.4: Counterweight to lift beam connection

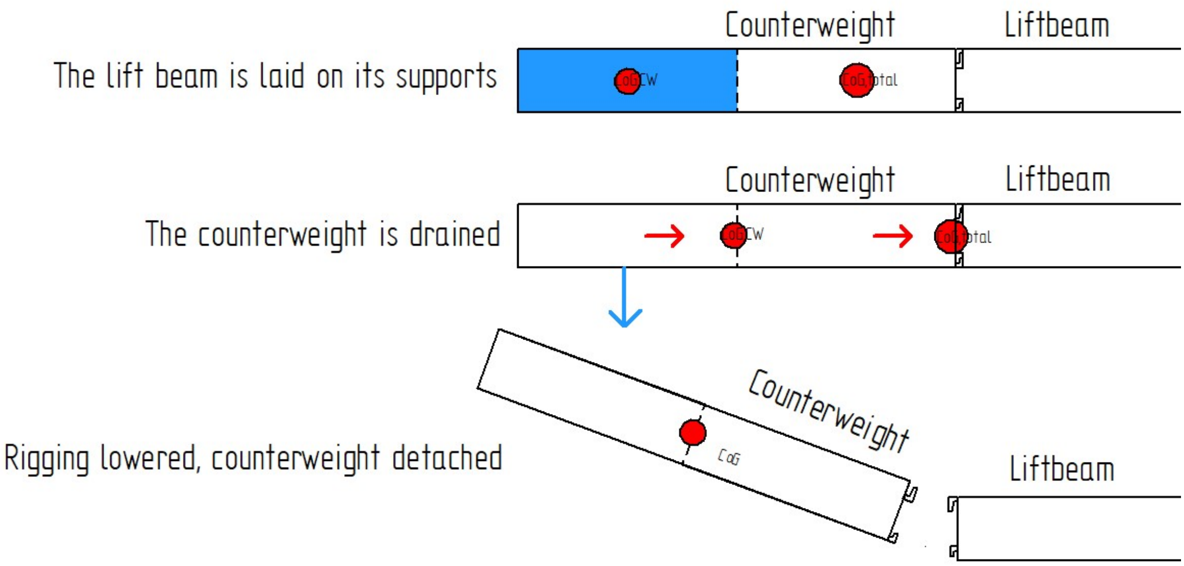

Figure 7.5: Detachment sequence of the counterweight

The design of the hooks is provided in Appendix F.2. After detachment the counterweight is lifted back on deck. Hereafter the counterweight is refilled and subsequently connected to the following lift beam.

7.1.4. Cross-beam installation phase

After installation of all the lift beams, installation of the two cross-beams follows. A temporary, but rigid connection is required for effective application of the cross-beams. A rigid connection will allow for moment transfer between the lift beams and the cross-beam and thereby redistribute the load over the lift beams. The connection also has to be temporary, since the cross-beam has to be separated from the lift beams after disposal of the topsides.

Two solutions have been identified for this problem. These solutions are only visualised, and therefore no design calculations have been performed. One option is to install the cross-beams on the same elevation as the lift beams. The elements are connected through an enclosed shape when the cross-beam is lifted up. More information about this option can be found in Appendix F.3. Another option is to install the cross-beams below the lift beams.This option is chosen, as it is expected that this method will provide a quicker installation. For the connection primary and secondary stabbing cones are used. An impression of the cross-beam-to-lift beam connection is shown in figure 7.6.

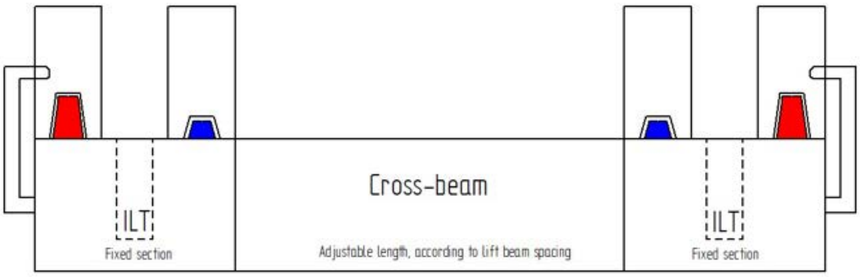

Figure 7.6: Cross-beam-to-lift beam connection

The primary stabbing cones are indicated in red, and are of larger size than the secondary stabbing cones, which are shown in blue. The tolerance between the stabbing cone and the lift beam receptor is also larger for the secondary stabbing cone. This effectively means that only the primary stabbing cones will have to be installed, whereas the installation of the secondary stabbing cones automatically follows. The load transfer between the cross-beam and the lift beam is based on normal forces and friction between the lift beam's tension flange and the compression flange of the cross-beam. The stabbing cones are primarily used to guide the installation of the cross-beam, and provide lateral stability. To ensure that the connection is maintained, and fully fixed, sideward elements are connected to the outer lift beams. These pin type elements are hydraulically driven and can therefore be remotely operated. In between adjacent lift beams an ILT interface is provided for the removal rigging. Hereby it has to be noted that significant strengthening of the cross-beam, around the ILT interface, will be required, to carry the horizontal shear forces that are exerted by the ILT. Finally it has to be noted that the length of the cross-beam's mid span can be adjusted to comply with varying lift beam spacing.

Alternatively it can be opted to only use the fixed section, which results in a total of four short cross-beams. In this case the pin elements have to be connected to each lift beam. An impression of this is shown in figure 7.7.

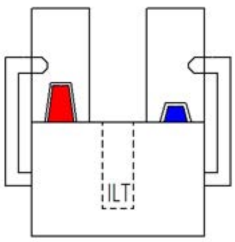

Figure 7.7: Short cross-beam alternative

A benefit of this alternative is that the cross-beam doesn't need to be modified for varying MSF leg spacing. The total installation time of these elements is on the other hand expected to increase as the number of operations increases. The effects of the short cross-beam alternative on the topsides' structural integrity are shown in Appendix F.3. It is found that the topsides has sufficient capacity for the lift beam setup consisting of short cross-beams. An increase in the UC's of the legs and the number of critical members is observed. However no failing members are identified, meaning that topsides removal is structurally feasible under this alternative setup.

For the lift beams topsides removal concept the original solution, depicted in figure 7.6, is chosen. The cross-beams are installed using a spreader bar, which is expected to result in less tilting of the cross-beam during the operation. An impression of the cross-beam installation is shown in figure 7.8.

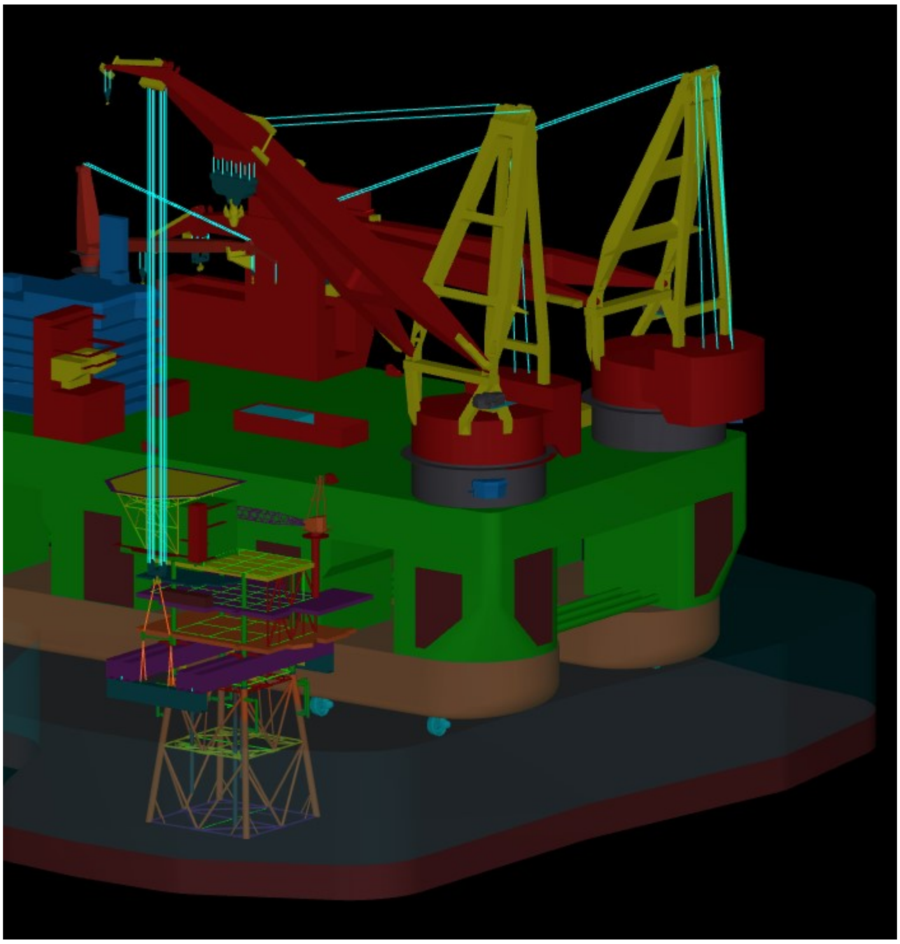

Figure 7.8: Installation of the cross-beam

7.1.5. Lift beam connection phase

After completing installation of the lift frame, the connection can be made with the MSF legs. The main activity during this phase is to create the holes for the pin-hole connection. Creating the holes can be done simultaneously for all four legs. It is essential that the holes are accurately aligned with each other in order to smoothly penetrate the pin without damaging any components and to avoid eccentric load transfer during lifting. Therefore this process takes place after positioning of the lift beams. Pin support sleeves,which are connected to the pin support frame, are used to ensure alignment of the holes with the pin. When the holes are completed, the pin is hydraulically driven into the hole. The pin's ends are finally secured with bolts to ensure connection with the support frame is maintained. The workmen perform the activities from work access platforms, which are installed prior to this phase.

7.1.6. Topsides removal phase

Installation of the removal rigging

During the connection phase, the removal rigging is prepared and the SSCV establishes its topsides removal position. It has been decided to use rigging arrangement A, as shown in figure 4.4. The 55-45 distribution corresponding to this rigging arrangement is favorable for the topsides. Also, the vertically oriented slings will not impose large side loads from the rigging. The topsides is planned to be lifted over the stern of the vessel, at an heading of 250 degrees and a crane radius of 48 meters. Prior to lifting the topsides off its substructure, the removal rigging has to be installed. Installation of the removal rigging is shown in figure 7.9.

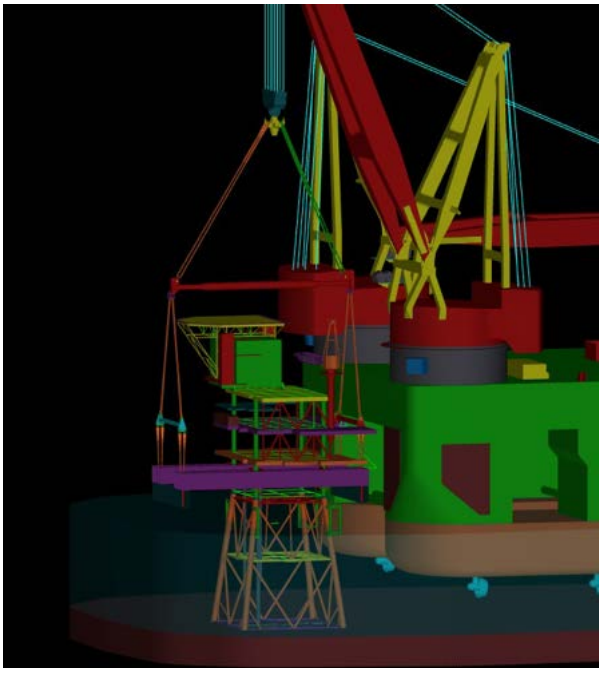

Figure 7.9: Installation of the removal rigging

For the rigging existing assets are used, except for the longitudinal spreader bar, which has to be modified due to the combination of a large load and a large span. The length of the upper rigging is such that there is an offset of approximately 1 meter between the hook and the CoG of the assembly. More information about the rigging can be found in Appendix F.4. As previously mentioned, ILT's will be used as lift points for topside removal. An ILT is a cylindrical shaped tool, equipped with sharp contact teeth over its height. An impression of an ILT is provided in figure 7.10.

Figure 7.10: Example of an ILT

The ILT's are slowly lowered into the ILT interfaces which are housed in the cross-beams. When the ILT is lifted, the teeth expand, and grip onto the ILT interface. It is thereby important that the ILT is vertically loaded. This way no external moment is applied to the ILT. An external moment could cause one part of the circumference to take up more of the load, and potentially contact may get lost with the other parts. The ILT can be operated remotely and provides a quick and safe solution to remove the topsides. Its application is especially useful for locations that are otherwise hard to reach. The ILT interface is a steel plate which has sufficient thickness to grip onto, and withstand the gripping forces. Stiffeners will be applied around the ILT interface to take up the horizontal contact force and distribute it to the cross-section of the cross-beam. After connecting the ILT's, the topsides is ready to be removed.

Static lift stability

During topsides removal, the lift points are located below the CoG of the assembly. Excessive tilting and shifting of the topsides can result in toppling of the lift object. This happens when the gravity and the sling forces can't provide a resisting moment against the tilt. This is the case when the CoG shifts out of the rigging envelope or when alignment between the lower rigging and upper rigging is reached. In this case, the rigging loads can't restrain the tilting motion of the topsides and the topsides will eventually fall over. This situation is governing over the transverse direction, where the spacing of the lift points is relatively short. The shorter this distance, the smaller the tilt or shift needs to be for the CoG to fall out of the rigging envelope.

It is thereby of importance to investigate the stability of the lift. The static stability of the lift is assessed in AGES. The sensitivity of the lift to toppling is assessed by imposing CoG inaccuracies to the lift object, and applying external loads to the system. Inaccuracies regarding the lift object's CoG will result in tilt, until the CoG is positioned right under the hook. In the early design phase it is suggested to consider a CoG envelope which has a size of 5% of the lift object's dimension in the respective direction [27].

The external loads cause an overturning moment of the lift object and hence also tilting of the topsides. Two types of external loads are considered; a wind load and an impact load. The wind load acts over the height of the topsides, and has its CoF positioned above the topsides CoG. For the wind speed profile the power law is used. The impact load could be caused by impact between the topsides and guides or bumpers, during set down of the topsides on deck. It is assumed that the impact load acts on the bottom of the MSF legs, since the lever arm of the load to the topsides CoG is largest in this case. The impact load can be taken as 5% of the unfactored weight of the lift object [45].

The largest overturning moment is reached when the wind load and impact load work in opposite directions. Eventually the governing case is assessed in which the CoG inaccuracies are included. Hereby a maximum wind speed can be determined for which toppling of the topsides won't occur. The results of the static lift analysis are provided in Appendix F.4. It was found that excluding the impact loads a maximum wind speed of 137 knots can be applied. Including the impact loads, the maximum wind speed for which toppling won't occur is equal to 112 knots.

Dynamic response of the topsides

Additionally, the dynamic response of the topsides during removal is assessed using LiftDyn. Limiting criteria are defined for which collision between the topsides and the rigging, and the rigging and SSCV, won't occur. Furthermore, limiting criteria are set on the rigging load fluctuation to examine whether slack of the rigging occurs. In this analysis no CoG inaccuracies are included. It is however advised to investigate whether CoG inaccuracies will have a significant effect on the operability of the operation. The results are provided in Appendix F.4. It was found that slack of slings M1 and M2 can occur for peak periods between 7 and 9 seconds and a wave height of approximately 6 meters. Regarding the relative motions of the assembly, it was found that the limits for these motions can be exceeded for peak periods greater than 10.5 seconds. Both these intervals, considering the allowable wave heights, are considered to be out of the danger zone of the operation.

After lifting the topsides off its substructure, the assembly is elevated and rotated towards the SSCV deck and subsequently lowered. These steps are shown in figures 7.11, 7.12 and 7.13 respectively.

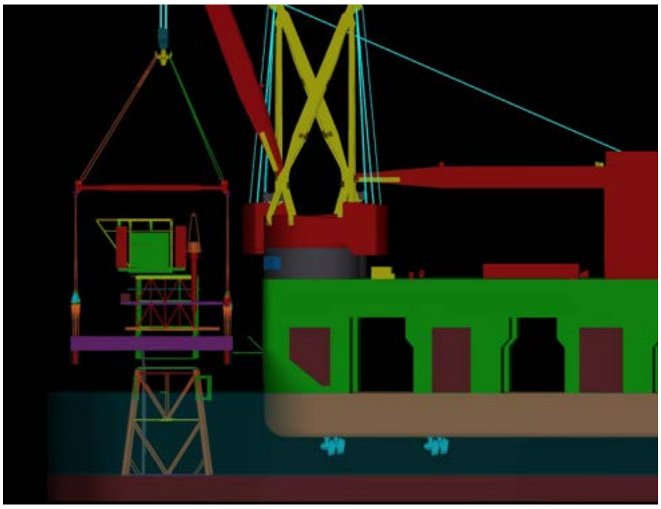

Figure 7.11: Lift topsides off substructure

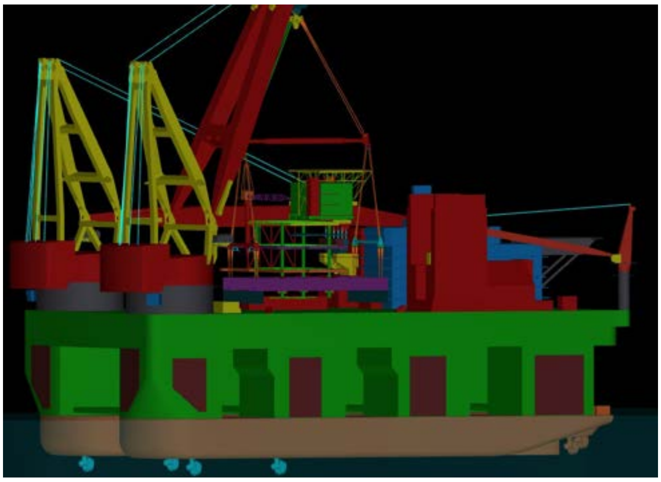

Figure 7.12: Rotate topsides to deck

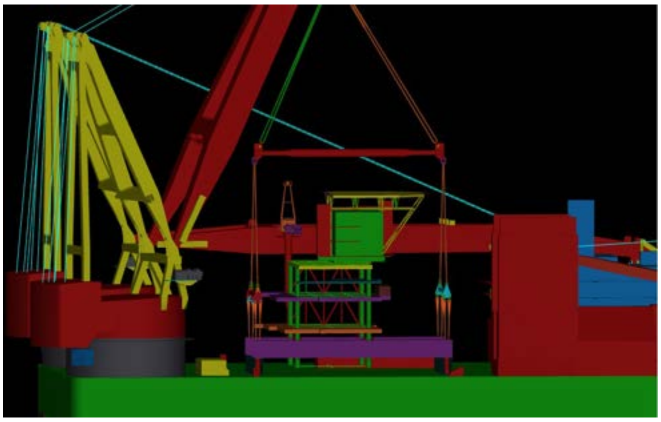

Figure 7.13: Lower topsides onto deck

7.1.7. Transportation and offloading phase

After placing the topsides on deck, the SSCV sails to calm waters. Here, the topsides, including lift frame is lifted onto a barge, which will transport the topsides to the destined yard. The topsides transfer to the barge is shown in figure 7.14.

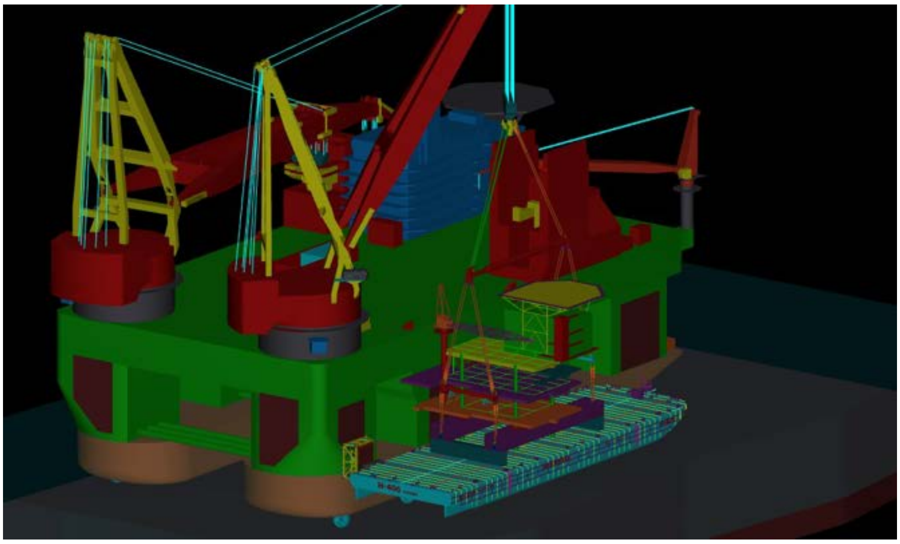

Figure 7.14: Lift topsides to barge for transportation

The barge is equipped with skids, or alternatively with SPMT's, on which the assembly is placed and the topsides is subsequently sea-fastened. Upon arrival at the yard, the barge is moored, and levelled with the quay, as shown in figure 7.15.

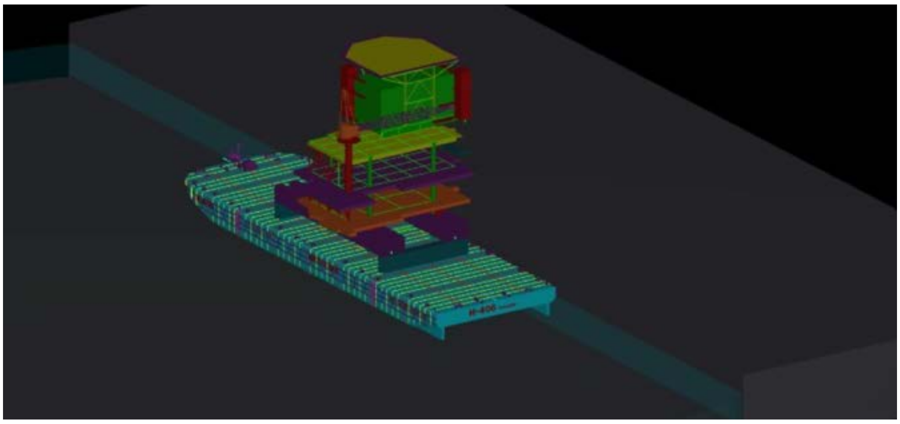

Figure 7.15: Topsides offloaded to quay by barge

The skids on deck of the barge are connected to skids on-shore, and the assembly is skidded to its final destination in this manner. With the use of SPMT's, the topsides can slowly be transported from the barge to the yard. The assembly is then elevated and the topsides is placed on a support structure. Finally the lift frame is disconnected and retrieved to be used for another topsides removal project.

7.2. Topsides removal time

7.2.1. Main activities

The lift beams topsides removal process can be divided in four stages: topsides preparation, lift frame installation, topsides removal and topsides offloading. An overview of the main activities in these stages is provided in figure 7.6. An estimate for the duration is provided for the first three stages in Appendix F.5. Here, also an overview of the sequence of the steps is shown.

Stage	Activity
Topside preparation	On-deck preparations
	Removal of under-deck obstructions
	Preparation of the MSF legs
	Welding of temporary supports onto the MSF legs
	Cutting free of the MSF legs
Lift frame installation	Install lift beams onto temporary support
	Drain the counterweight
	Disconnect the counterweight and lift back on deck
	Install the cross-beams
	Connect the lift beams with the MSF legs
Topside removal	Attach the removal rigging to the lift frame
	Lift the topside off its substructure and put the assembly on deck
Transportation and offloading	Sail to calm waters with the SSCV
	Lift the topside including lift frame onto a barge
	Topside including lift frame offloaded to yard

Figure 7.16: Lift beams topside removal main activities

The topsides preparation phase is executed well before actual topsides removal. In this stage a platform supply vessel will be needed to (de)mobilize workmen, equipment and materials and provide accommodation. The first two activities can be executed simultaneously. The last three steps should be performed in the given sequence. The leg has to be prepared before any activities are performed on it. Welding of the temporary supports should occur before cutting the MSF legs. This way the leg is not additionally loaded after cutting free from its substructure. It is estimated that approximately one week is required to complete the topsides preparation stage.

For the lift frame installation phase, the first three steps are repeated four times. After installation of each lift beam, the counterweight is refilled and connected to the following lift beam. Installation of a lift beam is estimated to take 30 minutes, and is performed in DP mode. Retrieval of the counterweight and preparations for the following lift are estimated to take one hour. Installation of the cross-beams is strongly dependant on the pitch and roll motions of the SSCV and is approximated to take one hour per cross-beam. Prior to connection of the lift beams to the MSF legs, holes have to be cut. This is done simultaneously for all four legs and is estimated to take a total of six hours. Penetration of the pin is hydraulically driven and is completed quickly. While the connection is being established, the SSCV will take its removal position. Hereby the functioning of the SSCV is optionally rechecked and the ballasting of the SSCV is adjusted prior to the lift.

Before lifting the topsides, the ILT's are lowered into the ILT interface. This process is estimated to take one hour. After connection of the ILT's the topsides is ready to be removed. The topsides is lifted off its substructure and put on deck. Lifting can be done relatively quickly at 3.4m/min using 60 sheaves. The lifting speed can be doubled by reducing the number of sheaves to 30. The capacity of the main hoist will decrease doing this, and therefore this could only be applied to the smaller platforms. The duration of topsides removal is mainly driven by ballasting of the SSCV. The total operation for lifting the topsides off its substructure and putting it on deck is approximated to take one hour.

After topsides removal the SSCV sails to a remote, calm area and drops the assembly off to a barge. Here, the assembly is sea-fastened and transported to the destined yard. Offloading of the assembly happens by means of skidding or using SPMT's. The topsides is eventually handed over to a support structure, the lift beams are disconnected, and retrieved to be prepared for another removal job.

7.2.2. Topsides removal time

The time required for installation of the lift frame and removal of the topside is one of the parameters to express the performance of the lift beams topsides removal concept. The total required SSCV time for the lift beams concept can be compared with the case for reversed installation. Through one-on-one sessions with company experts, estimates are obtained for the duration of the lift frame installation and topside removal stages. An overview of the time path is provided in Appendix F.5. It has been found that, excluding the waiting on weather time, the total duration for removal of reference topsides 14 is equal to 33 hours. The time starts from arrival of the SSCV, and ends when the topsides is lifted on deck of the SSCV.

Removal of reference topsides 14 is initially planned to be done with reversed installation. The total topsides removal time, excluding waiting on weather time, was estimated at 133 hours. This indicates an offshore SSCV time reduction of 75 %. Unfortunately, no data was available including waiting on weather time.

However for the lift beams concept, the weather sensitivity effects can still be included. The duration of the lift frame installation steps, and topsides removal steps are put in a sequence for this sake. For the installation of the lift beams and the cross-beams, and removal of the topsides, limiting criteria are applied for the lift object's motions. For all steps an operational limit is applied to the wind speed at 25 knots. The limiting motions for installation of the lift beam have been discussed in section 6.4.1. For installation of the cross-beams, the limiting heave motion is defined by the lift beams and the water surface, and is equal to 2.4 meters. The limiting sway motion is defined by the width of the lift beam, and is set at 1.11 meters. These values represent the maximum allowable single amplitude of the motions. Installation of the cross-beam is done with the use of a spreader bar, at a crane radius of 26.7 meters for the cross-beam near the SSCV's starboard, and at 79 meters for the other cross-beam. As previously, a SSCV heading of 160 degrees, and a slew angle of 90 degrees have been used. The limiting criteria for removal of the reference topsides are discussed in Appendix F.4. It has to be noted that the heading of the SSCV and the crane configuration are adjusted for this operation.

The waiting on weather time is determined with the in-house Sequencetool, and takes the sequence of the steps, the duration of the steps, and the limiting criteria per step into account. Originally, removal of reference topside 14 is planned in the month October. The total average waiting on weather time in this month is found to be 30 hours. This comes down to an expected total offshore SSCV time of 63 hours. An overview of the waiting time per step is provided in Appendix F.5. It has to be noted that the waiting on weather time is an average estimate based on a 20 year dataset. In reality the weather can strongly vary over relatively short spans. This is especially the case for the winter months.

7.3. Lift beams concept costs

The total costs for the lift beams concept are mainly composed of capital costs for the lift frame and the connection elements, operational costs for the supply vessel during the preparation phase, and costs for the SSCV during the topsides removal phase. The total costs for the lift beams concept are then compared to the costs for reversed installation. The costs for reversed installation are only expressed in operational costs for the SSCV. In both equations, the costs for workmen, additional equipment and materials is excluded. It therefore has to be noted that the economic comparison is somewhat incomplete. It has been decided to not take the aforementioned factors into account, since these variables are not known for the case of reversed installation. Excluding these factors from the costs of both methods will allow for a fair, yet incomplete, comparison. Furthermore it has to be noted that the sailing time of the SSCV to the location is not included. The topsides location differs for each project, and it is unknown from which location the SSCV departs.

The costs for the lift frame consist of material costs and fabrication costs. The material cost for S460 steel is equal to 1.30EUR/kg. The fabrication cost for the beam, excluding stiffeners , is equal to 1EUR/kg. The fabrication cost for stiffeners is higher due to the more complex welding process, and equals 2EUR/kg. Finally the costs for the connection elements between the lift beam and counterweight has to be taken into account. Due to its shape and location, the complexity of the welding and fitting increases, and therefore the fabrication costs are also estimated to be 2EUR/kg. For this connection S690 steel is used, which costs 2EUR/kg. The total costs per lift beam are then equal to:

$$Costs_{LB} = W_{dry,profile} * (1.30 + 1) + W_{dry,stiffeners} * (1.30 + 2) + W_{dry,connectionhooks} * (2 + 2) = 221 * 10^3 * 2.30 + 36 * 10^3 * 3.30 + 14.5 * 10^3 * 4 \approx 685,000EUR$$

For the cross-beams the same costs are assumed as for the lift beams. The total lift frame costs are therefore equal to:

$$Costs_{frame} = 6 * 685,000 = 4.1MEUR$$

The costs for the connection are composed of the costs for the hydraulic pin and the support frame. The costs per hydraulic pin, including corresponding components, is estimated at 175,000EUR. The pin support frame is made of S355 steel, for which the material costs are equal to 1EUR/kg. The fabrication costs for the support frame are estimated at 2EUR/kg. The total costs for the connection are then equal to:

$$Costs_{connection} = 4 * 175,000 + (8 * 22 * 10^3) * (2 + 1) = 1.23MEUR$$

The total capital costs for the lift frame, including connections, is approximately equal to 5.3 MEUR. It has to be noted that this value is based on topsides with a jacket substructure consisting of 4 legs.

The operational costs for the preparation phase are estimated by the costs for the support vessel, which is required for approximately one week. The day rate for such a vessel, including fuel, is estimated at 25,000EUR/day. The total costs for the operation phase are then estimated at:

$$Costs_{preparation} = 7 * 25,000 = 175,000EUR$$

Finally the costs for the topsides removal phase are estimated by the offshore SSCV time, which in general can be considered as the main driving factor for the topsides removal costs. Here, a fictive day rate is assumed for the Sleipnir of 1MEUR/day. The topsides removal costs, excluding waiting on weather time, are then equal to:

$$Costs_{topside,removal} = \frac{33}{24} * 1,000,000 = 1,375,000EUR$$

The total costs for removal of reference topsides 14, excluding waiting on weather, are then equal to:

$$Costs_{total} = 4.1 + 1.23 + 0.175 + 1.375 = 6.88MEUR$$

And including waiting on weather:

$$Costs_{total} = 4.1 + 1.23 + 0.175 + 2.625 = 8.13MEUR$$

The costs for removal of reference topsides 14, excluding waiting on weather time is equal to:

$$Costs_{rev.ins} = \frac{133}{24} * 1,000,000 = 5.54MEUR$$

It has to be noted that the waiting on weather time for reversed installation is expected to result in significantly higher costs. The number of operations is relatively large and the likelihood of delays on the critical path of topsides removal therefore increases. Including the waiting on weather time may therefore reduce the difference in costs for removal of reference topside 14.

The lift beams concept becomes only profitable if it can be reused for a numerous amount of times. The topsides removal time for the other topsides can't be determined, since it depends on a large number of variables, including the weight, composition and state of the topside. It however can be determined how much topsides, that are identical to reference topsides 14, have to be removed in order for the lift beams concept to become profitable. This is shown below. As previously discussed, the waiting on weather is not included in this relation, since this variable is unknown for the reversed installation case.

$$C_{capital} + n * 0.175 + n * 1.375 = n * 5.54$$

$$5.33 + 1.55n = 5.54n$$

$$n = 1.34$$

It can be seen that after removal of two such topsides, the lift beams concept appears to become profitable. This number could potentially be reduced to one topsides removal, when the waiting on weather time and the offshore man hours are included in the costs calculations. Furthermore it has to be noted that the waiting on weather time in the summer months is as low as 4 hours, resulting in a total operation time of 37 hours. A complete overview of the total expected operation time per month, including waiting on weather, is provided in Appendix F.5.

8 Conclusions and recommendations

In this section the main conclusions about the lift beams concept are drawn. Additionally, recommendations are provided for application of the lift beams concept and for improvement or further investigation of certain aspects.

8.1. Conclusions

- A single lift topsides removal concept using so-called lift beams has been designed and to a certain degree optimised. The design complies with a variety of modular built topsides in the SNS. The concept is based on a single crane lift, which allows to place the topsides on deck after removal.
- The lift beams are designed to withstand the governing load case, while complying with the dimensional criteria. A steel plated beam is used with a box-profile, made of S460NL steel. The design of the lift beams is optimised in order to minimise its weight. The dry weight of the lift beam for two-sided support, including stiffeners, is equal to 257 mT.
- The topsides can withstand it to be lifted by the lift beams. The MSF legs and the MSF deck are both found to be suitable connection locations. Eventually it is decided to connect the lift beams to the MSF legs.
- The optimal lift beam setup consists of two-sided leg support with a cross-beam on both ends of the lift beams. The optimal rigging arrangement consists of two transverse spreader bars, and one longitudinal spreader bar.
- A pin-hole connection is used for the connection between the lift beams and the MSF legs. The pin is hydraulically driven and is supported by a support frame on each end. The neutral axis of the lift beams is aligned with the neutral axis of the MSF legs. The topsides has sufficient capacity to withstand the loads for this connection.
- The lift beams are installed one-by-one with the use of a counterweight. The counterweight is a steel box filled with water, which is drained and disconnected after installation of the lift beam. Tugger lines are used to dampen the governing heave motion of the lift beam during installation.
- The cross-beams are installed below the lift beams with the use of stabbing cones. For the lift points, ILT’s are used, which are housed in the cross-beam.
- For reference topsides 14, the optimal lift setup for installation is at an SSCV heading of 160 degrees, a slew angle of 90 degrees and a crane radius of 45.5 meters. The duration for removal of reference topsides 14, excluding waiting on weather time, is estimated at 33 hours. In case of reversed installation, the removal time, excluding waiting on weather time, is equal to 133 hours. This implies an offshore SSCV time reduction of 75 %.
- For a lift frame consisting of four lift beams and two cross-beams, the capital costs for the lift beams concept are estimated at approximately 5 MEUR. Using a fictive day rate for the SSCV, the lift beams concept is expected to become profitable after the removal of two topsides, which are similar to reference topsides 14.
- The lift beams concept provides a relatively quick and cost-effective solution for the removal of lighter modular built topsides. Given the reusability of the concept, a relatively quick return on investment can be expected.

8.2. Recommendations

- For the smaller topsides in the batch, it is recommended to only use lift beams on the exterior of the MSF legs. It was shown that one-sided leg support, with cross-beams, can be sufficient regarding the structural integrity of the topsides. This is especially the case for the smaller topsides, where the weight of the lift beams is relatively high compared to the weight of the topsides. This setup will also allow for a shorter topsides removal time. The available under-deck space for these topsides is in general lower. The lift beam's limiting motions during installation can significantly be increased this way. This will eventually provide a wider range over the year, in which removal of such platforms can be achieved in a relatively quick manner.

- It is recommended to investigate the opportunities to perform the lift beams topsides removal concept with a dual crane lift. This could significantly improve the installation of the lift beams and the rigging, and hence the complete topsides removal process. Also it might not be necessary to weld temporary supports, reducing the preparation scope. For a dual crane lift, the topsides can't be placed on deck of the SSCV. However the assembly could potentially be transported, while suspended in the cranes, to calmer waters, where it is transferred to a barge. Also, the range of potential topsides for removal with the lift beams concept increases, as the lifting capacity increases.

- It is recommended to perform additional structural integrity analyses on the other topsides in the batch. This way it can be ensured what the limits for the other topsides are. It can be found that one-sided leg support is also sufficient for the larger topsides. If this is the case, the weight and costs of the lift frame can be reduced. Also the topsides removal time will reduce this way.

- The geometric lock has shown potential as a connection type between the lift beams and the MSF legs. One of the characteristics of this concept is that torsion of the lift beams is restrained and hence the use and installation of cross-beams could potentially be avoided. The modelling of this connection in SACS is based on certain assumptions. With these assumptions, deviations were observed with the model in Abaqus. It is therefore advised to further investigate the connection stiffness of this connection concept.

- Finally it is advised to further investigate the possibilities for the connection between the lift beams and the cross-beams. The current design is found to be somewhat complicated in its installation and retrieval after disposal of the topsides. It is also advised to investigate the possibilities of using short cross-beams, which only connect adjacent lift beams. The length of the cross-beams doesn't need to be modified for different MSF leg spacings in this case.

List of Figures

List of Tables

A
SSCV Sleipnir characteristics

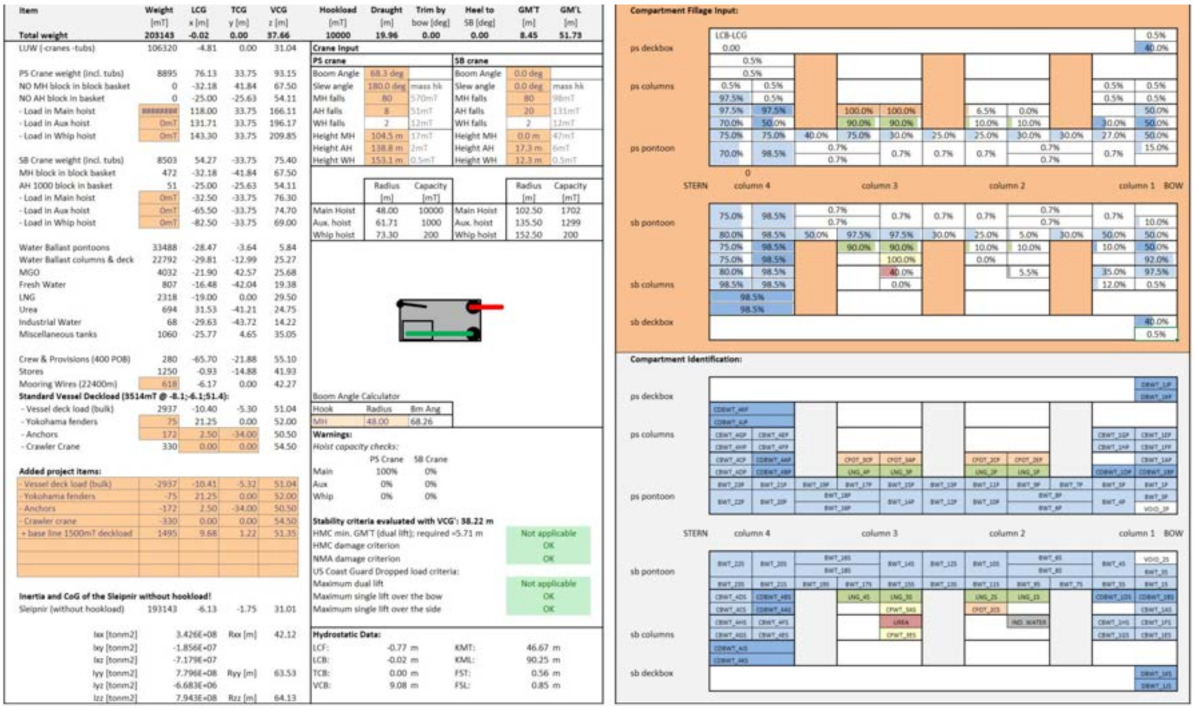

Figure A.1: Hydrostatic stability results

B
Design of the lift beams

B.1. Dimensional requirements

The maximum height of the lift beams follows from the available space between the cellar deck and jacket top horizontal elevation.

$$H_{max} = (H_{cellardeck} - H_{top.el.jacket}) - H_{clearance} \tag{B.1}$$

$$where : H_{clearance} = 2[m]$$

A height clearance of two meters is taken to account for:

- Sufficient space during installation
- Lift beam deflections during lifting
- Connection element dimensions
- Presence of under-deck obstructions

The governing lift beam height is based on reference topside 8. Figure B.1 gives an indication of this.

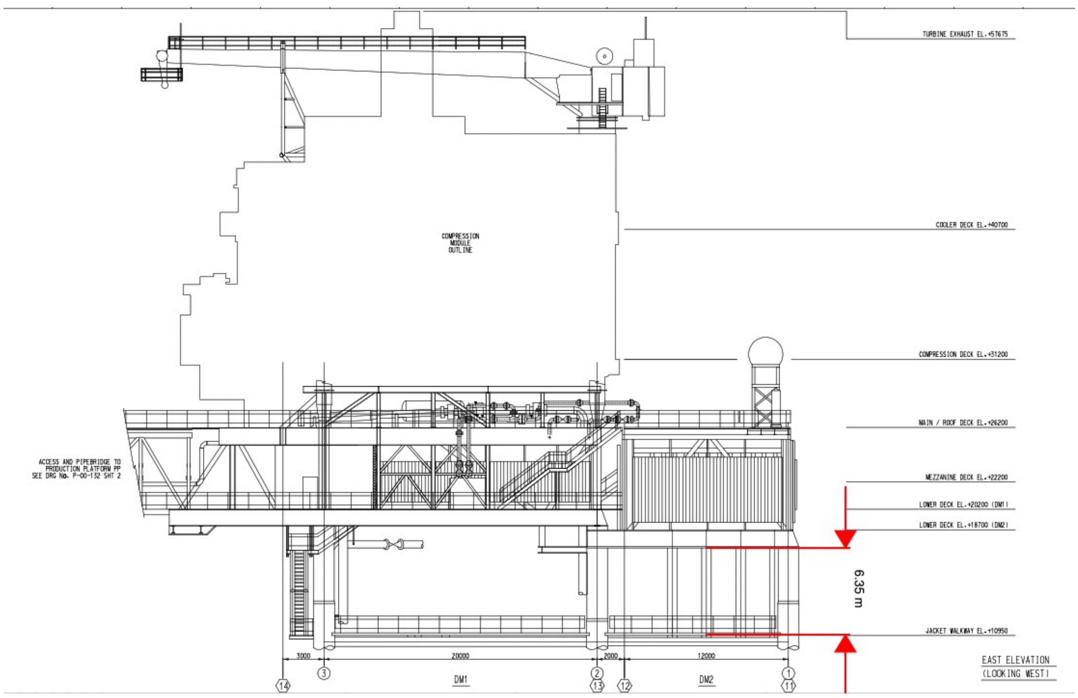

Figure B.1: Governing lift beam height

It follows that the maximum allowable lift beam height is equal to 4.35 meters. It has to be noted that the jacket walkway rails would have to be destructed for this.

The maximum width of the lift beams follows from the MSF leg spacing.The width is taken such that there is sufficient space for two lift beams between MSF legs.

$$B_{max} = \frac{B_{leg-spacing} - 2B_{clearance}}{2} \tag{B.2}$$

$$where : B_{clearance} = 2[m]$$

A width clearance of 2 meters is taken to account for:

- Sufficient space during installation
- Size of connection elements

The governing lift beam width is based on reference topside 2. The jacket leg spacing is shown in figure B.2.

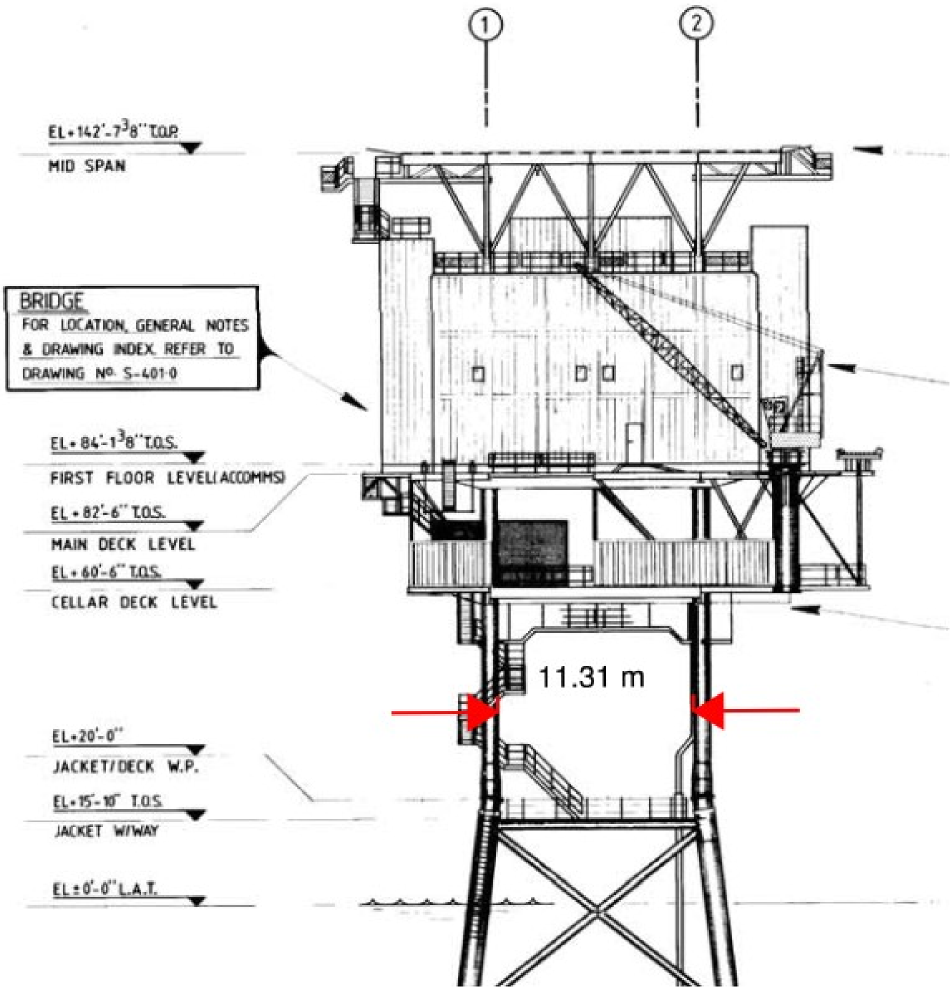

Figure B.2: Governing lift beam width

Applying equation B.2, it follows that the maximum allowable lift beam width is equal to 3.65 meters. The stairs from the cellar deck to the jacket walkway would have to be destructed prior to lift beam installation.

Finally, the minimum required length of the lift beams follows from the largest projected topside span:

$$L_{min} = L_{topside} + 2L_{clearance} \tag{B.3}$$

$$where : L_{clearance} = 2[m]$$

Clearance on both ends of the lift beam is taken to account for:

- Rigging clearances
- Installation offsets

The governing lift beam length is based on reference topside 7, which is shown in figure B.3.

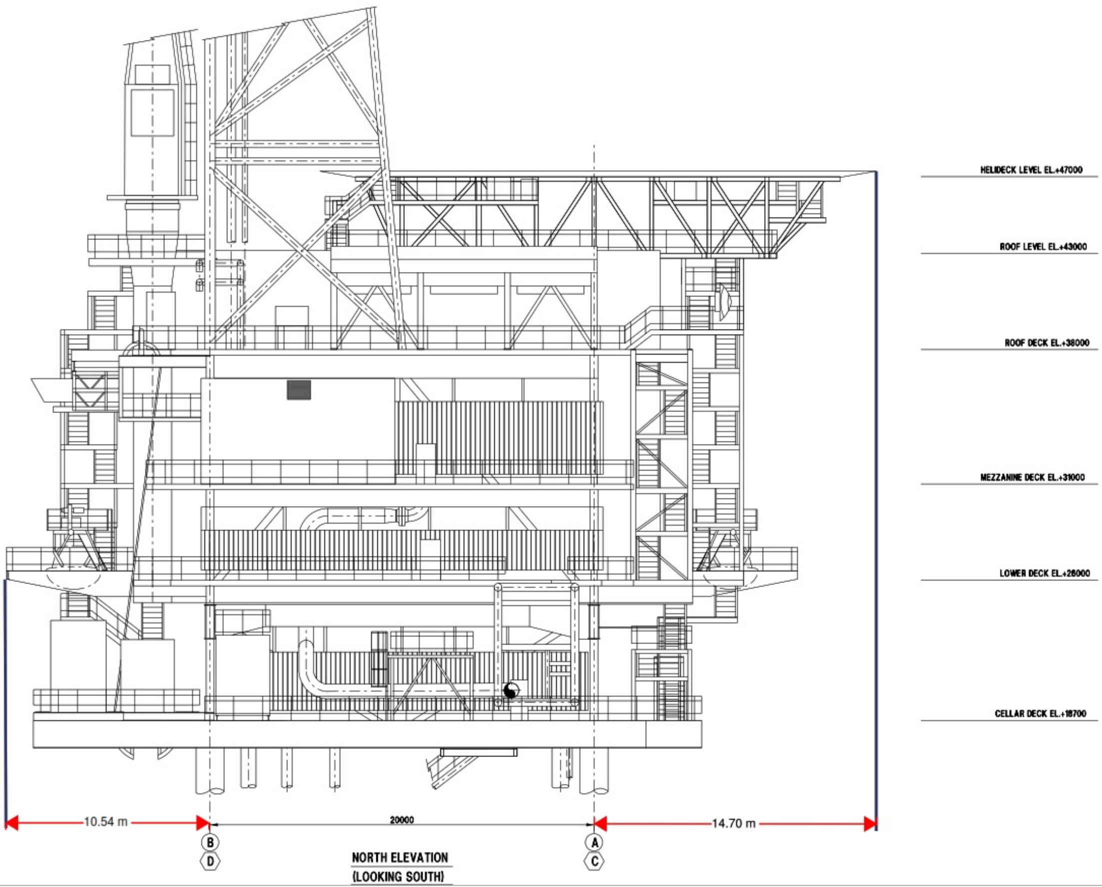

Figure B.3: Governing lift beam length

B.2. Indicative truss beam design

In this section an initial design for the truss is determined to get an indication on the potential weight that could be saved. Thereby it has to be noted that for simplicity, torsion is not included in the design of the truss. Also no punching shear check is performed. For further investigation it is advised to account for these aspects.

It has been decided that a Pratt truss is most suitable for the lift beams. An impression of the truss is provided in figure B.4.

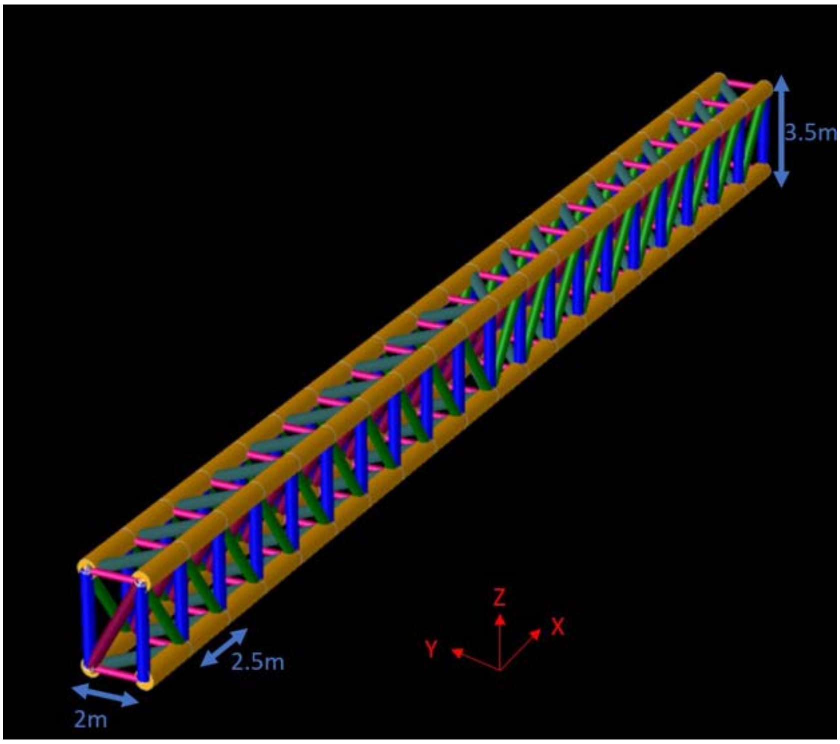

Figure B.4: Pratt truss design

Colours are used to indicate the different member types. The cross-sectional profiles and the corresponding properties are provided in table below.

Member	Profile	A[mm^2]	$I_{x/y}$ [mm^4]	r [mm]	L [mm]	KL/r [-]
Vertical (Blue)	CHS 406.4/16	19624	375	138	3500	25.3
Horizontal, x-z (Yellow)	CHS 711/50	103830	5703	234	2500	10.7
Diagonal, x-z (Green)	CHS 355.6/25	25965	357	117	4301	36.7
Horizontal, y-z (Pink)	CHS 101.6/5	1517	1.8	34	2000	58.5
Diagonal, x-y (Teal)	CHS 114.3/8	2672	3.8	38	4031	85.0
Diagonal, y-z (Burgundy)	CHS 139.7/10	4075	8.6	46	3202	87

The loads acting on each plane are shown in figures below. It is assumed that the vertical and longitudinal loads are equally distributed over the rows in the x-z plane. The effects of torsion are therefore for simplicity excluded.

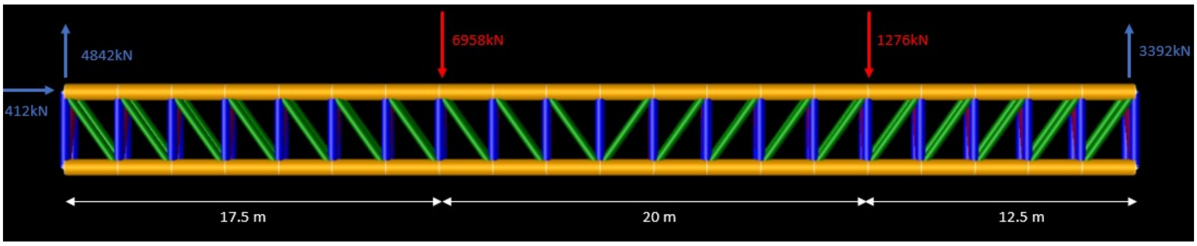

Figure B.5: Load case x-z plane

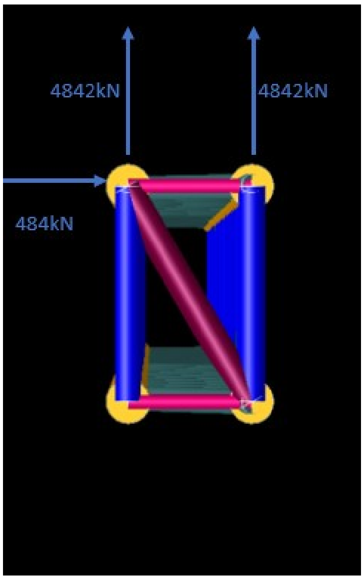

Figure B.6: Load case y-z plane

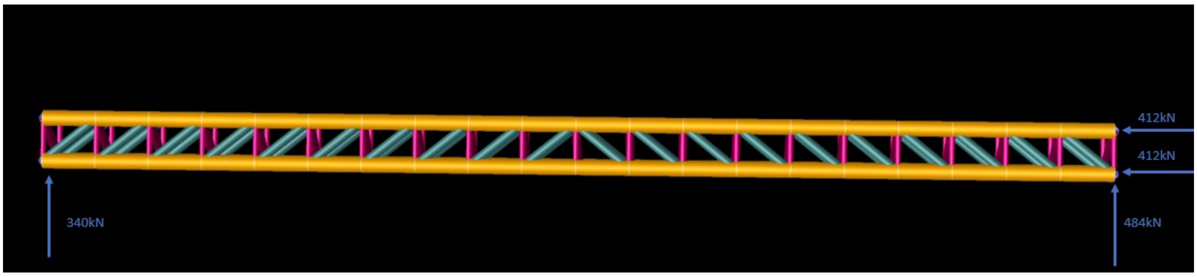

Figure B.7: Load case x-y plane

The truss structure is statically undetermined, and the load up take per member can't therefore be found from joint equilibrium. The load that is carried by each member, depends on the stiffness and orientation of the member. It is therefore recommended to get a better insight on the load uptake per member in order to improve their dimensions. Hereby, the layout of the truss and the spacing between members can be improved as well.

The member loads are approximated to be equal to:

$$F_{vert} = 4842kN$$

$$F_{diag,x-z} = \frac{4842}{cos(35.53)} = 5950kN$$

$$F_{hor,x-z} = 412 + \frac{17.5*4842+412*3.5/2}{3.5} + 484 * 17.5/2 = 26943kN$$

$$F_{hor,y-z} = 242kN$$

$$F_{diag,y-z} = 242/cos(60) = 484kN$$

$$F_{diag,x-y} = 2311/cos(51.34) = 388kN$$

The allowable stresses, the acting stresses and the unity checks for each member type are provided in table B.1. S460NL steel is used for the members.

Member	Critical buckling stress [MPa]	Acting stress [MPa]	UC [-]
Vertical	251.4	246.7	0.98
Horizontal, x-z	235.9	229.2	0.97
Diagonal, x-z	267.5	259.5	0.97
Horizontal, y-z	199.5	159.5	0.80
Diagonal, x-y	144.2	144.0	1.00
Diagonal, y-z	139.5	118.8	0.85

Table B.1: Overview of the UC's of the truss members

The critical buckling stress is determined with equations B.4 B.5. If $Kl/r \leq C_c$:

$$F_a = \frac{[1 - \frac{(Kl/r)^2]}{2C_c^2}]F_y}{\frac{5}{3} + \frac{3(Kl/r)}{8C_c} - \frac{(kl/r)^3}{8C_c^3}} \tag{B.4}$$

If $Kl/r > C_c$

$$F_a = \frac{12\pi^2 E}{23(Kl/r)^2} \tag{B.5}$$

Where:

$$C_c = \sqrt{\frac{2\pi^2 E}{F_y}} \tag{B.6}$$

It has to be noted that an additional punching shear check should be performed for the joints where the members meet the chord. The D/t ratio of the members may need to be adjusted to satisfy the check.

In figure B.8 the maximum combined unity checks and the failing members from SACS are shown.

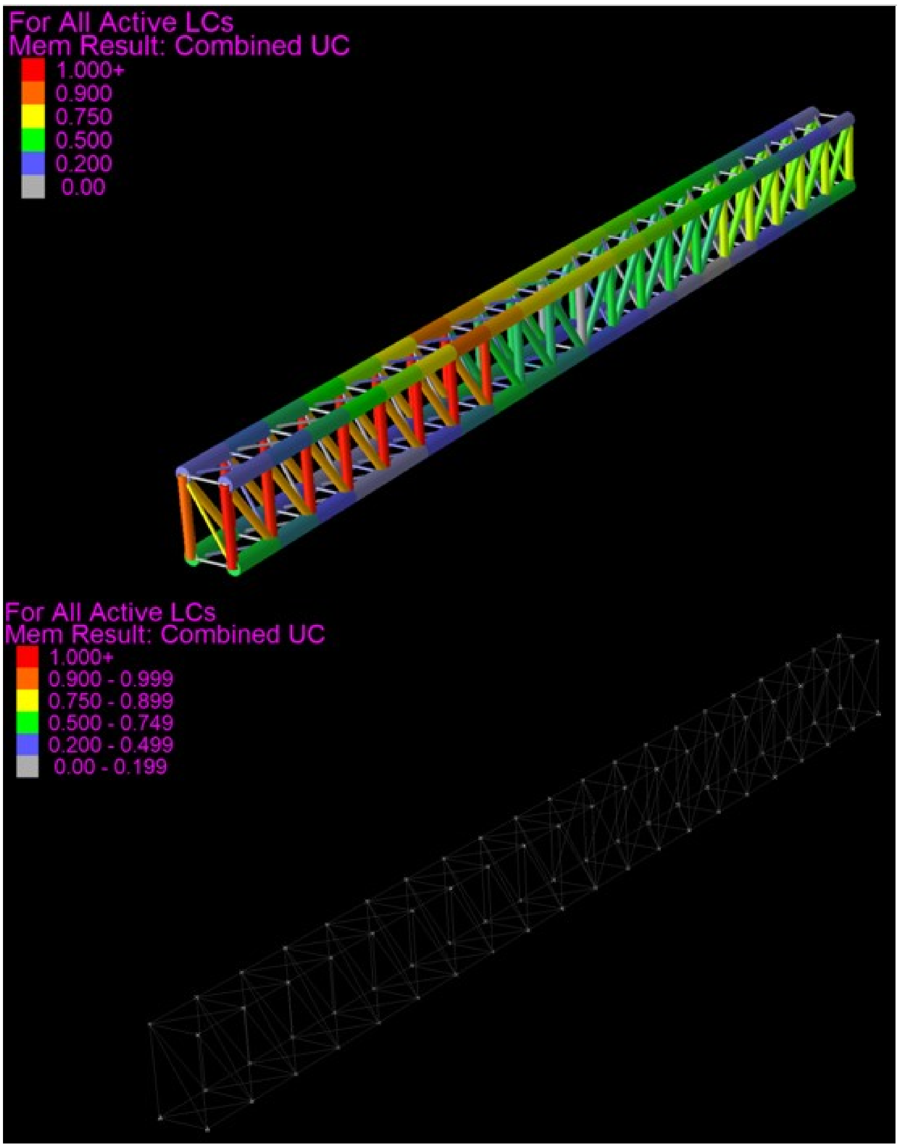

Figure B.8: Maximum combined unity checks (top) and failing members (bottom) in SACS

It can be seen that no failing members are identified. The unity checks of the horizontal and diagonal y-z member as well as the diagonal x-y member are far below the limit and their structural properties can likely be reduced. On the other hand, the effects of torsion will require increased structural properties of certain members. Taking all of this into account, it is considered that this initial design can be used as a reasonable indication for the weight of the lift beam when a truss structure is applied.
The total weight of the truss structure is equal to:

$$W_{truss} = \sum (A_i * L_i * n_i) * \rho_{st} = 227mT \tag{B.7}$$

B.3. Lift beam design

Description of Element	Width-Thickness Ratio	Limiting Width-Thickness Ratios: Compact	Limiting Width-Thickness Ratios: Noncompact[c]
Flanges of I-shaped rolled beams and channels in flexure[a]	b/t	$65/\sqrt{F_y}$	$95/\sqrt{F_y}$
Flanges of I-shaped welded beams in flexure	b/t	$65/\sqrt{F_y}$	$95/\sqrt{F_{yf}/k_c}$[e]
Outstanding legs of pairs of angles in continuous contact; angles or plates projecting from rolled beams or columns; stiffeners on plate girders	b/t	NA	$95/\sqrt{F_y}$
Angles or plates projecting from girders, built-up columns or other compression members; compression flanges of plate girders	b/t	NA	$95/\sqrt{F_y/k_c}$
Stems of tees	d/t	NA	$127/\sqrt{F_y}$
Unstiffened elements simply supported along one edge, such as legs of single-angle struts, legs of double-angle struts with separators and cross or star-shaped cross sections	b/t	NA	$76/\sqrt{F_y}$
Flanges of square and rectangular box and hollow structural sections of uniform thickness subject to bending or compression[d]; flange cover plates and diaphragm plates between lines of fasteners or welds	b/t	$190/\sqrt{F_y}$	$238/\sqrt{F_y}$
Unsupported width of cover plates perforated with a succession of access holes[b]	b/t	NA	$317/\sqrt{F_y}$
All other uniformly compressed stiffened elements, i.e., supported along two edges	b/t h/t_w	NA	$253/\sqrt{F_y}$
Webs in flexural compression[a]	d/t	$640/\sqrt{F_y}$	—
	h/t_w	—	$760/\sqrt{F_b}$
Webs in combined flexural and axial compression	d/t_w	for $f_a/F_y \le 0.16$ $\frac{640}{\sqrt{F_y}}\left(1 - 3.74\frac{f_a}{F_y}\right)$	—
		for $f_a/F_y > 0.16$ $257/\sqrt{F_y}$	
	h/t_w	—	$760/\sqrt{F_b}$
Circular hollow sections In axial compression In flexure	D/t	 $3{,}300/F_y$ $3{,}300/F_y$	 — —

[a]For hybrid beams, use the yield strength of the flange F_{yf} instead of F_y.
[b]Assumes net area of plate at widest hole.
[c]For design of slender sections that exceed the noncompact limits see Appendix B5.
[d]See also Sect. F3.1.
[e]$k_c = \frac{4.05}{(h/t)^{0.46}}$ if $h/t > 70$, otherwise $k_c = 1.0$.

Figure B.9: Element slenderness limits [10]

B.3.1. Reduced cross-sectional properties

As discussed in section 3.4.2, the cross-sectional elements for the two-sided support beam are classified as slender. The cross-sectional properties of slender elements are reduced by assuming an effective width. The effective width is applied for the loads that cause uniformly compressive stress in the elements [36]. The effective width of the flanges is determined with equation B.8, and the effective width of the webs with equation B.9.

$$B_e = \frac{253t_f}{\sqrt{f_{c,f}}} * (1 - \frac{50.3}{\frac{b}{t_f}\sqrt{f_{c,f}}}) = 2.2m \tag{B.8}$$

$$H_e = \frac{253t_w}{\sqrt{f_{c,w}}} * (1 - \frac{44.3}{\frac{h}{t_w}\sqrt{f_{c,w}}}) = 3.3m \tag{B.9}$$

Here, f_c is equal to the sum of compressive stresses in the element under consideration. The reduced cross-sectional properties are then simply determined by substituting $B = B_e$ and $H = H_e$. For strong-axis bending B_e is used for the width, as only the flanges are uniformly compressed under strong-axis bending. Similarly H_e is used as the effective width for weak-axis bending. For the axial compressive load, both B_e and H_e are used, since all elements are uniformly compressed by this load. Equations B.8, B.9 and B.10 are used to determine the reduced cross-sectional properties for the two-sided support beam. The reduced properties are applied in determining the allowable stresses.

$$W_{y,e,2} = \frac{1}{6}B_e H^2 - \frac{(B_e - 2t_w)(H - 2t_f)^3}{6H} = 0.83m^3 \tag{B.10}$$

$$W_{z,e,2} = \frac{1}{6}H_e B^2 - \frac{(H_e - 2t_f)(B - 2t_w)^3}{6B} = 0.32m^3 \tag{B.11}$$

$$A_{e,2} = B_e H_e - (B_e - 2t_w)(H_e - 2t_f) = 0.5m^2 \tag{B.12}$$

B.3.2. Acting stresses

Axial stresses

Axial stresses in the cross-section are caused by reaction force $R_{x,a}$. The stress is assumed to act uniformly over the cross-section.

$$f_a = \frac{R_{x,a}}{A} \tag{B.13}$$

Where:

$$A = B * H - (B - 2t_w) * (H - 2t_f) \tag{B.14}$$

$$f_{a,1} = \frac{1319kN}{0.83m^2} = 1.6MPa$$

$$f_{a,2} = \frac{823.4kN}{0.56m^2} = 1.5MPa$$

Bending stresses

The bending moments around the y- and z-axis both have their maximum at 17.25 meters from support A. $M_{y,max}$ causes strong-axis bending stresses, $f_{b,y}$, which are largest at the flanges of the profile, where $z = z_{max} = H/2$. The maximum value for $f_{b,z}$ is found on the outer edges of the profile, where $y = y_{max} = B/2$. It follows that the maxima override at the edge of the flange, with coordinate $(y, z) = (B/2, H/2)$.

$$f_{b,y,max} = \frac{M_y * z_{max}}{I_y} = \frac{M_y}{W_y} \tag{B.15}$$

$$f_{b,z,max} = \frac{M_z * y_{max}}{I_z} = \frac{M_z}{W_z} \tag{B.16}$$

Where:

$$W_y = \frac{BH^2}{6} - \frac{(B - 2t_w)(H - 2t_f)^3}{6H} \tag{B.17}$$

$$W_z = \frac{HB^2}{6} - \frac{(H-2t_f)(B-2t_w)^3}{6B} \tag{B.18}$$

It follows that:

$$f_{b,y,max,1} = \frac{273158.9kNm}{1.25m^3} = 217.7MPa$$

$$f_{b,y,max,2} = \frac{170530.3kNm}{0.83m^3} = 206.5MPa$$

$$f_{b,z,max,1} = \frac{13514.5kNm}{0.67m^3} = 20.1MPa$$

$$f_{b,z,max,2} = \frac{9350.9kNm}{0.39m^3} = 24.1MPa$$

Shear stresses

The shear stresses in the profile are caused by reaction forces $R_{z,a}$ and $R_{y,a}$, and torsional moment $M_{x,max}$. The maximum shear stresses are found between $x = 0$, at support A, and $x = 17.25$. Shear stresses due to $R_{z,a}$ are taken up by the webs, and shear stresses due to $R_{y,a}$ are taken up by the flanges. Their maximum value occurs at the shear center of the profile. It is assumed that the shear stresses follow a 60-40 distribution over the cross-sectional elements. This implies that 60% of the load is taken by one flange or web, and 40% by the other. The maximum shear stress is considered in assessing the maximum shear stress in the profile, which occurs in the web. The average shear stress is used in determining the maximum plate stress in the profile, which is assessed at the edges of the profile.

$$f_{v,z,av} = 0.6 * \frac{R_{z,a}}{h * t_w} \tag{B.19}$$

$$f_{v,y,av} = 0.6 * \frac{R_{y,a}}{b * t_f} \tag{B.20}$$

$$f_{v,z,max} = \frac{6}{5} * \frac{R_{z,a} * Q_z}{2 * I_y * t_w} \tag{B.21}$$

$$f_{v,y,max} = \frac{6}{5} * \frac{R_{y,a} * Q_y}{2 * I_z * t_w} \tag{B.22}$$

Where:

$$Q_z = s_z * \frac{A}{2}$$

$$Q_y = s_y * \frac{A}{2}$$

And:

$$s_z = \frac{H}{2} - \frac{(B*t_f)*\frac{t_f}{2} + 2*(\frac{(H-2*t_f)}{2}*t_w)*(\frac{(H-2*t_f)}{4}+t_w)}{B*t_f + 2*\frac{H-2*t_f}{2}*t_w}$$

$$s_y = \frac{B}{2} - \frac{((H-2*t_f)*t_w)*\frac{t_w}{2} + 2*(\frac{B}{2}*t_f)*\frac{B}{4}}{(H-2*t_f)*t_w + 2*(\frac{B}{2}*t_f)}$$

Torsional shear stresses due to $M_{x,max}$ are taken up by the webs and flanges and have a uniform value in the elements. For a long time, torsional shear stresses were determined using St.Venant's constant, I_t. However it was noticed that using I_t often leads to significant errors. For closed profiles, a more accurate estimate of the torsional shear stresses can be obtained by using the enclosed area, A_o, instead of I_t [30]. Equation B.23 is used in determining the torsional shear stresses

$$f_{v,t} = \frac{T}{2 * t_{w/f} * A_o} \tag{B.23}$$

It can be noted that the maximum torsional shear stress occurs in the element with the smallest thickness. The shear stresses for the one-sided support beam and two-sided support beam are provided below.

$$f_{v,z,av,1} = 0.6 * \frac{15669kN}{0.17m^2} = 56.4MPa$$

$$f_{v,z,av,2} = 0.6 * \frac{9782kN}{0.13m^2} = 46.5MPa$$

$$f_{v,y,av,1} = 0.6 * \frac{783.5kN}{0.25m^2} = 1.9MPa$$

$$f_{v,y,av,2} == 0.6 * \frac{489.1kN}{0.15m^2} = 1.9MPa$$

$$f_{v,z,max,1} = \frac{6}{5} * \frac{15669*0.70}{2*2.73*0.04} = 60.4MPa$$

$$f_{v,z,max,2} = \frac{6}{5} * \frac{9782*0.47}{2*1.80*0.03} = 50.7MPa$$

$$f_{v,y,max,1} = \frac{6}{5} * \frac{783.5*0.40}{2*0.92*0.09} = 2.3MPa$$

$$f_{v,y,max,2} == \frac{6}{5} * \frac{489.1*0.30}{2*0.43*0.07} = 2.4MPa$$

$$f_{v,t,fl,1} == \frac{39139.8}{2*0.09*11.54} = 18.8MPa$$

$$f_{v,t,fl,2} == \frac{20069.2}{2*0.07*9.37} = 15.3MPa$$

$$f_{v,t,wb,1} == \frac{39139.8}{2*0.04*11.54} = 42.4MPa$$

$$f_{v,t,wb,2} == \frac{20069.2}{2*0.03*9.37} = 35.7MPa$$

B.3.3. Allowable stresses

The allowable stresses in the cross-section are dependant on the slenderness and yield strength of the elements. For loads that cause uniformly compressive stresses in slender elements, reduced cross-sectional properties are used.

Allowable axial stress

The allowable axial stresses are limited by the critical buckling stress. Buckling will first occur around the weak-axis, which has the highest value for Kl_b/r. The allowable axial stresses in the cross-section are determined with equations B.24 and B.25.

For $Kl_b/r \geq C_c$:

$$F_a = \frac{[1 - \frac{(Kl_b/r)^2}{2C_c^2}]F_y}{\frac{5}{3} + \frac{3(Kl_b/r)}{8C_c} - \frac{(kl_b/r)^3}{8C_c^3}} \tag{B.24}$$

For $Kl_b/r < C_c$:

$$F_a = \frac{12\pi^2 E}{23(Kl_b/r)^2} \tag{B.25}$$

Where:

K = Buckling factor (= 1) [-]

l_b = Unbraced length (=20) [m]

$$C_c = \sqrt{\frac{2\pi^2 E}{F_y}}[-]$$

For the two-sided support beam, equation B.24 is reduced by a factor Q_a.

$$F_{a,2} = \frac{Q_a[1 - \frac{(Kl_b/r)^2}{2C_c^2}]F_y}{\frac{5}{3} + \frac{3(Kl_b/r)}{8C_c} - \frac{(kl_b/r)^3}{8C_c^3}} \tag{B.26}$$

And:

$$C_c = \sqrt{\frac{2\pi^2 E}{Q_a * F_y}}$$

Where:

$$Q_a = \frac{A_e}{A_{actual}}$$

The allowable axial stresses for the one-sided support beam and two-sided support beam are provided below.

$$(Kl_b/r)_1 = 18.9$$

$$(C_c)_1 = 97$$

$$F_{a,1} = 255.8MPa$$

$$(Kl_b/r)_2 = 22.9$$

$$(C_c)_2 = 100.6$$

$$Q_a = 0.89$$

$$F_{a,2} = 217.3MPa$$

The effects for lateral-torsional buckling can be considered by taking an equivalent slenderness ratio, and substituting it in equations B.24 and B.26. Here l_{lb} equals the distance between lateral supports.

$$(\frac{l_{lb}}{r})_{eq} = \sqrt{\frac{5.1 l_{ltb} W_y}{\sqrt{I_t I_z}}} \quad \text{(B.27)}$$

$$\frac{(l_{lb}}{r})_{eq1} = 7.4$$

$$\frac{(l_{lb}}{r})_{eq2} = 11.3$$

$$F_{a,LTB,1} = 258.8MPa$$

$$F_{a,LTB,2} = 227.1MPa$$

It can be seen that lateral-torsional buckling is not the governing buckling mechanism for the cross-sections, as box-type member are torsionally very stiff [39]. This can still be the case for cross-sections where $H >> B$.

Allowable bending stress

The allowable bending stress for compact elements equals:

$$F_b = 0.66F_y \quad \text{(B.28)}$$

For non-compact the allowable bending stress equals:

$$F_b = 0.60F_y \quad \text{(B.29)}$$

The allowable bending stress for slender elements is determined with equation B.30.

$$F_b = 0.60F_y * \frac{W}{W_e} \quad \text{(B.30)}$$

The allowable bending stresses for the one-sided support beam and two-sided support beam are provided below.

$$F_{b,y,1} = 0.6 * 400 = 240MPa$$

$$F_{b,y,2} = 0.6 * 410 * \frac{0.83}{0.83} = 246MPa$$

$$F_{b,z,1} = 0.6 * 440 = 264MPa$$

$$F_{b,z,2} = 0.6 * 440 * \frac{0.32}{0.39} = 217.5MPa$$

Allowable shear stress
The allowable shear stress in cross-section is independent of the element slenderness class. The web slenderness, h/t_w, however does play a role in the shear stress limit. If $h/t_w \leq \frac{380}{\sqrt{F_{y,w}}}$, the allowable shear stress is given by equation B.31. If not, equation B.32 is applied.

$$F_v = 0.40F_y \tag{B.31}$$

$$F_v = \frac{C_v}{2.89} * F_y \leq 0.4 * F_y \tag{B.32}$$

Where:

$$C_v = \frac{45000k_v}{F_y(\frac{h}{t_w})^2}$$
for $C_v < 0.8$

$$C_v = \frac{190}{h/t_w}\sqrt{\frac{k_v}{F_y}}$$
for $C_v > 0.8$

$$k_v = 4 + \frac{5.34}{(\frac{a}{h})^2} for a/h < 1.0$$

$$k_v = 5.34 + \frac{4}{(\frac{a}{h})^2} for a/h > 1.0$$

Parameter a, presents the clear distance between intermediate transverse stiffeners. The shorter the stiffener spacing, the larger the allowable shear stress. The allowable shear stress for the two profiles are provided below.

$$a_1 = 3.75m$$

$$kv_1 = 10.6$$

$$Cv_1 = 0.69$$

$$F_{v,1} = 0.24F_y = 104.7MPa$$

$$a_2 = 2.75m$$

$$kv_2 = 16.5$$

$$Cv_2 = 0.59$$

$$F_{v,1} = 0.20F_y = 90MPa$$

Allowable combined stress
Axial stresses and bending stresses both act in axial direction and hence their joint effect can be assessed. The maximum axial stress occurs on the edge of the compression flange, also indicated as point A in figure 3.3. The unity checks provided in equations B.33 and B.34 shall be satisfied.

$$\frac{f_a}{F_a} + \frac{C_{my}f_{by}}{(1-\frac{f_a}{F'_{ey}})F_{by}} + \frac{C_{mz}f_{bz}}{(1-\frac{f_a}{F'_{ez}})F_{bz}} \leq 1.0 \tag{B.33}$$

$$\frac{f_a}{0.60F_y} + \frac{f_{by}}{F_{by}} + \frac{f_{bz}}{F_{bz}} \leq 1.0 \tag{B.34}$$

Where:

$$C_{mx/y} = 0.85$$

$$F'_{ex/y} = \frac{12\pi^2 E}{23(Kl_b/r_b)^2}$$

For slender elements in the cross-section, the allowable stresses, using reduced cross-sectional properties, are applied. Besides the combined axial stress, Huber's equation is applied for the combined effect of axial stresses, bending stresses and shear stresses. The equation is a simplified version of the Von Mises stress equation.

$$\sigma_{HUB} = \sqrt{(\sigma_a + \sigma_b)^2 + 3(\tau_v + \tau_t)^2} \leq 0.66F_y \tag{B.35}$$

The combined stress according to Huber's equation has to be checked at point A and point B, indicated in figure 3.3. A limit is set to the maximum value of these points of $0.66F_y$. This limit is not specified in AISC 1989, but is widely adopted by HMC.

B.3.4. Unity checks

Unity checks for the bending stresses, shear stresses, axial stresses and their combined effect are determined to assess whether the cross-section has sufficient capacity to withstand the stress from the governing load case. The formula for the unity checks are provided below.

$$UC_b = \frac{f_{b,y} + f_{b,z}}{F_b}$$

$$UC_v = \frac{f_{v,z} + f_{v,t}}{F_v}$$

$$UC_a = \frac{f_a}{min(F_{a,bkl}, F_{a,ltb})}$$

$$UC_{b+a} = max(\frac{f_a}{F_a} + \frac{C_{my} f_{by}}{(1-\frac{f_a}{F'_{ey}})F_{by}} + \frac{C_{mz} f_{bz}}{(1-\frac{f_a}{F'_{ez}})F_{bz}}, \frac{f_a}{0.60F_y} + \frac{f_{by}}{F_{by}} + \frac{f_{bz}}{F_{bz}})$$

$$UC_{HUB} = max(\frac{\sqrt{(f_{b,y}+f_{b,z}+f_a)^2 + 3*(f_{v,z}+f_{v,t})^2}}{0.66F_{y_w}}, \frac{\sqrt{(f_{b,y}+f_{b,z}+f_a)^2 + 3*(f_{v,y}+f_{v,t})^2}}{0.66F_{y_f}})$$

For the one-sided support beam, the following unity checks are obtained:

$$UC_{b,1} = \frac{217.7+20.1}{240} = 1.0$$

$$UC_{v,1} = \frac{60.4+42.4}{104.7} = 0.98$$

$$UC_{a,1} = \frac{1.6}{255.8} = 0.006$$

$$UC_{b+a,1} = \frac{1.6}{255.8} + \frac{20.1}{440*0.6} + \frac{217.7}{400*0.6} = 0.99$$

$$UC_{HUB,1} = \frac{\sqrt{(208.9+20.1+1.6)^2 + 3*(56.4+42.4)^2}}{0.66*440} = 0.99$$

For the two-sided support beam, the following unity checks are obtained:

$$UC_{b,2} = \frac{206.5+24.1}{246} = 0.95$$

$$UC_{v,2} = \frac{50.7+35.7}{90} = 0.96$$

$$UC_{a,2} = \frac{1.6}{217.3} = 0.008$$

$$UC_{b+a,2} = \frac{1.6}{217.3} + \frac{24.1}{440*0.6*0.32/0.39} + \frac{206.5}{410*0.6} = 0.98$$

$$UC_{HUB,2} = \frac{\sqrt{(199.8+24.1*0.39/0.32+1.6)^2 + 3*(46.5+35.7)^2}}{0.66*440} = 0.93$$

B.3.5. Plating capacity

The extracts of the in-house plating capacity sheet for the one-sided support beam and two-sided support beam are provided in figures B.9 and B.10 respectively.

PLATING CAPACITY

BUCKLING RESISTANCE OF PLATES UNDER COMPRESSION

Support type: **Four sides supported**

Modulus of elasticity:	*210000*	[N/mm²]	
Poisson's ratio:	*0.3*	[-]	
Plate thickness:	*40*	[mm]	
Plate length:	*4170*	[mm]	
Plate width:	*3750*	[mm]	(Loaded)
Yield stress:	*440*	[N/mm²]	
Plate factor k:	4.000		
Design stress:	264.0	[N/mm²]	
b(eff)/t:	30.2		
Effective width:	1209.7	[mm]	
Section of curve:	**C - D**		
Critical stress:	**65**	**[N/mm²]**	
Design allowable load:	**16724**	**[kN]**	
Design specific allowable load:	**4460**	**[kN/m]**	

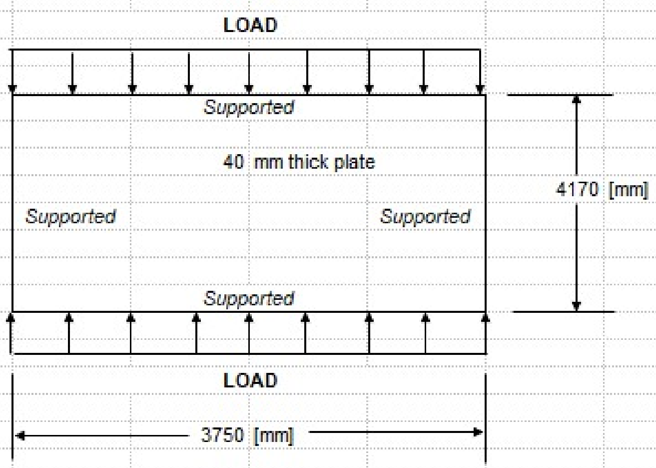

Figure B.10: Critical web plate buckling stress for the one-sided support beam

PLATING CAPACITY

BUCKLING RESISTANCE OF PLATES UNDER COMPRESSION

Support type:	**Four sides supported**		
Modulus of elasticity:	*210000*	[N/mm²]	
Poisson's ratio:	*0.3*	[-]	
Plate thickness:	*30*	[mm]	
Plate length:	*4210*	[mm]	
Plate width:	*2750*	[mm]	(Loaded)
Yield stress:	*440*	[N/mm²]	
Plate factor k:	4.000		
Design stress:	264.0	[N/mm²]	
b(eff)/t:	30.2		
Effective width:	907.2	[mm]	
Section of curve:	**C - D**		
Critical stress:	**68**	**[N/mm²]**	
Design allowable load:	**9433**	**[kN]**	
Design specific allowable load:	**3430**	**[kN/m]**	

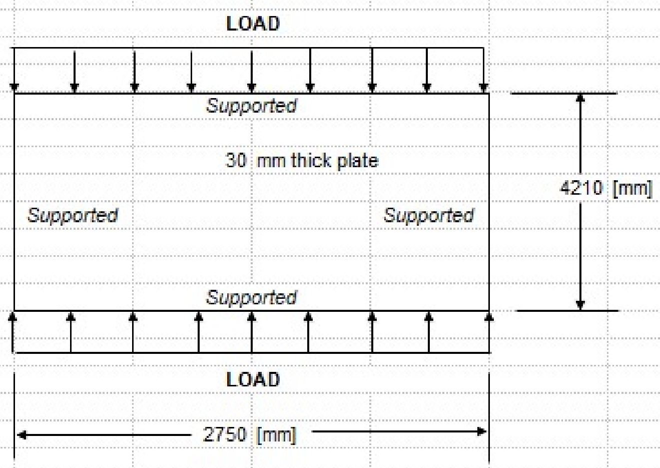

Figure B.11: Critical web plate buckling stress for the two-sided support beam

C

Topsides structural integrity analysis

C.1. SACS model setup

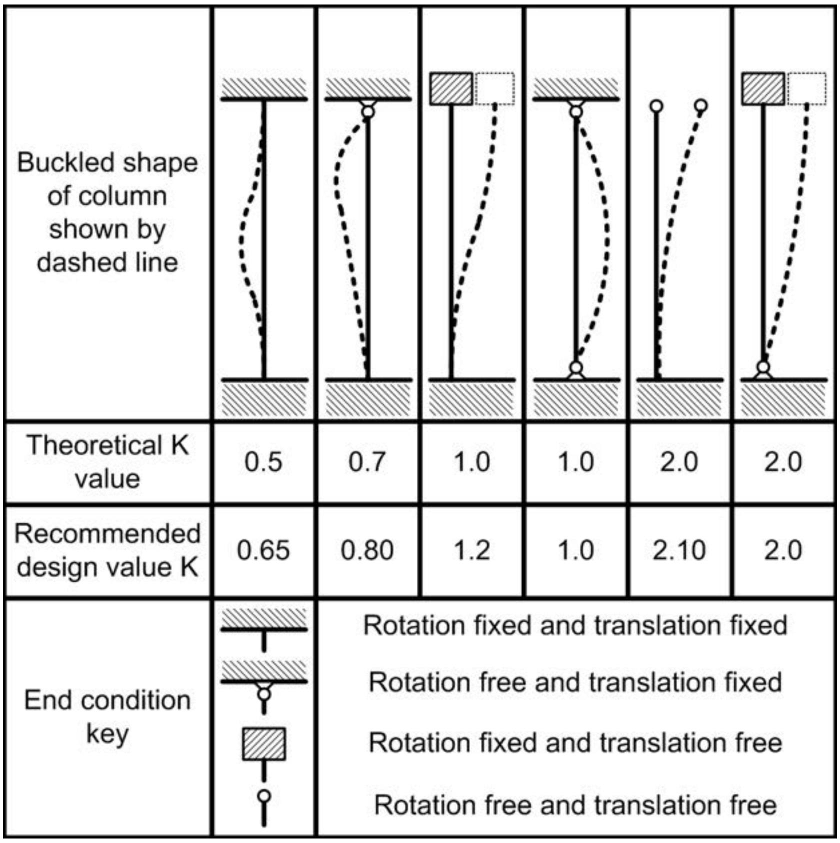

Figure C.1: Buckling factor for the MSF legs

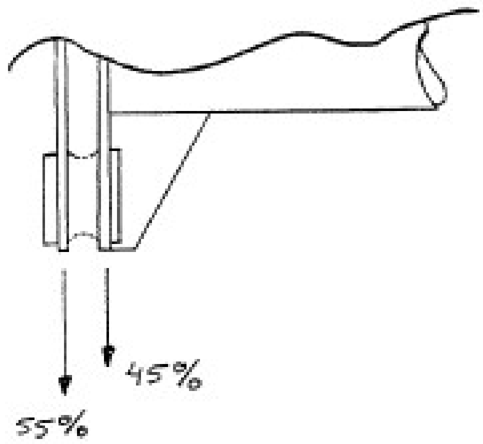

Figure C.2: Lift point friction distribution

C.2. SACS results

The design rigging loads, including μ_{DAF} and μ_{cont}, are determined according to equations 4.1 - 4.4.

C.2.1. MSF leg connections

One-sided leg support

The location of the lift points is provided in figure C.3.

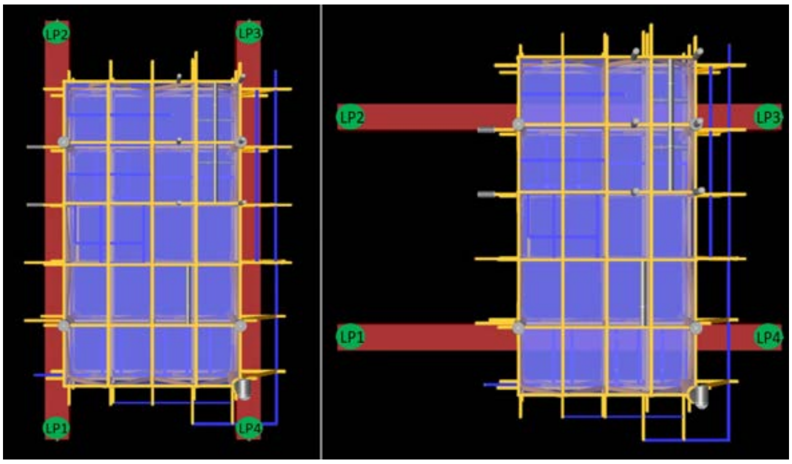

Figure C.3: 1-5 direction (left) E-B direction (right)

The equilibrium forces and the corresponding distribution over the diagonals is provided in table below.

Direction	$F_{LP1}[kN]$	$F_{LP2}[kN]$	$F_{LP3}[kN]$	$F_{LP4}[kN]$	μ_{2-4} [-]	μ_{1-3} [-]
1-5	6959	6394	7482	8135	0.502	0.498
E-B	6409	5598	7763	9200	0.511	0.489

Table C.1: Equilibrium load distribution over the lift points for the one-sided support models

A larger deviation in the equilibrium load distribution can be observed for the E-B direction. This is due to the position of the lift beams, where lift points 1 and 2 have a large arm with respect to the connection points. Also the position of the topside CoG, which is closer to row 1, plays a role here.
The vertical design rigging loads and side loads are provided in table below. The load case where majority of the hook load is taken by diagonal 2-4 has suffix 1, for the other diagonal suffix 2 is used.

Direction 1-5	$F_{LP1}[kN]$	$F_{LP2}[kN]$	$F_{LP3}[kN]$	$F_{LP4}[kN]$
$L64_1$	5533	7820	6055	9561
$L64_2$	8429	4923	8952	6664
$L54_1$	6257	7096	6779	8837
$L54_2$	7705	5648	8228	7388

Table C.2: Vertical rigging load distribution over the lift points for one-sided support in 1-5 direction

Direction 1-5	$F_{LP1}[kN]$	$F_{LP2}[kN]$	$F_{LP3}[kN]$	$F_{LP4}[kN]$
$L64_1$	277	391	303	478
$L64_2$	421	246	448	333
$L54_1$	313	355	339	442
$L54_2$	385	282	411	369

Table C.3: Rigging side load distribution over the lift points for one-sided support in 1-5 direction

Direction E-B	$F_{LP1}[kN]$	$F_{LP2}[kN]$	$F_{LP3}[kN]$	$F_{LP4}[kN]$
$L64_1$	5117	6890	6471	10492
$L64_2$	8014	3993	9368	7595
$L54_1$	5841	6165	7195	9768
$L54_2$	7289	4717	8644	8319

Table C.4: Vertical rigging load distribution over the lift points for one-sided support in E-B direction

Direction 1-5	$F_{LP1}[kN]$	$F_{LP2}[kN]$	$F_{LP3}[kN]$	$F_{LP4}[kN]$
$L64_1$	256	344	324	525
$L64_2$	401	200	468	380
$L54_1$	292	308	360	488
$L54_2$	364	236	432	416

Table C.5: Rigging side load distribution over the lift points for one-sided support in E-B direction

The load distribution over the rows for each load case is provided below.

Direction 1-5	**Equilibrium**	**L641**	**L642**	**L541**	**L542**
row 1-4	0.52	0.52	0.52	0.52	0.52
row 2-3	0.48	0.48	0.48	0.48	0.48
row 1-2	0.46	0.46	0.46	0.46	0.46
row 3-4	0.54	0.54	0.54	0.54	0.54
diag 2-4	0.501	0.60	0.40	0.55	0.45
diag 1-3	0.499	0.40	0.60	0.45	0.55

Table C.6: Load distribution over the lift point rows for one-sided leg support in 1-5 direction

Direction E-B	**Equilibrium**	**L641**	**L642**	**L541**	**L542**
row 1-4	0.54	0.54	0.54	0.54	0.54
row 2-3	0.46	0.46	0.46	0.46	0.46
row 1-2	0.41	0.41	0.41	0.41	0.41
row 3-4	0.59	0.59	0.59	0.59	0.59
diag 2-4	0.51	0.60	0.40	0.55	0.45
diag 1-3	0.49	0.40	0.60	0.45	0.55

Table C.7: Load distribution over the lift point rows for one-sided leg support in E-B direction

One-sided leg support with cross-beams

The location of the lift points is provided in figure C.4.

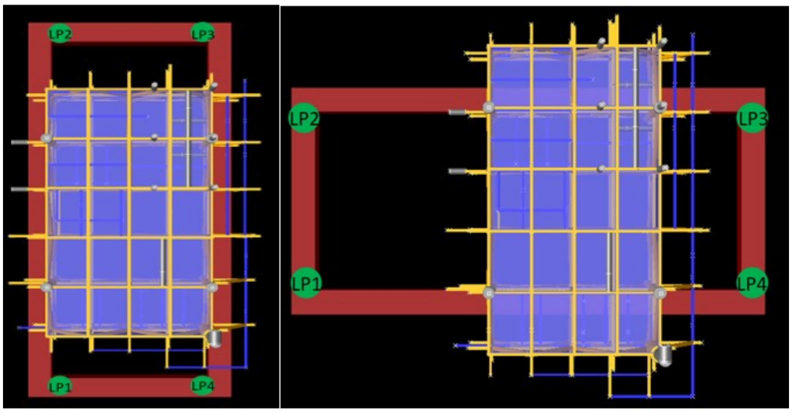

Figure C.4: 1-5 direction (left) E-B direction (right) for the one-sided leg support with cross-beams models

The CoG of the assembly and therefore the equilibrium distribution have changed slightly.

Direction	$F_{LP1}[kN]$	$F_{LP2}[kN]$	$F_{LP3}[kN]$	$F_{LP4}[kN]$	μ_{2-4} [-]	μ_{1-3} [-]
1-5	7883	7307	8430	9023	0.50	0.50
E-B	7444	6615	8697	10116	0.509	0.491

Table C.8: Equilibrium load distribution over the lift points for the one-sided support with cross-beams models

The design rigging loads are provided in tables below.

Direction 1-5	$F_{LP1}[kN]$	$F_{LP2}[kN]$	$F_{LP3}[kN]$	$F_{LP4}[kN]$
$L64_1$	6255	8935	6802	10651
$L64_2$	9519	5671	10067	7387
$L54_1$	7071	8119	7619	9835
$L54_2$	8703	6487	9251	8203

Table C.9: Vertical rigging load distribution over the lift points for one-sided support with cross-beams in 1-5 direction

Direction 1-5	$F_{LP1}[kN]$	$F_{LP2}[kN]$	$F_{LP3}[kN]$	$F_{LP4}[kN]$
$L64_1$	313	447	340	533
$L64_2$	476	284	503	369
$L54_1$	354	406	381	492
$L54_2$	435	324	463	410

Table C.10: Rigging side load distribution over the lift points for one-sided support with cross-beams in 1-5 direction

Direction E-B	$F_{LP1}[kN]$	$F_{LP2}[kN]$	$F_{LP3}[kN]$	$F_{LP4}[kN]$
$L64_1$	5948	8111	7201	11612
$L64_2$	9235	4824	10488	8325
$L54_1$	6770	7290	8022	10790
$L54_2$	8414	5646	9666	9147

Table C.11: Vertical rigging load distribution over the lift points for one-sided support with cross-beams in 1-5 direction

Direction E-B	$F_{LP1}[kN]$	$F_{LP2}[kN]$	$F_{LP3}[kN]$	$F_{LP4}[kN]$
$L64_1$	297	406	360	581
$L64_2$	462	241	524	416
$L54_1$	338	364	401	540
$L54_2$	421	282	483	457

Table C.12: Rigging side load distribution over the lift points for one-sided support with cross-beams in E-B direction

The load distribution over the rows for each load case is provided below.

Direction 1-5	**Equilibrium**	**L641**	**L642**	**L541**	**L542**
row 1-4	0.52	0.52	0.52	0.52	0.52
row 2-3	0.48	0.48	0.48	0.48	0.48
row 1-2	0.47	0.47	0.47	0.47	0.47
row 3-4	0.53	0.53	0.53	0.53	0.53
diag 2-4	0.50	0.60	0.40	0.55	0.45
diag 1-3	0.50	0.40	0.60	0.45	0.55

Table C.13: Load distribution over the lift point rows for one-sided leg support with cross-beams in 1-5 direction

Direction E-B	**Equilibrium**	**L641**	**L642**	**L541**	**L542**
row 1-4	0.53	0.53	0.53	0.53	0.53
row 2-3	0.47	0.47	0.47	0.47	0.47
row 1-2	0.43	0.43	0.43	0.43	0.43
row 3-4	0.57	0.57	0.57	0.57	0.57
diag 2-4	0.51	0.60	0.40	0.55	0.45
diag 1-3	0.49	0.40	0.60	0.45	0.55

Table C.14: Load distribution over the lift point rows for one-sided leg support with cross-beams in E-B direction

Two-sided leg support
The location of the lift points is provided in figure C.5.

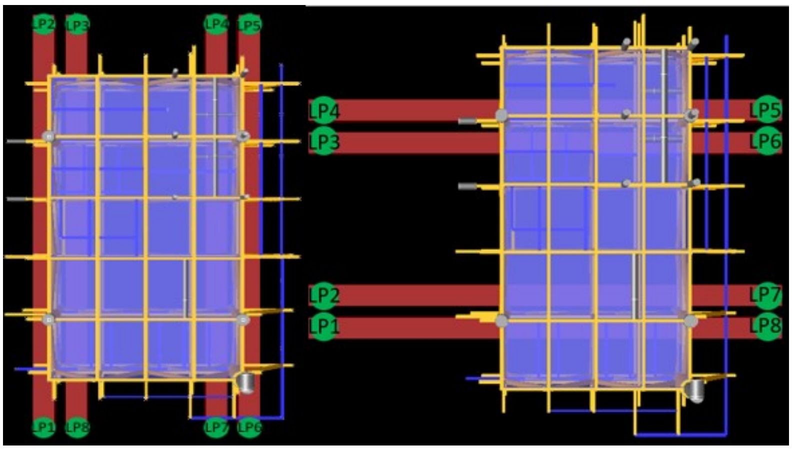

Figure C.5: 1-5 direction (left) E-B direction (right) for the two-sided leg support models

The equilibrium distribution over the lift points is provided below. The equilibrium load of adjacent lift beams is found to be approximately equal.

Direction	$F_{LP1,8}[kN]$	$F_{LP2,3}[kN]$	$F_{LP4,5}[kN]$	$F_{LP6,7}[kN]$	μ_{18-45}[-]	μ_{23-67}[-]
1-5	7678	7075	8201	8816	0.5	0.5

Table C.15: Equilibrium load distribution over the lift points for the two-sided support in 1-5 direction

Direction	$F_{LP1,2}[kN]$	$F_{LP3,4}[kN]$	$F_{LP5,6}[kN]$	$F_{LP7,8}[kN]$	μ_{12-56}[-]	μ_{34-78}[-]
E-B	7130	6276	8485	9878	0.492	0.508

Table C.16: Equilibrium load distribution over the lift points for the two-sided support in E-B direction

The design rigging loads are provided below. Four load cases are defined per load distribution. For the first load case, majority of the hook load is taken by diagonal 23-67 and 55% of the load is taken by the outer lift points. For the second load case, the same distribution is applied, with 55% of the load taken by the interior lift points. The third and fourth load case are defined in the same manner, but now majority of the hook load is taken by diagonal 18-45.

Direction 1-5	$F_{LP1}[kN]$	$F_{LP2}[kN]$	$F_{LP3}[kN]$	$F_{LP4}[kN]$	$F_{LP5}[kN]$	$F_{LP6}[kN]$	$F_{LP7}[kN]$	$F_{LP8}[kN]$
L641	3364	4806	3854	2990	3625	5677	4724	2728
L642	2729	3853	4807	3626	2990	4724	5677	3364
L643	5112	3059	2424	4420	5372	3930	3294	4158
L644	4159	2424	3060	5373	4419	3295	3930	5111
L541	3801	4370	3496	3348	4062	5241	4366	3086
L542	3086	3496	4370	4062	3347	4367	5240	3800
L543	4675	3496	2782	4062	4935	4367	3652	3800
L544	3801	2781	3496	4936	4062	3652	4366	4674

Table C.17: Vertical rigging load distribution over the lift points for two-sided support in 1-5 direction

Direction 1-5	$F_{LP1}[kN]$	$F_{LP2}[kN]$	$F_{LP3}[kN]$	$F_{LP4}[kN]$	$F_{LP5}[kN]$	$F_{LP6}[kN]$	$F_{LP7}[kN]$	$F_{LP8}[kN]$
L641	168	240	193	150	181	284	236	136
L642	136	193	240	181	149	236	284	168
L643	256	153	121	221	269	197	165	208
L644	208	121	153	269	221	165	196	256
L541	190	218	175	167	203	262	218	154
L542	154	175	219	203	167	218	262	190
L543	234	175	139	203	247	218	183	190
L544	190	139	175	247	203	183	218	234

Table C.18: Rigging side load distribution over the lift points for two-sided support in 1-5 direction

Direction E-B	$F_{LP1}[kN]$	$F_{LP2}[kN]$	$F_{LP3}[kN]$	$F_{LP4}[kN]$	$F_{LP5}[kN]$	$F_{LP6}[kN]$	$F_{LP7}[kN]$	$F_{LP8}[kN]$
L641	4903	3950	1959	2593	5580	4627	3759	4396
L642	3950	4903	2595	1958	4627	5581	4394	3761
L643	3156	2521	3389	4341	3833	3198	5189	6143
L644	2521	3156	4342	3387	3198	3833	6142	5190
L541	4467	3593	2317	3030	5144	4270	4116	4833
L542	3593	4466	3032	2315	4270	5144	4831	4118
L543	3593	2878	3032	3904	4270	3555	4831	5706
L544	2878	3593	3905	3030	3555	4270	5705	4833

Table C.19: Vertical rigging load distribution over the lift points for two-sided support in E-B direction

Direction E-B	$F_{LP1}[kN]$	$F_{LP2}[kN]$	$F_{LP3}[kN]$	$F_{LP4}[kN]$	$F_{LP5}[kN]$	$F_{LP6}[kN]$	$F_{LP7}[kN]$	$F_{LP8}[kN]$
L641	245	198	98	130	279	231	188	220
L642	198	245	130	98	231	279	220	188
L643	158	126	169	217	192	160	259	307
L644	126	158	217	169	160	192	307	260
L541	223	180	116	152	257	214	206	242
L542	180	223	152	116	213	257	242	206
L543	180	144	152	195	213	178	242	285
L544	144	180	195	152	178	214	285	242

Table C.20: Rigging side load distribution over the lift points for two-sided support in E-B direction

The load distribution over the rows for each load case are provided below.

Direction 1-5	Equilibrium	L641	L642	L643	L644	L541	L542	L543	L544
Row 18-23	0.464	0.464	0.464	0.464	0.464	0.464	0.464	0.464	0.464
Row 45-67	0.536	0.536	0.536	0.536	0.536	0.536	0.536	0.536	0.536
Row 23-45	0.481	0.481	0.481	0.481	0.481	0.481	0.481	0.481	0.481
Row 18-76	0.519	0.519	0.519	0.519	0.519	0.519	0.519	0.519	0.519
Diag 23-76	0.500	0.600	0.600	0.400	0.400	0.550	0.550	0.450	0.450
Diag 18-45	0.500	0.400	0.400	0.600	0.600	0.450	0.450	0.550	0.550

Table C.21: Load distribution over the lift point rows for two-sided leg support in 1-5 direction

Direction E-B	Equilibrium	L641	L642	L643	L644	L541	L542	L543	L544
Row 12-78	0.535	0.535	0.535	0.535	0.535	0.535	0.535	0.535	0.535
Row 34-65	0.465	0.465	0.465	0.465	0.465	0.465	0.465	0.465	0.465
Row 12-34	0.422	0.422	0.422	0.422	0.422	0.422	0.422	0.422	0.422
Row 87-65	0.578	0.578	0.578	0.578	0.578	0.578	0.578	0.578	0.578
Diag 12-65	0.492	0.600	0.600	0.400	0.400	0.550	0.550	0.450	0.450
Diag 87-34	0.508	0.400	0.400	0.600	0.600	0.450	0.450	0.550	0.550

Table C.22: Load distribution over the lift point rows for two-sided leg support in E-B direction

Two-sided leg support with cross-beams
The location of the lift points is provided in figure C.6.

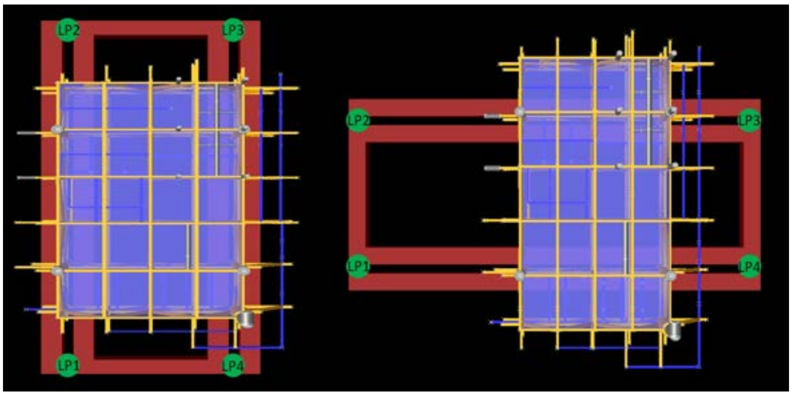

Figure C.6: 1-5 direction (left) E-B direction (right) for the two-sided leg support with cross-beams models

The equilibrium distribution over the lift points is provided below.

Direction	$F_{LP1}[kN]$	$F_{LP2}[kN]$	$F_{LP3}[kN]$	$F_{LP4}[kN]$	μ_{2-4} [-]	μ_{1-3} [-]
1-5	8277	7700	8825	9416	0.50	0.50
E-B	7835	6975	9088	10476	0.508	0.492

Table C.23: Equilibrium load distribution over the lift points for the two-sided support with cross-beams

The design rigging loads are provided below.

Direction 1-5	$F_{LP1}[kN]$	$F_{LP2}[kN]$	$F_{LP3}[kN]$	$F_{LP4}[kN]$
$L64_1$	6570	9407	7117	11123
$L64_2$	9992	5986	10539	7701
$L54_1$	7425	8552	7973	10268
$L54_2$	9136	6841	9684	8557

Table C.24: Vertical rigging load distribution over the lift points for two-sided support with cross-beams in 1-5 direction

Direction 1-5	$F_{LP1}[kN]$	$F_{LP2}[kN]$	$F_{LP3}[kN]$	$F_{LP4}[kN]$
$L64_1$	328	470	356	556
$L64_2$	500	299	527	385
$L54_1$	371	428	399	513
$L54_2$	457	342	484	428

Table C.25: Rigging side load distribution over the lift points for two-sided support with cross-beams in 1-5 direction

Direction E-B	$F_{LP1}[kN]$	$F_{LP2}[kN]$	$F_{LP3}[kN]$	$F_{LP4}[kN]$
$L64_1$	6249	8562	7501	12063
$L64_2$	9686	5124	10938	8625
$L54_1$	7108	7702	8360	11203
$L54_2$	8827	5984	10079	9484

Table C.26: Vertical rigging load distribution over the lift points for two-sided support with cross-beams in E-B direction

Direction E-B	$F_{LP1}[kN]$	$F_{LP2}[kN]$	$F_{LP3}[kN]$	$F_{LP4}[kN]$
$L64_1$	312	428	375	603
$L64_2$	484	256	547	431
$L54_1$	355	385	418	560
$L54_2$	441	299	504	474

Table C.27: Rigging side load distribution over the lift points for two-sided support with cross-beams in E-B direction

The load distribution over the rows for each load case are provided below.

Direction 1-5	**Equilibrium**	**L641**	**L642**	**L541**	**L542**
row 1-4	0.52	0.52	0.52	0.52	0.52
row 2-3	0.48	0.48	0.48	0.48	0.48
row 1-2	0.47	0.47	0.47	0.47	0.47
row 3-4	0.53	0.53	0.53	0.53	0.53
diag 2-4	0.50	0.60	0.40	0.55	0.45
diag 1-3	0.50	0.40	0.60	0.45	0.55

Table C.28: Load distribution over the lift point rows for two-sided leg support with cross-beams in 1-5 direction

Direction E-B	Equilibrium	L641	L642	L541	L542
row 1-4	0.53	0.53	0.53	0.53	0.53
row 2-3	0.47	0.47	0.47	0.47	0.47
row 1-2	0.43	0.43	0.43	0.43	0.43
row 3-4	0.57	0.57	0.57	0.57	0.57
diag 2-4	0.51	0.60	0.40	0.55	0.45
diag 1-3	0.49	0.40	0.60	0.45	0.55

Table C.29: Load distribution over the lift point rows for two-sided leg support with cross-beams in E-B direction

It can be seen that the same rigging load distribution is found as for the case with two lift beams with cross-beams. The position of the lift points and the weight distribution is the same for these cases.

C.2.2. MSF deck connection models

In this section the rigging loads and the dummy member loads are provided.

1-5 direction

The equilibrium load distribution over the lift points is given in table below.

$F_{LP1}[kN]$	$F_{LP2}[kN]$	$F_{LP3}[kN]$	$F_{LP4}[kN]$	$\mu_{24}[-]$	$\mu_{13}[-]$
6696	6217	8360	9048	0.503	0.497

Table C.30: Equilibrium load distribution over the lift points for MSF deck connection in 1-5 direction

The unfactored vertical and transverse rigging loads are provided in tables below.

Direction 1-5	$F_{LP1}[kN]$	$F_{LP2}[kN]$	$F_{LP3}[kN]$	$F_{LP4}[kN]$
$L64_1$	8264	4649	9928	7479
$L64_2$	5232	7681	6896	10511
$L54_1$	7506	5407	9170	8237
$L54_2$	5990	6923	7654	9753

Table C.31: Vertical rigging load distribution over the lift points for MSF deck connection in 1-5 direction

Direction 1-5	$F_{LP1}[kN]$	$F_{LP2}[kN]$	$F_{LP3}[kN]$	$F_{LP4}[kN]$
$L64_1$	413	232	496	374
$L64_2$	262	384	345	526
$L54_1$	375	270	458	412
$L54_2$	300	346	383	488

Table C.32: Rigging side load distribution over the lift points for MSF deck connection in 1-5 direction

Direction 1-5	Equilibrium	L641	L642	L541	L542
row 1-2	0.43	0.43	0.43	0.43	0.43
row 3-4	0.57	0.57	0.57	0.57	0.57
row 1-4	0.52	0.52	0.52	0.52	0.52
row 2-3	0.48	0.48	0.48	0.48	0.48
diag 2-4	0.50	0.40	0.60	0.45	0.55
diag 1-3	0.50	0.60	0.40	0.55	0.45

Table C.33: Load distribution over the lift point rows for MSF deck connection in 1-5 direction

The load out-put of the dummy members for the case without shim-plates is provided in figure C.7.

CA20- D1	CA20	DUM	L641	-4107.2915
			L642	-5696.9795
	D1		L641	-4107.2915
			L642	-5696.9795
CA30- D6	CA30	DUM	L641	-5585.8242
			L642	-5586.2134
	D6		L641	-5585.8242
			L642	-5586.2134
CA40- D11	CA40	DUM	L641	-3220.1482
			L642	-1662.8163
	D11		L641	-3220.1482
			L642	-1662.8163
CB30- D16	CB30	DUM	L641	-1063.4954
			L642	-1025.6508
	D16		L641	-1063.4954
			L642	-1025.6508
CC20- D2	CC20	DUM	L641	-332.3309
			L642	-653.0134
	D2		L641	-332.3309
			L642	-653.0134
CC30- D7	CC30	DUM	L641	764.0330
			L642	766.7925
	D7		L641	764.0330
			L642	766.7925
CC40- D12	CC40	DUM	L641	-469.8430
			L642	-99.1960
	D12		L641	-469.8430
			L642	-99.1960
CD20- D3	CD20	DUM	L641	-174.0963
			L642	-144.7032
	D3		L641	-174.0963
			L642	-144.7032
CD30- D8	CD30	DUM	L641	1487.2686
			L642	1455.1891
	D8		L641	1487.2686
			L642	1455.1891
CD40- D13	CD40	DUM	L641	14.4252
			L642	-39.6936
	D13		L641	14.4252
			L642	-39.6936
CE20- D4	CE20	DUM	L641	-1767.3574
			L642	-1149.6957
	D4		L641	-1767.3574
			L642	-1149.6957
CE30- D9	CE30	DUM	L641	-327.6705
			L642	-341.8857
	D9		L641	-327.6705
			L642	-341.8857
CE40- D14	CE40	DUM	L641	-280.0063
			L642	-915.6680
	D14		L641	-280.0063
			L642	-915.6680
CF20- D5	CF20	DUM	L641	-4113.0132
			L642	-2861.0752
	D5		L641	-4113.0132
			L642	-2861.0752
CF30- D10	CF30	DUM	L641	-5555.9355
			L642	-5527.0977
	D10		L641	-5555.9355
			L642	-5527.0977
CF40- D15	CF40	DUM	L641	-1101.0156
			L642	-2350.5930
	D15		L641	-1101.0156
			L642	-2350.5930

Figure C.7: Load out-put dummy members 1-5 direction

It can be seen that the outer dummy members 1, 5, 6, 10, 11 and 15 take up majority of the lift loads. It can also be noticed that a tension force is provided by dummy members 7 and 8, which is against the condition that these members can only provide a compression force. The tension forces in these members are required to obtain momentum balance. This implies that the topside can't be lifted under this setup, without the use of shim plates. The dummy load out-put with the use of shim plates is provided in figure C.8.

CA20-	D1	CA20	DUM	L641	-2194.8418
				L642	-3734.8606
		D1		L641	-2194.8418
				L642	-3734.8606
CA30-	D6	CA30	DUM	L641	-695.9688
				L642	-681.6900
		D6		L641	-695.9688
				L642	-681.6900
CA40-	D11	CA40	DUM	L641	-2593.3135
				L642	-1053.2056
		D11		L641	-2593.3135
				L642	-1053.2056
CB30-	D16	CB30	DUM	L641	-4705.7739
				L642	-4656.3989
		D16		L641	-4705.7739
				L642	-4656.3989
CC20-	D2	CC20	DUM	L641	-1588.5935
				L642	-1900.5918
		D2		L641	-1588.5935
				L642	-1900.5918
CC30-	D7	CC30	DUM	L641	0.0115
				L642	0.0221
		D7		L641	0.0115
				L642	0.0221
CC40-	D12	CC40	DUM	L641	-844.4060
				L642	-506.0297
		D12		L641	-844.4060
				L642	-506.0297
CD20-	D3	CD20	DUM	L641	-2150.7290
				L642	-2122.3760
		D3		L641	-2150.7290
				L642	-2122.3760
CD30-	D8	CD30	DUM	L641	-1358.4869
				L642	-1312.2700
		D8		L641	-1358.4869
				L642	-1312.2700
CD40-	D13	CD40	DUM	L641	-1709.7631
				L642	-1828.8470
		D13		L641	-1709.7631
				L642	-1828.8470
CE20-	D4	CE20	DUM	L641	-2585.3955
				L642	-1977.6350
		D4		L641	-2585.3955
				L642	-1977.6350
CE30-	D9	CE30	DUM	L641	-1407.6399
				L642	-1299.0143
		D9		L641	-1407.6399
				L642	-1299.0143
CE40-	D14	CE40	DUM	L641	-681.8235
				L642	-1657.2296
		D14		L641	-681.8235
				L642	-1657.2296
CF20-	D5	CF20	DUM	L641	-2747.2664
				L642	-1412.3994
		D5		L641	-2747.2664
				L642	-1412.3994
CF30-	D10	CF30	DUM	L641	-568.5273
				L642	-1024.8258
		D10		L641	-568.5273
				L642	-1024.8258
CF40-	D15	CF40	DUM	L641	0.0101
				L642	-665.0536
		D15		L641	0.0101
				L642	-665.0536

Figure C.8: Load out-put dummy members 1-5 direction with shimplates

It can be seen that a better load spread is obtained over the dummy members. Some members still take a significantly larger portion of the load than others. This is however necessary in order to obtain stability of the assembly. Furthermore, it is noticed that the dummy members only provide compression forces. Dummy members 7 and 15 do have a positive load output. However the magnitude of these loads is negligibly small, and hence it can be concluded that the compression only criterion is satisfied. The gap sizes of the dummy members are provided in table below.

Dummy member	Gap size [cm]
D1	4.5
D2	0.75
D3	0
D4	0.75
D5	2.5
D6	4
D7	0.75
D8	0
D9	0.75
D10	2.5
D11	3.5
D12	0.75
D13	0
D14	0.75
D15	2.5
D16	1.5

Table C.34: Overview of the optimal gap size for the dummy members in 1-5 direction

The gap size increases towards the outer column rows. This way it is ensured that the interior columns make contact first, before the exterior columns are activated. It has been noticed that the system is sensitive to relatively small changes in the shim plate thickness. This makes the load transfer per column somewhat unpredictable. It also implies that this method of load transfer is sensitive for fabrication and installation offsets.

E-B direction

The equilibrium load distribution over the lift points is given in table below.

$F_{LP1}[kN]$	$F_{LP2}[kN]$	$F_{LP3}[kN]$	$F_{LP4}[kN]$	$\mu_{24}[-]$	$\mu_{13}[-]$
7980	7329	9232	10830	0.513	0.487

Table C.35: Equilibrium load distribution over the lift points for MSF deck connection in E-B direction

The unfactored vertical and transverse rigging loads are provided in tables below.

Direction 1-5	$F_{LP1}[kN]$	$F_{LP2}[kN]$	$F_{LP3}[kN]$	$F_{LP4}[kN]$
$L64_1$	6448	8861	7700	12361
$L64_2$	9985	5324	11237	8824
$L54_1$	7332	7977	8585	11477
$L54_2$	9101	6208	10353	9709

Table C.36: Vertical rigging load distribution over the lift points for MSF deck connection in E-B direction

Direction 1-5	$F_{LP1}[kN]$	$F_{LP2}[kN]$	$F_{LP3}[kN]$	$F_{LP4}[kN]$
$L64_1$	322	443	385	618
$L64_2$	499	266	562	441
$L54_1$	367	399	429	574
$L54_2$	455	310	518	485

Table C.37: Rigging side load distribution over the lift points for MSF deck connection in E-B direction

Direction 1-5	Equilibrium	L641	L642	L541	L542
row 1-4	0.53	0.53	0.53	0.53	0.53
row 2-3	0.47	0.47	0.47	0.47	0.47
row 1-2	0.43	0.43	0.43	0.43	0.43
row 3-4	0.57	0.57	0.57	0.57	0.57
diag 1-3	0.49	0.40	0.60	0.45	0.55
diag 2-4	0.51	0.60	0.40	0.55	0.45

Table C.38: Load distribution over the lift point rows for MSF deck connection in E-B direction

The load out-put of the dummy members for the case without shim-plates is provided in figure C.9.

CA10-	D1	CA10	DUM	C641	-7602.1992
				C642	-3338.2278
		D1		C641	-7602.1992
				C642	-3338.2278
CA20-	D2	CA20	DUM	C641	428.6826
				C642	259.9450
		D2		C641	428.6826
				C642	259.9450
CA30-	D3	CA30	DUM	C641	1418.0219
				C642	1365.3745
		D3		C641	1418.0219
				C642	1365.3745
CA40-	D4	CA40	DUM	C641	193.9830
				C642	155.3034
		D4		C641	193.9830
				C642	155.3034
CA50-	D5	CA50	DUM	C641	-2389.1460
				C642	-6334.2183
		D5		C641	-2389.1460
				C642	-6334.2183
CC10-	D6	CC10	DUM	C641	-5173.5503
				C642	-5015.8496
		D6		C641	-5173.5503
				C642	-5015.8496
CC20-	D7	CC20	DUM	C641	213.6531
				C642	200.8993
		D7		C641	213.6531
				C642	200.8993
CC30-	D8	CC30	DUM	C641	967.5991
				C642	1191.6897
		D8		C641	967.5991
				C642	1191.6897
CC40-	D9	CC40	DUM	C641	334.8064
				C642	356.7052
		D9		C641	334.8064
				C642	356.7052
CC50-	D10	CC50	DUM	C641	-4305.3022
				C642	-4759.4229
		D10		C641	-4305.3022
				C642	-4759.4229
CD10-	D11	CD10	DUM	C641	-4689.7544
				C642	-4899.3252
		D11		C641	-4689.7544
				C642	-4899.3252
CD20-	D12	CD20	DUM	C641	170.7977
				C642	111.8359
		D12		C641	170.7977
				C642	111.8359
CD30-	D13	CD30	DUM	C641	860.4503
				C642	779.2581
		D13		C641	860.4503
				C642	779.2581
CD40-	D14	CD40	DUM	C641	293.5582
				C642	290.5570
		D14		C641	293.5582
				C642	290.5570
CD50-	D15	CD50	DUM	C641	-4294.3584
				C642	-3993.9431
		D15		C641	-4294.3584
				C642	-3993.9431
CF10-	D16	CF10	DUM	C641	-2267.8660
				C642	-6142.7095
		D16		C641	-2267.8660
				C642	-6142.7095
CF20-	D17	CF20	DUM	C641	206.5906
				C642	168.2906
		D17		C641	206.5906
				C642	168.2906
CF30-	D18	CF30	DUM	C641	1312.6119
				C642	1009.1448
		D18		C641	1312.6119
				C642	1009.1448
CF40-	D19	CF40	DUM	C641	221.9418
				C642	155.3794
		D19		C641	221.9418
				C642	155.3794
CF50-	D20	CF50	DUM	C641	-5607.7769
				C642	-1267.9442
		D20		C641	-5607.7769
				C642	-1267.9442

Figure C.9: Load out-put dummy members E-B direction

Similar observations can be made as for the 1-5 direction. It can be noticed that only the outer dummy members produce a compression force. The interior columns are all loaded on tension, which is considered to be invalid. A reason for this is the reduced spacing between connection elements. The topside also doesn't 'lean' towards a particular side. The dummy load-output when shim plates are applied, is shown in figure C.10.

CA10- D1	CA10	DUM	C641	-2785.6990
			C642	0.0187
	D1		C641	-2785.6990
			C642	0.0187
CA20- D2	CA20	DUM	C641	-1330.6857
			C642	0.0319
	D2		C641	-1330.6857
			C642	0.0319
CA30- D3	CA30	DUM	C641	-4202.1909
			C642	-6181.6943
	D3		C641	-4202.1909
			C642	-6181.6943
CA40- D4	CA40	DUM	C641	0.0333
			C642	-1131.0939
	D4		C641	0.0333
			C642	-1131.0939
CA50- D5	CA50	DUM	C641	0.0216
			C642	-920.3816
	D5		C641	0.0216
			C642	-920.3816
CC10- D6	CC10	DUM	C641	-17.9575
			C642	0.0212
	D6		C641	-17.9575
			C642	0.0212
CC20- D7	CC20	DUM	C641	-1453.9904
			C642	-1200.3972
	D7		C641	-1453.9904
			C642	-1200.3972
CC30- D8	CC30	DUM	C641	-6078.4956
			C642	-6126.9810
	D8		C641	-6078.4956
			C642	-6126.9810
CC40- D9	CC40	DUM	C641	0.0398
			C642	-253.2595
	D9		C641	0.0398
			C642	-253.2595
CC50- D10	CC50	DUM	C641	0.0261
			C642	0.0215
	D10		C641	0.0261
			C642	0.0215
CD10- D11	CD10	DUM	C641	0.0158
			C642	-550.5565
	D11		C641	0.0158
			C642	-550.5565
CD20- D12	CD20	DUM	C641	-769.9427
			C642	-1377.0806
	D12		C641	-769.9427
			C642	-1377.0806
CD30- D13	CD30	DUM	C641	-6094.0640
			C642	-5598.9771
	D13		C641	-6094.0640
			C642	-5598.9771
CD40- D14	CD40	DUM	C641	-494.2419
			C642	0.0370
	D14		C641	-494.2419
			C642	0.0370
CD50- D15	CD50	DUM	C641	0.0146
			C642	0.0127
	D15		C641	0.0146
			C642	0.0127
CF10- D16	CF10	DUM	C641	0.0209
			C642	-2326.9983
	D16		C641	0.0209
			C642	-2326.9983
CF20- D17	CF20	DUM	C641	0.0218
			C642	-1190.6111
	D17		C641	0.0218
			C642	-1190.6111
CF30- D18	CF30	DUM	C641	-4779.1699
			C642	-2849.5754
	D18		C641	-4779.1699
			C642	-2849.5754
CF40- D19	CF40	DUM	C641	-1032.6548
			C642	0.0192
	D19		C641	-1032.6548
			C642	0.0192
CF50- D20	CF50	DUM	C641	-668.5233
			C642	0.0117
	D20		C641	-668.5233
			C642	0.0117

Figure C.10: Load out-put dummy members E-B direction with shim plates

The gap sizes for the dummy members are provided in table below. It can be noticed that the gap sizes are ordered in a more structured manner. This was possible due to the fact that the topside is lifted in a centric manner.

Dummy member	**Gap size [cm]**
D1	2.5
D2	0.75
D3	0
D4	0.75
D5	2.5
D6	2.5
D7	0.75
D8	0
D9	0.75
D10	2.5
D11	2.5
D12	0.75
D13	0
D14	0.75
D15	2.5
D16	2.5
D17	0.75
D18	0
D19	0.75
D20	2.5

Table C.39: Overview of the optimal gap size for the dummy members in E-B direction

C.3. Verification of the results

C.3.1. Rigging loads

The design rigging loads for the 60-40 and 55-45 distribution are provided in Appendix C.2. The loads differ from the equilibrium load distribution, and therefore it has to be checked whether the load output per lift point row remains the same. Stable lifting of the topside is secured in this way. The load output per row is expressed as a fraction of the total rigging load. Looking at these tables in section C.2., it can be seen that the load output per row remains the same for all load cases. Only the diagonals, on which the varying load distribution is imposed, take up different portions of the total rigging load. It can be concluded that the rigging loads are implemented correctly this way.

C.3.2. Boundary conditions

In verifying the boundary conditions, the two beams 1-5 direction model for load case L641 is examined in this section.

Pinned connection

It is expected that mainly forces in transverse and vertical direction are transferred to the MSF legs, as only forces in these directions are applied to the system. The beam along row 1, which is connected to leg joints PB10 and PE10, is examined. First the force balance in z-direction is considered, as shown in figure C.11.

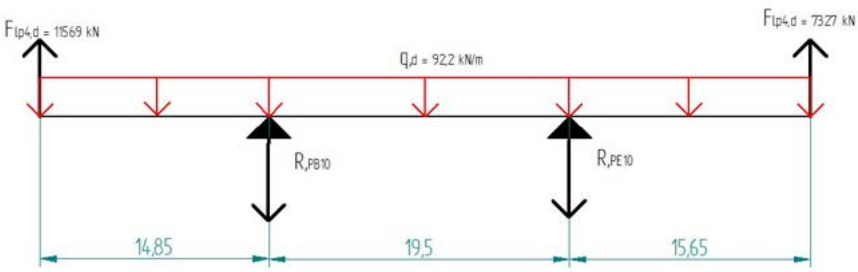

Figure C.11: Vertical force balance, pinned connection

The loads that are shown in this figure are the design loads. The previously shown unfactored rigging loads are multiplied with a factor of 1.21. The same holds for the self-weight of the lift beam, which becomes: $q_{beam1,d} = 76.2 * 1.21 = 92.2kN/m$
It follows that:

$$R_{PB10} = \frac{11569 * (14.85 + 19.5) - 7327 * 15.65 - 92.2 * 50 * 19.5/2}{19.5} = 12194kN \quad \text{(C.1)}$$

And:

$$R_{PE10} = 11569 + 7327 - 12194 - 50 * 92.2 = 2092kN \quad \text{(C.2)}$$

It can be noticed that lifting the topsides off its equilibrium, results in large deviations between the leg reaction forces. The spring reaction forces from $K_{z,1}$ and $K_{z,2}$ also have to be taken into account. $K_{z,1}$ is located above PE10 and the spring reaction force, $F_{K_{z,1}}$, has a magnitude of 29 kN downwards. $F_{K_{z,2}}$ is located above PB10 and equals 47 kN, acting downwards as well.
Finally the effects of eccentric lifting also have to be taken into account. The CoG of the assembly and the CoF of the rigging loads are used for this. The coordinates of these points are provided in table below.

	x	y	z
$CoG_{assembly}$	0.703	15.599	21.973
$CoF_{rigging}$	0.753	15.573	15.000

Table C.40: Topsides CoG and rigging load CoF coordinates in 1-5 direction for one-sided leg support

Eccentricity in x-direction will result in an overturning moment around the y-axis. This overturning moment is decoupled over rows 1 and 5. This results in a reduction of the reaction forces at PB10 and PE10.

$$M_y = (CoF_x - CoG_x) * F_{rig,d} \tag{C.3}$$

And:

$$F_z = \frac{M_y}{2 * 18} = 48.7kN \tag{C.4}$$

Similarly, eccentricity in y-direction will result in an overturning moment around the x-axis. The overturning moment is decoupled over rows B and E, which result in an additional compressive force in PB10 and a tensile force in PE10.

$$M_x = (CoF_y - CoG_y) * F_{rig,d} \tag{C.5}$$

And:

$$F_z = \frac{M_x}{2 * 19.5} = \pm 23.4kN \tag{C.6}$$

When decoupling the moments it is assumed that both legs take 50% of the load. The final vertical reaction forces of the legs are equal to:

$$R_{z,PB10} = 12194 + 47 - 49 - 23 = 12169kN \tag{C.7}$$

And:

$$R_{z,PE10} = 2092 + 29 - 49 + 23 = 2095kN \tag{C.8}$$

It can be seen that the force contributions due to the overturning moment acting on the topside are relatively small. The off-equilibrium leg reaction forces are the main contributors to the unfavorable topsides loading.
Similarly a force balance in x-direction can be considered, as shown in figure C.12.

Figure C.12: Horizontal force balance, pinned connection

No additional load components due to eccentric lifting or spring forces are applicable in this direction. Using equations C.1 and C.2 it follows that:

$$R_{x,PB10} = 724kN \tag{C.9}$$

And:

$$R_{x,PE10} = 220kN \tag{C.10}$$

The obtained results are now compared to the nodal forces of PB10 and PE10. In figure C.13 the load extract from SACS is shown.

PB10-CB10	PB10	482	L641	-12305.8867	724.5948	1492.9307	0.0000	0.0000	0.0000
	CB10		L641	-12271.1475	724.5948	1492.9307	0.0000	2985.8552	1449.1864
PB50-CB50	PB50	482	L641	-2004.8898	-210.7138	1206.5519	0.0000	0.0000	0.0000
	CB50		L641	-1970.1508	-210.7138	1206.5519	0.0000	2413.0986	-421.4267
PE10-CE10	PE10	482	L641	-2014.3684	220.4155	-1492.9307	0.0000	0.0000	0.0000
	CE10		L641	-1979.6293	220.4155	-1492.9307	0.0000	-2985.8552	440.8301

Figure C.13: Nodal forces acting on nodes PB10 and PE10 for a pinned connection

It can be seen that the obtained leg forces in x- and z-direction are reasonably close to the values from SACS. It can also be seen that no moments are transferred to the MSF leg nodes. Surprisingly a relatively large force in longitudinal direction of the lift beam is found to be acting on the MSF legs. The force equals 1493 kN for both PB10 and PE10. As no loads are applied to the model in this direction it is suspected that these loads follow from bending of the lift beam. This can also be seen in the opposing direction of the force for legs PB10 and PE10. As the lift beam bends the MSF legs are both pushed inwards, hence the force in longitudinal direction should be different in sign for these nodes. It is found that this longitudinal shear force is caused by bending of the lift beam [37]. The force follows from the moment difference between the MSF legs:

$$F_y = \frac{M_{PB10} - M_{PE10}}{2y} = \frac{161631.95 - 103371.09}{2 * 19.5} = 1494kN \tag{C.11}$$

This consequently results in a jump in the moment line at the connection with the MSF legs. The moment and shear line of the lift beam is split up in three parts : LP4-PB10, PB10-PE10 and PE10-LP3, as shown below.

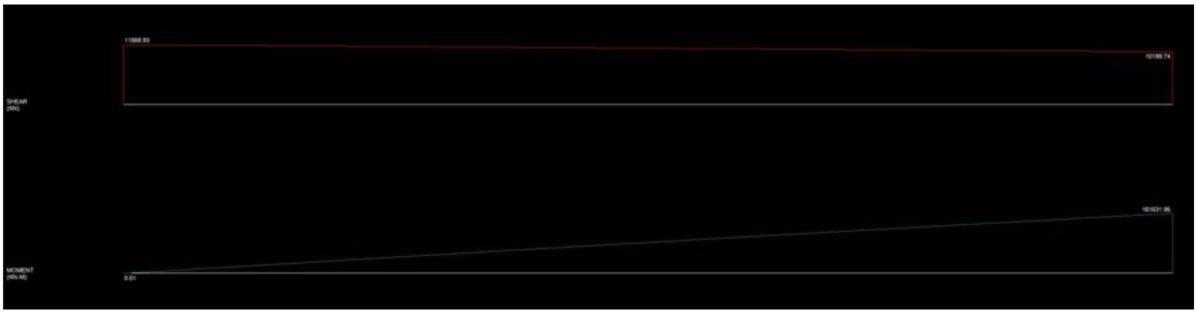

Figure C.14: Moment and shear line for section LP4-PB10

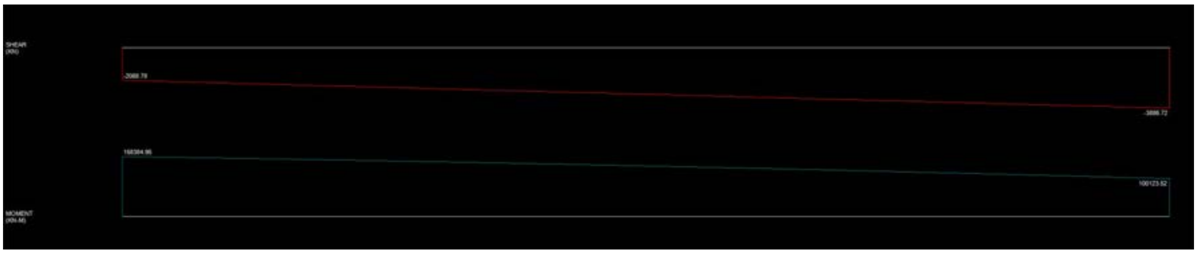

Figure C.15: Moment and shear line for section PB10-PE10

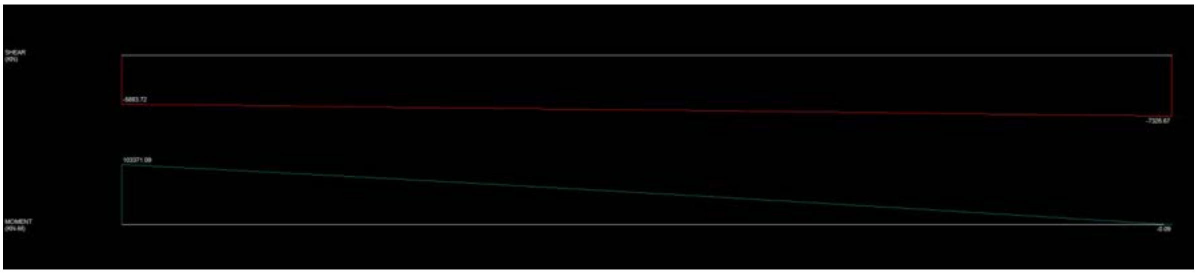

Figure C.16: Moment and shear line for section PE10-LP3

At PB10 a jump in the moment line of 161632-158385 = 3247 kNm is observed. Similarly for PE10 a moment jump of 103371-100124 = 3247 kNm is found. The moment jump follow from the distance of the longitudinal shear force to the neutral axis of the lift beam: 1494 * 4.35/2 = 3247 kNm.

Finally the lift beam end is restrained against torsion as a pinned connection is used without a cross-beam. The twist resisting moment is shown in figure C.17.

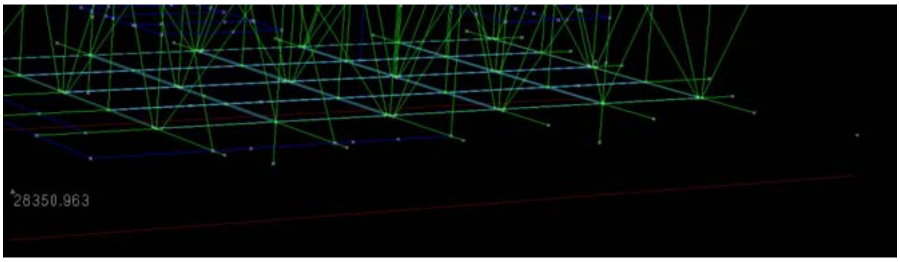

Figure C.17: Torsional reaction moment lift beam LP4-LP3

It can be seen that this moment equals 28351 kNm. This moment is approximated with the follow relation:

$$M_{torsion} = (R_{z,PB10} + R_{z,PE10}) * (B/2 + D_O/2) + (R_{x,PB10} + R_{x,PE10}) * (H/2) = 26678kNm \quad (C.12)$$

Clamped connection

The forces and moments that are transferred to the MSF legs for a clamped connection are verified by engineering judgement. Figure C.18 shows the reaction forces and moments for legs PB10 and PE10 according to SACS.

PB10-CB10	PB10	482	L641	-12005.9316	711.1879	4866.4736	-339.3785	-13979.6758	13966.4697
	CB10		L641	-11971.1934	711.1879	4866.4736	-339.3785	-4246.7480	15388.8438
PB50-CB50	PB50	482	L641	-2230.8857	-225.6303	4110.3218	34.2885	-7166.4028	-12041.3301
	CB50		L641	-2196.1465	-225.6303	4110.3218	34.2885	1054.2218	-12492.5908
PE10-CE10	PE10	482	L641	-2314.3245	233.8223	-4866.4736	77.9462	8130.5508	14384.4922
	CE10		L641	-2279.5857	233.8223	-4866.4736	77.9462	-1602.3766	14852.1357

Figure C.18: Nodal forces acting on nodes PB10 and PE10 for a clamped connection

It can be seen that the reaction forces in x- and z-direction are similar as for the pinned case. The longitudinal shear force increases from 1494 kN to 4866 kN. The same jump in the bending moment line is observed, which is equal to $2.175 * 4866 = 10584kNm$. The torsional moment of 28351 kNm is now spread as a weak-axis bending moment of 13980 kNm to leg PB10 and 14384.5 kNm to leg PE10. The other moments are dependent on the stiffness of the MSF legs and the rotation of the lift beam. The forces and moments that are transferred for a clamped connection are considered to be correct.

C.3.3. UC

The combined UC of MSF leg PB10 for load case L641, is reviewed for each removal setup in 1-5 direction. For simplicity only the pinned connection is considered. It is aimed to get more insight in how much of the leg capacity is taken by which type of loading. This way it can also be checked whether changes in the removal setup lead to expected differences. Figure 6 shows the locally defined coordinate system of the MSF leg, with z pointing in the direction of the lift beams.

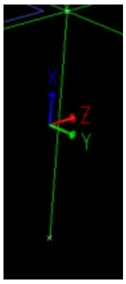

Figure C.19: Local coordinates of leg PB10

The relevant structural properties of the MSF legs are provided in table below.

A_{axial}	0.186	$[m^2]$
A_{shear}	0.093	$[m^2]$
W_x	0.052	$[m^4]$
W_y	0.052	$[m^4]$
F_y	335	$[MPa]$

Table C.41: Properties MSF leg

The maximum combined UC of the MSF legs occurs at the interface with the MSF deck. The individual UC's that are considered are:

$$F_a = \frac{R_{z,PB10}}{A_{axial}} \tag{C.13}$$

$$F_{by} = \frac{M_{y,PB10}}{W_y} \tag{C.14}$$

$$F_{bz} = \frac{M_{z,PB10}}{W_z} \tag{C.15}$$

$$F_v = \frac{\sqrt{F_z^2 + F_y^2}}{A_{shear}} \tag{C.16}$$

Figure C.20 shows the UC's for the two lift beams model.

Stress	Actual	Allowa...	Ratio
Euler	-65.81	18054.60	0.00
Fa	-65.81	197.43	0.33
-Fby	57.09	251.25	0.21
-Fbz	27.71	251.25	0.05
Fv	17.80	134.00	0.13
Ftor	0.00	134.00	0.00

Figure C.20: Overview of the MSF leg UC's for one-sided leg support

The stresses are checked with the forces from SACS in figure C.13.

$$F_a = \frac{12306}{0.186} = 66MPa$$

$$F_{by} = \frac{1494*2}{0.052} = 57MPa$$

$$F_{bz} = \frac{724*2}{0.052} = 28MPa$$

$$F_v = \frac{\sqrt{724^2+1494^2}}{0.093} = 18MPa$$

It can be seen that most of the MSF leg's capacity is taken by the vertical load and the moment around the y-axis. The vertical load is needed to lift the topsides off its place, and has increased due to the rigging load distribution. For a 60-40 distribution, the difference in leg reaction force can be approximated with equations below.

$$R_{PB10,60-40} \approx \frac{1.2 * F_{LP4,eq} * (19.5 + 14.85) - \frac{F_{LP3,eq}}{1.2} * 15.65 - q_{beam} * 50 * \frac{19.5}{2}}{19.5} \tag{C.17}$$

$$R_{PB10,eq} = \frac{F_{LP4,eq} * (19.5 + 14.85) - F_{LP3,eq} * 15.65 - q_{beam} * 50 * \frac{19.5}{2}}{19.5} \tag{C.18}$$

Subtracting equation C.18 from C.17:

$$R_{PB10,60-40} - R_{PB10,eq} = \frac{0.2 * F_{LP4,eq} * (19.5 + 14.85) + 0.17 * F_{LP3,eq} * 15.65}{19.5} = 4703kN \tag{C.19}$$

The actual difference between the PB10 equilibrium reaction force and the PB10 reaction force for a 60-40 distribution equals $12306 - 7768 = 4538kN$ The difference in results follows from the fact that the rigging loads do not exactly increase or decrease by a factor of 1.2. Nonetheless it can be seen that the leg reaction force increases by almost 60%.
The y-moment is a consequence of the longitudinal shear force and is not required to lift the topside off its substructure. If possible it would be valuable if the longitudinal shear force could be reduced or if possible eliminated. Finally the moment acting around the z-axis is caused by the transverse reaction force in y-direction. Under this setup the transfer of this force, and the corresponding moment can't be avoided. Figure C.21 shows the UC's of PB10 when cross-beams are added to the lift beam setup.

Stress	Actual	Allowa...	Ratio
Euler	-50.75	18054.60	0.00
Fa	-50.75	197.43	0.26
-Fby	85.74	251.25	0.34
-Fbz	-14.98	251.25	0.01
Fv	24.41	134.00	0.18
Ftor	0.00	134.00	0.00

Figure C.21: Overview of the MSF leg UC's for one-sided leg support with cross-beams

It can be seen that the vertical load has reduced, while the rigging loads have increased. This implies that the cross-beams redistribute the loads over the connection points. This shows to be quite useful for the leg's structural integrity, since the transferred loads approach the equilibrium case. Furthermore it is noticed that F_{by} and F_v have slightly increased, implying that the longitudinal shear force increases when cross-beams are added. The lift beams are stiffer now and therefore there is more resistance to bending of the lift beams. F_{bz} shows a strong decrease and change of sign. This likely implies that the cross-beam takes up part of the transverse load, and provides a horizontal reaction force to the lift beams. This could also partially follow from the resistance against torsion of the lift beams. Figure C.22 shows the UC's for the two-sided leg support setup.

Stress	Actual	Allowa...	Ratio
Euler	-54.94	18054.60	0.00
Fa	-54.94	197.43	0.28
-Fby	58.24	251.25	0.23
-Fbz	1.36	251.25	0.00
Fv	16.34	134.00	0.12
Ftor	0.00	134.00	0.00

Figure C.22: Overview of the MSF leg UC's for two-sided leg support

Compared to the one-sided leg support setup, it is noticed that the vertical load acting on PB10 has reduced, while the total weight of the assembly has increased. The MSF leg is loaded in a less eccentric manner. Decoupling of the weak-axis bending moment, acting on the MSF leg, therefore results in a lower added vertical load component. It could also imply that redistribution over the MSF leg row takes place due to the two-sided leg support. F_{by} increases slightly as a longitudinal shear force acts from both sides of the MSF leg in the same direction. What is mainly achieved is the strong reduction in F_{bz}. This follows from the fact that the lift point side loads counteract each other and that the leg is lifted in a less eccentric manner. Finally the results are provided for the two-sided leg support with cross-beams setup.

Stress	Actual	Allowa...	Ratio
Euler	-51.43	18054.60	0.00
Fa	-51.43	197.43	0.26
-Fby	73.68	251.25	0.29
-Fbz	-2.76	251.25	0.00
Fv	20.68	134.00	0.15
Ftor	0.00	134.00	0.00

Figure C.23: Overview of the MSF leg UC's for the four beams with cross-beams model

Compared to two-sided leg support without cross-beams, primarily an increase in F_{by} and F_v is observed, which is caused by the stiffer lift beams support, resulting in a larger longitudinal shear force. Correspondingly, a slight increase for F_v is observed, which is caused by the increased longitudinal shear force and increased side loads. The vertical load has slightly reduced as a consequence of the load redistribution.

D

The connection between the lift beams and the topside

D.1. The connection concepts

In this section the full range of connection concepts that have been considered is shown. The characteristics of each concept are briefly discussed. In the end an overview is provided of the challenges, and the advantages and disadvantages of each concept.

D.1.1. Gripper frame

An impression of the gripper frame is provided in figures D.1 and D.2.

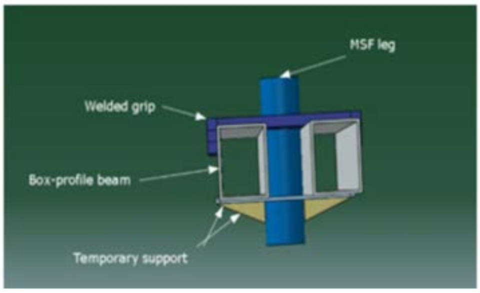

Figure D.1: Impression of the gripper frame

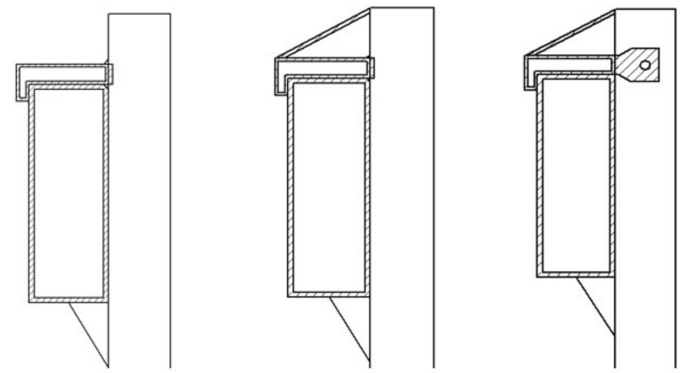

Figure D.2: Variations of the gripper frame

For this connection concept a gripper shaped frame is installed onto the MSF leg. During lifting the lift beam pushes against the frame, which transfers the load to the MSF leg. Outward twist of the lift beam is restrained by the leg of the gripper frame. Bending of the frame therefore imposes torsional shear stresses to the lift beam. The leg of the gripper frame also resists weak-axis bending of the lift beam. To reduce deflection of the gripper frame, the free-end could be braced, as indicated in figure D.2. This way, the loads are also introduced in a more favorable manner to the MSF leg. To avoid the extensive under-deck welding scope, the frame could also be connected to the leg with the use of a pin, as shown on the right in figure D.2. This connection with the MSF leg will also eliminate leg reaction moments.

D.1.2. Gripper

Another method to lift the topside by its MSF legs is to use a gripper, which is equipped on the lift beam. Figure D.3 illustrates this connection type.

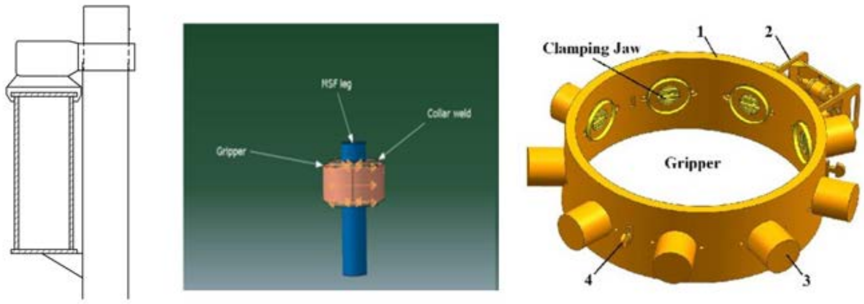

Figure D.3: Gripper connection [46]

Lifting with the use of a gripper is based on friction. The loads that are transferred for this connection concept are expected to be very large. A collar could be welded onto the MSF leg to take up these loads. This will allow to use the same diameter gripper for different leg diameters. Another option is to strengthen the leg by means of grouting. The concrete will provide sufficient inner pressure to withstand the loads from the gripper. Different grippers would be needed for different leg diameters if this option is chosen. It has to be noted that the gripper has to be strong enough to prevent torsion of the lift beam.

D.1.3. Enclosed shells

A variation to the gripper concept, is to form an enclosed shape, which pushes against a collar, rather than gripping onto it. An impression of this is provided in figure D.4.

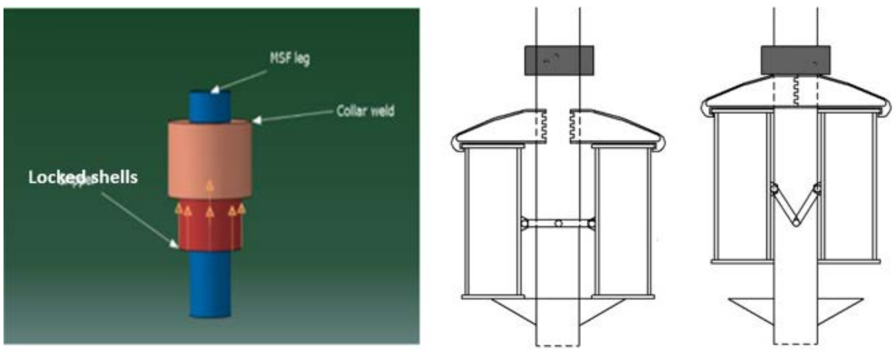

Figure D.4: Enclosed shells

The enclosed shape is formed by two shells which are attached on top of the lift beams. When the lift beams are lifted upwards, the lift beams will rotate towards the leg and form the enclosed shape. The rotation can be around a hinge, which is located in the middle of a transverse element, connected to the lift beams. The connection will require a lot of precision to ensure that the enclosed shape can be created. Disconnection is achieved by simply lowering the rigging.

D.1.4. Geometric lock

The geometric lock forms an enclosed shape between the lift beams and the MSF leg. A wedge shaped collar is welded onto the MSF leg and the lift beam has a trapezoidal shape to achieve this. Other variations can be thought of to establish this enclosed shape. An impression of this connection concept is provided in figure D.5.

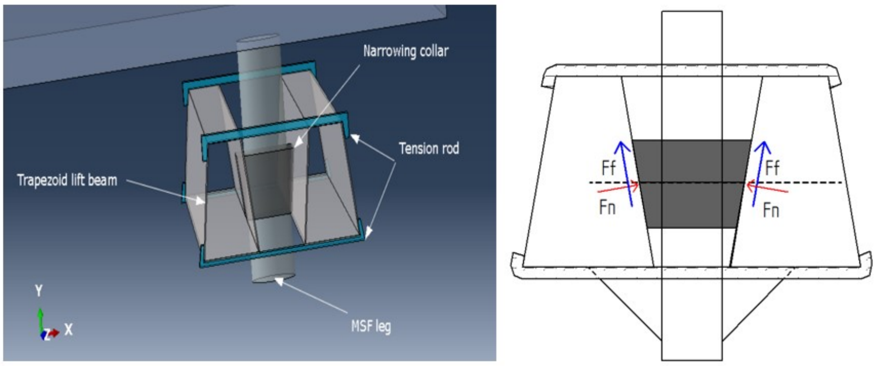

Figure D.5: Geometric lock

Lifting is based on friction and normal forces for this concept. When the lift beams are lifted upwards, mainly normal forces are transferred between the lift beams and the wedge. These normal forces will push the lift beams outwards during lifting. The tension rods, which are attached to the top and bottom of the lift beams, will ensure that contact is maintained.

D.1.5. Pin-hole connection

The pin-hole connection is previously used for the lifting and upending of large diameter piles. The pin penetrates a hole that is formed onto the MSF leg. Lifting with this concept is based on bearing between the pin and the shells of the MSF leg. Figure D.6 illustrates variations of this connection concept.

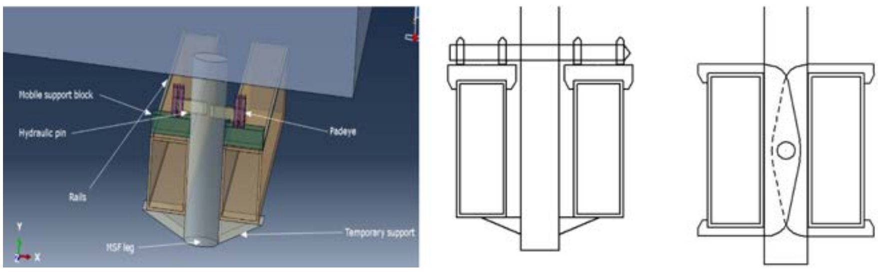

Figure D.6: Pin-hole connection

When the pin pushes against the shell of the MSF leg, the pin will somewhat deflect, and the orientation of the contact force changes. This could result in the pin being pushed out of the hole. This could be prevented by using one large pin instead of two separate pins. Another option is to change the orientation of the pin in the direction of the lift beams. This way outward twist of the lift beams is prevented, and the pin can be positioned at the neutral axis of the lift beam.

D.1.6. Steel-on-steel/ shim plates

This connection concept is used to connect the lift beams to the MSF deck. As was shown in chapter 4, it is essential that the interior columns of the topside are also activated during lifting. As discussed shim plates could be used for this purpose, which are varying in thickness, and are positioned at the location of the connection point. Another possibility could be to use a thick, flexible, rubber-like material, which can take up under-deck unevenness and activate the interior columns due to its flexibility. An impression of this is provided in figure D.7.

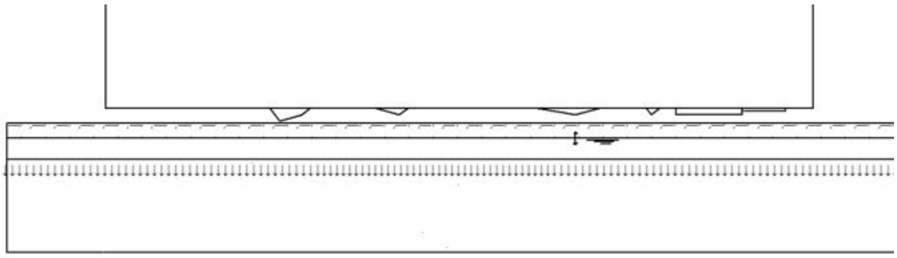

Figure D.7: Steel-on-steel

The rubber material will have to be thick enough to activate all columns and equally distribute the load over the length of the lift beam.

D.1.7. Hydraulic jacks

An alternative to the shim plates is the use of hydraulic jacks. This way a more controlled load transfer can be achieved. An impression of this is provided in figure D.8.

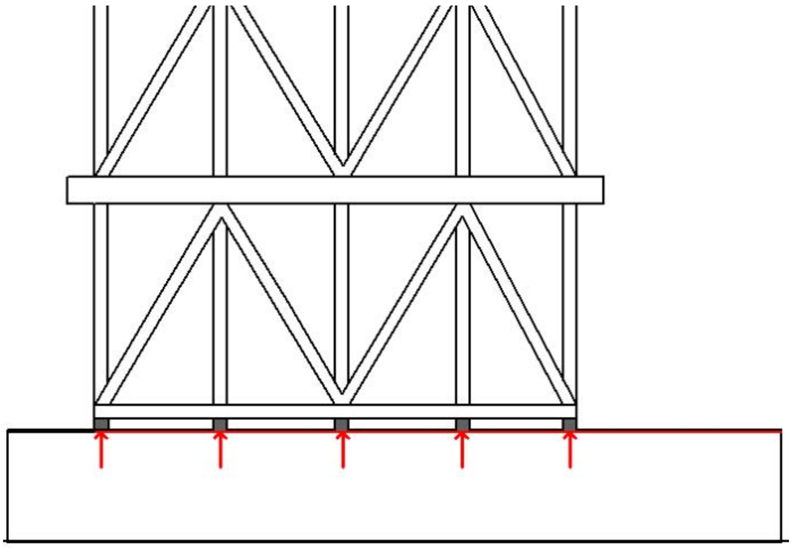

Figure D.8: Hydraulic jacks

The load out-put of the jacks can be controlled by manipulating the hydraulics fluid. The hydraulic system could be housed inside the lift beams. The hydraulic jacks are on-shore positioned on the lift beams, based on the location of the connection points. it is important that a flat, even surface is prepared at the connection location. Expansion of the jacks could be used to overbridge obstructions

D.1.8. Connection concepts initial assessment

	Advantages	Disadvantages/ challenges
Gripper frame	The leg of the frame restrains torsion and weak axis bending of the lift beam	Installation of the gripper frame will be complicated
		Due to the size and location of the gripper frame, its installation will only be possible after lift beam installation
		Adequate working space and work access is required for this.
		The relativelty heavy frame would have to be hoisted, from the topside, to the required elevation.
		The height of the gripper frame (~0.5m) will limit the height of the lift beams.
		The under-deck welding scope is large, and would have to be applied to each topside.
		Moments due to torsion and weak-axis bending are introduced to the leg.
Gripper	Strong, reliable connection	A radial force, which is about 5 to 6 times larger than the required vertical load, is exerted onto the MSF leg.
		Welding of collars will be required to grip onto.
		Grouting the leg will result in difficulties on how to seal the grouting. Castellation cut not be possible this way
		Hence there will be a large under-deck welding scope
		Height limitations
		How to connect the grippers to the lift beam?
		Gripper has to be strong enough to prevent torsion of the lift beam
Enclosed shells	No need for strengthening of the MSF leg, smaller collars can be used to push against	The shells will bend, and the reaction bending moment has to be provided by the MSF leg
	Easy to disconnect	Installation of the enclosed shape will require a lot of precision, in order for the shapes to connect with eachother
	Cheap solution	The height of the hinged transverse member would have to be at the right elevation for this.
	Only vertical load transferred to the lift beams	Also, an effenaar will be required to ensure that both beams are lifted simultaneously with the same load.
		To achieve this connection a rigid cross-beam, connected to all the lift beams, can't be used.
Geometric lock	Quick disconnection after topside removal.	Connection will require the installation of the tension rods in the critical path
	No need for additional tools, connection integrated along the length of the lift beam	The working principle of this connection strongly depends on the properties of the tension rods
	Relatively easy installation, no height/width restrictions for the lift beam	Large contact forces, which are much larger than the required vertical lift force. Local strengthening of the lift beams
	Engangement of the connection simply achieved by hoisting	How to take friction into account? -> conservative approach will have to be taken
		Under-deck welding scope
		Which tolerance/ clearance to take between the wedge and the lift beam?
Pin-hole connection	Connecting the pin in longitudinal direction of the lift beams, won't need twist restrainme	Can the leg provide sufficient bearing area to withstand the loads?
	Using one large pin instead of two, will also solve the pin being pushed out of the hole	If the pin is transversly connected to the lift beam, torsion will be introduced to the lift beam.
	Drop-shaped holes could be used, which narrow down towards the lift load direction	Due to second order effects the pin will be pushed out of the hole.
	Support sleaves could be used as well	Twist of the lift beam therefore must be restrained
	Simple connection and disconnection	Large holes will be required. Risk of alignment of the holes
	Small preparation scope, no welding	
	Proven technology	
Steel-on-steel	A rubber layer could be used to take up deck unevenness and to deal	Varying stiffness between the lift beam and the topside
	with varying connection locations	How to deal with under-deck unevenness
	A large amount of potential connection locations	A small deviation in the shim-plate thickness will have a significant impact on the load transfer
	No welding needed	Does the deck have sufficient capacity?
	Beneficial load transfer for the lift beams	Statically undetermined, weakest member at connection interface becomes governing
		Sufficient 'flat' area required
Hydraulic jacks	Controlled load output	Sufficient stroke required to overbridge obstructions/unevenness
	Load independent of rigging load distribution	A cross-beam will be needed to provide lateral stability
	, and stiffness of the lift beams and MSF deck , when hydraulically linked	How to position the lift beams? -> large temporary support structure required
	Large amount of potential lift points, good load spread voor topside and lift beams	
	Positioning of the jacks easily determined, based on structural drawings of the MSF	

Figure D.9: Connection concepts initial assessment

D.2. Connection concept design

D.2.1. Pin-hole design

Pin design

First the bearing capacity of the MSF leg is checked as this is expected be the governing factor in the pin design. The first step is to determine the leg shell reaction forces, R_A and R_B.

$$R_{z,A} = F_{d,z,A} + \frac{M_y}{D_{leg} - t_{leg}} = 18.43MN \tag{D.1}$$

$$R_{z,B} = F_{d,z,B} - \frac{M_y}{D_{leg} - t_{leg}} = 10.69MN \tag{D.2}$$

Where:

$$M_y = (F_{d,x,A} + F_{d,x,B}) * 2.175 \tag{D.3}$$

The longitudinal reaction force, R_x, is assumed to act on side A only. The transverse reaction forces, R_y, are equal to the transverse side loads.

$$R_{x,A} = F_{x,z,A} + F_{x,z,B} = 1.46MN \tag{D.4}$$

$$R_{x,B} = 0MN \tag{D.5}$$

$$R_{y,A} = F_{d,y,A} = 0.80MN \tag{D.6}$$

$$R_{y,B} = F_{d,y,B} = 0.66MN \tag{D.7}$$

The bearing resistance of the MSF leg is determined with equation D.8.

$$F_{br,Rd} = \frac{f * k_1 * \alpha_b * F_u * D_{pin} * t_{leg}}{\gamma_{M2}} = 22.60MN \tag{D.8}$$

Where:

f	factor for oversized hole (= 0.8)	[-]
k_1	Bearing parameter 1 (= 2.5)	[-]
α_b	Bearing parameter 2 (= 1.0)	[-]
F_u	Shell tensile strength (= 470)	[MPa]
F_{up}	Pin tensile strength (= 850)	[MPa]
γ_{M2}	Material factor for bolted connections (= 1.3)	[-]

The bearing parameters are determined with equations D.9 and D.10.

$$k_1 = min(2.8 * \frac{e_2}{D_{hole}} - 1.7, 2.5) \tag{D.9}$$

$$\alpha_b = min(\frac{e_1}{3D_{hole}}, \frac{F_{up}}{F_u}, 1.0) \tag{D.10}$$

An additional ULS load factor, γ_{ULS}, of 1.2 is applied to the maximum vertical leg reaction force $R_{z,A}$.

$$R_{A,Ed} = \gamma_{ULS} * R_{z,A} = 22.12MN \tag{D.11}$$

The bearing unity check of the MSF leg equals:

$$UC_{br,leg} = \frac{R_{A,Ed}}{F_{br,Rd}} = 0.98 \tag{D.12}$$

It can be concluded that the MSF leg is able to withstand the bearing load that is exerted by the hydraulic pin during lifting. It is now left to determine whether the hydraulic pin has sufficient capacity for the governing load case. The structural properties of the pin and spacing between the support frame and leg support are provided in table below.

A_{pin}	0.307	[m^2]
W_{pin}	0.024	[m^3]
$F_{y,pin}$	590	[MPa]
$F_{u,pin}$	780	[MPa]
E	210	[GPa]
L_{pin}	2500	[mm]
$x_{CL_{leg}-CL_{frame}}$	385	[mm]

Table D.1: Properties of the hydraulic pin

The maximum shear force in the pin is equal to normal force $F_{N,pin}$, which acts on support A.

$$F_{N,pin} = \sqrt{R_{z,A}^2 + R_{y,A}^2} = 18.45MN \tag{D.13}$$

The maximum bending moment in the pin, $M_{N,pin}$ occurs at leg shell A and equals:

$$M_{N,pin} = F_{N,pin} * x_{CL_{leg,shell}-CL_{frame}} = 7.10MNm \tag{D.14}$$

The LRFD design shear force and moment, $F_{v,Ed,pin}$ and $M_{Ed,pin}$ are determined by multiplying the previously obtained values with γ_{ULS}. The shear resistance and moment resistance of the pin are determined with equations D.17 and D.18.

$$F_{v,Ed,pin} = F_{N,pin} * \gamma_{ULS} = 22.14MN \tag{D.15}$$

$$M_{Ed,pin} = M_{N,pin} * \gamma_{ULS} = 8.52MNm \tag{D.16}$$

$$F_{v,Rd,pin} = \frac{0.6 * A_{pin} * F_{u,pin}}{\gamma_{M2}} = 110.5MN \tag{D.17}$$

$$M_{Rd,pin} = \frac{1.5 * W_{pin} * F_{y,pin}}{\gamma_{M0}} = 18.5MNm \tag{D.18}$$

	Yield strength [MPa] as function of material thickness [mm]							
Steel grade	0 <t <16	16 <t <40	40 <t <63	63 <t <80	80 <t <100	100 <t <150	150 <t <200	200 <t <250
S355J2+N	355	345	335	325	315	295	275	255

Table D.2: Yield strength of S355J2+N steel as a function of material thickness

In equation D.18, γ_{M0} represents the pin bending material factor and equals 1.15, according to Norsok [12]. The pin unity checks for shear, bending and their combination are provided below.

$$UC_{v,pin} = \frac{F_{v,Ed,pin}}{F_{v,Rd,pin}} = 0.20 \tag{D.19}$$

$$UC_{b,pin} = \frac{M_{Ed,pin}}{M_{Rd,pin}} = 0.46 \tag{D.20}$$

$$UC_{com,pin} = (UC_{v,pin})^2 + (UC_{b,pin})^2 = 0.25 \tag{D.21}$$

Finally the pin is checked on its bearing capacity.

$$F_{br,Rd,pin} = \frac{1.5 * t_{leg} * D_{pin} * F_{y,pin}}{\gamma_{M0}} = 24.05MN \tag{D.22}$$

$$UC_{br,pin} = \frac{F_{v,Ed,pin}}{F_{br,Rd,pin}} = 0.93 \tag{D.23}$$

Support frame design

The rules of thumb for the dimensions of the main plate and cheek plate are provided below [34].

$$r_{main} = 1.75 * d_{pin} \tag{D.24}$$

$$r_{cheek} = 1.50 * d_{pin} \tag{D.25}$$

$$t_{main} = (0.3 - 0.5) * d_{pin} \tag{D.26}$$

$$t_{cheek} \leq 0.5 * t_{main} \tag{D.27}$$

$$w(weldlegsize) \leq t_{cheek} - 5mm \tag{D.28}$$

The yield strength as a function of material thickness for S355J2+N is given in table below.
On section A only a shear force is acting.

$$F_{shear,A} = F_h = 3244kN$$

$$A_{shear,A} = 0.13 * t_{main} = 0.13 * 0.25 = 0.0325m^2$$

$$f_{v,A} = 3244/0.0325 = 99.82MPa$$

$$Fv = 0.4 * 255 = 102MPa$$

$$UCv, A = \frac{99.82}{102} = 0.98[-]$$

On section B an axial load and a bending moment are acting.

$$F_{axial,B} = 3244kN$$

$$M_B = -F_v * x_v + F_h * (z_h + t_f/2 + h_b/2) = 700kNm$$

$$A_B = h_B * t_{main} = 0.09m^2$$

$$w_B = \frac{1}{6} * t_{main} * h_B^2 = 0.0054m^3$$

$$\sigma_{t,B} = \frac{3244}{0.09} = 35.92MPa$$

$$\sigma_{b,B} = \frac{700}{0.0054} = 128.8MPa$$

$$UC_{t+b,B} = \frac{35.92}{0.6*255} + \frac{128.8}{0.66*255} = 1.0[-]$$

On section C, an axial force, a shear force and a moment are acting.

$$F_{axial,C} = 3244kN$$

$$F_{shear,C} = 12300kN$$

$$M_C = -F_v * x_v + F_h * (z_h + t_f/2 + h_C/2) = 1104kNm$$

$$A_C = h_C * t_{main} = 0.15m^2$$

$$w_C = \frac{1}{6} * t_{main} * h_C^2 = 0.016m^3$$

$$\sigma_{t,C} = \frac{3244}{0.15} = 21.27MPa$$

$$\sigma_{v,C} = \frac{12300}{0.15} = 80.66MPa$$

$$\sigma_{b,C} = \frac{1104}{0.016} = 71.18MPa$$

$$UC_{VM,C} = \frac{\sqrt{(21.27+71.18)^2+3*80.66^2)}}{0.66*255} = 1.0[-]$$

Section D is under an angle of 29 degrees with respect to the horizontal.

$$M_D = F_h * (z_h + h_D/2 * sin(29)) - F_v * (1.094 - h_D/2 * cos(29) - e) = 9119kNm$$

$$F_{axial,D} * sin(61) + F_{shear,D} * sin(29) = 12300$$

$$F_{axial,D} * cos(61) - F_{shear,D} * cos(29) = 3244$$

$$F_{axial,D} = 12330kN$$

$$F_{shear,D} = 3126kN$$

$$A_D = h_D * t_{main} = 0.33m^2$$

$$w_D = \frac{1}{6} * t_{main} * h_D^2 = 0.074m^3$$

$$\sigma_{t,D} = \frac{12330}{0.33} = 31.08MPa$$

$$\sigma_{v,D} = \frac{3126}{0.33} = 9.40MPa$$

$$\sigma_{b,D} = \frac{9119}{0.074} = 123.73MPa$$

$$UC_{VM,D} = \frac{\sqrt{(31.08+123.73)^2+3*9.40^2)}}{0.66*255} = 0.93[-]$$

The largest moment is found to be acting on section E.

$$M_E = F_h * z_h - F_v * (x_v - t_w/2 - e - h_E/2) = 9533kNm$$

$$F_{axial,E} = 12300kN$$

$$F_{shear,E} = 3244kN$$

$$A_E = h_E * t_{main} = 0.35m^2$$

$$w_E = \frac{1}{6} * t_{main} * h_E^2 = 0.082m^3$$

$$\sigma_{t,E} = \frac{12300}{0.35} = 35.14MPa$$

$$\sigma_{v,E} = \frac{3244}{0.35} = 9.29MPa$$

$$\sigma_{b,E} = \frac{9533}{0.082} = 116.73MPa$$

$$UC_{a+b,E} = \frac{35.14}{0.6*255} + \frac{116.73}{0.66*255} = 0.92[-]$$

Section F is finally checked to verify that the width below the lift point is sufficient to withstand the stresses in the main plate.

$$F_{shear,F} = 3244kN$$

$$M_F = F_h * (4350/2 - r_{main}) = 3508kNm$$

$$A_F = h_F * t_{main} = 0.42m^2$$

$$w_F = \frac{1}{6} * t_{main} * h_F^2 = 0.116m^3$$

$$\sigma_{v,F} = \frac{3244}{0.42} = 7.77MPa$$

$$\sigma_{b,F} = \frac{3508}{0.116} = 30.18MPa$$

$$UC_{VM,F} = \frac{\sqrt{(30.18^2 + 3*7.77^2)}}{0.66*255} = 0.20[-]$$

Padeye capacity check

PADEYE CAPACITY

Sling Load		12300	[kN]	
Consequence Factor		1.30	[-]	
Padeye Design load Fdl:		15990	[kN]	
	Manual input			
Shackle:		22400	[kN]	
Pin diameter D:		625	[mm]	
Inside width W:			[mm]	
Inside length L:			[mm]	
Material properties padeye:				
Modulus of elasticity E:		200000	[N/mm²]	
Minimum yield stress σ_y:		355	[N/mm²]	
Minimum tensile strength σ_t:		510	[N/mm²]	
Hardness Brinell Factor Fhb:		5.6	[-]	

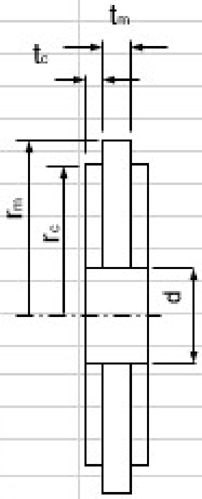

[Ref. SC-292 table 5.1-1]

Padeye dimensions:				
Pinhole diameter d:	(d = Min. D+4, Max. 1.04×D)	635	[mm]	OK
Mainplate radius r_m:	(r_m≥1.75×D)	1094	[mm]	OK
Mainplate thickness tm:	(tm = 0.30 ~ 0.50×D)	250	[mm]	OK
Cheekplate radius r_c:	(r_c2 ≥ 1.50×D)	938	[mm]	OK
Cheekplate thickness t_c:	(t_c <= 0.5×t_m)	125	[mm]	OK
Weld cheek - main plate w:	(w ≤ tc-5)	30	[mm]	OK
Spacer plate thickness			[mm]	
Section length $\gamma-\gamma$		1100	[mm]	

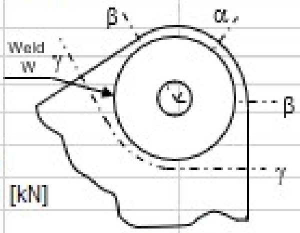

! TOTAL PADEYE THICKNESS > (W-4 MM OR W × 0.92)

Output summary:			
Governing U.C. =	**0.55**		
Max. design load Fdl =	**22400**	[kN]	
1. d ≤ 1.04×D --> Bearing stress check	Fp =	51.2	[N/mm²]
	U.C. =	**0.16**	
2. Shear stress at section $\alpha-\alpha$	Fs =	25.2	[N/mm²]
	U.C. =	**0.18**	
3. Tensile stress at section $\beta-\beta$	Ft =	22.9	[N/mm²]
	U.C. =	**0.14**	
4. Shear stress at weld cheek plate - main plate	Fs =	63.9	[N/mm²]
	U.C. =	**0.45**	
5. Tear out stress at section $\gamma-\gamma$	Fs =	58.1	[N/mm²]
(Only applicable if cheeck plates are used)	U.C. =	**0.41**	
6. Shackle capacity	U.C. =	**0.55**	

Figure D.10: Padeye capcity check

Local bearing stiffeners

$$UC_{web,yielding} = \frac{(\frac{R}{t_w*(N+5k)})}{0.66F_{y,w}} = 3.53 \tag{D.29}$$

$$UC_{web,crippling} = \frac{R}{67.5t_w^2[1+3*\frac{N}{d}(\frac{t_w}{t_f})^{1.5}]\sqrt{F_{y,w}t_f/t_w}} = 2.38 \tag{D.30}$$

For flanges restrained against rotation, sidesway web buckling will not occur when:

$$\frac{d_c/t_w}{l_b/b_f} > 2.3 \tag{D.31}$$

Where:

R	Concentrated load (= 2765)	[kips]
N	Bearing length (= $t_{main,plate} = 9.84$)	[in]
k	Web toe radius (= $t_w = 1.18$)	[in]
$F_{y,w}$	Web yield strength (= 63.82)	[ksi]
d	web height (= 171.26)	[in]
d_c	d - 2k (= 165.75)	[in]
l_b	Unrestrained length (=787.4)	[in]

D.2.2. Geometric lock design

Lift beam design

Acting stresses

Axial stresses

Axial stresses in the cross-section are caused by reaction force $R_{x,a}$. The stress is assumed to act uniformly over the cross-section.

$$f_a = \frac{R_{x,a}}{A} \tag{D.32}$$

Where:

$$A = \frac{B_{top}+B_{bottom}}{2}*H - \frac{B_{top,red}+B_{bottom,red}}{2}*H_{red} \tag{D.33}$$

$$B_{top,red} = B_{top} + 2*t_f*cos(80.22) - 2*t_w/cos(80.22) \tag{D.34}$$

$$B_{bottom,red} = B_{bottom} - 2*t_f*cos(80.22) - 2*t_w/cos(80.22) \tag{D.35}$$

$$H_{red} = H - 2*t_f \tag{D.36}$$

$$f_a = \frac{824kN}{0.87m^2} = 0.95MPa$$

Bending stresses

The bending moments around the y- and z-axis both have their maximum at 17.25 meters from support A. $M_{y,max}$ causes strong-axis bending stresses, $f_{b,y}$, which are largest at the flanges of the profile, where $z = z_{max} = H/2$. The maximum value for $f_{b,z}$ is found on the outer edges of the profile, where $y = y_{max} = B_{bottom}/2$. It follows that the maxima override at the edge of the tension flange, with coordinate $(y,z) = (B_{bottom}/2, -H/2)$.

$$f_{b,y,max} = \frac{M_y*z_{max}}{I_y} = \frac{M_y}{W_y} \tag{D.37}$$

$$f_{b,z,max} = \frac{M_z*y_{max}}{I_z} = \frac{M_z}{W_z} \tag{D.38}$$

Where:

$$W_y = \frac{H^2*(B_{top}^2+B_{bottom}^2+4*B_{top}*B_{bottom})}{12*(B_{top}+2*B_{bottom})} - \frac{H_{red}^2*(B_{top,red}^2+B_{bottom,red}^2+4*B_{top,red}*B_{bottom,red})}{12*(B_{top,red}+2*B_{bottom,red})} \tag{D.39}$$

It follows that:

$$f_{b,y,max} = \frac{170530.3kNm}{0.837m^3} = 203.8MPa$$

$$f_{b,z,max} = \frac{9054.5kNm}{0.33m^3} = 27.5MPa$$

Shear stresses

The shear stresses in the profile are caused by reaction forces $R_{z,a}$ and $R_{y,a}$, and torsional moment $M_{x,max}$. The maximum shear stresses are found between $x = 0$, at support A, and $x = 17.25$. Shear stresses due to $R_{z,a}$ are taken up by the webs, and shear stresses due to $R_{y,a}$ are taken up by the flanges. Their maximum value occurs at the shear center of the profile. It is assumed that the shear stresses follow a 60-40 distribution over the cross-sectional elements. This implies that 60% of the load is taken by one flange or web, and 40% by the other. The maximum shear stress is expected to occur in the web, since the vertical shear force is governing. Also the torsional shear stress will be largest in the web due to its smaller thickness. The average shear stress is used in determining the maximum plate stress in the profile, which is assessed at the edges of the profile.

$$f_{v,z,av} = 0.6 * \frac{R_{z,a}}{h * t_w} \tag{D.40}$$

$$f_{v,y,av} = 0.6 * \frac{R_{y,a}}{b * t_f} \tag{D.41}$$

$$f_{v,z,max} = \frac{6}{5} * \frac{R_{z,a} * Q_z}{2 * I_y * t_w} \tag{D.42}$$

$$f_{v,y,max} = \frac{6}{5} * \frac{R_{y,a} * Q_y}{2 * I_z * t_w} \tag{D.43}$$

Where:

$$Q_z = s_z * \frac{A}{2}$$

$$Q_y = s_y * \frac{A}{2}$$

And:

$$c = \frac{H}{3} * (2 * B_{top} + B_{bottom})/(B_{top} + B_{bottom})$$

$$s_z = c-(B_{bottom}*t_f*\frac{t_f}{2}+2*t_f*(c-t_f/sin(80.22))*((c-t_f)/2+t_f))/(B_{bottom}*t_f+2*t_f*(c-t_f)/sin(80.22))$$

Torsional shear stresses due to $M_{x,max}$ are taken up by the webs and flanges and have a uniform value in the elements. For a long time, torsional shear stresses were determined using St.Venant's constant, I_t. However it was noticed that using I_t often leads to significant errors. For closed profiles, a more accurate estimate of the torsional shear stresses can be obtained by using the enclosed area, A_o, instead of I_t [30]. Equation B.23 is used in determining the torsional shear stresses

$$f_{v,t} = \frac{T}{2 * t_{w/f} * A_o} \tag{D.44}$$

It can be noted that the maximum torsional shear stress occurs in the element with the smallest thickness. The shear stresses for the trapezoid beam are provided below.

$$f_{v,z,av} = 0.6 * \frac{9782kN}{0.164m^2} = 36.2MPa$$

$$f_{v,y,av} = 0.6 * \frac{489.1kN}{0.36m^2} = 0.7MPa$$

$$f_{v,z,max} = \frac{6}{5} * \frac{9782*1.07}{2*2.75*0.04} = 58.1MPa$$

$$f_{v,t,fl} == \frac{14141.1}{2*0.12*8.92} = 6.6MPa$$

$$f_{v,t,wb} == \frac{14141.1}{2*0.04*8.92} = 19.8MPa$$

Allowable stresses The allowable stresses in the cross-section are dependant on the slenderness and yield strength of the elements.

Allowable axial stress
The allowable axial stresses are limited by the critical buckling stress. Buckling will first occur around the weak-axis, which has the highest value for Kl_b/r. The allowable axial stresses in the cross-section are determined with equations D.45 and D.46.
For $Kl_b/r \geq C_c$:

$$F_a = \frac{[1 - \frac{(Kl_b/r)^2]}{2C_c^2}]F_y}{\frac{5}{3} + \frac{3(Kl_b/r)}{8C_c} - \frac{(kl_b/r)^3}{8C_c^3}} \tag{D.45}$$

For $Kl_b/r < C_c$:

$$F_a = \frac{12\pi^2 E}{23(Kl_b/r)^2} \tag{D.46}$$

Where:

K = Buckling factor (= 1) [-]

l_b = Unbraced length (=20) [m]

$$C_c = \sqrt{\frac{2\pi^2 E}{F_y}}[-]$$

The allowable axial stresses for the one-sided support beam and two-sided support beam are provided below.

$$(Kl_b/r)_1 = 18.9$$

$$(C_c)_1 = 97$$

$$F_a = 244.9MPa$$

As for the box-profile beam, the effects for lateral-torsional buckling are not governing and hence the allowable axial stress for this phenomenon is not determined.

Allowable bending stress
The allowable bending stress for compact elements equals:

$$F_b = 0.66F_y \tag{D.47}$$

For non-compact the allowable bending stress equals:

$$F_b = 0.60F_y \tag{D.48}$$

The allowable bending stresses are provided below.

$$F_{b,y} = 0.6 * 440 = 264MPa$$

$$F_{b,z} = 0.66 * 380 = 251MPa$$

Allowable shear stress

The allowable shear stress in cross-section is independent of the element slenderness class. The web slenderness, h/t_w, however does play a role in the shear stress limit. If $h/t_w \leq \frac{380}{\sqrt{F_{y,w}}}$, the allowable shear stress is given by equation D.49. If not, equation D.50 is applied.

$$F_v = 0.40F_y \tag{D.49}$$

$$F_v = \frac{C_v}{2.89} * F_y \leq 0.4 * F_y \tag{D.50}$$

Where:

$$C_v = \frac{45000k_v}{F_y(\frac{h}{t_w})^2}$$
for $C_v < 0.8$

$$C_v = \frac{190}{h/t_w}\sqrt{\frac{k_v}{F_y}}$$
for $C_v > 0.8$

$$k_v = 4 + \frac{5.34}{(\frac{a}{h})^2} for a/h < 1.0$$

$$k_v = 5.34 + \frac{4}{(\frac{a}{h})^2} for a/h > 1.0$$

Parameter a, presents the clear distance between intermediate transverse stiffeners. The shorter the stiffener spacing, the larger the allowable shear stress.

$$a = 5m$$

$$k_v = 8.04$$

$$C_v = 0.52$$

$$F_v = 0.18F_y = 79.4MPa$$

Allowable combined stress

Axial stresses and bending stresses both act in axial direction and hence their joint effect can be assessed. The maximum axial stress occurs on the edge of the compression flange, also indicated as point A in figure 3.3. The unity checks provided in equations D.51 and D.52 shall be satisfied.

$$\frac{f_a}{F_a} + \frac{C_{my}f_{by}}{(1 - \frac{f_a}{F'_{ey}})F_{by}} + \frac{C_{mz}f_{bz}}{(1 - \frac{f_a}{F'_{ez}})F_{bz}} \leq 1.0 \tag{D.51}$$

$$\frac{f_a}{0.60F_y} + \frac{f_{by}}{F_{by}} + \frac{f_{bz}}{F_{bz}} \leq 1.0 \tag{D.52}$$

Where:

$$C_{mx/y} = 0.85$$

$$F'_{ex/y} = \frac{12\pi^2 E}{23(Kl_b/r_b)^2}$$

For slender elements in the cross-section, the allowable stresses, using reduced cross-sectional properties, are applied. Besides the combined axial stress, Huber's equation is applied for the combined effect of axial stresses, bending stresses and shear stresses. The equation is a simplified version of the Von Mises stress equation.

$$\sigma_{HUB} = \sqrt{(\sigma_a + \sigma_b)^2 + 3(\tau_v + \tau_t)^2} \leq 0.66F_y \tag{D.53}$$

The combined stress according to Huber's equation has to be checked at point A and point B, indicated in figure 3.3. A limit is set to the maximum value of these points of $0.66F_y$. This limit is not specified in AISC 1989, but is widely adopted by HMC.

Unity checks

Unity checks for the bending stresses, shear stresses, axial stresses and their combined effect are determined to assess whether the cross-section has sufficient capacity to withstand the stress from the governing load case. The formula for the unity checks are provided below.

$$UC_b = \frac{f_{b,y}+f_{b,z}}{F_b}$$

$$UC_v = \frac{f_{v,z}+f_{v,t}}{F_v}$$

$$UC_a = \frac{f_a}{min(F_{a,bkl}, F_{a,ltb})}$$

$$UC_{b+a} = max(\frac{f_a}{F_a} + \frac{C_{my} f_{by}}{(1-\frac{f_a}{F'_{ey}})F_{by}} + \frac{C_{mz} f_{bz}}{(1-\frac{f_a}{F'_{ez}})F_{bz}}, \frac{f_a}{0.60F_y} + \frac{f_{by}}{F_{by}} + \frac{f_{bz}}{F_{bz}})$$

$$UC_{HUB} = max(\frac{\sqrt{(f_{b,y}+f_{b,z}+f_a)^2+3*(f_{v,z}+f_{v,t})^2}}{0.66F_{y_w}}, \frac{\sqrt{(f_{b,y}+f_{b,z}+f_a)^2+3*(f_{v,y}+f_{v,t})^2}}{0.66F_{y_f}})$$

For the trapezoidal beam, the following unity checks are obtained:

$$UC_b = \frac{203.8+27.5}{251} = 0.92$$

$$UC_v = \frac{58.1+19.8}{79.4} = 0.98$$

$$UC_a = \frac{0.95}{245} = 0.004$$

$$UC_{b+a} = \frac{0.95}{245} + \frac{204}{251} + \frac{27.5}{264} = 0.92$$

$$UC_{HUB} = \frac{\sqrt{(203.8+0.95+27.5)^2+3*(6.6+0.68)^2}}{0.66*380} = 0.93$$

Abaqus results

The tension rods are designed to take up the maximum tension force for the governing load case. The axial forces in the upper tensions rods and the lower tensions rods are plotted in figures D.11 and D.12 respectively.

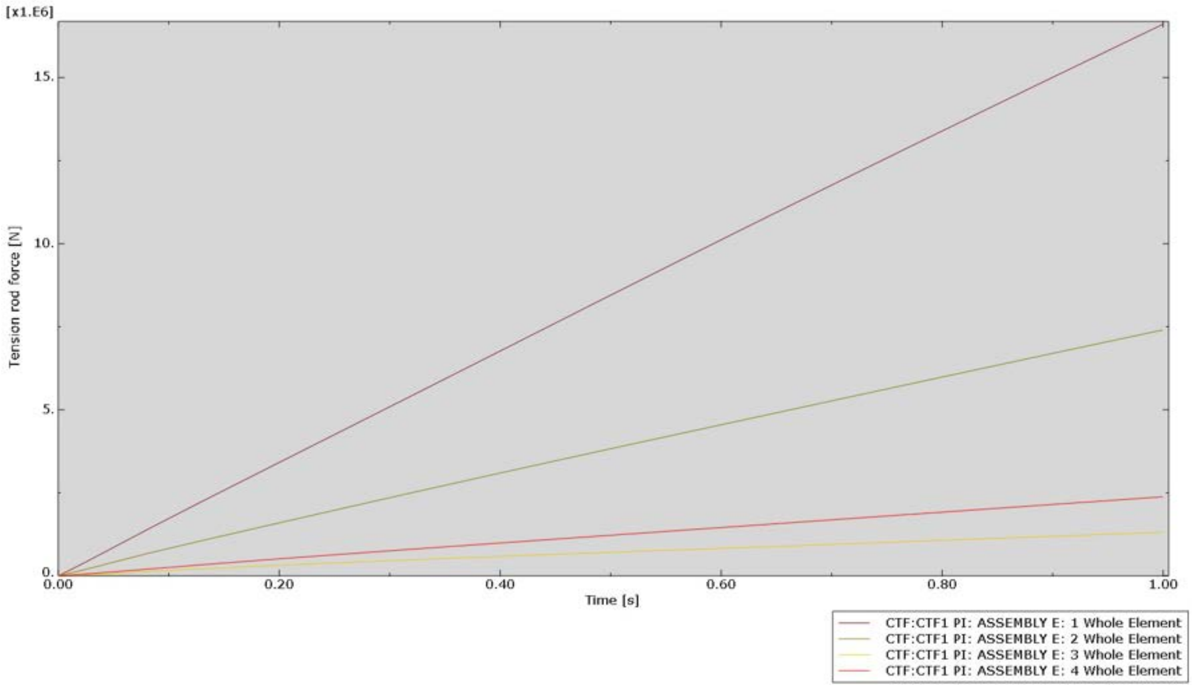

Figure D.11: Axial force top tension rods

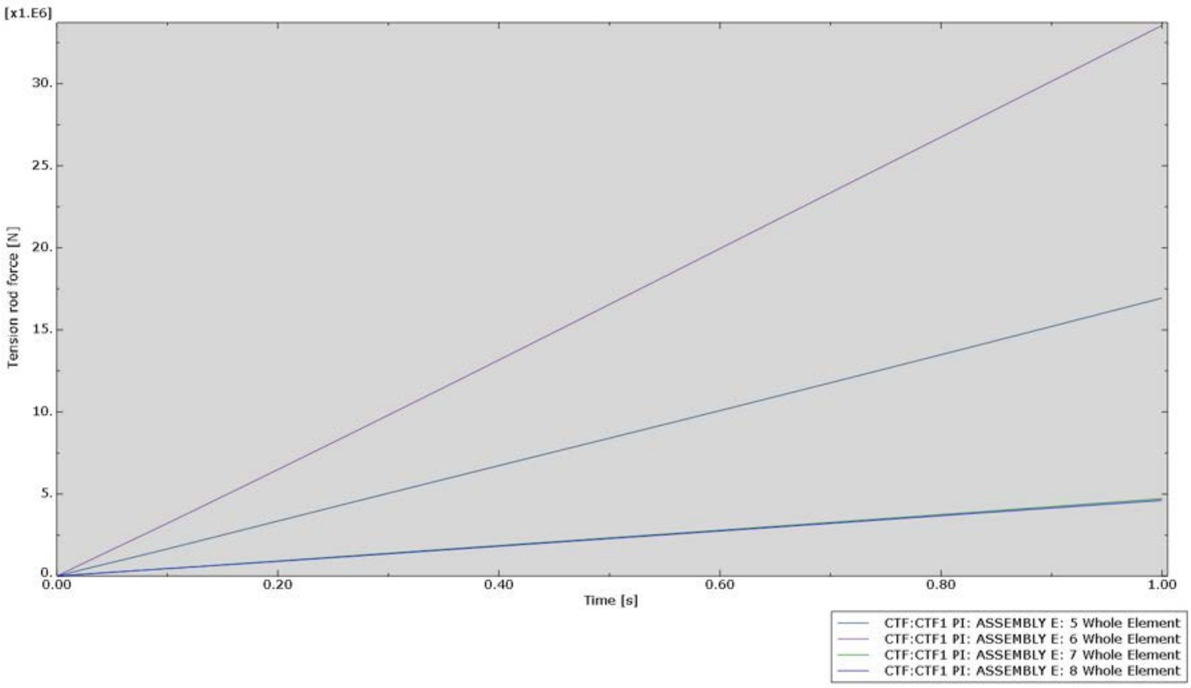

Figure D.12: Axial force bottom tension rods

The maximum plate stresses in the lift beam's contact surface are shown in figure D.13.

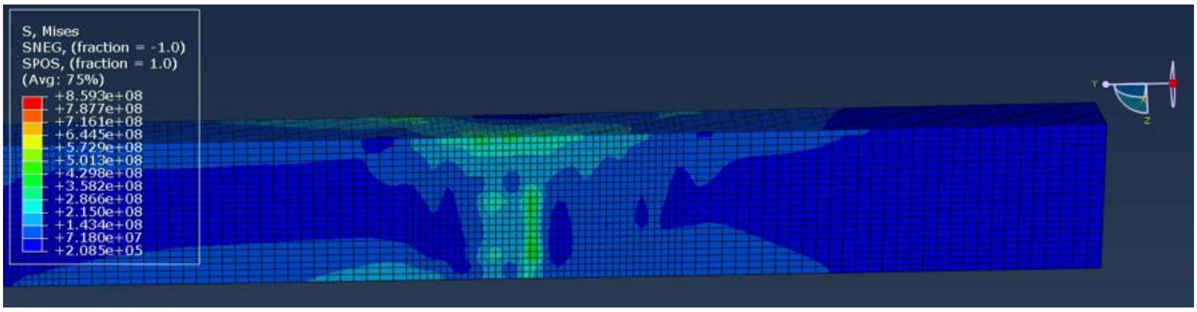

Figure D.13: The Von Mises stresses in the lift beam's contact surface

The average Von Mises stress is taken at the teal coloured nodes, and is equal to 272 MPa. The assumed average stress is plotted in figure D.14.

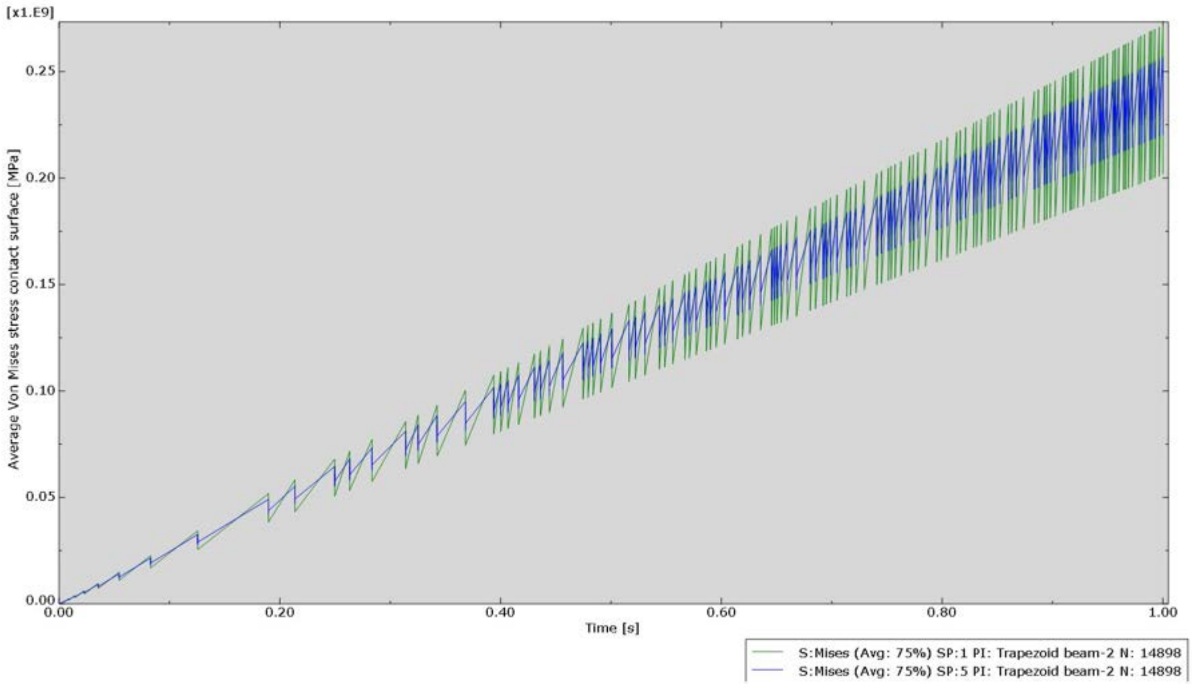

Figure D.14: Average Von Mises stress in the lift beam's contact surface

A rapidly fluctuating stress can be observed over time, which is likely caused by transfer of contact stresses between adjacent nodes.

The Von Mises stresses in the governing leg are provided in figure D.15.

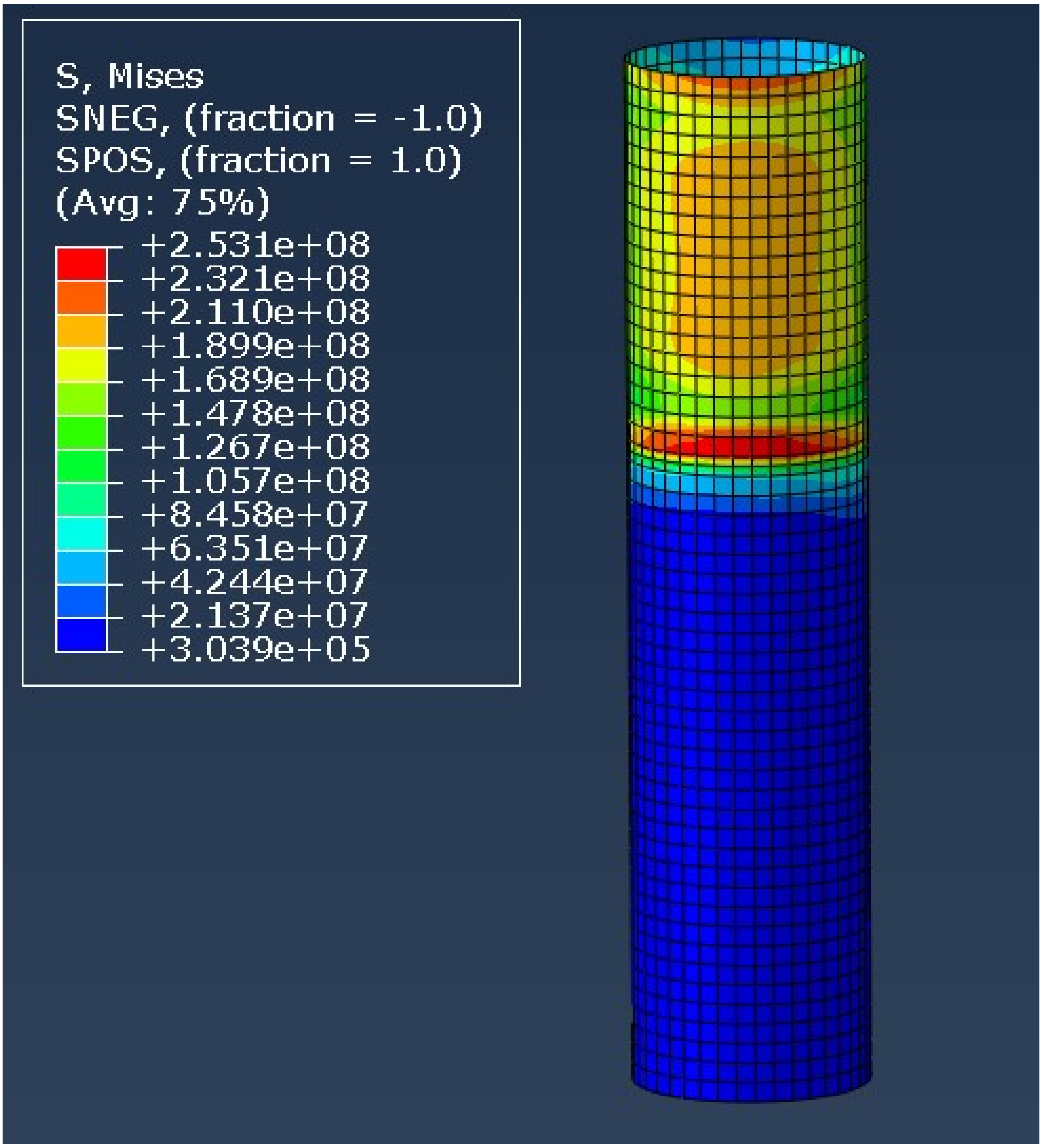

Figure D.15: Von Mises stress in the governing MSF leg

The Von Mises stresses in the wedge are provided in figure D.16.

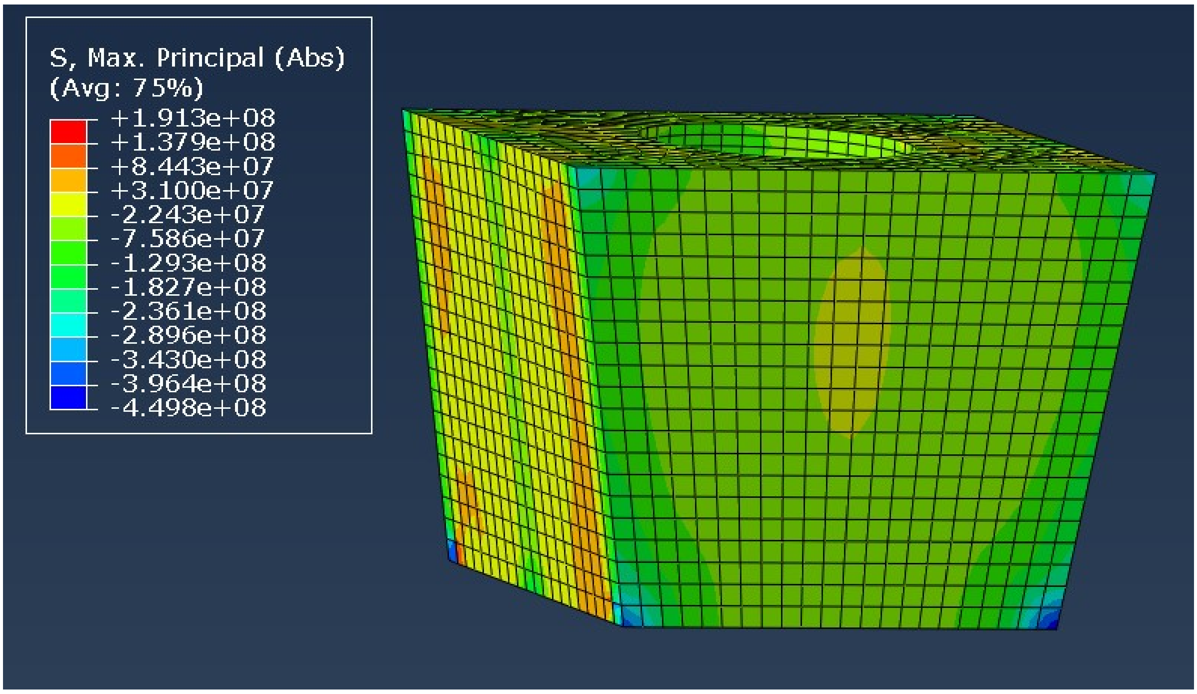

Figure D.16: Von Mises stress in the governing wedge

Verification of the results

The stability of the model is assessed by comparing the stabilizing dissipation energy with the system's internal energy. The results are plotted in figures D.16 and D.17.

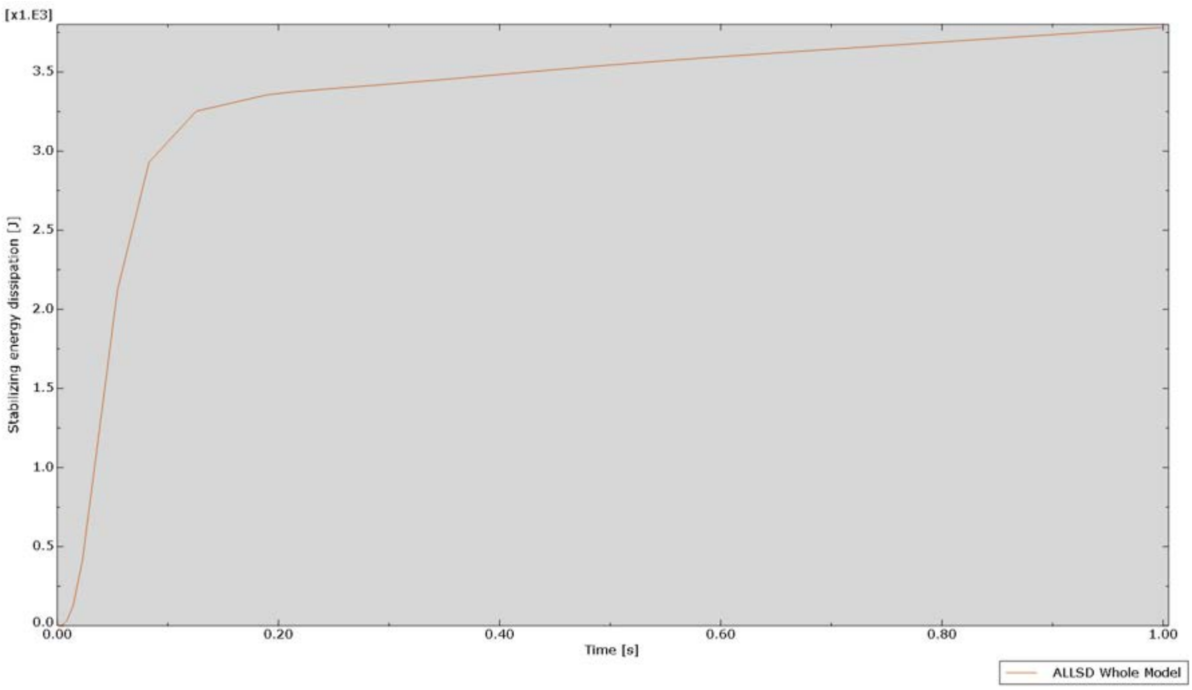

Figure D.17: Stabilizing energy dissipation for the whole model

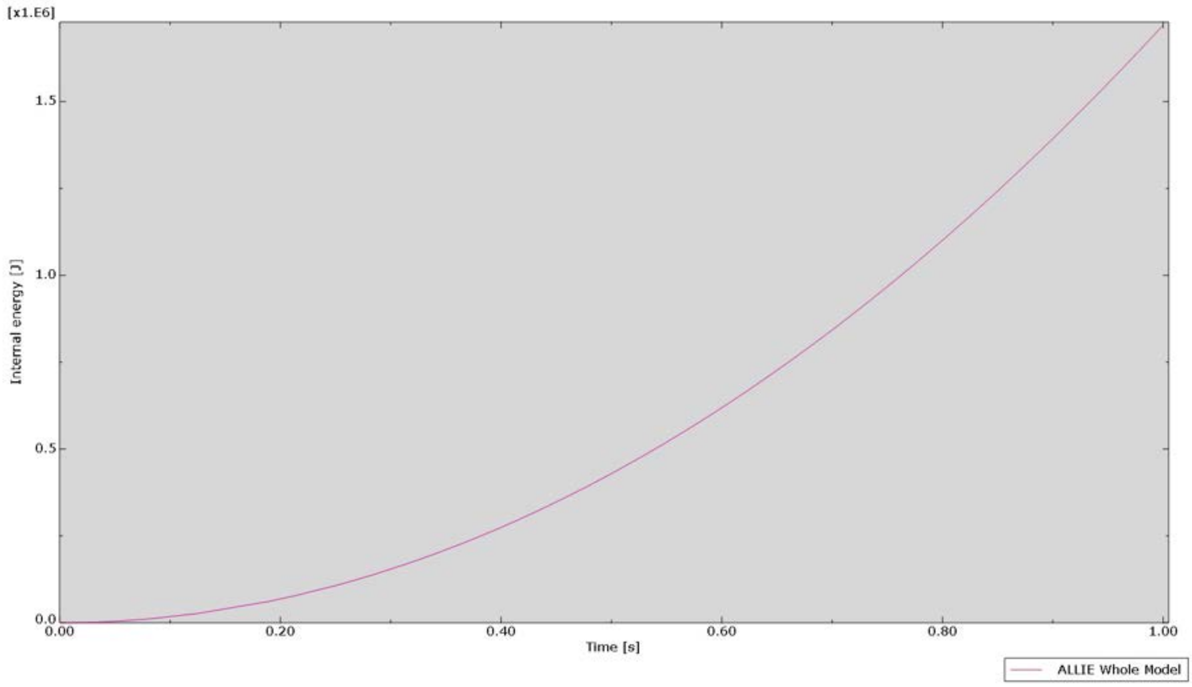

Figure D.18: Internal energy for the whole model

The energy dissipation term is equal to 3.8 kJ. The internal energy of the model is equal to 1.7 MJ. This comes down to a dissipated energy percentage of 0.2 %. This is considered to be too low to have any significant influence on the system's response.
It is also checked whether the loads are taken by the system as expected. The reaction forces and moments for leg A and B are provided in table below.

	Leg_A	Leg_B
$R_x [kN]$	27	120
$R_y [kN]$	1.2	13
$R_z [kN]$	4500	25500
$M_x [kNm]$	400	6000
M_y [kNm]	3400	4000
M_z [kNm]	22	70

The transverse reaction forces, R_x, are relatively small, since the tension rods, the lift beams and the wedge take up most of the horizontal component of the contact load. The longitudinal reaction force, R_y is negligibly small as there are no loads imposed in this direction. The vertical reaction forces are checked on the vertical force equilibrium. A simplification of the load case is provided in figure D.19.

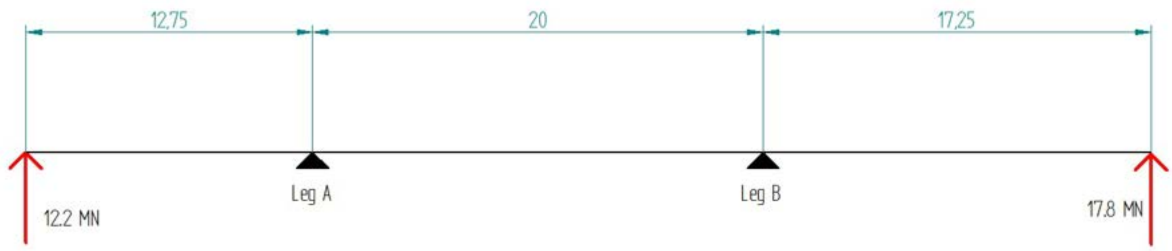

Figure D.19: Vertical force equilibrium

It follows that:

$$R_{z,a} = \frac{12.2 * 32.75 - 17.8 * 17.25}{20} = 4.6MN \tag{D.54}$$

And:

$$R_{z,b} = \frac{17.8 * 37.25 - 12.2 * 12.75}{20} = 25.4MN \tag{D.55}$$

Approximately the same results are found for the vertical reaction forces, implying that the loads are appropriately transferred through the system. Finally the reaction moments are shortly assessed. The strong axis bending moments, M_y, that are transferred to the legs are dependant of the stiffness of the contact elements and therefore can't be assessed quantitatively. Relatively speaking, it is expected that the strong axis bending moment in leg B is significantly larger than in leg A. The weak axis bending moment can be estimated by multiplying the difference in vertical load between beam 1 and beam 2, with the arm, which is equal to $B_{wedge,top}/2$.

$$M_y = ((6.7 - 5.5) + (9.8 - 8)) * 2.73/2 = 4100kNm \tag{D.56}$$

The torsional reaction moment, M_z, is as expected negligibly small. It is concluded that the load is correctly carried by the system and hence the model is verified.

The governing stresses in the leg, the lift beam's contact surface and the wedge are shown below for load case L641 in 1-5 direction.

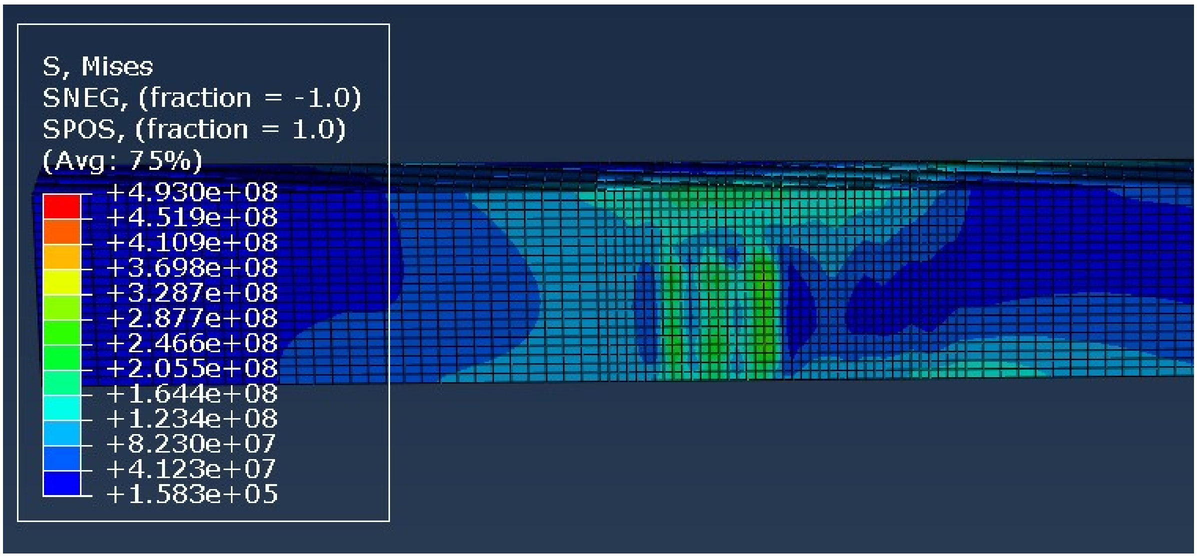

Figure D.20: Maximum plate stresses in the lift beam's contact surface for LC641

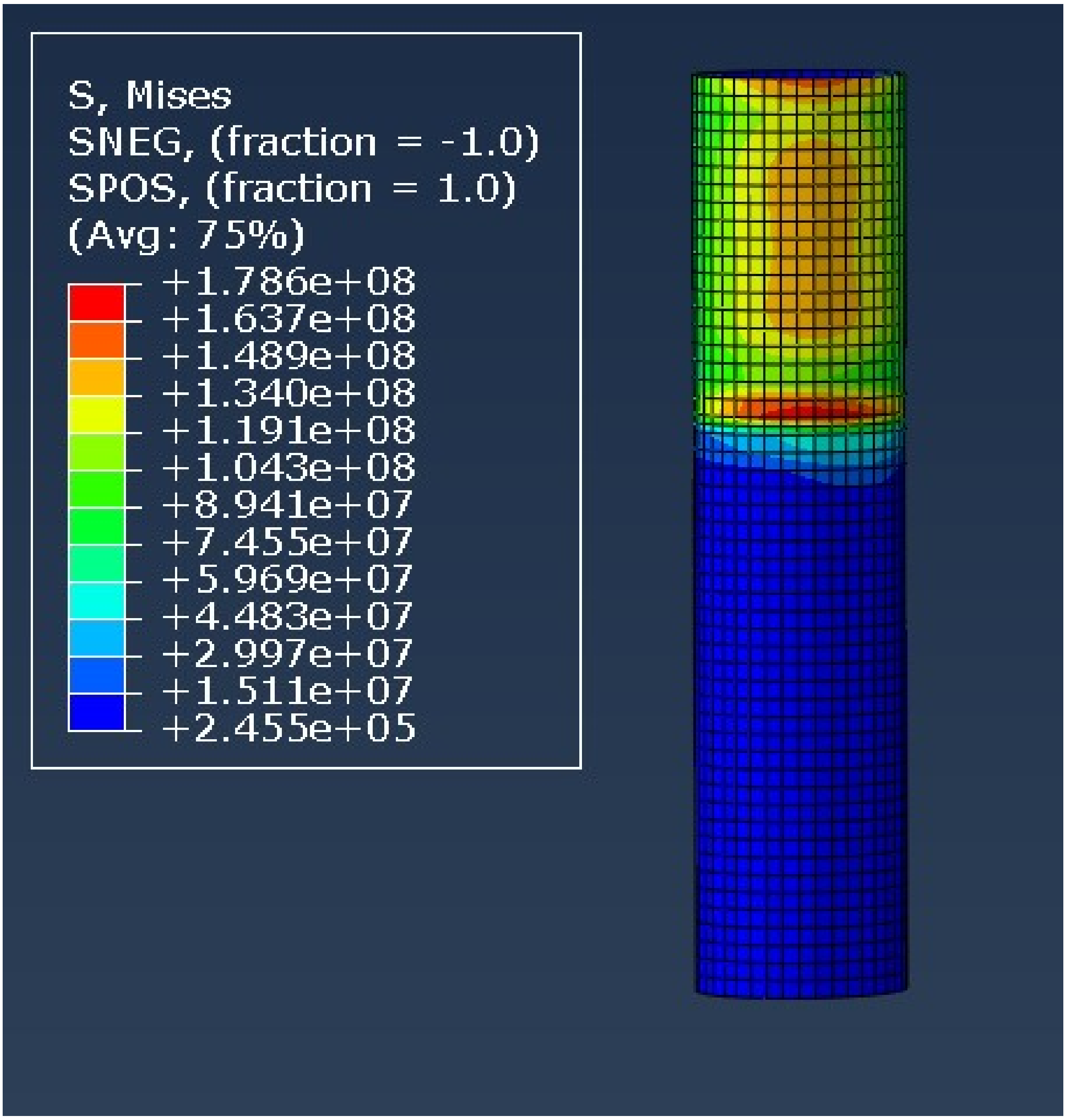

Figure D.21: Maximum stresses in the governing MSF leg for LC641

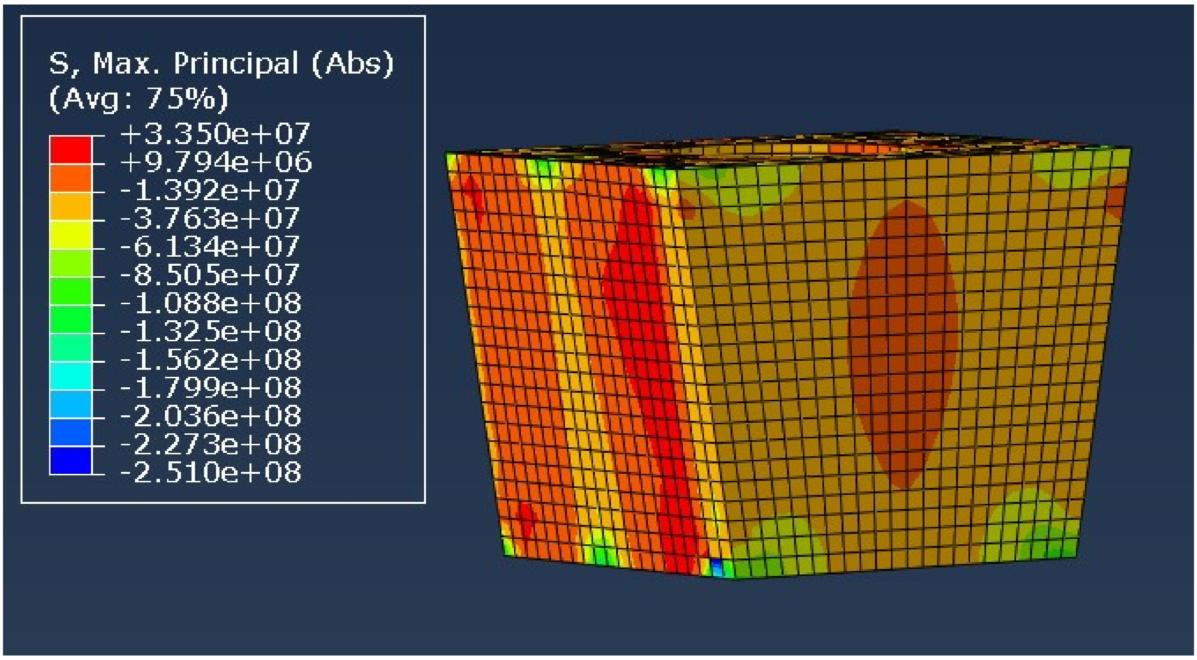

Figure D.22: Maximum stresses in the wedge's contact surface

The maximum stress in the MSF leg, excluding the peak stresses, is found to be approximately 150 MPa. The UC for the MSF leg is therefore:

$$UC_{VM,PB10} = \frac{150}{0.66*335} = 0.68$$

The maximum combined UC for PB10 under the same load case in SACS is found to be 0.66. It can therefore be concluded that the MSF legs can withstand the contact loads for this load case.

D.2.3. Hydraulic jack design

The UC's for web yielding and web crippling are determined with equations D.35 and D.36. A 60-40 distribution is assumed over the webs.

$$UC_{web,yielding} = \frac{\left(\frac{0.6*R}{t_w*(N+5k)}\right)}{0.66F_{y,w}} = 0.99 \tag{D.57}$$

$$UC_{web,crippling} = \frac{0.6*R}{67.5t_w^2[1+3*\frac{N}{d}(\frac{t_w}{t_f})^{1.5}]\sqrt{F_{y,w}t_f/t_w}} = 1.04 \tag{D.58}$$

Where:

R	= 2205	[kips]
N	= 20.87 (= D_{body})	[in]
k	Web toe radius (= t_w = 1.18)	[in]
t_f	= 2.76	[in]
$F_{y,w}$	Web yield strength (= 63.82)	[ksi]
d	web height (= 165.75)	[in]

The resultant forces of the hydraulic jacks groups, for direction 1-5, are determined with equations D.37, D.38 and D.39.

$$F_{Res1} + F_{Res2} + F_{Res3} = F_{topside} \tag{D.59}$$

$$F_{Res1} * x_1 + F_{Res2} * x_2 - F_{Res3} * x_3 = 0 \tag{D.60}$$

$$F_{Res1} * y_1 - F_{Res2} * y_2 - F_{Res3} * y_3 = 0 \tag{D.61}$$

Where for direction 1-5:

$F_{topside}$	= 25839	[kN]
x_1	= 0.95	[m]
x_2	= 3.2	[m]
x_3	= 3.55	[m]
y_1	= 8.72	[m]
y_2	= 10.78	[m]
y_3	= 10.78	[m]

It follows that:

$F_{res,1}$ = 14280 kN

$F_{res,2}$ = 4056 kN

$F_{res,3}$ = 7503 kN

And:

$$F_{jack,1} = \frac{14280}{7} = 2040kN$$

$$F_{jack,2} = \frac{4056}{6} = 676kN$$

$$F_{jack,3} = \frac{7503}{3} = 2501kN$$

Similarly for direction E-B it follows that:

$$F_{Res1} + F_{Res2} + F_{Res3} = F_{topside} \tag{D.62}$$

$$F_{Res1} * x_1 - F_{Res2} * x_2 - F_{Res3} * x_3 = 0 \tag{D.63}$$

$$F_{Res1} * y_1 + F_{Res2} * y_2 - F_{Res3} * y_3 = 0 \tag{D.64}$$

Where for direction 1-5:

$F_{topside}$	= 25839	[kN]
x_1	= 7.7	[m]
x_2	= 3.55	[m]
x_3	= 3.55	[m]
y_1	= 1.03	[m]
y_2	= 10.78	[m]
y_3	= 8.72	[m]

It follows that:

$F_{res,1}$ = 8144 kN

$F_{res,2}$ = 7488 kN

$F_{res,3}$ = 10206 kN

And:

$$F_{jack,1} = \frac{8144}{8} = 1018kN$$

$$F_{jack,2} = \frac{7488}{6} = 1248kN$$

$$F_{jack,3} = \frac{10206}{6} = 1701kN$$

E

Installation of the lift beams

E.1. Lift beam installation concepts

In this section the full range of considered installation concepts is shown. The characteristics of each concept are briefly discussed. Hereafter an assessment follows, from which the most promising installation concepts have been selected.

E.1.1. Rectangular frame

The rectangular frame consists of two lift beams, attached to a cross-beam on each end. Installation of the rectangular frame is achieved by lifting the frame over the topside and subsequently lowering it to the required elevation. An impression of the rectangular frame is provided in figure E.1.

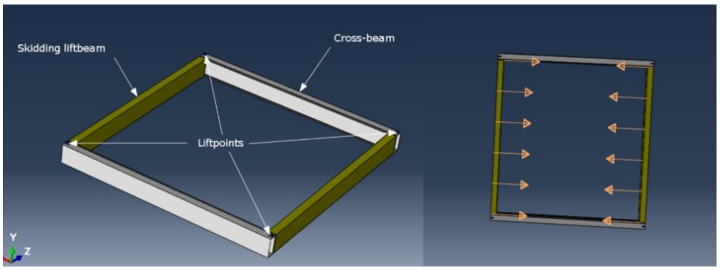

Figure E.1: The rectangular frame

The frame's lift points are located on the stationary cross-beams. The lift beams are allowed to skid over the cross-beams to the connection point.

E.1.2. Forklift frame

The forklift frame consists of a cross-beam on which on one end the lift beams are attached and on the other end a counterweight. The forklift frame is illustrated in figure E.2.

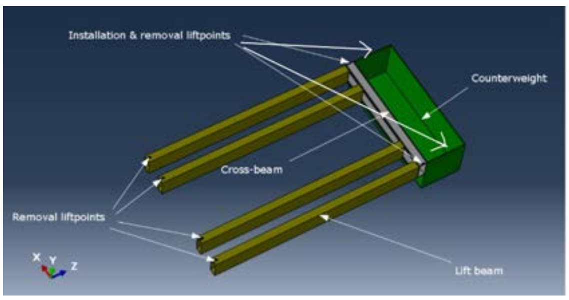

Figure E.2: The forklift frame

For the installation of the forklift frame, the lift points attached to the counterweight are used. The counterweight should be chosen such that the CoG of the assembly lies within the lift point envelope. The forklift frame is lowered to the required elevation and slowly shoved below the topside. The removal lift points are attached to the lift beams' free ends and to the cross-beam

E.1.3. Two-way forklift frame

An alternative to the forklift frame is the two-way forklift frame. Here, the counterweight is provided by the lift beams themselves. An impression of this concept is shown in figure E.3.

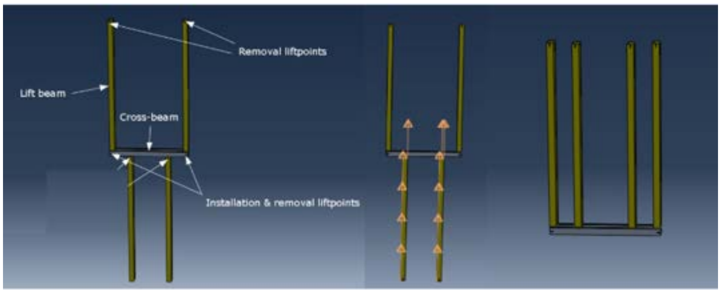

Figure E.3: The two-way forklift frame

The frame consists of a cross-beam with lift beams attached to it on both sides. The lift beams, oriented away from the vessel are first installed onto their temporary supports, while the lift beams pointing towards the vessel are providing the counterweight. After installation of the first lift beams, several options exist. The most complicated solution would be that the counterweight providing lift beams are allowed to skids through the cross-beam to their temporary supports. A more feasible alternative is that the installed lift beams can be detached from the cross-beam, where after the cross-beam and counterweight providing lift beams are lifted back on deck. New lift beams are installed at the position of the installed lift beams, and the process is repeated, but now for the interior lift beams.

E.1.4. Beam-per-beam crane vessel

The lift beams can also be installed one-by-one. This will increase the installation time, but the operation will become less sensitive. The option also exists to install the lift beams by a smaller HLV with this concept. Installation of the beams one-by-one can be achieved with the use of a counterweight. For the outer lift beams installation can also be achieved with a spreader bar, which is oriented parallel to the lift beam. An impression of these solutions is provided in figure E.4.

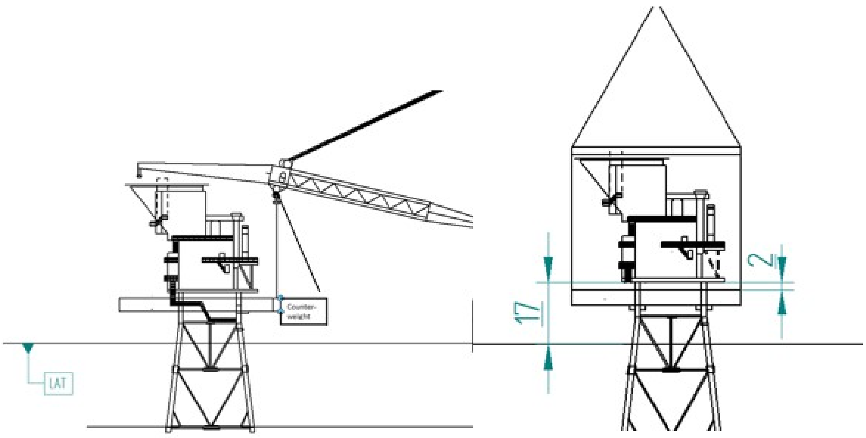

Figure E.4: Beam-per-beam installation

E.1.5. Skidding

Finally the lift beams can installed by means of skidding. This process can be performed by a barge. Installation through skidding is shown in figure E.5.

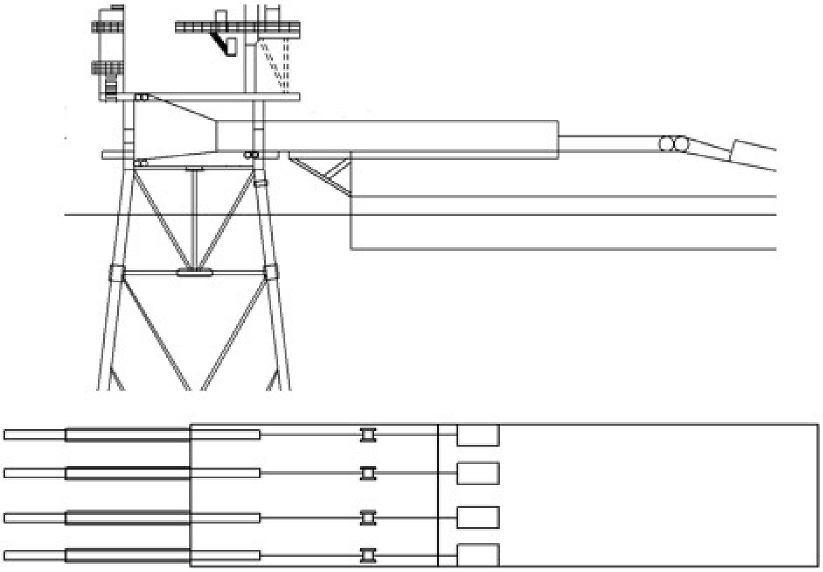

Figure E.5: Lift beams skidding

To reach the required elevation, a support frame has to be built on the barge, which stretches over the stern of barge to hand over the lift beams to the temporary supports. Potentially skid beams could be used, which can be connected to the temporary supports. Hereby, additional supports would be required in between temporary supports. Skidding is driven by push and pull units which are installed on the barge. The opportunity exists to skid the lift beams simultaneously onto their supports.

E.1.6. Installation concepts initial assessment

	Advantages/opportunities	Disadvantages/ challenges
Rectangular frame	Quick installation	Clearances to be observed at many locations simultaneously
	Potential direct removal -> Same rigging could be used during installation and removal	Skidding of the beams introduces risk of system breakdown
	Heave compensator could be used to dampen the motions of the frame, while the lift beams are skidding	How to deal with the CoG shift when the lift beams are skidding?
	Use leg mating units to absorb potential impact loads	Only one-sided leg support possible
	The frame remains the same for different topsides, no changes required.	Connection with the cross-beam will be costly
		Low workability due to size and weight of the frame
		How to deal with combination of skidding motions and vessel motions?
Forklift frame	A guide and bumper system could be used to take up potential impact loads and guide the lift beams in position	Stabbing the fork below the platform without damaging vital components of the platform is challenging
	ILT's could be used for quick, remote connection of the removal rigging	Deflection of the lift beams due to their own weight
	The size of the forklift frame could be reduced to two beams	Using water balast as main tuning parameter might be challenging
	Install the fork with two blocks, making the concept independent of the water ballasting	Large size and weight of the frame
	Two-sided leg support	How to stay close to the connection points while maintaining sufficient clearance
	Quick installation, no mechanics required	Reattaching the rigging
	Add a cross-beam to the lift beams' free ends to absorb rigging sideloads	Large lateral and vertical motions during installation
	Use one of the outer lift beams as an alignment guide	
Two-way forklift frame	Use a tandheugel mechanism for the skidding (as used for jack-ups)	Complex, costly connection with the cross-beam, lots of mechanics
	ILT's	How to lift the frame back on deck? CoG shift after installation of the first beams
	Two-sided leg support	How to reattach the rigging?
	Add a cross-beam to the lift beams' free ends to absorb rigging sideloads	How to change the spacing of the beams for different topside geometries?
	No counterweight needed	How to house the skidding while hoisting a large load?
	1 outer, 1 inner beam in first step, better clearance and stability during installation	
Beam-per-beam installation	Install the outer lift beams with the use of a spreader bar	balancing the beam using water ballast as main tuning parameter is difficult and needs to be done for each beam individual.
	add two beams closing the frame after the individually installed beams running through the platform are in place	Hand-over system required
	to absorb the aforementioned compression forces	
	Strength is that the installation of individual beams is relatively easy in comparison to installing multiple beams in one go	
	Easier to maintain clearance	
	Use Aegir dual block for installation for steering and lifting	
Skidding	Use of relatively cheap equipment	keeping control over the floating body whilst working in close proximity of the platform (mooring)
	Clamp the beams on the outer end of the barge	wave induced motions of floating body in combination with moving number of rigidly supported beams
	Install a continuous skid connecting the barge with the temporary supports	underneath the platform cause belly & head aches
		How to deal with potential impact?
		Relative heave motions
		How to maintain lateral position?
		equipment will be needed for long time and outfitting barge has cost impact and impact on barge schedule as well

Figure E.6: Installation concepts initial assessment

E.2. Lift analysis

E.2.1. Lift beam installation rigging

The properties of the rigging that is used for installation of the lift beam-counterweight assembly is provided in table E.1. The lift-beam counterweight assembly is modelled in AGES to check the static stability of the assembly, and to obtain the force in each sling under the given setup. It has to be noted that for two of the lift points non-existent copies of existing slings are used.

Ref. sling	Lift point	L [m]	k [kN/m]	SWL [mT]	Force [kN]	UC [-]
1	LP1	27.985	28900	700	2708	0.394
2	LP2	29.488	28000	700	2677	0.390
2	LP3	29.488	28000	700	2677	0.390
1	LP4	27.985	28900	700	2708	0.394

Table E.1: Properties of the lift beam installation rigging

The slings are modelled in LiftDyn as in-line connector, which are given a stiffness and pre-tension. The stiffness is described by the relation, $\frac{EA}{L}$ and provides stiffness to the lift object in a specific direction at a specific location. The pre-tension is the sling force that is found in AGES, and is needed to provide static equilibrium to the assembly. Based on the SSCV properties, the lift object properties and the sling properties, the dynamic response of the system can be obtained.

E.2.2. Limiting criteria

The limiting criterion for the single sway amplitude is defined for the case where one of the interior lift beams is already installed. This governing case is shown in figure E.7.

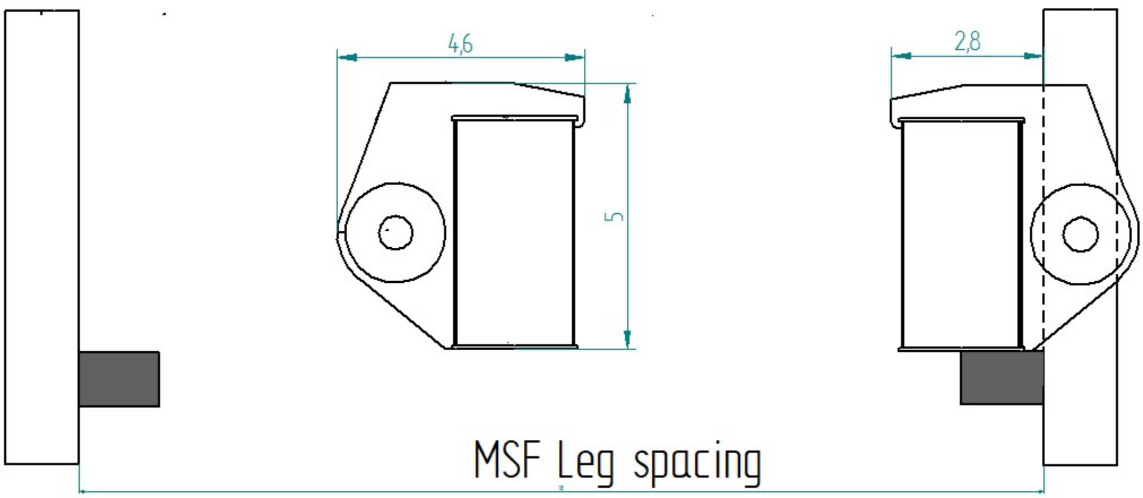

Figure E.7: Governing case for the limiting sway motion

The limiting sway single amplitude depends on the MSF leg spacing and hence the orientation of the lift beams.
The limiting sway single amplitude for the 1-5 direction is equal to:

$$Sway_{SA,1-5} = \frac{18-1.22-4.6-2.8}{2} = 4.7m$$

The limiting sway single amplitude for the E-B direction is equal to:

$$Sway_{SA,E-B} = \frac{19.5-1.22-4.6-2.8}{2} = 5.4m$$

The limiting heave single amplitude is the same for both directions, since it is determined by the MSF deck elevation and the top horizontal elevation.

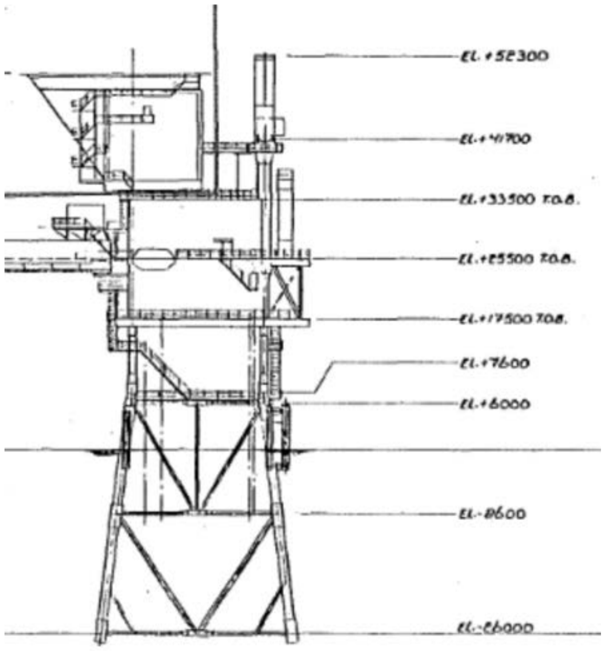

Figure E.8: Reference platform 14 front view

$$Heave_{SA} = \frac{16.5-7.6-5}{2} = 1.95m$$

In figure E.9 a top view of reference platform 7 is shown, indicating the different rows. It can be seen that the platform north has an offset of 20 degrees with respect to the true north.

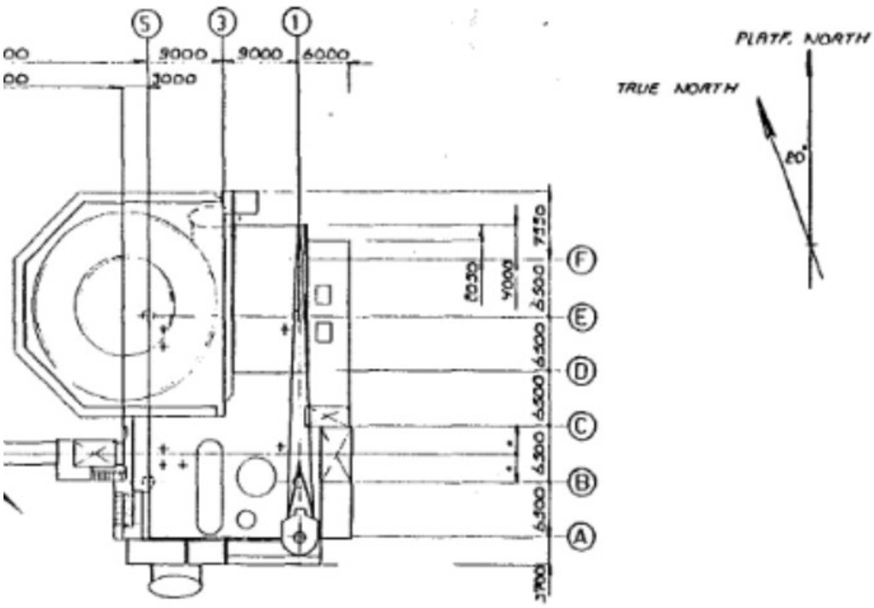

Figure E.9: Reference platform 14 top view

E.2.3. Unrestrained case

The eigenmodes between 0 and 16 seconds for the different crane radii are shown in tables below.

R = 45.5 m, 16 eigenmodes total	
Eigenmode	Eigenperiode [s]
$Pitch_{LB-CW,1}$	10.6
$Roll_{LB-CW}$	6.07
$Pitch_{LB-CW,2}$	1.13
$Pitch_{crane,1}$	1.03
$Pitch_{crane,2}$	0.71
$Heave_{LB-CW}$	0.45
$Elongation_{rigging}$	0.29

Table E.2: Overview of the eigenmodes with an eigenperiod between 0 and 16 seconds for a crane radius of 45.5 meters

R = 63.5 m, 17 eigenmodes total	
Eigenmode	Eigenperiode [s]
$Pitch_{SSCV}$	15.20
$Pitch_{LB-CW,1}$	10.47
$Roll_{LB-CW}$	6.02
$Pitch_{crane,1}$	1.16
$Pitch_{LB-CW,2}$	1.13
$Pitch_{crane,2}$	0.66
$Heave_{LB-CW}$	0.45
$Elongation_{rigging}$	0.28

Table E.3: Overview of the eigenmodes with an eigenperiod between 0 and 16 seconds for a crane radius of 63.5 meters

R = 82 m, 17 eigenmodes total	
Eigenmode	Eigenperiode [s]
$Pitch_{SSCV}$	15.34
$Pitch_{LB-CW,1}$	10.16
$Roll_{LB-CW}$	5.9
$Pitch_{crane,1}$	1.38
$Pitch_{LB-CW,2}$	1.13
$Pitch_{crane,2}$	0.61
$Heave_{LB-CW}$	0.45
$Elongation_{rigging}$	0.26

Table E.4: Overview of the eigenmodes with an eigenperiod between 0 and 16 seconds for a crane radius of 82 meters

R = 100 m, 18 eigenmodes total	
Eigenmode	Eigenperiode [s]
$Roll_{SSCV}$	13.28
$Pitch_{SSCV}$	11.94
$Pitch_{LB-CW,1}$	8.91
$Roll_{LB-CW}$	5.38
$Pitch_{crane,1}$	1.87
$Pitch_{LB-CW,2}$	1.13
$Pitch_{crane,2}$	0.54
$Heave_{LB-CW}$	0.45
$Elongation_{rigging}$	0.21

Table E.5: Overview of the eigenmodes with an eigenperiod between 0 and 16 seconds for a crane radius of 100 meters

It can be seen that for a change in crane radius, different eigenmodes are found for the system. Except for a crane radius of 45.5 meters, a pitch eigenmode of the SSCV is found within the eigenperiod range of interest. For a crane radius of 100 meters an additional roll eigenmode of the SSCV is found. It has to be noted that the eigenperiods of the SSCV's pitch and roll motion appear to be relatively low. The possible source for this could be the discretisation of the SSCV when determining the hydrodynamic properties of the SSCV for a given water depth. A physical reason for the relatively low eigenmodes of the SSCV is the shallow water depth in which the operation is performed. The shallower this water depth the lower the displaced volume of the SSCV and hence the lower the hydrostatic stiffness of the SSCV. The same could apply to the added mass and damping. As there is uncertainty about this, it is strongly advised to reassess these eigenmodes.

The eigenperiod of the pitch and roll eigenmodes of the lift beam-counterweight assembly decreases as the crane radius increases. An interesting finding is the constant eigenperiod for the second pitch mode and the heave mode of the lift beam-counterweight assembly. Finally it can be seen that the eigenmode of the rigging can be excited. The eigenperiod of this eigenmode decreases as the crane radius increases. As the crane radius increases, the length of the main hoist decreaes, resulting in an increasing stiffness. An increasing stiffness implies an increasing eigenfrequency, and hence a decreasing eigenperiod.

To check the magnitude of the eigenmode excitation and to verify whether the right eigenmodes are observed, a few RAO's for the lift beam's tip motions are plotted. The RAO of the lift beam's tip heave motion for a crane radius of 45.5 meters is provided in figure E.10

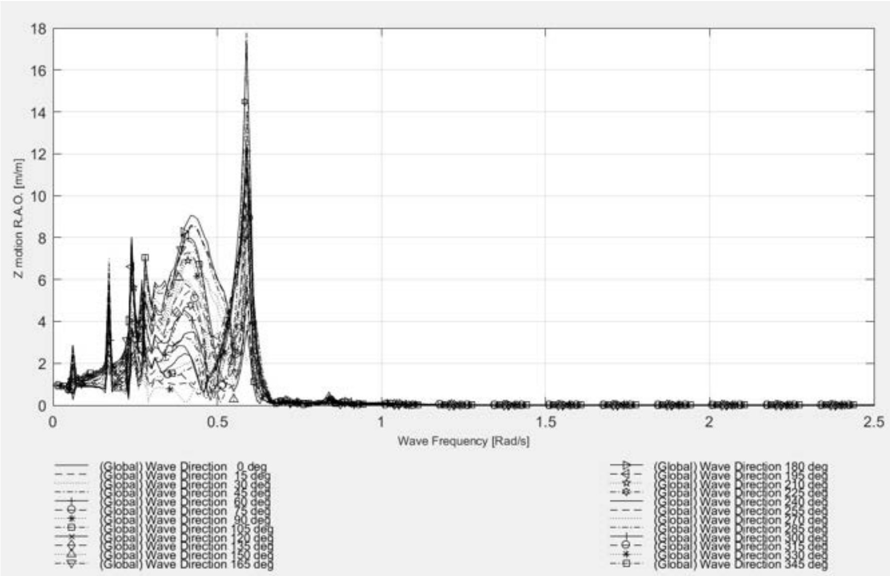

Figure E.10: RAO of tip's heave motion for a crane radius of 45.5 meters

A strong peak around a wave frequency of approximately 0.6 rad/s can be observed. This is equal to an eigenperiod of 10.5 seconds, corresponding to the pitch eigenmode of the lift object. The peaks with a lower wave frequency are out of the range of interest. The RAO for the tip's heave motion for a crane radius of 100 meters is plotted in figure E.11.

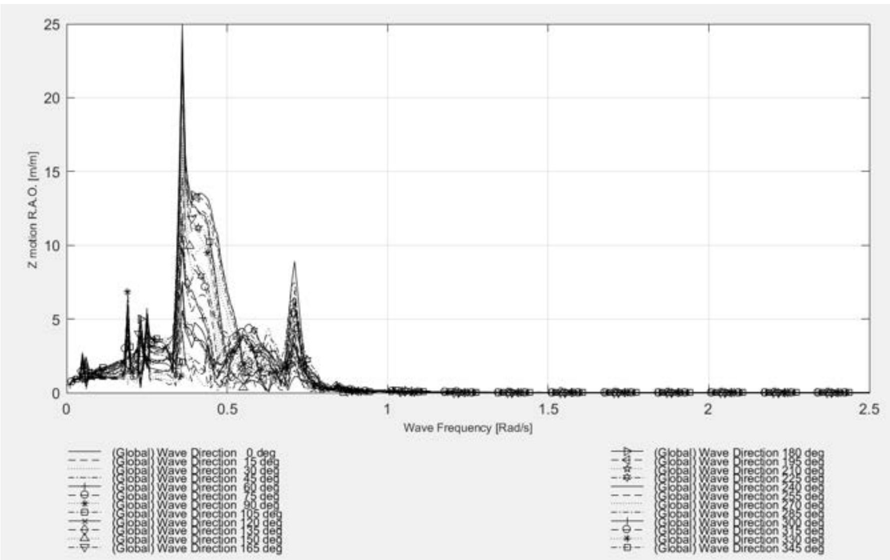

Figure E.11: RAO of tip's heave motion for a crane radius of 100 meters

Similarly a peak at a wave frequency of approximately 0.7 seconds is found, corresponding to the lift object's pitch eigenmode with an eigenperiod of 8.91 seconds. The other peak around a wave frequency of 0.3 seconds corresponds to another pitch eigenmode of the lift object, which is out of range of the wave periods under consideration. The RAO of the tip's sway motion at a radius of 100 meters is shown in figure E.11.

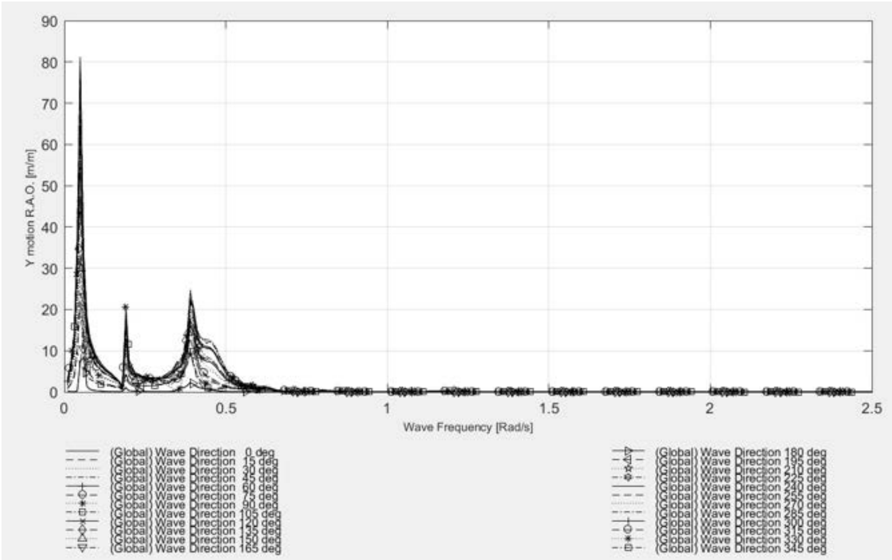

Figure E.12: RAO of tip's sway motion for a crane radius of 100 meters

The peak that is found around 0.45 rad/s corresponds to the SSCV's roll eigenmode with an eigenperiod of 13.28 seconds.

The operability plots, for the combined limiting criteria, for the different crane radii are provided in figures below.

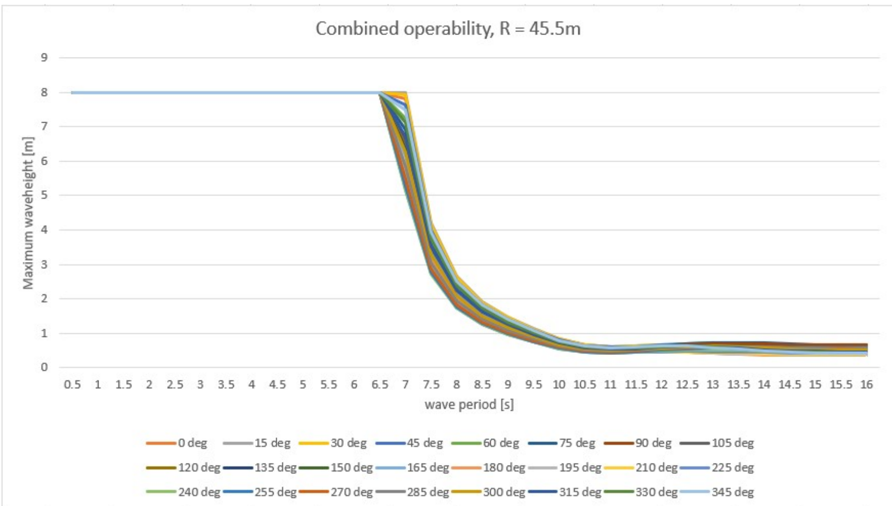

Figure E.13: Operability plot for a crane radius of 45.5 meters

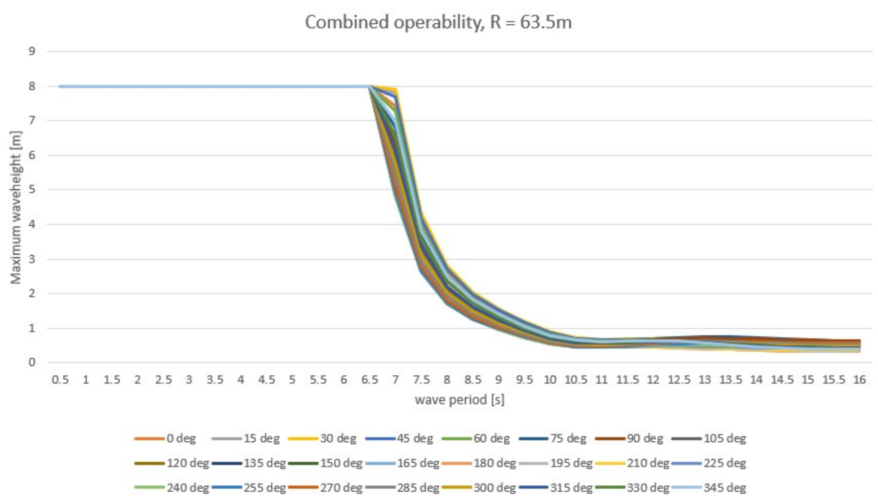

Figure E.14: Operability plot for a crane radius of 63.5 meters

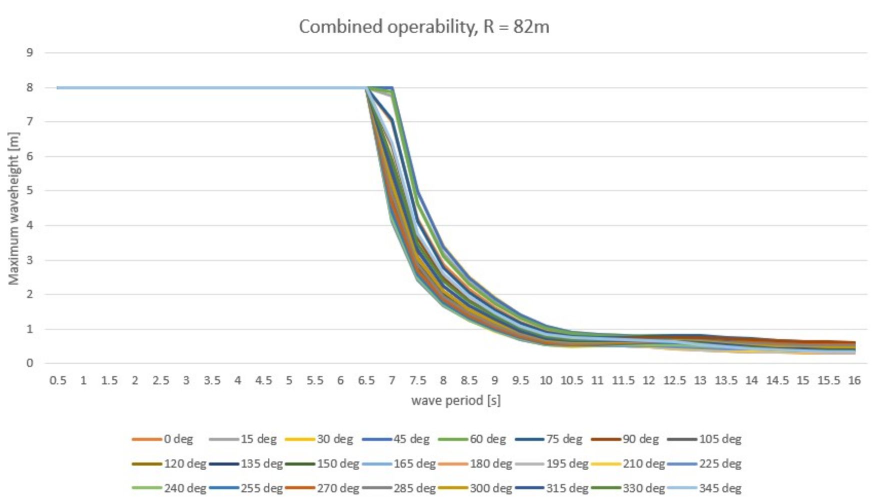

Figure E.15: Operability plot for a crane radius of 82 meters

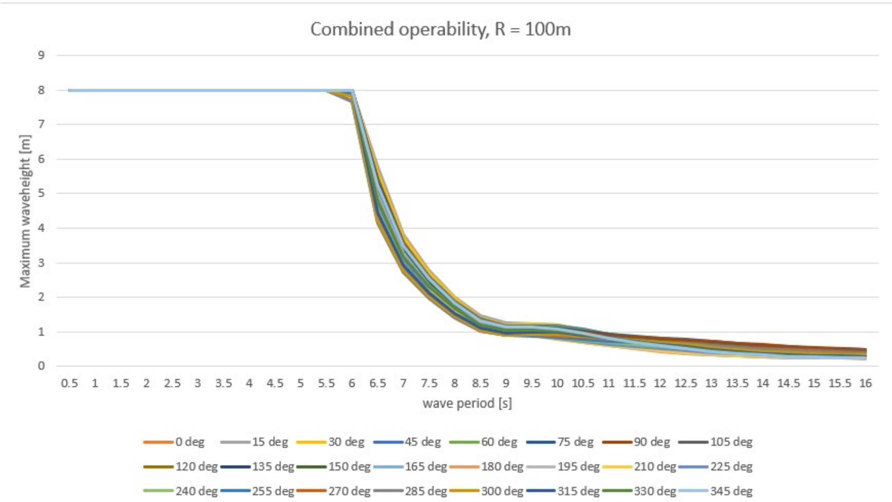

Figure E.16: Operability plot for a crane radius of 100 meters

The average waiting on weather time for the different crane radii and vessel headings is provided in tables below.

R = 45.5 m, average WoW [hrs]	
340 deg	250 deg
36	25
24	19
22	13
9	7
3	2
2	2
1	1
2	2
8	6
16	12
22	15
37	22

Table E.6: The average waiting on weather time[hrs] for a crane radius of 45.5 meters

R = 63.5 m, average WoW [hrs]	
340 deg	250 deg
37	24
28	18
25	11
10	6
3	2
2	1
1	1
2	2
8	5
18	11
24	14
40	19

Table E.7: The average waiting on weather time[hrs] for a crane radius of 63.5 meters

R = 82 m, average WoW [hrs]	
340 deg	250 deg
40	18
30	14
29	8
11	4
4	1
2	1
2	1
3	1
8	4
19	8
26	11
45	15

Table E.8: The average waiting on weather time[hrs] for a crane radius of 82 meters

R = 100 m, average WoW [hrs]	
340 deg	250 deg
46	26
38	18
32	12
11	6
3	2
2	2
2	2
3	2
9	6
19	10
28	14
45	19

Table E.9: The average waiting on weather time[hrs] for a crane radius of 100 meters

The dominant wave direction over the year is provided in figure E.17.

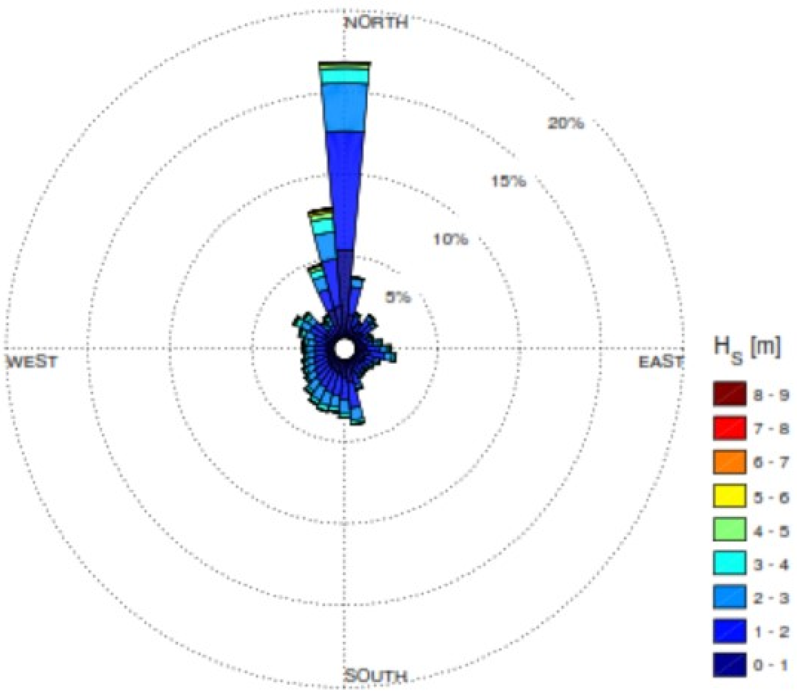

Figure E.17: Dominant wave direction over the year

The yearly workability based on the wind speed is limited to 80% as shown in figure E.18.

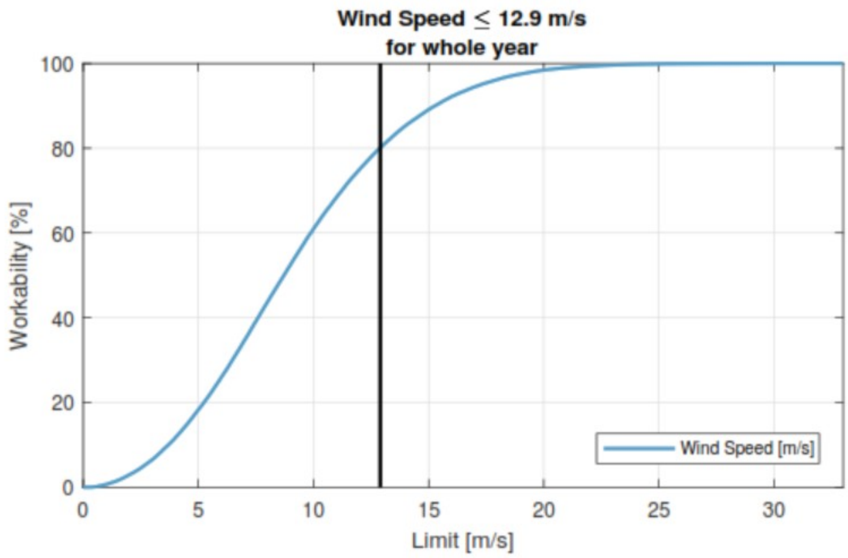

Figure E.18: Yearly workability based on the limiting wind speed

E.2.4. Tugger lines

The RAO for the tip's heave motion with the use of tugger lines is shown in figure E.17.

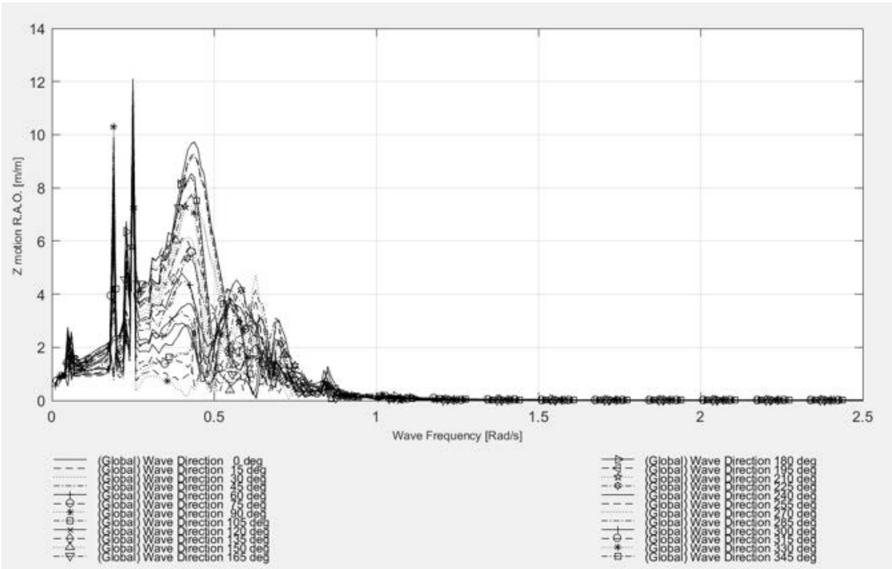

Figure E.19: Tip's heave motion RAO with tugger lines

It can be seen that the peaks around a wave frequency of 0.4 rad/s and 0.7 rad/s have decreased by approximately 50%. It can be seen that the damping has resulted in flatter, less distinct peaks.

F

Case study on the lift beams concept

F.1. Preparation phase

The temporary supports are designed to carry the design weight of the lift beams. The maximum reaction force for the temporary supports follows from momentum balance in the E-B direction and is equal to:

$$F_z = \frac{25-11.15}{18} * 264.2 * 9.81 = 1994kN$$

For the temporary supports, an HEA 900 profile is used. The free end of the temporary support is braced in order to reduce the deflection and load of the temporary support. For both elements S355 steel is used. An impression of the load case is provided in figure F.1.

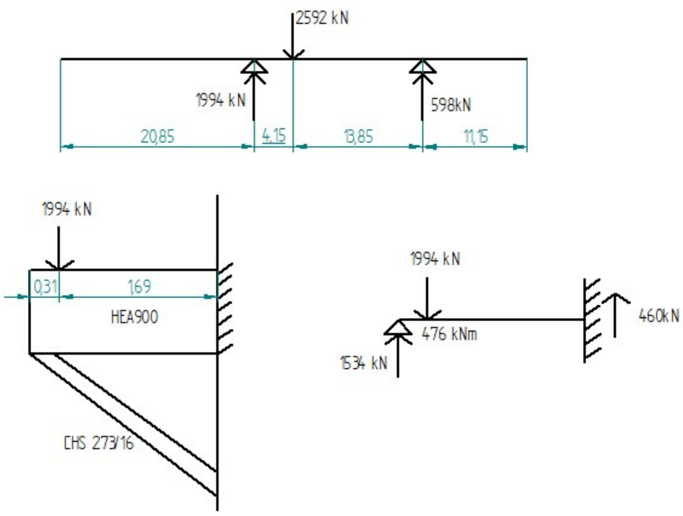

Figure F.1: Temporary support load case

The properties of the elements, and their respective governing UC is provided below.

HEA900		
Aweb	0.0133	m^2
wy	0.0092	m^3
UC_combo	0.92	[-]
CHS 273/16		
Aax	0.013	m^2
UC_axial	1.00	[-]

F.2. Lift beam-to-counterweight connection

The connection between the lift beam and the counterweight must carry the weight of the lift beam and the corresponding overturning moment. The design of the upper and lower hook is provided in figure F.2.

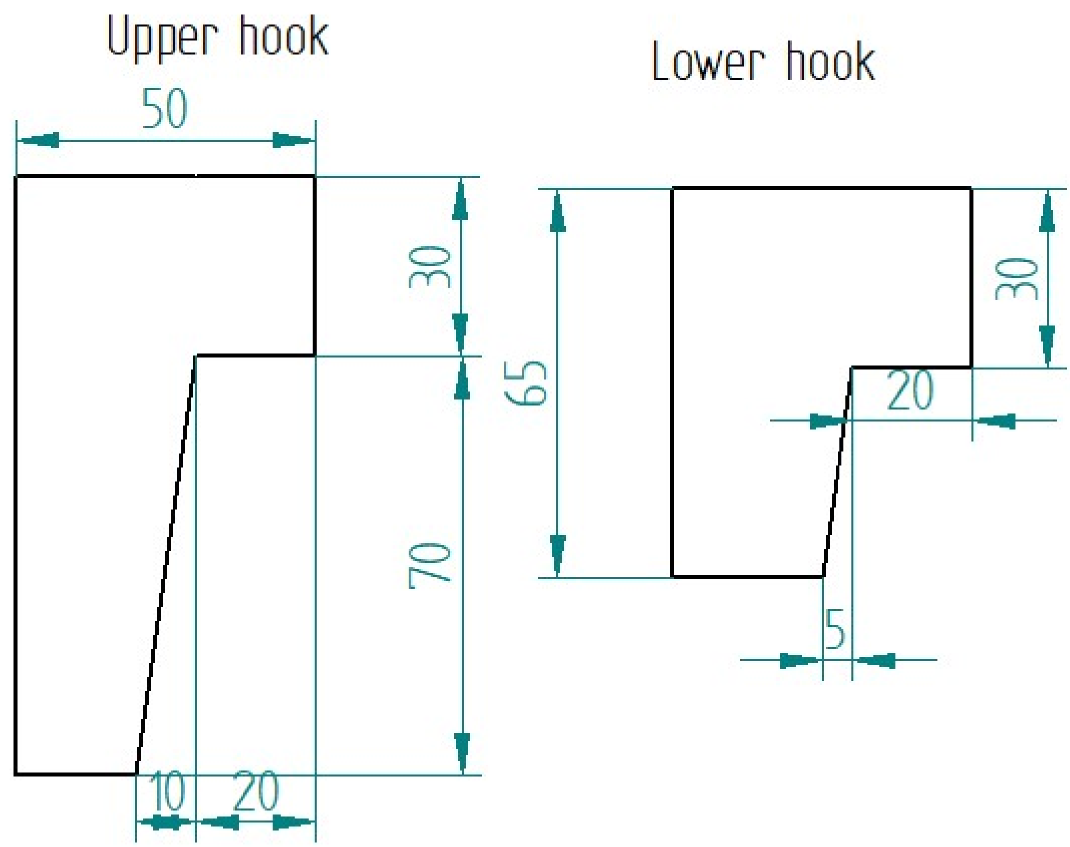

Figure F.2: Dimensions of the upper and lower hook

The hooks have an in-plane width of 3.22 meters. This means that the hooks stick out 0.5 meters on each side of the lift beam. High grade S690 steel is used for the hooks to withstand the relatively large bending moment. The yield strength, taking the material thickness into account, is equal to 550 MPa. The overturning moment is decoupled in a normal force, acting on the tilted side of both hooks. The loads acting on the hooks are shown in figure F.3.

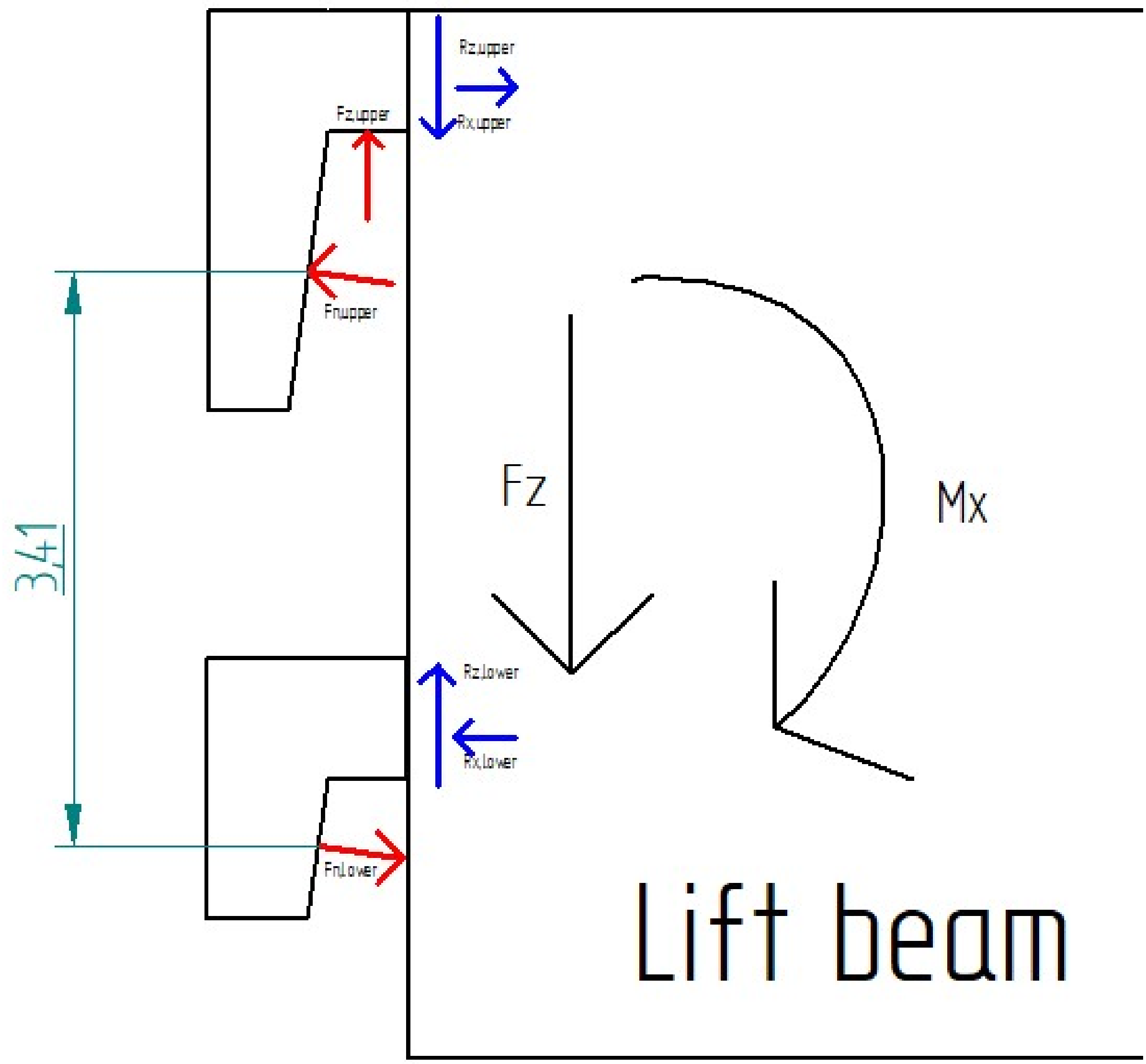

Figure F.3: Loads acting on the hooks

Here, F_z follows from the weight of the lift beam, and is equal to 3195.5 kN. The bending moment is equal to 79885.8 kNm. The magnitude of the connection forces and the hook reaction forces is provided in table below.

Fn,upper	24189	kN
Fn,lower	24189	kN
Fz,,upper	3196	kN
Rz,upper	6562	kN
Rx,upper	23954	kN
Rz,lower	3367	kN
Rx,lower	23954	kN

The lower hook on the counterweight side is cut short to ensure only $F_{n,lower}$ is transferred. The unity checks at two cuts are examined, at the interface with the lift beam, and at the location of the normal forces. The sections are shown in figure F.4.

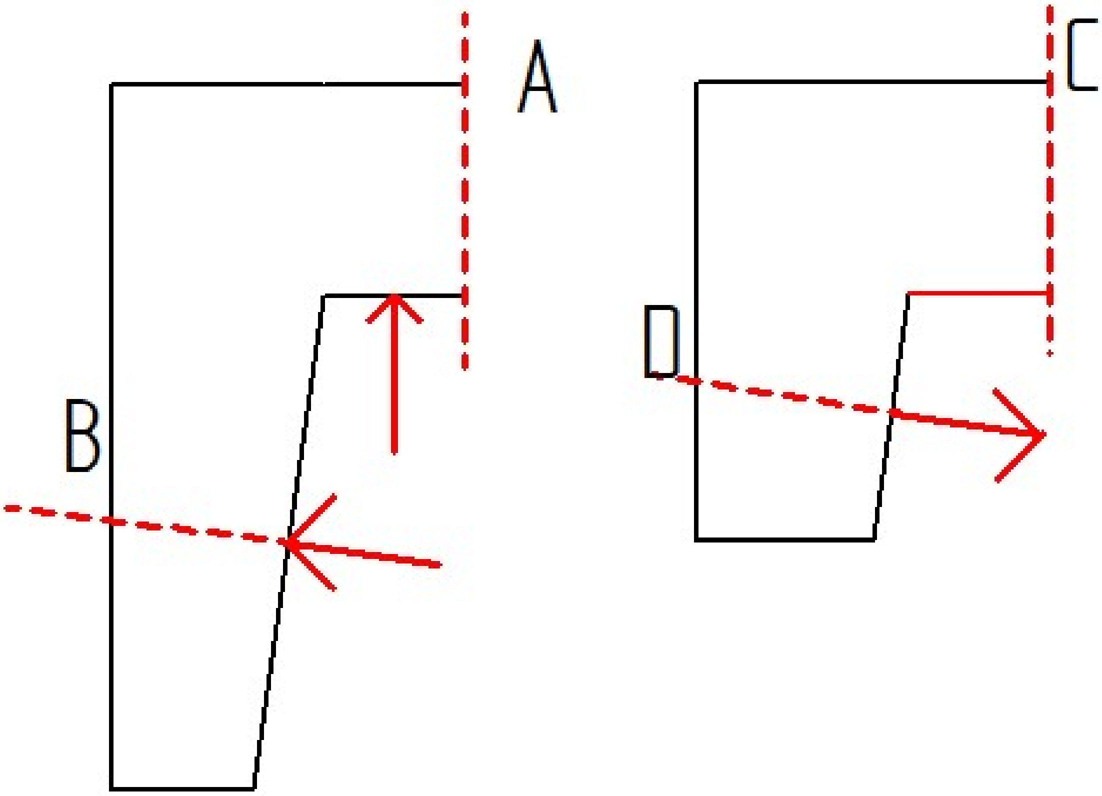

Figure F.4: Governing sections

The governing unity check for these sections can be found in table below.

Upper hook		
Section A	0.96	[-]
Section B	0.93	[-]
Lower hook		
Section C	0.75	[-]
Section D	0.64	[-]

F.3. Cross-beam-to-lift beam connection

F.3.1. Hook connection

Here the option is shown where the cross-beam is installed on the same elevation as the lift beam. An impression of this is provided in figure F.5.

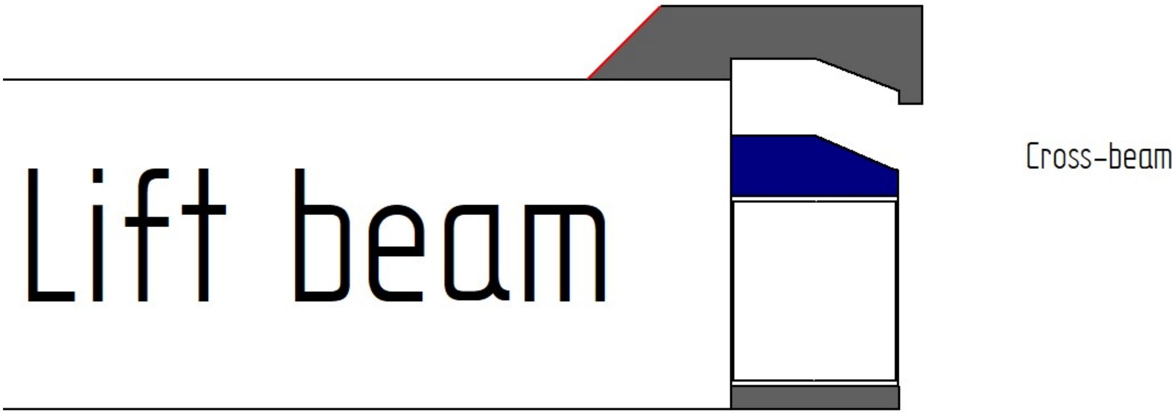

Figure F.5: Cross-beam-to-lift beam connection

The cross-beam can be designed to be of shorter height than the lift beams. The moments acting on the cross-beam are significantly lower, and hence less moment of inertia around the strong axis is required. Supports are welded onto the lower flange of the lift beam, on which the cross-beam can be temporarily laid. On top of the lift beam, a hook is installed, which forms an enclosed shape with the top of the cross-beam, when the cross-beam is lifted upwards. This way a rigid connection is formed between the lift beams and the cross-beam which will allow for force and moment transfer and will therefore allow for redistribution of the load path. The length of the mid span of the cross-beam can be adjusted to comply with different lift beam spacing. This is indicated in figure F.6.

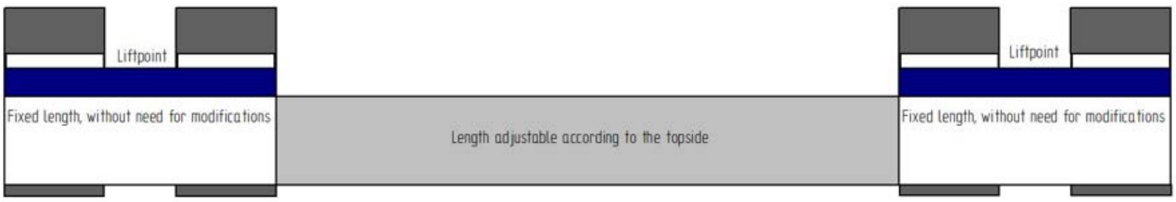

Figure F.6: Adjustable cross-beam length, front view

Local strengthening of the lift beam will be required to take up the load that is transferred from the hook. Similarly the cross-beam has to be strengthened at the location of the load transfer. As previously discussed, the design of this connection, and the local strengthening, is considered to be out of the scope of this project. Eventually it has been decided to go for the option where the cross-beam is installed below the lift beams. It is expected that installation of the cross-beam can easier be achieved this way. Also the connection remains fixed for that connection, when the rigging is lowered.

F.3.2. Short cross-beam alternative

It can also be decided to use a short cross-beam, which is connected between adjacent beams. It has to be noted that this alternative is only suitable for the two-sided leg support case. This will result in a total of four short cross-beams. The benefit of this alternative solution is that there is no need to adjust the length of the cross-beam for different MSF leg spacing. This way also the weight of the assembly is reduced.

However the installation time to install all of the four cross-beams is expected to be larger. Also this variant will only allow for load distribution amongst adjacent beams. To investigate the effects on the topsides structural integrity, the new lift beam setup is modelled in SACS. This is done for the E-B direction with the pin-hole connection. An impression of the SACS model is shown in figure F.7.

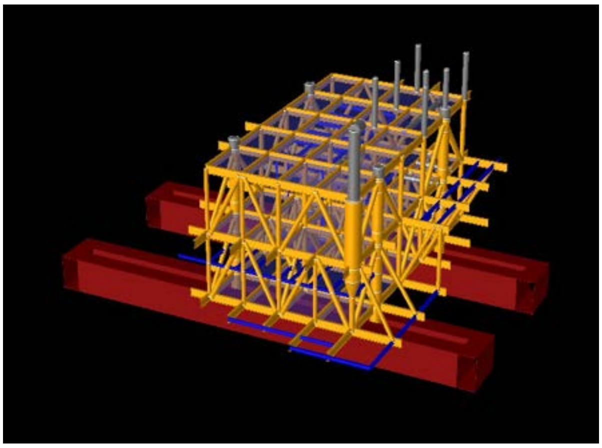

Figure F.7: Impression of the SACS model for the short cross-beam alternative

The topsides structural integrity results for the 55-45 rigging load distribution case are provided in table below.

E-B direction, 55-45 dist, pin-hole connection					
UC_{PB10}	UC_{PB50}	UC_{PE10}	UC_{PE50}	n_{crit}	n_{fail}
0.53	0.54	0.50	0.44	13	0

Compared to the results for the full span cross-beam, as shown in table 5.10, an increase in the UC's of the legs can be observed. Also the number of critical members has increased from five to thirteen. Looking at the UC's for leg PB10, an increase in the vertical load can be observed as expected. Also the strong-axis and weak-axis bending moment acting on the leg have increased.

However no failing members are identified under this setup. The short cross-beam alternative could therefore potentially provide a more efficient solution for topsides removal. No definitive conclusions can be drawn at this point. It is therefore strongly advised to further investigate this solution.

F.4. Topsides removal phase

F.4.1. Removal rigging

For removal of the topsides it has been chosen to use rigging arrangement A, which is shown in figure 4.4. As was shown in the structural integrity analyses a 55-45 rigging distribution is much more favorable for the topsides structural integrity. Rigging arrangement B is eventually not chosen because of the lateral component of the lower rigging, which would impose significant lateral loads to the system. These loads would partially be taken by the MSF legs and would result in a relatively large weak-axis bending moment. Furthermore, the use of ILT's requires vertical slings, since its load transfer is based on horizontal shear forces, and hence the rigging may not impose a moment to the ILT.
An overview of the removal rigging for reference topsides 14 is presented in figure F.8.

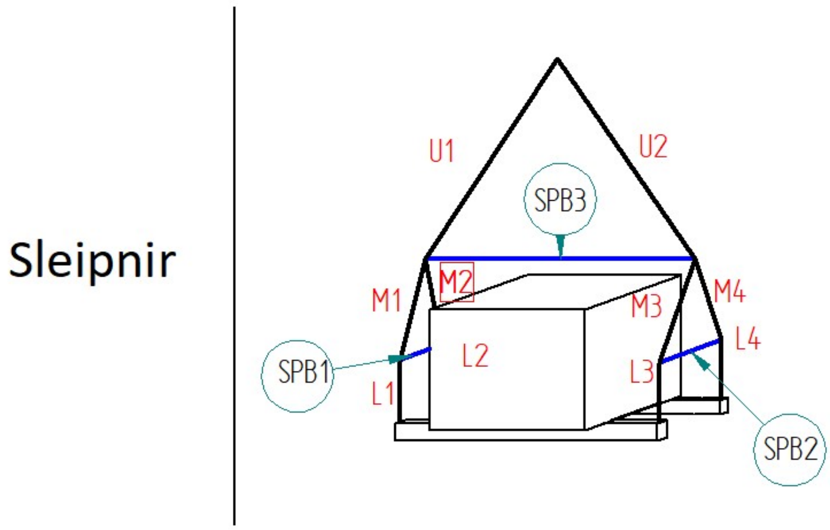

Figure F.8: Overview of the rigging for removal of reference topsides 14

The properties of the slings are provided in table below.

Sling	Length [m]	SWL [mT]	Stiffness [kN/m]	Single/Doubled
L1	13.46	2000	212800	Doubled
L2	13.48	2200	206900	Doubled
L3	13.31	2400	217400	Doubled
L4	13.29	2400	215900	Doubled
M1	31.46	2200	97100	Doubled
M2	31.46	2200	97100	Doubled
M3	31.27	2200	95800	Doubled
M4	31.27	2200	95800	Doubled
U1	43.33	5200	209100	Doubled
U2	46.47	4180	119700	Doubled

As can be seen all the slings are doubled, which implies that the sling travels twice between lift points. It has to be noted that for slings M1 and M3 copies are used for the neighbouring slings.

For SPB1 and SPB2, existing spreader bars are used, which have sufficient capacity for removal of reference topsides 14. For SPB3 an existing spreader bar (SPB1) is modified. The diameter of the tube is increased to 2 meters, and the wall thickness to 60 mm. The tube capacity of the modified spreader bar is checked using an in-house spreader bar capacity sheet. An extract of this sheet is provided in figure F.9.

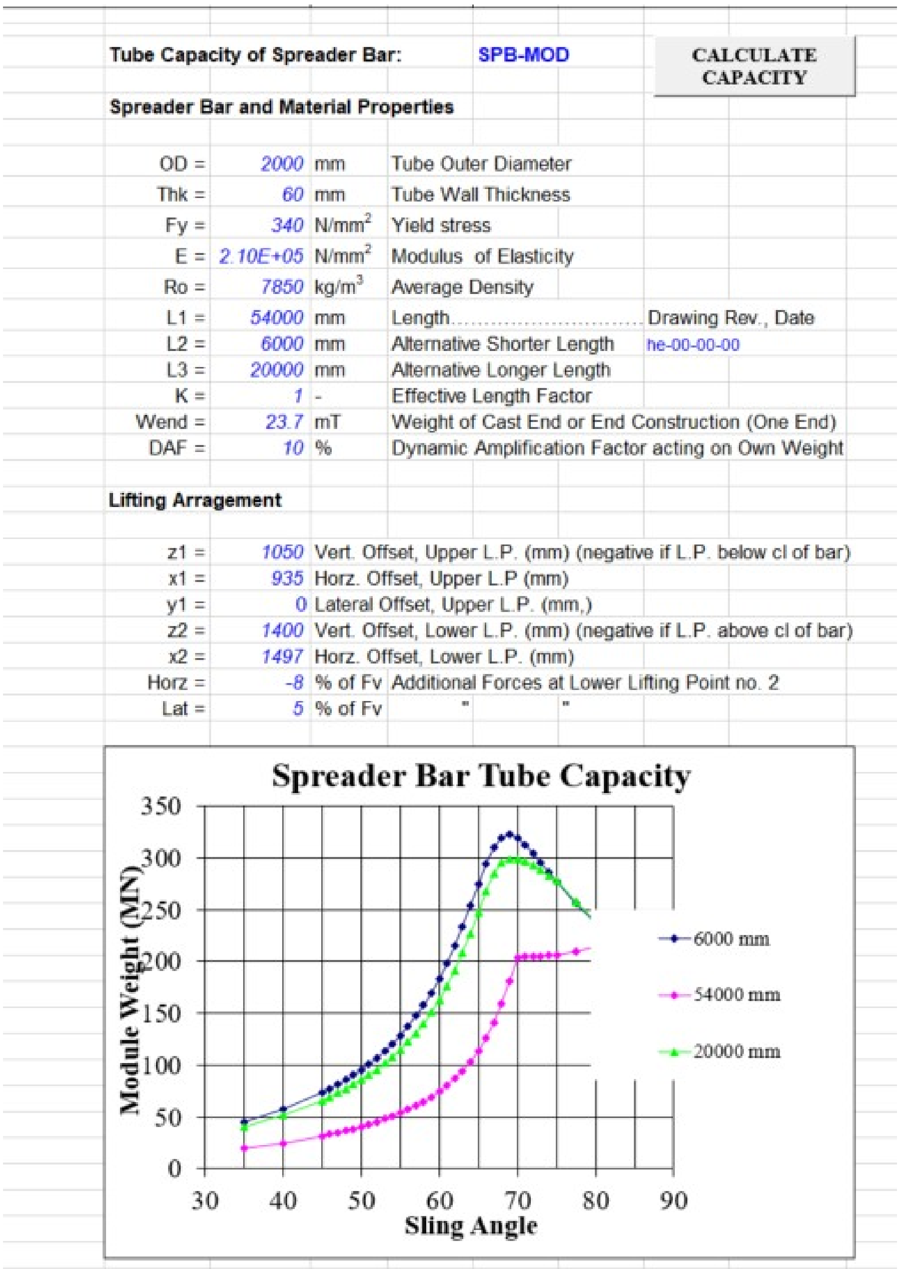
Tube Capacity of Spreader Bar: SPB-MOD — CALCULATE CAPACITY

Spreader Bar and Material Properties

OD =	2000	mm	Tube Outer Diameter
Thk =	60	mm	Tube Wall Thickness
Fy =	340	N/mm²	Yield stress
E =	2.10E+05	N/mm²	Modulus of Elasticity
Ro =	7850	kg/m³	Average Density
L1 =	54000	mm	Length............................ Drawing Rev., Date
L2 =	6000	mm	Alternative Shorter Length he-00-00-00
L3 =	20000	mm	Alternative Longer Length
K =	1	-	Effective Length Factor
Wend =	23.7	mT	Weight of Cast End or End Construction (One End)
DAF =	10	%	Dynamic Amplification Factor acting on Own Weight

Lifting Arragement

z1 =	1050		Vert. Offset, Upper L.P. (mm) (negative if L.P. below cl of bar)
x1 =	935		Horz. Offset, Upper L.P (mm)
y1 =	0		Lateral Offset, Upper L.P. (mm,)
z2 =	1400		Vert. Offset, Lower L.P. (mm) (negative if L.P. above cl of bar)
x2 =	1497		Horz. Offset, Lower L.P. (mm)
Horz =	-8	% of Fv	Additional Forces at Lower Lifting Point no. 2
Lat =	5	% of Fv	" "

Figure F.9: Extract of the spreader bar capacity sheet

The capacity of the tube increases as the angle of the slings increases. This follows from the fact that for an increasing sling angle, the sling force decreases since the lateral component of the sling force decreases. A transition piece with a slope of 1:6 is used to connect the 2 meter diameter tube with the 1.4 meter diameter end cast.

Also the lift points are modified using an in-house lift point capacity sheet. The new dimensions of the lower lift points and the upper lift points are shown in figures F.10 and F.11 respectively. It has to be noted that the weld between the lift points and the end cast needs to be examined.

PADEYE CAPACITY

Sling Load		16000	[kN]	
Consequence Factor		1.00	[-]	
Padeye Design load Fdl:		16000	[kN]	
	Manual input			
Shackle:		17168	[kN]	
Pin diameter D:		360	[mm]	
Inside width W:		500	[mm]	
Inside length L:		1120	[mm]	
Material properties padeye:				
Modulus of elasticity E:		210000	[N/mm²]	
Minimum yield stress σy:		345	[N/mm²]	
Minimum tensile strength σt:		510	[N/mm²]	
Hardness Brinell Factor Fhb:		5.6	[-]	
				[Ref. SC-292 table 5.1-1]
Padeye dimensions:				
Pinhole diameter d:	(d = Min. D+4, Max. 1.04×D)	370	[mm]	OK
Mainplate radius rm:	(rm ≥ 1.75×D)	650	[mm]	OK
Mainplate thickness tm:	(tm = 0.30 ~ 0.50×D)	180	[mm]	OK
Cheekplate radius rc:	(rc2 ≥ 1.50×D)	540	[mm]	OK
Cheekplate thickness tc:	(tc <= 0.5×tm)	90	[mm]	OK
Weld cheek - main plate w:	(w ≤ tc-5)	60	[mm]	OK
Spacer plate thickness		50	[mm]	
Section length γ–γ		700	[mm]	
Output summary:				
Governing U.C. =		**0.93**		
Max. design load Fdl =		**17168**	[kN]	
1. d ≤ 1.04×D --> Bearing stress check		Fp =	123.5	[N/mm²]
		U.C. =	**0.40**	
2. Shear stress at section α–α		Fs =	59.6	[N/mm²]
		U.C. =	**0.43**	
3. Tensile stress at section β–β		Ft =	54.2	[N/mm²]
		U.C. =	**0.35**	
4. Shear stress at weld cheek plate - main plate		Fs =	55.6	[N/mm²]
		U.C. =	**0.40**	
5. Tear out stress at section γ–γ (Only applicable if cheeck plates are used)		Fs =	127.0	[N/mm²]
		U.C. =	**0.92**	
6. Shackle capacity		**U.C. =**	**0.93**	

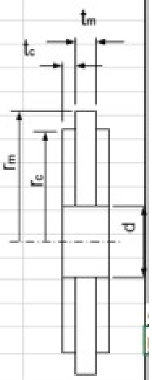

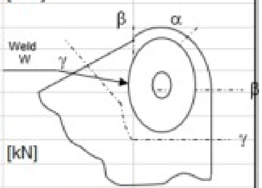

Calc. Acc. To Heerema SC-292 Criteria for lift point design, Revision C (December 2014)
Allowable stress according to AISC
Eighth Revision: January 2016

Figure F.10: Extract of the lower lift point capacity sheet

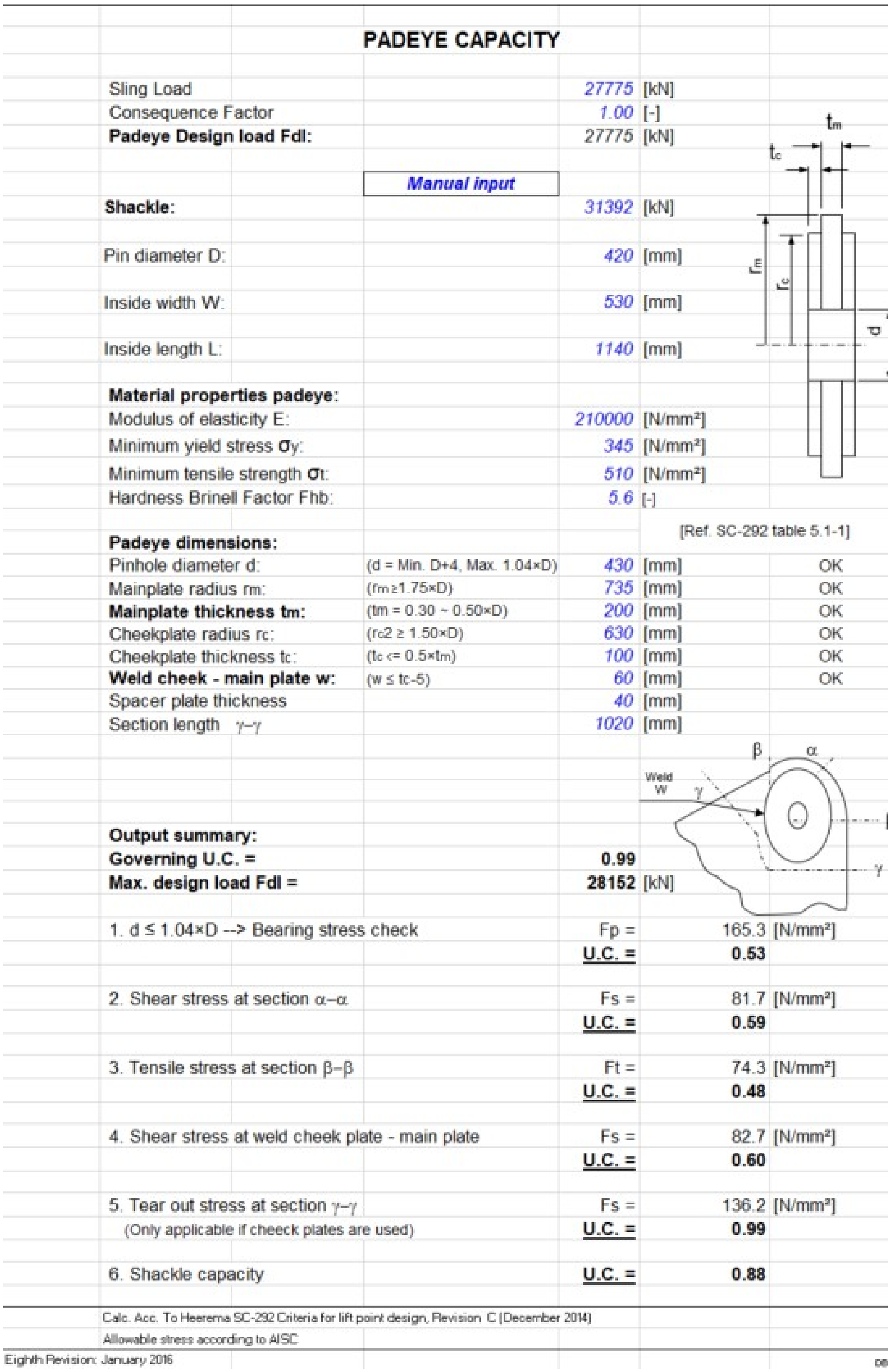

PADEYE CAPACITY

Sling Load		27775	[kN]	
Consequence Factor		1.00	[-]	
Padeye Design load Fdl:		27775	[kN]	
	Manual input			
Shackle:		31392	[kN]	
Pin diameter D:		420	[mm]	
Inside width W:		530	[mm]	
Inside length L:		1140	[mm]	
Material properties padeye:				
Modulus of elasticity E:		210000	[N/mm²]	
Minimum yield stress σ_y:		345	[N/mm²]	
Minimum tensile strength σ_t:		510	[N/mm²]	
Hardness Brinell Factor Fhb:		5.6	[-]	
			[Ref. SC-292 table 5.1-1]	
Padeye dimensions:				
Pinhole diameter d:	(d = Min. D+4, Max. 1.04×D)	430	[mm]	OK
Mainplate radius r_m:	($r_m \geq 1.75\times D$)	735	[mm]	OK
Mainplate thickness t_m:	(t_m = 0.30 ~ 0.50×D)	200	[mm]	OK
Cheekplate radius r_c:	($r_{c2} \geq 1.50\times D$)	630	[mm]	OK
Cheekplate thickness t_c:	($t_c \leq 0.5\times t_m$)	100	[mm]	OK
Weld cheek - main plate w:	($w \leq t_c-5$)	60	[mm]	OK
Spacer plate thickness		40	[mm]	
Section length $\gamma-\gamma$		1020	[mm]	
Output summary:				
Governing U.C. =		**0.99**		
Max. design load Fdl =		**28152**	[kN]	
1. d ≤ 1.04×D --> Bearing stress check		Fp =	165.3	[N/mm²]
		U.C. =	**0.53**	
2. Shear stress at section $\alpha-\alpha$		Fs =	81.7	[N/mm²]
		U.C. =	**0.59**	
3. Tensile stress at section $\beta-\beta$		Ft =	74.3	[N/mm²]
		U.C. =	**0.48**	
4. Shear stress at weld cheek plate - main plate		Fs =	82.7	[N/mm²]
		U.C. =	**0.60**	
5. Tear out stress at section $\gamma-\gamma$		Fs =	136.2	[N/mm²]
(Only applicable if cheeck plates are used)		U.C. =	**0.99**	
6. Shackle capacity		U.C. =	**0.88**	

Calc. Acc. To Heerema SC-292 Criteria for lift point design, Revision C (December 2014)
Allowable stress according to AISC
Eighth Revision: January 2016

Figure F.11: Extract of the upper lift point capacity sheet

F.4.2. Static lift analysis of the topsides

A static lift analysis is performed on reference topsides 14 to examine the stability of the lift setup. As the lift points are located below the CoG of the lift object the possibility of toppling exists. Therefore the sensitivity of the lift setup to toppling is assessed. AGES is used to assess the static stability of the lift setup. The rigging properties described in F.4.1 are used as input. For simplicity the same working line is taken for the doubled slings. An impression of the model is shown in figure F.12.

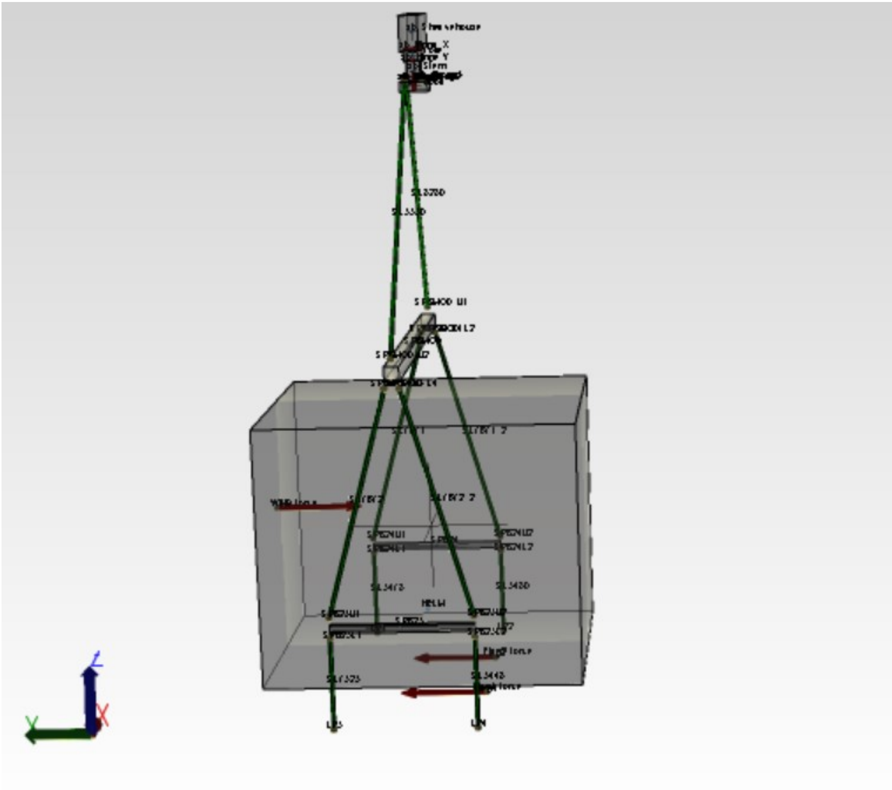

Figure F.12: Impression of the model in AGES

The topsides is modelled as a block which captures the topsides envelope. The lift points are modelled as POI's which are attached to the main body. The lift points are located 4.5 meters below deck, and are distanced at 19.5 meters over the transverse direction.

The properties of the assembly are including the presence of the helideck and the LQ, and are summarized in table below.

Element	Width (x) [m]	Length (y) [m]	Height (z) [m]	CoG_x [m]	CoG_y [m]	CoG_z [m]	Mass [mT]
Main body	39.5	43.7	36	2.25	1.62	-11.4	4935

Table F.1: Properties of the assembly block

The position of the CoG is given with respect to the geometrical center of the block. In assessing the stability of the lift setup an envelope is used for the CoG, which is 5% of the topsides dimensions in the respective direction. For simplicity, no offset is given to the CoG z-coordinate. It can however be noted that an increase in the vertical distance between the CoG and the lift points will further enhance the instability phenomena. The coordinates of the CoG envelope and the lift points with respect to the geometrical center are provided in table below.

Point	x	y	z
CoG_0	2.25	1.62	36
CoG_1	3.24	2.71	-11.4
CoG_2	1.26	2.71	-11.4
CoG_3	3.24	0.53	-11.4
CoG_4	1.26	0.53	-11.4
LP_1	-25.75	11.65	-22.5
LP_2	-25.75	-7.85	-22.5
LP_3	24.25	11.65	-22.5
LP_4	24.25	-7.85	-22.5

Table F.2: Overview of the CoG envelope coordinates and the lift point coordinates

First the case is examined where solely inaccuracies in the CoG are considered. Hereby it is also aimed to examine whether the UC's of the rigging remains within limits. The UC's of the rigging and the tilt of the topsides for the different CoG locations is provided in table F.3

CoG case	xtilt [%]	ytilt [%]	maximum UC [-]
0	-1.48	-1.1	0.73(L4)
1	-4.1	3.3	0.79(M3)
2	1.1	3.3	0.75(U1)
3	-4.1	-5.5	0.88(L4)
4	1.1	-5.5	0.81(L4)

Table F.3: Overview of the assembly tilt and maximum rigging UC for the different CoG cases

It can be seen that the tilt is limited to 4.1 % around the x-axis and 5.5% around the y-axis. These changes in tilt are considered to be reasonable. Furthermore it can be noticed that the rigging has sufficient capacity to deal with CoG inaccuracies.

Furthermore the effects of rigging elongation to the rigging load distribution, and the tilt of the assembly are examined. Hereby the length of the rigging from one of the lift points to the hook is increased by one times the diameter of the rigging under consideration. the results are shown in table F.4.

Case	Alteration of sling length	Diag dist(LP1/LP4-LP2/LP3)	Elongated string	xtilt	ytilt
Normal lift	-	54.8/45.2	-	-0.34	2.38
Skew load case 1	L1, M1, U1	51.9/48.1	LP1	1.44	4.16
Skew load case 2	L2, M2, U1	57.7/42.3	LP2	1.45	0.53
Skew load case 3	L3, M3, U2	57.4/42.6	LP3	-1.97	4.69
Skew load case 4	L4, M4, U2	52.2/47.8	LP4	-1.88	0.12

Table F.4: Overview of the assembly tilt and maximum rigging UC for the different CoG cases

It can be seen that for the normal case, the diagonal rigging load distribution follows a 55-45 distribution as expected. Increasing the string length results in a lower force uptake, as the assembly will tilt towards the 'shorter' rigging side, which is stiffer and quicker under tension.

External loads are applied to the system to examine the lift setup's sensitivity to toppling. The external loads will provide an overturning moment, which will result in tilting and shifting of the topsides. At a certain point, the gravity of the assembly cannot provide a resisting moment against the externally applied overturning moment. When this point is reached, toppling of the topsides will occur. Toppling of the topsides directly results in failure of the lift, with the lift object likely falling in the water. Besides pollution of the environment, the SSCV can get damaged in the fall. Two types of external loads are considered, a wind load and an impact load.

For the wind load, the wind-induced drag force is considered, as described by equation F.2.

$$F_w = \frac{1}{2} C_D \rho_{air} B \int_{17}^{53} U(z)|U(z)|dz \tag{F.1}$$

Where:

C_D = 0.95 [-]

ρ_{air} = 1.225 $[kg/m^3]$

B = 39.5 $[m]$

For the wind speed profile the power law is used, which is shown in equation F.1.

$$U(z) = U(H) * (\frac{z}{H})^{\alpha} \tag{F.2}$$

The power law exponent, α, may be taken as 0.12 for an open sea with waves [14]. The reference wind speed, $U(H)$, is generally taken at an elevation of 10 meters with respect to the waterline. The wind force can then be expressed as:

$$F_w = 22.98 * \int_{17}^{53} (0.76U(H))^2 z^{0.24} dz \tag{F.3}$$

The wind force as a function of the wind speed is plotted in figure F.13.

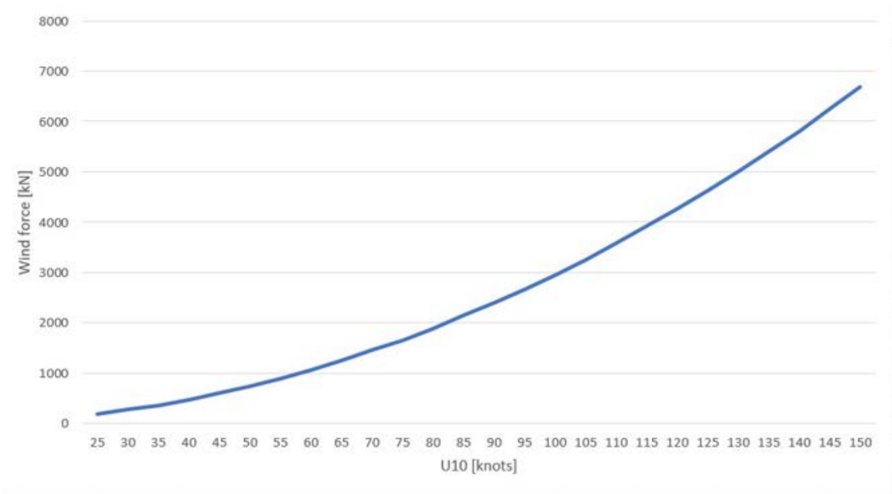

Figure F.13: Wind force as a function of U(10)

The center of force of the wind load acts 3 meters above the geometrical center of the topsides. First the lift setup's sensitivity to toppling is examined when only a wind load is applied. This is done for the different CoG cases, as described in table F.2. The wind load acts in transverse direction (y-axis), since the spacing of the lift points is relatively short in this direction. The governing direction of the wind load depends on the CoG case. The governing wind direction works in the direction where the distance between the assembly's CoG and any of the lift points is smallest. The smaller this distance,

the smaller the shift or tilt of the topsides is required at which toppling will occur. As the topsides tilts, the transverse spreader bars SPB1 and SPB2 also tilt to a point where they are parallel with the topsides. The same holds for SPB3. At a certain shift and tilt, the middle rigging aligns with the upper rigging, which implies that the adjacent rigging can't provide a restoring force, with toppling as a result.
It is found that for a wind load equal to 5520 kN, the topsides will topple. This corresponds to a wind speed of 137 knots. The external moment caused by the wind load is equal to 82 MNm. The equilibrium position of the assembly, just before the limiting wind load is reached, is depicted in figure F.14.

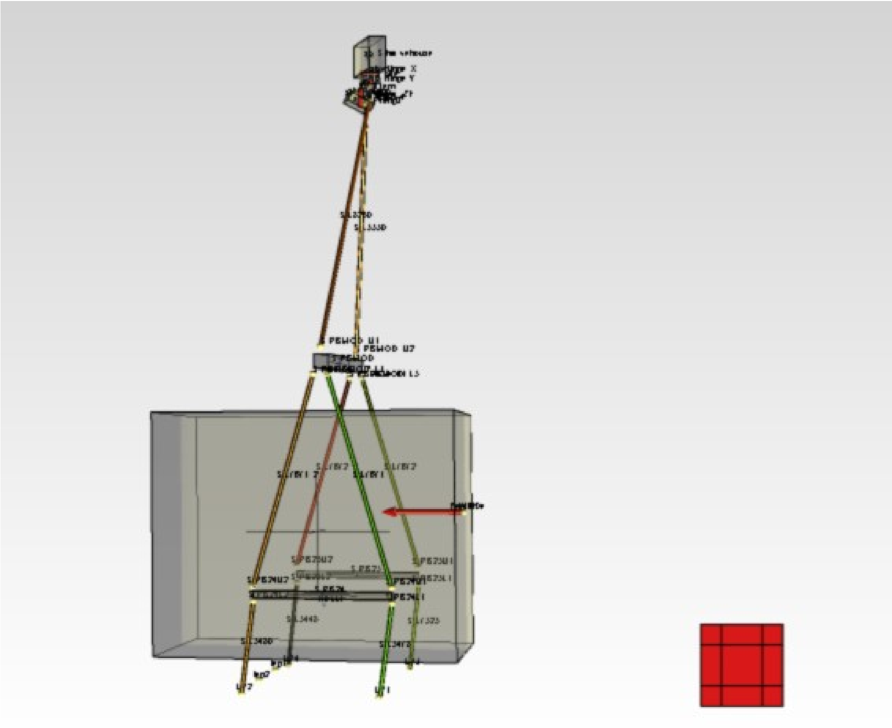

Figure F.14: Equilibrium position of the assembly just before the limiting wind load is reached

Furthermore an impact load is considered acting on both legs and is equal to 5% of the unfactored weight of the topsides.

$$F_{imp,leg} = 0.05 * 4935 * 9.81/1.21 = 2000.5kN \tag{F.4}$$

The legs are located 22 meters below the geometrical center of the topsides. The impact load is simultaneously applied with the wind load. Hereby the governing case follows when the loads act in opposite direction, working as a couple on the assembly. For the same reasons, the governing CoG location is for CoG_3.

It is found that in combination with the impact loads, for a wind load of 3700 kN the topsides will topple. This corresponds to a wind speed of 112 knots. The equilibrium position of the assembly just before the critical wind load is reached, is shown in figure F.15.

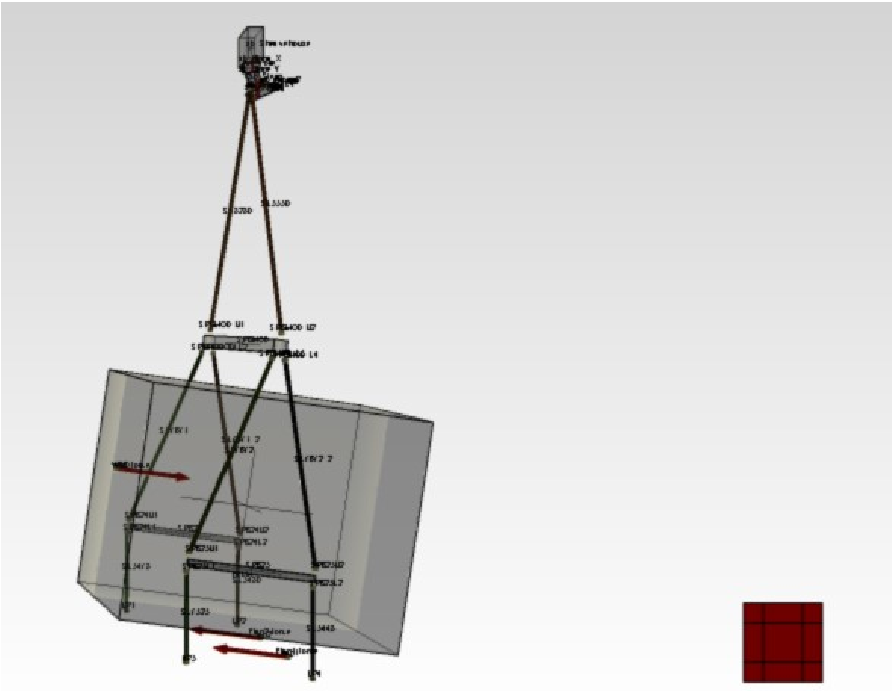

Figure F.15: Equilibrium position of the assembly just before the limiting wind load is reached, including impact loads

F.4.3. Dynamic response of the topsides

Now that the static stability of the system is assessed, the dynamic response will be investigated. For this exercise no CoG shift is considered. It is however recommended to investigate whether significant changes in the dynamic response will be observed when CoG inaccuracies are included. An impression of the model in LiftDyn is shown in figure F.16.

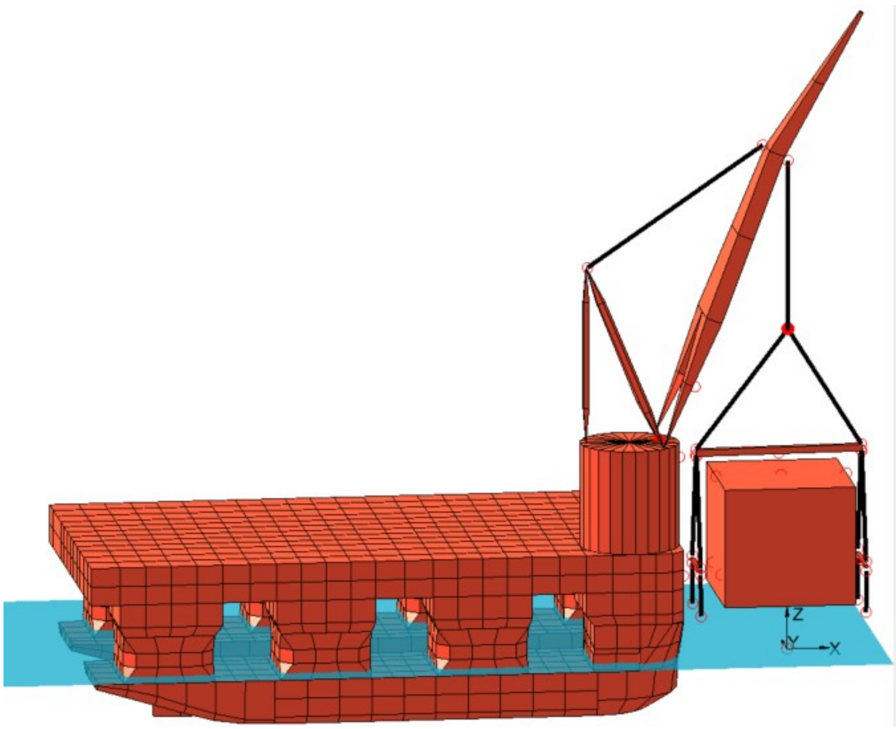

Figure F.16: LiftDyn model for removal of reference topsides 14

The static equilibrium position of the topsides and the rigging arrangement from AGES is implemented in LiftDyn. The stiffness of the slings and the sling force for the equilibrium position are used as input for the connectors in LiftDyn.

Limiting criteria are applied for which collision between the rigging and the topsides, and between the rigging and the SSCV is prevented. This is done by setting a limit to the relative motion between the points of interest. The value of this motion is equal to the distance between these points, taking an extra margin of 1 meter into account. Furthermore a limit is applied to the force fluctuation in the connector, which is equal to 90% of the static sling force. This is done to examine whether slack will occur in the rigging. Slack will result in instability as the sling under consideration won't be under tension. An overview of the limiting criteria is provided in table below.

Limiting criterion	Single amplitude	Unit
F_{L1}	9265	kN
F_{L2}	10038	kN
F_{L3}	11789	kN
F_{L4}	12937	kN
F_{M1}	10076	kN
F_{M2}	10835	kN
F_{M3}	12745	kN
F_{M4}	13848	kN
F_{U1}	26471	kN
F_{U2}	30826	kN
$x_{SPB1-SSCV}$	3.75	m
$x_{SPB1-top}$	4.68	m
$x_{SPB2-top}$	6.73	m
$x_{SPB3-SSCV}$	4.24	m
$z_{SPB3-top}$	5.78	m

Table F.5: Overview of the limiting criteria for removal of reference topsides 14

Using a JONSWAP spectrum, the RAO's of the limiting criteria can be determined, as well as the operability for each criterion. This is done in similar fashion as for installation of the lift beams. The combined operability of the limiting criteria is provided in figure F.17.

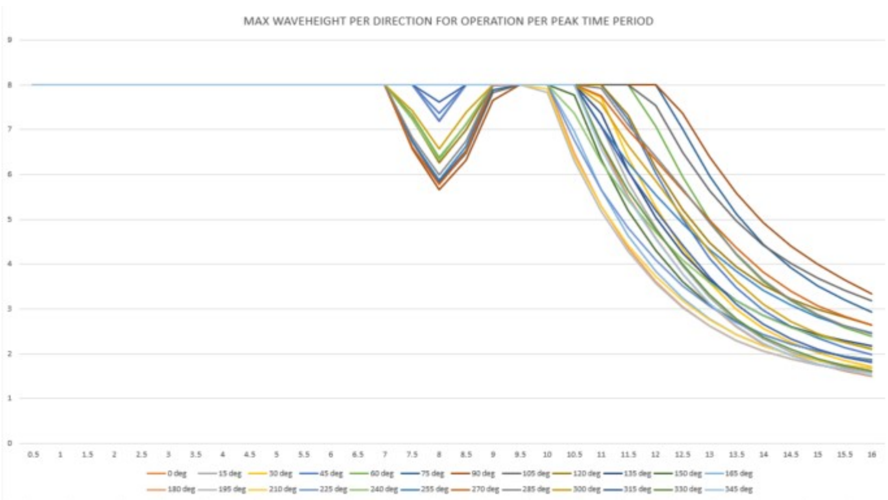

Figure F.17: Combined operability of the limiting criteria for removal of reference topsides 14

The drop in operability for a peak period between 7 and 9 seconds is for the slack criterion for slings M1 and M2. As was shown in the static lift analysis, it is likely that one of these slings will align with the upper rigging, when excessive tilting and shifting of the topsides is reached. The operability in this period drops from a maximum allowable wave height of 8 meters to approximately 6 meters. Waves with such peak periods and wave heights are not considered to be likely expected and hence this drop can be considered as irrelevant. Furthermore a drop in the operability is observed for peak periods higher than 10.5 seconds. This is for the limiting criterion for the relative motion between SPB1 and the hull of the SSCV, and the relative motion between SPB3 and the hull of the SSCV. This motion is likely excited by pitching of the SSCV and the side lead angle of the assembly. The peak periods above 10.5 seconds are however not expected to represent a large portion of the wave energy, and are therefore not considered as critical. In general it can therefore be concluded that the dynamic response of the topsides during removal is limited.

F.5. Topsides removal time path

The time path is divided in three stages: a general preparatory phase, installation of the lift frame, and removal of the topsides. Figure F.18 provides the time path of the preparatory phase.

Figure F.18: Time path general preparatory phase

Upon arrival at the location of the platform, the functioning of the SSCV's DP system has to be tested and the SSCV has to establish its position. Hereafter a landing area is prepared and a gangway is installed to provide access from the SSCV to the topsides. Final checks are performed on the topsides to ensure that the topsides' state is as expected. After completing the final platform preparations, installation of the lift frame can start.In figure 7.8 the time path of the lift frame installation is shown.

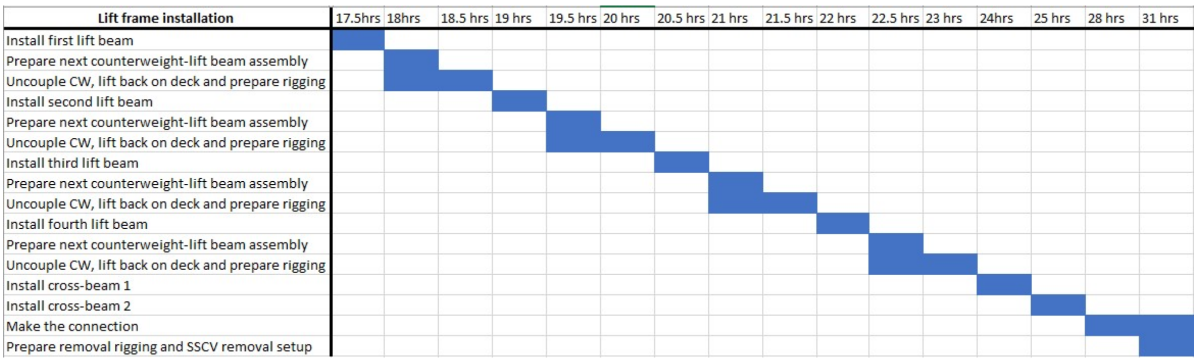

Figure F.19: Time path lift frame installation phase

As previously discussed, the installation of the lift beams, including retrieval of the counterweight and preparation of the next lift beam, takes approximately 1.5 hours. Preparation of the next lift beam can be performed by the portside crane, while the installation of another lift beam is ongoing. This process is repeated until all lift beams are installed. The installation of the cross-beams follows, which is estimated to take 2 hours in total. In total it takes 8 hours to install the lift frame, and six hours until the connection is established. In the connection phase, the SSCV's removal setup can be prepared, as well as the removal rigging. Finally the time path of topsides removal is shown.

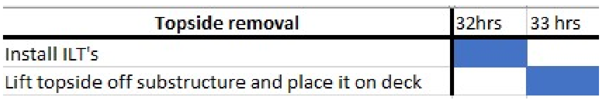

Figure F.20: Time path topside lift

It can be seen that in total 33 hours are required for removal of reference topsides 14. This duration is excluding the waiting on weather time.
An overview of the sequence of steps is provided in figure F.21.

1	PREPARATIONS	17
2	LB1 AANBRENGEN	0.5
3	CW RETRIEVAL & PREPARATIONS 1	1
4	LB 2 AANBRENGEN	0.5
5	CW RETRIEVAL & PREPARATIONS 2	1
6	LB3 AANBRENGEN	0.5
7	CW RETRIEVAL & PREPARATIONS 3	1
8	LB4 AANBRENGEN	0.5
9	CW RETRIEVAL & PREPARATIONS 4	1
10	CONNECTION	6
11	INSTALL CROSS-BEAM 1	1
12	INSTALL CROSS-BEAM 2	1
13	INSTALL ILT'S	1
14	TOPSIDE LIFT & PLACE ON DECK	1

Figure F.21: Overview of the installation and removal steps

The average waiting on weather time and total operation time per step, for each month is provided in figures F.22 and F.23 respectively.

Average waiting time [hrs] incl. WoW and delay [hrs]:

Period	1	2	3	4	5	6	7	8	9	10	11	12	13	14	Total	Total [days]
01.Jan - 31.Jan	55	0	2	0	0	0	1	0	0	5	8	8	0	1	80	3.3
01.Feb - 29.Feb	29	1	1	0	0	0	1	0	0	3	5	11	0	0	53	2.2
01.Mar - 31.Mar	16	0	1	0	0	0	0	0	0	3	4	8	0	0	34	1.4
01.Apr - 30.Apr	6	0	0	0	0	0	0	0	0	1	1	2	0	0	11	0.5
01.May - 31.May	3	0	0	0	0	0	0	0	0	0	0	1	0	0	5	0.2
01.Jun - 30.Jun	3	0	0	0	0	0	0	0	0	0	0	0	0	0	4	0.2
01.Jul - 31.Jul	3	0	0	0	0	0	0	0	0	0	0	0	0	0	4	0.1
01.Aug - 31.Aug	4	0	0	0	0	0	0	0	0	1	0	0	0	0	6	0.2
01.Sep - 30.Sep	12	0	0	0	0	0	0	0	0	2	1	1	0	0	17	0.7
01.Oct - 31.Oct	17	0	1	0	0	0	2	0	0	3	2	4	0	0	30	1.3
01.Nov - 30.Nov	23	0	1	0	0	0	1	0	0	5	4	8	0	1	44	1.8
01.Dec - 30.Dec	31	1	2	0	0	0	1	0	0	6	7	9	0	1	59	2.4
01.Jan - 31.Dec	17	0	1	0	0	0	1	0	0	2	3	4	0	0	29	1.2

Figure F.22: Overview of the average waiting time

Period	1	2	3	4	5	6	7	8	9	10	11	12	13	14	Total	Total [days]
01.Jan - 31.Jan	72	1	3	1	1	1	2	1	1	11	9	9	1	2	113	4.7
01.Feb - 29.Feb	46	2	2	1	1	1	2	1	1	9	6	12	1	1	86	3.6
01.Mar - 31.Mar	33	1	2	1	1	1	1	1	1	9	5	9	1	1	67	2.8
01.Apr - 30.Apr	23	1	1	1	1	1	1	1	1	7	2	3	1	1	44	1.8
01.May - 31.May	20	1	1	1	1	1	1	1	1	6	1	2	1	1	38	1.6
01.Jun - 30.Jun	20	1	1	1	1	1	1	1	1	6	1	1	1	1	37	1.5
01.Jul - 31.Jul	20	1	1	1	1	1	1	1	1	6	1	1	1	1	37	1.5
01.Aug - 31.Aug	21	1	1	1	1	1	1	1	1	7	1	1	1	1	39	1.6
01.Sep - 30.Sep	29	1	1	1	1	1	1	1	1	8	2	2	1	1	50	2.1
01.Oct - 31.Oct	34	1	2	1	1	1	3	1	1	9	3	5	1	1	63	2.6
01.Nov - 30.Nov	40	1	2	1	1	1	2	1	1	11	5	9	1	2	77	3.2
01.Dec - 30.Dec	48	2	3	1	1	1	2	1	1	12	8	10	1	2	92	3.8
01.Jan - 31.Dec	34	1	2	1	1	1	2	1	1	8	4	5	1	1	62	2.6
Nett span	17	1	1	1	1	1	1	1	1	6	1	1	1	1	33	1.4

Figure F.23: Overview of the total operation time

The values in the figures are average waiting times, which are based on a data set spanning over more than 20 years. It has to be noted that in reality the weather can strongly vary over short time spans, especially in the winter months.

Bibliography

[1] Pioneering spirit. URL https://allseas.com/equipment/pioneering-spirit/.

[2] URL https://www.bsee.gov/public-faqs/what-is-decommissioning-of-offshore-platforms.

[3] Helm platform. URL https://www.marinetraffic.com/am/photos/picture/ships_id/1397350/244105000.

[4] URL https://www.rystadenergy.com/newsevents/news/press-releases/global-oil-gas-decommissioning-costs-to-total-\protect\TU\textdollar42-billion-through-2024-dominated-by-uk-north-sea/.

[5] Brent delta platform lift. URL https://www.shell.co.uk/sustainability/decommissioning/brent-field-decommissioning/brent-delta-topside-lift.html.

[6] Sean. URL https://onedyas.com/project/sean-2/.

[7] Sleipnir clearance criteria for topside installation in dynamic positioning mode approach.

[8] The claw. URL https://www.vbar.com/Claw/index.html.

[9] Vb10,000. URL https://www.vbar.com/vb10000/index.html.

[10] Specification for structural steel buildings. 1989.

[11] Emerging heavy lift technology for the offshore decommissioning industry. 2001. URL http://www.gard.no/web/updates/content/53272/emerging-heavy-lift-technology-for-the-offshore-decommissioning-industry.

[12] Design of steel structures. 2004.

[13] Eurocode 3: Design of steel structures - part 1-8: Design of joints. 2005.

[14] Environmental conditions and environmental loads. 2010.

[15] Decommissioning of north sea oil and gas facilities an introductory assessment of potential impacts, costs and opportunities. 2011. URL https://ecoeffective.biz/wp-content/uploads/2016/02/LNS200_Report-analysis-of-decommissioning-options-for-North-Sea-oil-and-gas-facilities_LiNSI_DEF-copy-kopie.pdf.

[16] How it works. 2011. URL http://vtruss.com/howitworks/index.html.

[17] Decommissioning in the north sea, review of decommissioning capacity]. *Decom North Sea*, page 11, 2014. URL https://decomnorthsea.com/uploads/pdfs/projects/Decommissioning-in-the-North-Sea-Demand-vs-Capacity_low-res.pdf.

[18] Monthly mechanics: Truss bridges. 2016. URL https://perchpro.com/2016/12/02/monthly-mechanics-truss-bridges/.

[19] Cessation. 2017. URL https://frigg.industriminne.no/en/2017/10/05/cessation-2/.

[20] Ospar inventory of offshore installations - 2017. 2017. URL https://odims.ospar.org/maps/new?layer=geonode:ospar_offshore_installations_2017_01_001.

[21] Ospar inventory of offshore installations - 2017. 2017. URL https://odims.ospar.org/documents/1623.

[22] Tapered sections. 2017. URL https://konstru.zendesk.com/hc/en-us/articles/115002091811-Tapered-Sections.

[23] Heerema sleipnir stability booklet. 2019. URL https://instore.hmc-heerema.com/department/engineering/teammarineengineering/library/BargeVesselMarine/Sleipnir/V0119-335-131-JSL-A-MI-0001.pdf.

[24] Decommissioning insight 2019. page 4, 2019. URL https://oilandgasuk.co.uk/wp-content/uploads/2019/11/OGUK-Decommissioning-Insight-2019.pdf.

[25] Brent delta topside decommissioning close-out report. 2019. URL https://assets.publishing.service.gov.uk/government/uploads/system/uploads/attachment_data/file/865827/Brent_Delta_Topside_Close_Out_Report.pdf.

[26] Conductor and topsides removal/jacket preparations progress report 6. 2019. URL https://instore.hmc-heerema.com/department/technologyworldwide/teamgeneraltechnology/library/PictureProgressReport/Jotun%20-%20EPRD%20B%20Platform/I0475%20Jotun%20B%20-%20Progress%20Report%20No.%206.pdf.

[27] Marine operations and marine warranty. 2020.

[28] Offshore platform/topsides. 2020. URL https://www.edgenmurray.com/post/offshore-platform-topsides/.

[29] Decommissioning insight 2020. 2020. URL https://oilandgasuk.co.uk/wp-content/uploads/2019/11/Decommissioning-Insight-2020-OGUK.pdf?

[30] A.S. Malik A.F. Hughes, D.C. Iles. Design of steel beams in torsion. 2011. URL https://www.steelconstruction.info/images/6/6f/Sci_p385.pdf.

[31] B.F.C. Fontoura C. Rebelo L.S. da Silva M. Veljkovic A.M.P de Jesus, R. Matos. A comparison of the fatigue behavior between s355 and s690 steel grades. *Journal of Constructional Steel Research*, 79, 2012. doi: 10.1016/j.csr.2012.07.021. URL https://www.sciencedirect.com/science/article/pii/S0143974X12001782.

[32] G.J. Arends. Handleiding ontwerpen draagconstructies - dimensionering en controle-berekening van liggers, kolommen en vakwerken. 2017.

[33] M.S. Love A.S. Bull. Worldwide oil and gas platform decommissioning: A review of practices and reefing options. *Ocean Coastal Management*, 168, 2019. doi: 10.1016/j.ocecoaman.2018.10.024. URL https://www.sciencedirect.com/science/article/pii/S0964569118304484.

[34] C. Barclay. Lift point design sc-292. 2014.

[35] C. Barclay. Single crane lift systems sc-201. 2016.

[36] O.W. Blodgett. Design of welded structures. 1967.

[37] J.W. Welleman C. Hartsuijker.

[38] C. Clement. Offshore heavy lift design and operations: Sling tension in heavy lifts with quadruple sling arrangement. 2015. doi: 10.13140/RG.2.1.4891.9286. URL https://www.researchgate.net/publication/306000332_Offshore_Heavy_Lift_Design_and_Operations_Sling_Tension_in_Heavy_Lifts_with_Quadruple_Sling_Arrangement.

[39] T.V. Galambos. Guide to stability design criteria for metal structures, 4th ed. 1988. URL https://www.academia.edu/RegisterToDownload/BulkDownload.

[40] F. Sliggers J.S. Hoving. Lecture notes oe44096 bottom founded offshore structures- decommissioning, msc offshore dredging engineering, tu delft. 2018. URL https://brightspace.tudelft.nl/d2l/le/content/127582/viewContent/1181145/View.

[41] F. G. Larminie, R. B. Clark, J. K. Rudd, and M. L. Tasker. The history and future of north sea oil and gas: An environmental perspective [and discussion]. *Philosophical Transactions of the Royal Society of London. Series B, Biological Sciences*, 316(1181):487–493, 1987. ISSN 00804622. URL http://www.jstor.org/stable/2396591.

[42] CUT UK Ltd. Castellated step cut. URL https://www.cut-group.com/special-dwcms/castellated-step-cut/.

[43] F. Corvaro F. Polonara M. Leporini, B. Marchetti. Reconversion of offshore oil and gas platforms into renewable energy sites production: Assessment of different scenarios. *Renewable Energy*, 135, 2018. doi: 10.1016/j.renene.2018.12.073. URL https://www.sciencedirect.com/science/article/abs/pii/S0960148118315209.

[44] B. Donnay O. Hechler, G. Axmann. The right choice of steel - according to the eurocode -. 2009.

[45] P. Schoenmaekers. Design of guidance systems for lifting and placement sc-251. 2019.

[46] Yu Wentai, Sidie Yang, Shunqing Liu, Tao Liu, and Haixia Gong. The relationship between the depth embedded pipe pile and the force of clamping jaw. *IOP Conference Series: Materials Science and Engineering*, 452:022052, 12 2018. doi: 10.1088/1757-899X/452/2/022052.